

# Sheffield Hallam University

*Independent component analysis techniques and their performance evaluation for electroencephalography.*

VIGON, Laurence Celine.

Available from the Sheffield Hallam University Research Archive (SHURA) at:

<http://shura.shu.ac.uk/20479/>

## A Sheffield Hallam University thesis

This thesis is protected by copyright which belongs to the author.

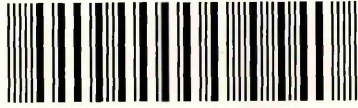
The content must not be changed in any way or sold commercially in any format or medium without the formal permission of the author.

When referring to this work, full bibliographic details including the author, title, awarding institution and date of the thesis must be given.

Please visit <http://shura.shu.ac.uk/20479/> and <http://shura.shu.ac.uk/information.html> for further details about copyright and re-use permissions.

CAMPUS, POND STREET,  
SHEFFIELD, S1 1

101 715 635 2



**Fines are charged at 50p per hour**

19/10/04 *afm*

REFERENCE

ProQuest Number: 10701126

All rights reserved

INFORMATION TO ALL USERS

The quality of this reproduction is dependent upon the quality of the copy submitted.

In the unlikely event that the author did not send a complete manuscript and there are missing pages, these will be noted. Also, if material had to be removed, a note will indicate the deletion.



ProQuest 10701126

Published by ProQuest LLC (2017). Copyright of the Dissertation is held by the Author.

All rights reserved.

This work is protected against unauthorized copying under Title 17, United States Code  
Microform Edition © ProQuest LLC.

ProQuest LLC.  
789 East Eisenhower Parkway  
P.O. Box 1346  
Ann Arbor, MI 48106 – 1346

# **Independent Component Analysis Techniques And Their Performance Evaluation For Electroencephalography**

Laurence Céline Vigon

A thesis submitted in partial fulfilment of the requirements of  
Sheffield Hallam University  
for the degree of Doctor of Philosophy

April 2002

Collaborating Organisation: Sheffield University  
Department of Psychology





I dedicate this thesis to my beloved parents Georges and Nelly Vigon,  
and to my dearest sister Corinne Vigon, for always keeping faith in me  
and for their stimulating words of support and encouragement,  
which made the successful completion of this work possible.

# Acknowledgements

I am grateful to have received the joint Sheffield Hallam University - Sheffield University research grant which gave me the opportunity to pursue my PhD studies and carry out this study within the research community of both Universities.

I would like to deeply thank Prof A.K. Ray, head for research of the Electronics group, who kindly helped me with financial assistance during my final year and made it possible for me to complete my PhD.

I would like to express my very special thanks and profound gratefulness to Prof J.E.W. Mayhew for his continuous and most valuable help and guidance as a supervisor during the project, and to Dr N.A. Taroyan and Prof J.P. Frisby for their active collaboration to the study and for numerous and valuable discussions. I am very grateful to Dr Peter Furness for helping with the data recording procedures, to Dr David Buckley for his help in designing the experiment, and to Drs David Johnston and Olivier Pascalis for valuable discussions. Everyone in the Vision Research Unit at Psychology Department – Sheffield University, provided a warm welcome to this wonderful research environment and made it possible for me to use their facilities and equipments, and with their kind help and assistance to design experiments and record a considerable amount of data. I benefited greatly from this collaboration which provided me with a deeper understanding of neuroscience and the clinical importance of this area of research. And my special thanks also go out to the kind co-operation of all the subjects who took part in the electroencephalogram data recordings.

Most of all, I would like to express my most sincere gratitude and deepest thankfulness to my dear director of studies, Dr Reza Saatchi, for offering me this project and for providing me with continuous help and assistance all throughout the project. I have benefited greatly from his valuable expertise in Digital Signal Processing and Artificial Intelligence, and I greatly appreciated the help he provided in my understanding of the signal processing techniques used in the study. His considerable energy and enthusiastic ideas, as well as his useful advice made this 3-year journey an exciting, fruitful and most enjoyable one. I would like to deeply thank Dr Reza Saatchi also for his continual guidance, his many words of support and encouragement, and for his admirable patience, immense kindness and infinite generosity which made this study possible.

# Declaration

No portion of the work referred to in this thesis has been submitted in support of an application for another degree or qualification to this or any other university, institute of learning or industrial organisation.

Laurence Céline Vigon

April 2002

# Abstract

The ongoing electrical activity of the brain is known as the electroencephalogram (EEG). Evoked potentials (EPs) are voltage deviations in the EEG elicited in association with stimuli. EPs provide clinical information by allowing an insight into neurological processes. The amplitude of EPs is typically several times less than the background EEG. The background EEG has the effect of obscuring the EPs and therefore appropriate signal processing is required for their recovery.

The EEG waveforms recorded from electrodes placed on the scalp contains the ongoing background EEG, EPs from various brain sources as well as signal components with sources external to the brain. An example of externally generated signal which is picked up by the electrodes on the scalp is the electrooculogram (EOG). This signal is generated by the eyes when eye movements or blinks are performed.

Saccade-related EEG waveforms were recorded from 7 normal subjects. A signal source separation technique, namely the independent component analysis (ICA) algorithm of Bell and Sejnowski (hereafter referred to as BS\_ICA), was employed to analyse the recorded waveforms. The effectiveness of the BS\_ICA algorithm as well as that of the ICA algorithm of Cardoso, was investigated for removing ocular artefact (OA) from the EEG. It was quantitatively demonstrated that both ICA algorithms were more effective than the conventional correlation-based techniques for removing the OA from the EEG.

A novel iterative synchronised averaging method for EPs was devised. The method optimally synchronised the waveforms from successive trials with respect to the event of interest prior to averaging and thus preserved the features of the signals components that were time-locked to the event.

The recorded EEG waveforms were analysed using BS\_ICA and saccade-related components (frontal and occipital pre-saccadic potentials, and the lambda wave) were extracted and their scalp topographies were obtained. This initial study highlighted some limitations of the conventional ICA approach of Bell and Sejnowski for analysing saccade-related EEG waveforms.

Novel techniques were devised in order to improve the performance of the ICA algorithm of Bell and Sejnowski for extracting the lambda wave EP component. One approach involved designing a template-model that represented the temporal characteristics of a lambda wave. Its incorporation into the BS\_ICA algorithm improved the signal source separation ability of the algorithm for extracting the lambda wave from the EEG waveforms. The second approach increased the effective length of the recorded EEG traces prior to their processing by the BS\_ICA algorithm. This involved abutting EEG traces from an appropriate number of successive trials (a trial was a set of waveforms recorded from 64 electrode locations in a experiment involving a saccade performance). It was quantitatively demonstrated that the process of abutting EEG waveforms was a valuable pre-processing operation for the ICA algorithm of Bell and Sejnowski when extracting the lambda wave.

A Fuzzy logic method was implemented to identify BS\_ICA-extracted single-trial saccade-related lambda waves. The method provided an effective means to automate the identification of the lambda waves extracted by BS\_ICA. The approach correctly identified the single-trial lambda waves with an Accuracy of 97.4%.

# Nomenclature

## List of abbreviations (in alphabetical order)

ANOVA	Analysis-of-variance
BS_ICA	ICA algorithm of Bell and Sejnowski
BSS	Blind Signal Separation
DAC	Data Acquisition Computer
ECG	Electrocardiogram
EGI	Electrical Geodesic Incorporation
EEG	Electroencephalogram
EMG	Electromyogram
EOG	Electoocculogram
EOG <sub>L</sub>	Left EOG channel
EOG <sub>R</sub>	Right EOG channel
EP	Evoked Potential
ERP	Event-Related Potential
Ext.ICA	Extended version of the ICA algorithm of Bell and Sejnowski
FCM	Fuzzy C-Means
GSN	Geodesic Sensor Net
GSNIC	Geodesic Sensor Net Interface Cable
ICA	Independent Component Analysis
Infomax	Information Maximisation
JADE	Joint Approximate Diagonalisation Eigen-matrices
ms	Milliseconds
MI	Mutual Information
Net Amps	Net Amplifier unit
NLPCA	Non-linear Principal Component Analysis
NS	Negative Shift
OA	Ocular Artefact
PCA	Principal Component Analysis
RLS	Recursive Least Square
SAS	Statistical Analysis System
SNR	Signal-to-Noise Ratio

Std	Standard deviation
STDR	Standard Deviation Ratio
SSS	Signal Source Separation
SVD	Single Value Decomposition
USB	Universal Serial Bus
$\mu\text{V}$	Microvolts

## List of symbols

$N$	number of time points in a waveform
$n$	number of original sources and number of recorded (measured) mixtures (i.e. number of channels)
$i, j, k, l, r$	counting index which take positive integer values
$t$	digital sample (time) index which take positive integer values
$S = \{s_1, \dots, s_n\}$	matrix of original sources signals
$X = \{x_1, \dots, x_n\}$	matrix of recorded mixtures
$N = \{n_1, \dots, n_n\}$	Noise matrix
$U = \{u_1, \dots, u_n\}$	matrix of estimated underlying signals
$A = \begin{bmatrix} a_{11} & \dots & a_{1n} \\ \dots & \dots & \dots \\ a_{n1} & \dots & a_{nn} \end{bmatrix}$	mixing matrix where the $a_{ij}$ are the mixing coefficients
$W = \begin{bmatrix} w_{11} & \dots & w_{1n} \\ \dots & \dots & \dots \\ w_{n1} & \dots & w_{nn} \end{bmatrix}$	unmixing (or separating) matrix where the $w_{ij}$ are referred to as weights (or unmixing coefficients).
$f$	function that relates the measured signals to the transmitted signals
$P$	matrix of normalised (i.e. no amplitude information) principal components
$M = \begin{bmatrix} M_{11} & \dots & M_{1n} \\ \dots & \dots & \dots \\ M_{n1} & \dots & M_{nn} \end{bmatrix}$	eigen-matrix (set of linear weights factors) or mapping matrix
$\lambda = \{ \lambda_1, \dots, \lambda_n \}$	matrix of eigen-values
$T = \{ T_1, \dots, T_n \}$	matrix of eigen-vectors

$L$	matrix of non-normalised (i.e. that contain amplitude information) principal components
$R_x$	covariance (correlation) matrices of mixtures $X$
$R_y$	covariance (correlation) matrix of output signals $Y$
$R_s$	covariance (correlation) matrix of source signals $S$
$R_v$	covariance (correlation) matrix of whitened mixtures $V$
$p(), q()$	probability distribution functions
$E[.]$	expectation operation
$J_2(.)$	NLPCA cost function
$g(.)$	non-linear transfer function
$\ln(.)$	Natural logarithm function
$v$	whitened mixture
$y$	output of tranfert function $g(.)$
$D, h, m$	intermediate variables used for computational purposes.
$Q$	inverse correlation matrix of the input signals in the RLS algorithm
$e$	estimated error
$\beta$	constant forgetting term
$Tri[.]$	operation that computes the upper triangular part of a matrix
$O_x(.)$	whitening operation
$Y$	probability distribution
$H(.)$	Entropy measure
$I(.)$	Mutual information
$\frac{\partial}{\partial W}$	First derivative with respect to weight $W$
$\propto$	proportional to
$W_o$	bias weight matrix
$W_{opt}$	optimum value for $W$
$J$	Jacobian matrix
$\Delta W$	Rate of change in the weight matrix $W$
$\Delta W_o$	Rate of change in the bias weight matrix $W_o$
$\eta_n$	Learning rates
$m_1, m_2, m_3$	gradients of the lambda wave template model
$\phi, \phi_s, \phi_{si}$	model cost-function, smallest cost-function value, normalising factor

$C_1$	constant that controls the contribution of the model to the BS_ICA algorithm
$C_2$	constant that controls the contribution of the error to the model cost-function
$C_x$	Finite fourth-order cumulants of mixture $X$
$K_4$	Kurtosis
$C()$	function of $C_x$
$Cum^{(n)}(.)$	$n$ th-order cumulants function
$diag(.)$	diagonalisation operation
$\Sigma$	sum operation
$I_n$	Identity matrix
$V$	matrix of whitened mixtures
$T$	transpose operator
$-I$	inverse operator
$H$ (or #)	Hermetian operator (or pseudo-inverse operator)
$\wedge$	Estimation operaor
$-$	Conjugate operator
$ \cdot $	norm (or absolute function)
$\sqrt{\cdot}$	square route function
$\tanh()$	hyperbolic tangent function
$Z$	Unitary matrix
$B = \begin{bmatrix} B_{11} & \dots & B_{1n} \\ \dots & \dots & \dots \\ B_{n1} & \dots & B_{nn} \end{bmatrix}$	Set of matrices (input to the joint diagonalisation process)
$\hat{\theta}$	fraction symbol
$p$	row vector
$o$	original signal
$r$	recovered signal
$k_1, k_2$	scaling factors
$\varepsilon$	Euclidean distance
$\rho$	correlation coefficient
$S_i$	Sum of normalised contributions of a component to all electrodes
$S_\lambda$	Sum of normalised contributions of a component to the parieto-occipital area of the cerebral cortex

$S$	topographic feature (percentage of $S_\lambda$ over $S_l$ ).
$A_1, A_2$	names of the electrodes located on the scalp region near the ears
$C_3, C_4, C_z$	names of the electrodes located in the central region of the scalp
$F_3, F_4, F_7, F_8, F_z$	names of the electrodes located in the frontal region of the scalp
$Fp_1, Fp_2$	names of the electrodes located in the frontal pole region of the scalp
$P_3, P_4, P_z$	names of the electrodes located in the parietal region of the scalp
$O_1, O_2, O_z$	names of the electrodes located in the occipital region of the scalp
$T_3, T_4, T_5, T_6$	names of the electrodes located in the temporal region of the scalp
$f_1, f_2, f_3$	temporal features of the lambda wave
$\alpha$	viewing angle
$F$	set of BS_ICA-extracted component waveforms
$v$	cluster prototype (mean) in fuzzy c-means clustering algorithm
$\xi$	iteration number in fuzzy c-means clustering algorithm
$\mu_{ik}$	membership value of a waveform $k$ to a class $i$
$d_{ik}$	distance between a pattern $k$ and the $i$ th cluster center
$\Psi$	matrix of degree of membership values
$\delta$	fuzzification factor
$\%C$	percentage of waveforms classified to a category
$\tau$	iteration termination tolerance in fuzzy c-means clustering algorithm

# List of Figures

**Fig.1.1** A typical lambda wave together with its saccadic EOG waveform.

**Fig.2.1** The signal source separation (SSS) principle.

**Fig.2.2** Block diagram of the operation of NLPKA when applied to 2 sources;  $O_x(\cdot)$  is the whitening process of the mixtures.

**Fig.2.3** The information theoretic principle

**Fig.2.4** Optimal information flow in sigmoidal neurons [1.9]

**Fig.2.5** A diagram to illustrate the operation of BS\_ICA.

**Fig.2.6** A diagram to illustrate the operation of JADE: inverting  $A$  by chaining a whitener and a unitary matrix.

**Fig.3.1** Spike-shaped EOG waveform caused by blinks.

**Fig.3.2** Square-like waveforms caused by saccadic eye movements.

**Fig.4.1** The international 10-20 system of electrode placement: (a) top view and (b) side view of the head with the alpha-numeric designation of electrodes placement on the scalp for the EEG recordings.

**Fig.4.2** The Electrical Geodesics Inc. (EGI) system.

**Fig.4.3** The Electrical Geodesics sensor network (GSN) of 64 electrodes.

**Fig.4.4** Subject wearing the 64-channel GSN.

**Fig.4.5** A representation of the checkerboard showing the directions of saccade and the viewing angle.

**Fig.4.6** Composition of the recorded trials.

**Fig.5.1** Typical distributions of transformed EEG waveforms (the horizontal axis is amplitude in  $\mu V^2$  and the vertical axis is frequency of occurrence for an amplitude range).

**Fig.5.2** Typical plots of original EEG (a), EOG (b), contaminated EEG (c), contaminated EOG (d), recovered EEG waveforms using JADE (e), extended ICA (f), EOG subtraction (g) and PCA (h). The vertical axis is amplitude in  $\mu V^2$  and horizontal axis is time in seconds.

**Fig.5.3** Plots of standard deviation ratio (STDR) (a-d), correlation coefficient (e-h) and Euclidean distance (i-l) parameters for JADE, extended-ICA, EOG subtraction and PCA algorithms. The horizontal axis is trial number for all plots.

**Fig.5.4** Plots to demonstrate the effect of noise on the performances of extended-ICA (-■-), JADE (-◆-), PCA (-×-) and EOG subtraction (-▲-). The horizontal axis is signal to noise ratio (SNR).

**Fig.6.1** Flowchart of the iterative time-synchronisation operation.

**Fig.6.2** Scaled eye-movement EOG waveform and its first derivative.

**Fig.6.3** Spatial averaging operation: (a) the Electrical Geodesics sensor network of 64 electrodes and (b) the International 10-20 system of electrode placement with the alphanumeric designation of electrodes placement on the scalp for the EEG.

**Fig.6.4** Averaged EEG waveform with lambda wave features: (a) not-abutted, (b) abutted for 3 trials. Vertical arrow indicates the average stimulus onset.

**Fig.6.5** Averaged eye-movement EOG waveform: (a) not-abutted, (b) abutted for 3 trials. Vertical arrow indicates the average stimulus onset.

**Fig.6.6** Block diagram of the main data processing operations and analysis procedures.

**Fig.6.7** (a) The averaged eye-movement EOG waveform before synchronisation, (b) the saccade offsets distribution. (c) the averaged eye-movement EOG waveform after synchronisation, (d) the saccade offsets distribution.

**Fig.6.8** The lambda wave (top) and eye-movement EOG waveform (bottom) obtained by (a) averaging without time-synchronisation, (b) averaging with time-synchronisation. The vertical arrow indicates the average stimulus onset.

**Fig.6.9** The 22 averaged waveforms displayed (a) in a clinical format and (b) with their amplitude range and time-course information. In (b), the vertical axis is in microvolts and the horizontal axis is in second.

**Fig.6.10** (a) Correlation coefficient values and (b) Euclidean distance values, between the original and recovered EEG waveforms.

**Fig.6.11** (a) Mean correlation coefficient values and (b) mean Euclidean distance values, (across the four mixing ratios), between the original and recovered EOG waveforms.

**Fig.6.12** The extracted EOG<sub>L</sub> waveform.

**Fig.6.13** The extracted EOG<sub>R</sub> waveform.

**Fig.6.14** The pre-saccadic potential extracted in the frontal area.

**Fig.6.15** The lambda wave component.

**Fig.6.16** The pre-saccadic potential extracted in the occipital area.

**Fig.6.17** BS\_ICA-extracted lambda waves (top row) and eye-movements (bottom row) together with their respective scalp distributions for ((a), (b)) the not-abutted and ((c), (d)) the abutted approaches. The vertical arrow indicates the average stimulus onset.

**Fig.7.1** A model of the lambda wave represented by three straight lines.

**Fig.7.2** The model-based BS\_ICA operation.

**Fig.7.3** Two Lambda wave components extracted by BS\_ICA (top and middle) with their respective scalp distributions (side) and the corresponding extracted EOG component (bottom) for (a) BS\_ICA without model, (b) model-based BS\_ICA. The vertical arrow indicates the average stimulus onset.

**Fig.7.4** (a) The training results when no SF was incorporated into the model cost function. (b)-(h) The effect of gradually increasing the contribution of the SF to the model cost function by increasing the value of constant ratio  $C_1/C_2$ .

**Fig.7.5** Effect of the feedback-error on the dropping effect caused by overtraining. (a) and (c) Training results for model without smoothing factor. (b) and (d) Same information when the smoothing factor is incorporated into the model.

**Fig.7.6** (a) The training results for a value of  $C_1$  ( $C_1=54$ ) when the model does not work. (b) The same training results for the same value of  $C_1$  ( $C_1=54$ ) when the error-feedback was incorporated into the model cost function.

**Fig.8.1** (a) The BS\_ICA-extracted lambda wave. (b) The corresponding EOG component. The vertical arrow indicates the averaged stimulus.

**Fig.8.2** Subject 1: Typical NLPCA extracted lambda waves with their scalp distributions (top three rows) and the corresponding extracted EOG waveforms with their scalp distributions (bottom row).

**Fig.8.3** Subject 2: The NLPCA extracted lambda waves with their scalp distributions (top three rows) and the corresponding extracted EOG waveforms with their scalp distributions (bottom row).

**Fig.8.4** Subject 3: The NLPCA extracted lambda waves with their scalp distributions (top three rows) and the corresponding extracted EOG waveforms with their scalp distributions (bottom row).

**Fig.8.5** Subject 4: The NLPCA extracted lambda waves with their scalp distributions (top three rows) and the corresponding extracted EOG waveforms with their scalp distributions (bottom row).

**Fig.9.1** (a) Binary clustering membership functions and (b) Fuzzy logic clustering membership functions.

**Fig.9.2** Operations involved for fuzzy C-means clustering.

**Fig.9.3** Plot of the features of BS\_ICA-extracted single-trial components identified as either the lambda waves (o) or non-lambda waves (+). (a) and (b) represent the gradients ( $m_1$ ,  $m_2$  and  $m_3$ ) features, (c) and (d) the scalp topography feature ( $S$ ).

**Fig.10.1** Results of the single-trial BS\_ICA-extracted lambda waves classification for the fuzzy c-means clustering approach.

# List of Tables

**Table 2.1** A review on the work reported on signal source separation (SSS) since 1986. **Part A** and **B** described general purpose methods, **Part C** deals the non-linear mixing, **Part D** deals with the non-stationary condition, **Part E** deals with unequal number of mixtures and sources.

**Table 5.1** A review of reported work on ocular artefact removal over the past 20 years.

**Table 5.2** Means and variances for the three parameters over 32 trials.

**Table 5.3** Tukey's test (at level of significance 0.05) for pair-wise differences between algorithms.

**Table 5.4** Performance evaluation results when the mixing matrix  $A = \begin{bmatrix} 0.5 & 0.2 \\ 0.3 & 0.5 \end{bmatrix}$ .

**Table 5.5** Results obtained when the algorithms were applied to four transformed EEG sources.

**Table 6.1** The mixing coefficients used to generate the EEG mixtures

**Table 6.2** Mean and standard deviation (std) values (across the four mixing ratios) for  $\rho$  and  $\varepsilon$  (in  $\mu\text{V}$ ) for different lengths of waveforms.

**Table 6.3** Summary of the analysis results for the temporal features of the lambda wave when assessing four methods to recover the lambda wave component.

**Table 6.4** Summary of the analysis results for the scalp distribution and amplitude range features when assessing four methods to recover the lambda wave component (std = standard deviation).

**Table 7.1** The mixing ratios.

**Table 7.2** Correlation coefficient ( $\rho$ ) and Euclidean distance ( $\varepsilon$ ) values for the two BS\_ICA approaches for (a) the EEG waveform and (b) the EOG waveform.

**Table 7.3** Mean and standard deviation (Std) values of  $\rho$  and  $\varepsilon$  (in  $\mu\text{V}$ ) for the data shown in Table 2, for (a) EEG and (b) the EOG waveforms.

**Table 7.4** Correlation coefficients ( $\rho$ ) and Euclidean distance ( $\varepsilon$  in  $\mu\text{V}$ ) for the approaches. The total power of each signal within the mixtures were less than its power before mixing.

**Table 7.5** Summary of the analysis results for the temporal features of the lambda wave when assessing the two BS\_ICA-based approaches to recover the lambda wave component.

**Table 7.6** Summary of the analysis results for the scalp distribution and amplitude range features when assessing the two ICA-based approaches to recover the lambda wave component (std = standard deviation).

**Table 8.1** Summary of the analysis results for four temporal features of the lambda wave across the 7 subjects, when assessing the NLPCA approach to recover the lambda wave component.

**Table 9.1** Performance results of the fuzzy c-means clustering algorithm, with fuzzification factor ( $\delta$ ) = 2 and number of iteration ( $\xi$ ) = 10.

# List of Publications

1. Vigon, L., Saatchi, R., Mayhew, J.E.W. and Fernandes, R.: 'Quantitative evaluation of techniques for ocular artifact filtering of EEG waveforms', *IEE Proceedings - Science, Measurement and Technology*, 2000, **147** (5), pp.219-228.
2. Vigon, L., Saatchi, R., Mayhew, J.E.W., Taroyan, N.A., Frisby, J.P., Johnston, D. and Pascalis, O.: 'Independent Component Analysis of Saccade Related Electroencephalogram Waveforms', *Electronics letters*, 2000, **36** (12), pp.1006-1007.
3. Taroyan, N.A., Vigon, L., Saatchi, R., Mayhew, J.E.W. and Frisby, J.P.: 'Extracting the Lambda Wave Using Model-Based Independent Component Analysis', Symposium on Eye Movements and Vision in the Natural World, Amsterdam, September 27-29 2000, pp.123-124.
4. Vigon, L., Saatchi, R., Mayhew, J.E.W., Taroyan, N.A., Frisby, J.P.: 'Signal Source Separation of Saccade-Related Evoked Potentials', *Clinical Neurophysiology Proceedings (formerly Electroencephalography and Clinical Neurophysiology)*, **112** (6) (June 2001 issue), The British Society for Clinical Neurophysiology meeting, London, 20 October 2000, pp.1117-1118.
5. Vigon, L., Saatchi, R.: 'Adaptive non-linear principal component analysis for the extraction of a saccade related EEG component called the lambda wave', *IEE Conference Proceedings on Intelligent Sensor Processing*, Birmingham, 14 February 2001, pp.19/1-19/6.
6. Vigon, L., Saatchi, R., Mayhew, J.E.W., Taroyan, N.A., Frisby, J.P.: 'The Effect of Signal Length on the Performance Of Independent Component Analysis For Extracting the Lambda Wave', *Medical, Biological Engineering & Computing (MBEC)*, 2002, **40**, pp.260-268.
7. Vigon, L., Saatchi, R., Mayhew, J.E.W., Taroyan, N.A., Frisby, J.P., Buckley, D.: 'Model-Based Independent Component Analysis for Extracting the Lambda Wave from the EEG', *IEE Proceedings - Vision, Image and Signal Processing*, 2001 (submitted).
8. R. Saatchi, L. Vigon, "Fuzzy Clustering Identification of ICA-Extracted Single-Trial Lambda Waves", *IEE Proceedings - Science, Measurement and Technology*, 2002 (submitted).

# Contents

Acknowledgements.....	i
Declaration.....	ii
Abstract.....	iii
Nomenclature.....	iv
List of Figures.....	ix
List of Tables.....	xiv
List of Publications.....	xvi
Contents.....	xvii
<b>Chapter 1. Introduction</b>	<b>1</b>
1.1 Chapter Summary.....	1
1.2 Background of the study.....	1
1.3 Aims and objectives of the study.....	5
1.4 Original contribution.....	8
1.5 Organisation of thesis.....	9
<b>Chapter 2. Signal Source Separation Principles</b>	<b>12</b>
2.1 Chapter summary.....	12
2.2 The objectives of signal source separation.....	12
2.3 A review of the most relevant SSS techniques.....	14
2.4 A brief review of the principal component analysis (PCA) .....	21
2.5 A brief overview of the non-linear PCA (NLPCA) approach.....	22
2.6 Independent component analysis of Bell and Sejnowski (BS_ICA).....	24
2.6.1 Assumptions and general principle.....	24
2.6.2 The information theoretic principle.....	25
2.6.3 A neural network implementation of BS_ICA.....	28
2.6.3.1 Principle of maximum entropy preservation (infomax).....	29
2.6.3.2 The BS_ICA learning rule.....	29
2.6.4 Mathematical analysis and derivation of the BS_ICA learning rule.....	31
2.6.5 The extended version of the BS_ICA learning rule.....	39
2.6.6 Mode of operation of BS_ICA.....	40

2.7 ICA using the joint diagonalisation of Eigen matrices (JADE).....	41
2.7.1 Definition and assumptions.....	41
2.7.2 JADE principle and mathematical analysis.....	42
2.7.2.1 Concept.....	42
2.7.2.2 Whitening.....	43
2.7.2.3 Simplification of the SSS problem.....	45
2.7.2.4 Determining the unitary matrix through joint-diagonalisation.....	45
2.7.2.5 Summary of the main steps of the JADE algorithm.....	47
2.8 Conclusion.....	48
<b>Chapter 3. Description of Signals Included in the Study</b>	<b>49</b>
3.1 Chapter summary.....	49
3.2 Electroencephalogram (EEG).....	50
3.3 Evoked potentials (EPs) and event-related potentials (ERPs) .....	50
3.3.1 EPs/ERPs characteristics.....	50
3.3.2 ERP analysis .....	51
3.3.3 Clinical and other applications of ERPs.....	52
3.4 Electrooculogram (EOG).....	52
3.4.1 EOG characteristics.....	52
3.4.2 EOG filtering.....	54
3.5 Saccade-related evoked potentials.....	54
3.5.1 Types of saccade-related EPs.....	55
3.5.2 Saccade-related EP/ERP model.....	56
3.6 Analysis of the data considered in this study.....	57
3.7 Conclusion.....	58
<b>Chapter 4. Data Recording Experimental Methodology</b>	<b>59</b>
4.1 Chapter summary.....	59
4.2 Data recording system set-up.....	59
4.3 Electrical Geodesic Inc. (EGI) EEG recording system.....	61
4.3.1 The Geodesic sensor net (GSN) .....	61
4.3.2 The Geodesic sensor net interface cable (GSNIC) .....	63
4.3.3 The Net Amps amplifier unit.....	63
4.3.4 The data acquisition computer (DAC) .....	64

4.3.5	The Net Station software.....	64
4.4	Data recording procedure.....	65
4.4.1	First set of experimental data: EOG filtering from the EEG waveforms.....	65
4.4.2	Second set of experimental data: saccade-related EEG and EOG waveforms.....	66
4.5	Conclusion.....	68

**Chapter 5. Analysis of Conventional and Signal Source Separation Approaches  
for Removing Ocular Artefact from the EEG 70**

5.1	Chapter summary.....	70
5.2	Introduction.....	70
5.3	A brief overview of the EOG subtraction method.....	77
5.4	Experimental procedures.....	78
5.4.1	Experimental methods.....	78
5.4.2	Source signals and mixtures generation.....	79
5.4.3	Procedures to enable JADE and Extended-ICA deal with the problems of amplitude scaling and channel permutation.....	82
5.4.4	Parameters for evaluating the OA removal methods.....	83
5.4.5	Statistical tests for determining the significance of differences.....	84
5.5	Results and discussion.....	84
5.5.1	Single EEG and EOG data set analysis.....	85
5.5.2	Analysis to determine the effect of mixing matrix.....	89
5.5.3	Effect of additive Gaussian noise.....	90
5.5.4	Multiple EEG channels analysis.....	91
5.6	Key observations of this Part of the the study.....	91
5.7	Conclusion.....	93

**Chapter 6. The Effect of Signal Length on the Performance of Independent  
Component Analysis For Extracting the Lambda Wave 94**

6.1	Chapter summary.....	94
6.2	Introduction.....	94
6.3	Experimental Method.....	95
6.3.1	Pre-processing procedures.....	95
6.3.2	Iterative Time-Synchronisation Operation and its Evaluation .....	95
6.3.3	Averaging process.....	96

6.3.3.1 Spatial Averaging.....	99
6.3.3.2 Temporal Averaging.....	100
6.3.4 Whitening process and Application of BS_ICA.....	100
6.3.5 Backprojection of the separated components.....	101
6.3.6 Analysis procedure.....	101
6.3.7 Summary diagram for the data processing and analysis procedures .....	104
6.4 Results and discussion.....	105
6.4.1 Iterative time-synchronised averaging.....	105
6.4.2 BS_ICA applied to artificial mixtures.....	107
6.4.3 BS_ICA applied to 22 spatially and temporally averaged waveforms.....	110
6.4.3.1 BS_ICA extraction of three saccade-related EPs components.....	110
6.4.3.2 The effect of signal length on the performance of BS_ICA for extracting the lambda wave.....	113
6.5 Conclusion.....	117

**Chapter 7. Model-Based Independent Component Analysis for Extracting the  
Lambda Wave 119**

7.1 Chapter summary.....	119
7.2 Introduction.....	119
7.3 Experimental procedure.....	120
7.3.1 Outline of the procedure for extracting the lambda wave.....	120
7.3.2 Design of the model-based BS_ICA for the lambda wave extraction.....	120
7.3.2.1 Development of a model for the lambda wave.....	121
7.3.2.2 Development of a suitable cost-function.....	123
7.3.2.3 Development of a model tracking algorithm.....	123
7.3.2.4 Integration of the model into the BS_ICA algorithm.....	123
7.4 Analysis procedure.....	125
7.5 Results and discussion.....	126
7.5.1 Simulated signal mixtures.....	126
7.5.2 BS_ICA applied to the 22-averaged waveforms.....	129
7.6 Discussion on the effects of the error feedback.....	132
7.7 Conclusion.....	136

<b>Chapter 8. An Analysis of Adaptive Non-linear PCA for EEG Signal Source Separation and the Extraction of the Lambda Wave</b>	<b>137</b>
8.1 Chapter summary.....	137
8.2 Introduction.....	137
8.3 Experimental procedure.....	138
8.3.1 Data analysis.....	139
8.3.2 Signal source separation using NLPCA.....	139
8.4 Results and discussion.....	139
8.5 Conclusion.....	146
<b>Chapter 9. Fuzzy Clustering Identification of BS_ICA-Extracted Single-Trial Lambda Waves</b>	<b>147</b>
9.1 Chapter summary.....	147
9.2 Introduction.....	147
9.3 Fuzzy C-Means (FCM) Clustering Pattern Recognition Method.....	148
9.4 Experimental method.....	150
9.4.1 Operations for Extracting the Single-Trial Components from EEG Mixtures...	150
9.4.2 Inspection of BS_ICA-Extracted Components.....	151
9.4.3 Lambda Wave Representation by Feature Set.....	151
9.4.4 Classification of the BS_ICA-Extracted Components.....	152
9.5 Results and Discussion .....	153
9.6 Conclusion.....	156
<b>Chapter 10. Summary of overall results, Conclusions and Future Works</b>	<b>157</b>
10.1 Chapter summary.....	157
10.2 Summary of the overall results.....	157
10.3 Thesis conclusion.....	164
10.4 Suggestions for future work.....	167
10.4.1 Non-linear ICA .....	167
10.4.2 A Bayesian-based model approach to ICA .....	168
10.4.3 Final remarks.....	168

References... .....170

Appendix A – Refereed Journal Publications.....189

# Chapter 1. Introduction

## 1.1 Chapter Summary

In this chapter the background of the study is provided. The aims and objectives of the research are stated and an outline of the thesis is included.

## 1.2 Background of the Study

Electroencephalogram (EEG) is a record of the electrical activity of the brain. It contains valuable information about the brain functions and its abnormalities. Evoked potentials (EPs) are voltage deviations in the EEG which are time-locked to the onset of stimuli. They contain information about the neuronal mechanisms involved in sensory functions.

They are caused by external stimuli or cognitive processes triggered by external events. EPs have found numerous applications in clinical neurophysiology and psychiatry. This is because their recording is non-invasive and accurate, and they are consistently shown to be an indicator of brain functions and its abnormalities. For example, visual EPs have proved valuable in improving the understanding of dyslexia and were used as an objective method for early diagnosis of dyslexia [1.1][1.2].

This study was based on a saccade-related visual EP called the lambda wave. Saccades are rapid changes in the orientation of the eyes for realigning the visual axes on objects of interest. Dysfunction in this system may affect various visual functions such as depth perception and reading [1.3]. The lambda wave is believed to be related to visual information processing triggered by the relative movement of features of the visual field across the retina [1.4]. The lambda wave has a number of sub-components. These are generated by the brain when a subject visually follows a target stimulus (such as a red square) appearing at different locations on a black and white checkerboard background. These sub-components are time-locked to the saccade onset (i.e. initiation of the eye-movement) and its offset (i.e. termination of the eye-movement) [1.5]. One of these sub-components has a pronounced positive peak which appears within a 200 ms time window after the saccade offset [1.5]. A typical lambda wave together with its saccadic eye-movement EOG waveform are shown in Fig.1.1.

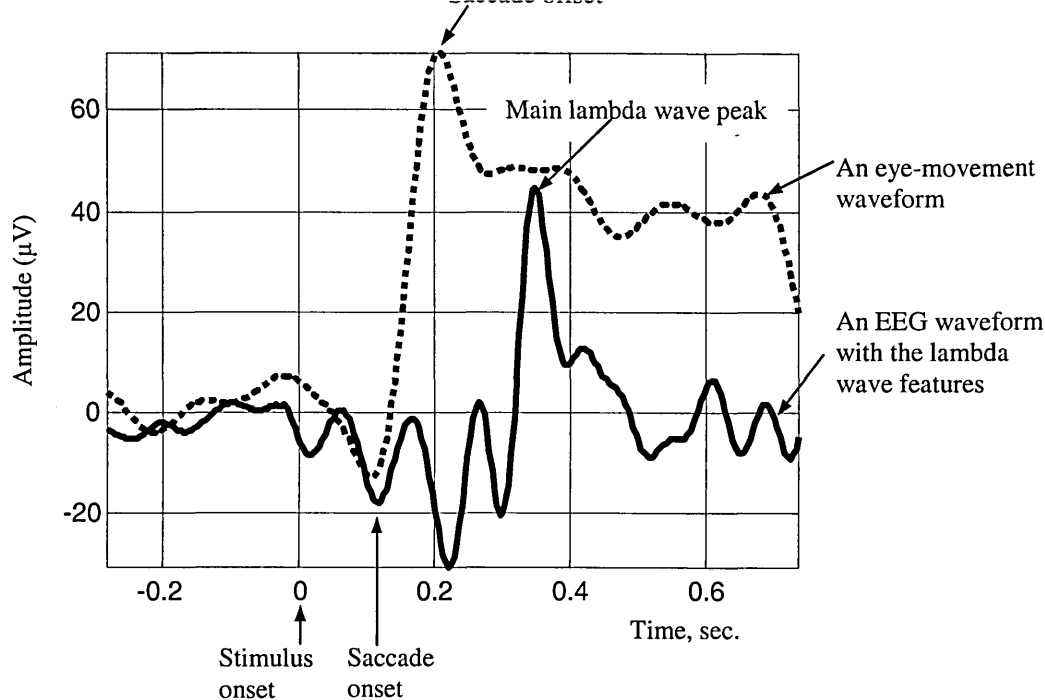


**Fig.1.1** A typical lambda wave together with its saccadic EOG waveform.

It is reported that the lambda wave originates in the parieto-occipital area (back of the head) of the cerebral cortex [1.6]. The study of the saccade-related EPs provides valuable information about how the brain deals with vision when eye-movements are performed [1.7].

Saccade-related EEG waveforms recorded from electrodes placed on the scalp contain a mixture of signals. These are:

- i) Saccade-related EP components (for example the lambda wave).
- ii) Non-saccade-related EEG components, i.e. the background EEG and stimulus time-locked EP components that are not related to the saccade.
- iii) The contaminating electrophysiological signals such as the electrooculogram (EOG). EOG is generated by the eyes when eye-movements or blinks are performed. Other contaminating electrophysiological signals include for example muscle activity (electromyogram, EMG) and the heart beat (electrocardiogram, ECG).
- iv) Non-electrophysiological (external) contaminating signals, for example the noise generated by the recording system and the 50 hertz mains interference.

The conventional method for recovering EPs from the background EEG is based on averaging. Using this method a large number (typically about 50) of EEG waveforms are

recorded and then averaged. Averaging is a valuable pre-processing tool prior to signal source separation as it can improve the signal-to-noise ratio. However, the EP recovered using this method remains a mixture of signal components from a number of different sources.

Therefore, signal source separation techniques that allow the recorded EEG waveforms to be unmixed are valuable for extracting and studying specific EP components such as the lambda wave. A detailed review of signal source separation methods is provided in Chapter 2. Techniques that can be used for this purpose are called independent component analysis (ICA) techniques. The goal of ICA techniques is to recover the independent source signals given only the recorded mixtures. ICA techniques are reviewed in reference [1.8]. Bell and Sejnowski [1.9] proposed a method for implementing ICA that extracts independent components by maximising the joint entropy (i.e. minimising the mutual information) of the separated components. Cardoso [1.10] proposed an approach for implementing ICA which exploits the fourth-order cumulant. The operation of the ICA algorithm of Bell and Sejnowski [1.9] (hereafter referred to as BS\_ICA) is based on a number of assumptions. These are: (i) the mixing process is linear, (ii) not more than one source signal has a Gaussian distribution, (iii) the source signals are stationary and statistically independent. When BS\_ICA is applied to the EEG waveforms, the source signals are considered to be concurrent electromagnetic activities that are temporally independent of each other and that are generated by spatially fixed sources. These signals are mixed as they propagate from their sources to the electrode locations on the scalp.

ERPs are susceptible to contaminations from various electrophysiological signals. The most serious of these (which are picked up by the electrodes on the scalp) is the electrooculogram (EOG). The human eye contains an electric dipole with a positive cornea and negative retina. As a result of eye movements or blinks, the electric dipole changes causing the voltage potential known as EOG. A fraction of the EOG spreads across the scalp and it is superimposed on the EEG, causing it serious contamination. The current method of OA removal is based on correlation-based techniques. A detailed review of some of the most relevant work done in the area of OA removal is provided in Chapter 5. In this study, the performances of two ICA-based approaches, namely the ICA algorithm of Bell and Sejnowski (BS\_ICA) [1.9] and the joint diagonalisation of eigen matrices (hereafter referred

to as JADE) algorithm of Cardoso [1.10], were quantitatively assessed and compared to that of two correlation-based methods for removing EOG based contamination from the EEG.

The features of EPs contained in successive EEG recordings can vary slightly in time, due to cognitive and electrophysiological effects. A novel iterative synchronised averaging method for EPs was devised. The method provided the ability to optimally synchronise the trials with respect to an event of interest prior to averaging, in order to preserve the signals components that are time-locked to the event.

For the EEG to conform to the stationarity requirement of BS\_ICA, the statistical properties of its signal components should be time invariant. However, EEG signal components (such as EPs) are short-duration transient signals and may not fully conform to the stationarity assumption of BS\_ICA. In this study a method was devised to increase the effective length of the EEG traces containing the EPs so as to increase their stationarity pre-requisite. The performance of BS\_ICA for extracting the lambda wave was assessed for different lengths of EEG waveforms.

BS\_ICA was investigated and applied to the recorded saccade-related waveforms. This enabled the extraction of a number of EP components related to the performance and generation of saccadic eye movements, and their scalp topographies to be obtained. These were: the frontal and occipital pre-saccadic potentials, and the lambda wave. This initial study also highlighted some limitations of BS\_ICA for analysing saccade-related EEG waveforms.

The ICA algorithm of Bell and Sejnowski (BS\_ICA) [1.9] does not allow prior knowledge of the source signals to be incorporated as part of its signal separation operation. Prior information, when available can aid the extraction of a component of interest. Therefore it may prove valuable to incorporate such prior information into the algorithm. In this study, a novel template-model that represented the temporal characteristics of a saccade-related EP called the lambda wave was developed. A method for its incorporation into the BS\_ICA algorithm was devised and implemented. The signal source separation ability of this model-based BS\_ICA algorithm for extracting the lambda wave from the EEG waveforms was investigated and its performance was compared to that of the conventional (model-less) BS\_ICA technique.

Nonlinear principal component analysis (NLPCA) is a recursive least-square based signal separation algorithm [1.11]. In this study, NLPCA technique was applied to saccade-related signals and its performance was compared to that of BS\_ICA. The results obtained with NLPCA provided further insight into the functioning of the brain during the performance of a saccadic eye movement.

The application of BS\_ICA to  $n$  recorded EEG waveforms resulted in  $n$  independent signal components. These components were originally visually inspected to identify a specific EP. The task of visual identification of specific EPs (specially when dealing with single-trials) can be time consuming and requires an expert familiar with the characteristic features of the desired component. A fuzzy c-means method that automated the process of identifying the single-trial lambda waves extracted by BS\_ICA from the recorded EEG waveforms was implemented and its effectiveness was investigated.

### **1.3 Aims and Objectives of the Study**

The aim of the study was to develop and apply novel signal processing techniques to improve the estimation, analysis and interpretation of EPs. The objectives are listed below and introduced as highlighted in the original proposal.

#### **1. Recording of saccade-related electroencephalogram (EEG) signal waveforms**

In this study, saccade-related EEG waveforms will be recorded from 7 subjects using an Electrical Geodesics Inc. (EGI) EEG recording machine. A variety of skills will be learnt and mastered in order to conduct a saccade-related experiment successfully. These will include for example practical skills related to utilising the EEG recording equipments (such as applying a network of electrodes on a subject's scalp) and softwares (for example to initialise parameters of the EEG recording machine, display the data on the screen and store the recorded data to the hard-drive for later processing and analysis). Prior to recording the data, an appropriate saccade-related experiment will be designed with the collaboration of clinicians to enable brain activity related to eye-movements to be monitored and studied.

## **2. Investigation of the effectiveness of independent component analysis (ICA) techniques for performing electrooculogram (EOG) filtering of the EEG - Comparison of ICA-based methods with correlation-based methods for EEG ocular artefact (OA) removal**

In this study, the performances of two main signal source separation techniques, namely the independent component analysis algorithm of Bell and Sejnowski (BS\_ICA) [1.9] and the joint approximation diagonalisation of eigen-matrices (JADE) algorithm of Cardoso [1.10] will be quantitatively assessed and compared to that of existing correlation-based methods for removing EOG based contamination from the EEG. The correlation-based methods to be investigated in the study will be principal component analysis (PCA) [1.12] and the EOG subtraction method [1.13]. The effect of additive noise on the performance of the four approaches will also be investigated.

## **3. Investigation of BS\_ICA for extracting saccade-related EEG components**

The Independent component analysis of Bell and Sejnowski (BS\_ICA) will be applied to the recorded saccade-related waveforms so as to enable the extraction of a number of EP components related to the performance and generation of saccadic eye movements, and their scalp topographies will be obtained. The components of interest are: the frontal and occipital pre-saccadic potentials, and the lambda wave.

## **4. Devise techniques to improve the performance of BS\_ICA for extracting the lambda wave – Three approaches.**

Novel procedures will be developed in order to improve the performances of BS\_ICA to extract an EP signal of interest called the lambda-wave. Three approaches will be investigated.

The first approach will consist of devising an iterative synchronisation procedure to optimally time synchronise the waveforms with respect to an event of interest prior to averaging, in order to preserve the signals components that are time-locked to the event. The performances of the iterative time synchronisation process will be quantitatively

evaluated and assessed for preserving the features of EP components in the EEG, prior to input to the BS\_ICA algorithm.

The second approach will consist of devising a method to increase the effective length of the EEG waveforms processed by BS\_ICA in order to enhance their stationarity property and thus to make them more suitable for BS\_ICA signal source separation. The performance of a process which involves abutting EEG waveforms prior to BS\_ICA will be quantitatively assessed when extracting the lambda wave.

The third approach will consist of developing a novel model-based BS\_ICA algorithm to extract the lambda wave from the EEG waveforms. This will include developing a template-model that represents the temporal characteristics of a saccade-related EP called the lambda wave and incorporate it into the BS\_ICA algorithm. The conventional BS\_ICA techniques do not allow prior knowledge of the source signals to be incorporated as part of the algorithm's signal separation operation. Prior information, when available can aid the extraction of a component of interest. Therefore it may prove valuable to incorporate such prior information into the algorithm. The signal source separation ability of the developed model-based BS\_ICA will be investigated and its performance for extracting the lambda wave will be compared to that of a conventional (model-less) BS\_ICA technique.

## **5. Investigate nonlinear principal component analysis (NLPCA) performance for extracting the lambda wave**

Nonlinear principal component analysis (NLPCA) is a recursive least-square based signal separation algorithm signal separation technique. Signal source separation algorithms such as the ICA algorithm of Bell and Sejnowski maximises entropy in order to extract signal components. However NLPCA uses a recursive least square algorithm for tracking signal subspaces in the data. In this study, NLPCA technique will be applied to saccade-related signals and its performance will be compared to that of ICA algorithm of Bell and Sejnowski [1.9].

## 6. Devise a method for automating the identification of BS\_ICA-extracted lambda waves

A fuzzy logic based method will be implemented to automate the process of identifying the single-trial lambda waves extracted by BS\_ICA from the recorded EEG waveforms. The application of BS\_ICA to  $n$  recorded EEG waveforms resulted in  $n$  independent signal components. These components originally were visually inspected to identify a specific EP such as the lambda wave. The task of visual identification of specific EPs (specially when dealing with single-trials) can be time consuming and requires an expert familiar with the characteristic features of the desired component. The performance of a fuzzy c-means clustering pattern recognition approach to perform the identification of the single-trial BS\_ICA-extracted lambda waves will be assessed.

### 1.4 Original Contribution

Novel ICA-based signal processing procedures were developed for the analysis and quantification of techniques employed for the extraction of saccade-related EP components from the recorded EEG waveforms. The original contributions of the study are as follows:

- Development of a procedure that enabled the quantitative assessment of four methods employed to perform OA removal of the EEG. (chapter 5)
- Development of an iterative synchronisation procedure that enabled the features of the saccade-related component signals to be preserved during averaging. (chapter 6)
- Development of an abutted-trial averaging procedure that enabled the stationary properties of the EEG waveforms to be enhanced prior to BS\_ICA application. (chapter 6)
- Using BS\_ICA, the characteristics of the temporal and spatial relationships of three saccade-related EP components were analysed. The EP components were: the frontal and occipital pre-saccadic potentials, and the lambda wave. (chapter 6)

- Development of a novel model-based BS\_ICA approach that enabled a priori knowledge of the EP component of interest called the lambda wave to be incorporated into the BS\_ICA algorithm for improving its performance for extracting the lambda wave. (chapter 7)
- An analysis of saccade-related EEG waveforms using nonlinear PCA technique that provided a new insight into the scalp distribution of the brain mechanisms involved in the generation and performance of saccades. (chapter 8)
- Implementation of a Fuzzy logic based procedure that enabled the automation of the identification of BS\_ICA-extracted single-trial lambda waves. (chapter 9)

## 1.5 Organisation of Thesis

An outline of the organisation of the thesis is provided in this section.

Chapter 1: The background of the study is provided. The aims and objectives of the research are identified and an outline of the thesis is given.

Chapter 2: The theoretical background of the signal processing techniques used in the study is provided. The discussion concentrates mainly on two signal source separation algorithms, namely the ICA algorithm of Bell and Sejnowski [1.9] and the JADE algorithm of Cardoso [1.10]. The methods of PCA [1.12] and NLPCA [1.11] are also explained in this chapter.

Chapter 3: The signals used in the study are described. The discussion concentrates on saccade-related EPs.

Chapter 4: The experimental procedures and methodologies used to record the signal waveforms are described. This includes a description of the data recording system/set-up and the design and implementation of the experiments.

Chapter 5: An analysis of signal source separation approaches for removing ocular artefact from the EEG is provided. The methods were the ICA algorithm of Bell and Sejnowski [1.9], the JADE algorithm of Cardoso [1.10], the PCA data decomposition [1.12] method

and the EOG subtraction method [1.13]. Procedures to quantify the algorithms performances are developed and explained. The results obtained when using each method to remove OA from the EEG are provided.

Chapter 6: Procedures to improve the performances of BS\_ICA to extract an EP signal of interest called the lambda-wave are described. Three approaches are provided.

The first approach is a iterative synchronisation procedure devised to optimally time synchronise the waveforms with respect to an event of interest prior to averaging, in order to preserve the signals components that are time-locked to the event. A detailed description of the algorithm is provided and the results of the effects of the iterative synchronisation process on the averaged waveforms are provided.

The second approach is a method devised to increase the effective length of the EEG waveforms processed by BS\_ICA. The performance of BS\_ICA for extracting the lambda wave is assessed for different lengths of EEG waveforms. The results of applying BS\_ICA to the abutted waveforms and to the not-abutted waveforms are provided. Results for both simulated waveforms and saccade-related waveforms are shown. Plots of the BS\_ICA-extracted lambda wave components waveforms produced by the two approaches (BS\_ICA applied to abutted and not-abutted waveforms) are provided and the results are compared.

Chapter 7: The design of a model-based BS\_ICA algorithm for improving the extraction of a saccade-related ERP component called the lambda wave is provided. The procedures used to develop (i) a model for the lambda wave, (ii) a suitable cost-function for incorporation into the BS\_ICA algorithm and (iii) a model tracking algorithm are described and explained. The results of applying the model-based BS\_ICA algorithm to both simulated waveforms and saccade-related waveforms are shown. The results of comparing the performances of the model-based BS\_ICA algorithm with that of conventional (model-less) BS\_ICA are discussed. Plots of the BS\_ICA-extracted lambda wave components produced by the two approaches (with and without model) are provided and the results are compared.

Chapter 8: The performance of the adaptive NLPCA method for the EEG signal source separation and extraction of the lambda wave is investigated. The methodology and results are discussed. The findings of this investigation are compared with the results obtained

using the ICA algorithm of Bell and Sejnowski [1.9]. Plots of the waveforms produced by the two approaches are provided and the results are compared.

Chapter 9: A method that automates the process of identifying the single-trial lambda waves extracted by BS\_ICA from the recorded saccade-related EEG waveforms is implemented. The performance of a fuzzy c-means clustering based pattern recognition approach is investigated for this purpose and the results obtained are provided.

Chapter 10: A summary of the overall results, a conclusion to the study and future works are provided.

## **Chapter 2. Signal Source Separation (SSS) Principles**

### **2.1 Chapter Summary**

An overview of the signal processing techniques used in the study is included in this chapter. A general introduction to signal source separation (SSS) principles is initially provided. The most relevant SSS studies over the past fifteen years are reviewed. The discussion concentrates mainly on the independent component analysis (ICA) of Bell and Sejnowski [1.9] and the joint approximation diagonalisation of eigen-matrices (JADE) of Cardoso [1.10]. The related methods of principal component analysis (PCA) [1.12] and non-linear principal component analysis (NLPCA) [1.11] are also described.

### **2.2 The Objectives of Signal Source Separation**

Consider for example a situation where there are a number of signals emitted by some physical objects or sources. These sources could be, for instance, different brain areas emitting electric signals, people speaking in the same room, emitting speech signals, or mobile phones emitting their radio waves. Further, assume that there are several sensors or receivers placed at different locations so that each one records a mixture of the original emitted signals with slightly different weights, depending on the distance between the sources and the sensors. When several signals are transmitted down the same medium at the same time, it is often difficult to identify them at the receiving-end (sensor) as they are very likely to have been mixed together during transmission. One must therefore attempt to separate the different signals in the recorded mixtures in order to retrieve the original signals.

Techniques such as matched filters exist and often require prior knowledge of the dynamics of the signals. In cases where both the source signals and the way the signals were mixed are unknown, it is not possible to design appropriate processing to optimally separate them. Therefore methods that can separate signals from mixtures without the need for prior information about the dynamics of the signal sources are valuable. These methods are called Blind source separation (BSS). The goal of BSS (hereafter referred to as SSS for signal source separation) is to recover independent sources given only sensor

observations that are mixtures of the original signals. The technique is said to be ‘blind’ because it assumes no a priori knowledge of:

- 1- the characteristics of the signals that have been mixed,
- 2- the number of original sources in the mixtures,
- 3- the physical properties of the transmitting medium,
- 4- the mixing relation between original sources and observations.

The principle of SSS is illustrated in Fig.2.1.

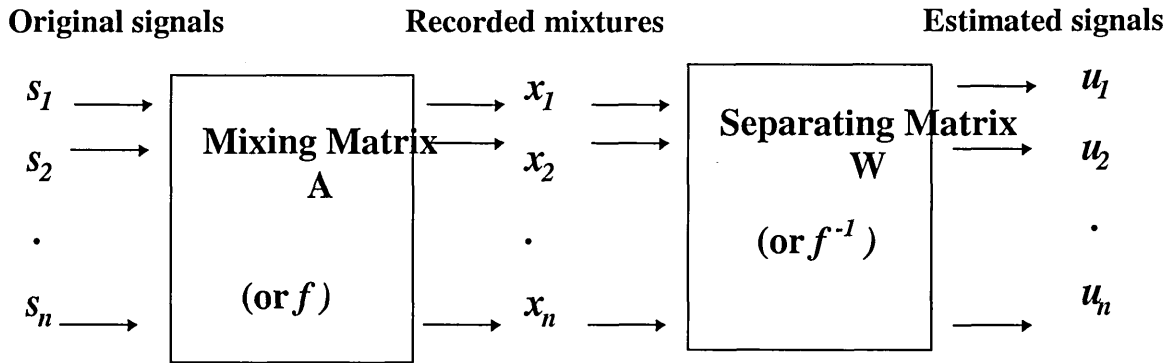


**Fig.2.1** The signal source separation (SSS) principle.

The technique assumes that  $n$  sources transmit certain signals  $s_i$ , which, after transmission through an arbitrary medium, are measured by  $n$  sensors  $x_i$ . Note that for simplicity, the case where the number of sensors is set equal to the number of sources will be used all throughout the thesis. The measured signals will be related to the transmitted signals by some unknown function  $f$ , referred to as the mixing relation. With added measurement noise  $n_i$ , this becomes,

$$x_i = f(s_1, \dots, s_n) + n_i \quad (2.1)$$

The aim is to find a separating matrix  $W \approx A^{-1}$  and thus to estimate the original signals  $u_i$  as shown in Fig.2.1 by the operation:

$$u_i = f^{-1}(x_1, \dots, x_n) \quad (2.2)$$

The estimated signals  $u_i$  are the underlying components that describe the essential structure of the data (recorded mixtures). These components correspond to some physical causes

that were involved in the processes that generated the mixtures. In most cases,  $f$  is considered a linear function because the interpretation of the representation is simpler, and so is its computation. Thus every component  $u_i$  is expressed as a linear combination of the observed variables:

$$u_i = \sum_{j=1}^n w_{ij} x_j \quad (2.3)$$

where  $w_{ij}$  are the coefficients of the separating matrix  $W$  that define the representation. The problem can then be rephrased as the problem of determining the coefficients  $w_{ij}$ . Using linear algebra, the linear transformation in (2.3) can be expressed as a matrix multiplication

$$\begin{pmatrix} u_1 \\ \cdot \\ \cdot \\ u_n \end{pmatrix} = W \begin{pmatrix} x_1 \\ \cdot \\ \cdot \\ x_n \end{pmatrix} \quad (2.4)$$

It can be safely assumed that the mixing coefficients are different enough to make the matrix that they form ( $A$ ) invertible. Thus there exist a matrix  $W$  with coefficients  $w_{ij}$  so that the  $u_i$  can be separated.  $W$  will be determined by the statistical properties of the transformed components  $u_i$ .

### 2.3 A review of the most relevant SSS techniques

This section provides an account of the most relevant work in the area of SSS. Table 2.1 contains some of the main techniques that have been reported recently.

**Table 2.1** A review on the work reported on signal source separation (SSS) since 1986. **Part A** and **B** described general purpose methods, **Part C** deals the non-linear mixing, **Part D** deals with the non-stationary condition, **Part E** deals with unequal number of mixtures and sources.

Part A Method	Comments	Authors associated with the method.
Simple feedback neural network	The seminal work to the problem of blind separation of sources was carried out by Herault and Jutten [2.1][2.2] where they introduced an adaptive algorithm in a simple feedback architecture whose learning rule based on a neural-based approach was able to separate simultaneously several unknown independent sources. Their approach has been further developed by other authors ([2.3] to [2.5]).	[2.1] to [2.5]
Cumulant-based cost functions	Comon[2.6] elaborated the concept of independent component analysis and proposed cumulant-based cost functions related to the approximate minimisation of mutual information between the sensors.	[2.6]
Decorrelation-based method	The notion of factorial code was explored by Attick and uses decorrelation as a strategy for visual processing [2.7]. Principal component analysis (PCA) [1.12] is a popular tool for multivariate data analysis and was used by a number of authors ([2.8] to [2.10]). Both decorrelation techniques were shown to only reduce a large number of variables to fewer components that are independent up to second order statistics of one another and account for the maximal amount of variance in the original data.	[1.12] [2.7] to [2.10]
Unsupervised learning rules based on the principle of redundancy reduction	In parallel to blind separation studies, unsupervised learning rules based on information theory were proposed by Linsker [2.11]. The goal was to maximise the mutual information between the inputs and outputs of a neural network. This approach is related to the principle of redundancy reduction suggested by Barlow [2.12] as a coding strategy in neurons. Each neuron should encode features that are as statistically independent as possible from other neurons over a natural ensemble of inputs. Nardal and Parga [2.13] applied the technique to the low-noise case and showed that the maximum mutual information between inputs and outputs of a neural processor implied that the output distribution was factorial, i.e. the multivariate probability density function (pdf) can be factorised as a product of pdfs.	[2.11] to [2.13]
Stochastic gradient Learning rules	Roth and Baram [2.14] and Bell and Sejnowski [1.9] independently derived stochastic gradient learning rules for the maximisation of the mutual information between the inputs and the outputs of a neural network and applied them, respectively, to forecasting, time series analysis and for the separation of sources. Bell and Sejnowski put the blind source separation problem into an information-theoretic framework and demonstrated the separation and deconvolution of mixed sources. However their adaptive learning rules are only suitable for super-Gaussian (with positive kurtosis) sources and fails to separate sub-Gaussian sources that have negative kurtosis.	[1.9] [2.14]
Joint Approximate Diagonalisation of Eigenmatrices (JADE) algorithm	An adaptive method similar to the cumulant-based cost functions approach introduced by Comon [2.6] was proposed by Cardoso and Laheld [2.15]. This approach is related to the principle of JADE [1.10], originally developed by Cardoso and Souloumiac [2.16], which exploits higher-order statistical independencies through the maximisation of some criteria based on the fourth-order cumulants of the observations (mixtures) and uses joint diagonalisation as a unitary optimiser for performing the maximisation. Contrary to many algorithms, JADE does not operate on the data themselves but on a statistical representation of them. It was successfully applied to the SSS of artificially mixed and numerically simulated audio-signals in the telecommunications domain [2.15].	[1.10] [2.6] [2.15] [2.16]

Table 2.1 Part A (continued)

Method	Comments	Authors associated with the method.
Maximum Likelihood Estimation (MLE)	Other algorithms for performing ICA have been proposed from different viewpoints. First proposed by Gaeta and Lacoume [2.17] and elaborated by Pham <i>et al.</i> [2.18], the maximum likelihood approach for blind separation of sources was shown by a number of authors ([2.19] to [2.21]) to be equivalent to the infomax approach described by Bell and Sejnowski.	[2.17] to [2.21]
Exploratory Projection Pursuit (EPP) network and Multiple output EPP network	Based on information-theoretic indices, this approach uses marginal negentropy (also known as negative entropy), as a projection index and showed that kurtosis seeking projection pursuit will extract one of the underlying sources from a linear mixture [2.22]. By choosing Negentropy as PP index, the learning rule is able to blindly separate out mixed sub-linear and super-Gaussian sources distributions [2.23]. Lee <i>et al.</i> [2.24] showed it to be an extension of the infomax principle satisfying a general stability criterion and preserving the simple architecture of Bell and Sejnowski. A multiple output EPP network was developed by Girolami and Fyfe [2.25], to allow full separation of all the underlying sources.	[2.22] to [2.25]
Nonlinear PCA algorithms	Developed by a large number of authors ([1.11],[2.26] to [2.31]), this approach can also be viewed from the infomax principle since they approximately minimise the sum of squares of the fourth-order marginal cumulants and therefore approximately minimise the mutual information of the network outputs [2.31]. A review of this method and its relation with other methods was carried out by Karhunen <i>et al</i> [2.32].	[1.11] [2.26] to [2.32]
A family of Fixed-point algorithms for ICA	This algorithm uses kurtosis as a contrast function and finds the relevant extrema of such contrast function by the use of a fixed-point iteration scheme [2.34][2.35]. They contain no user-defined parameters, they are very simple to program, they require no pre-whitening of the data, their fast cubic convergence can be proven analytically and in some choices of the non-linearity, they are much more robust against outliers than conventional ICA algorithms. Karhunen <i>et al.</i> [2.37] applied the technique to the blind separation of EEG sources and image feature extraction.	[2.33] to [2.37]
Bussang algorithm	Based on Bussang cost functions, this algorithm was shown to relate to the infomax principle. The connection first elucidated by Lambert [2.38] was confirmed by Lee <i>et al.</i> [2.39].	[2.38] [2.39]
Natural Gradient as an optimiser for infomax	When optimised using the natural gradient of Amari [2.40] or equivalently the relative gradient of Cardoso and Laheld [2.15], the original infomax learning rule for SSS gives superior computational efficiency as this avoids matrix inversion and speed up convergence.	[2.15] [2.40]

Lee *et al.* [2.41] showed how all of these seemingly different approaches can be put into a unifying frame work for the source separation problem based on the information-theoretic approach.

ICA is a relatively new method and generally applicable to several problems in signal processing. Extensive simulations have been performed to demonstrate the power of the learning algorithm and successful results in EEG, fMRI, speech recognition and face recognition systems indicate the power and optimistic hope in the new paradigm.

However, ICA makes a number of assumptions on the physical properties of the signals and mixing process (more details are provided in section 2.6 on assumptions made by the ICA algorithm of Bell and Sejnowski (BS\_ICA)) and the challenge lies in dealing with real world data, where the assumptions made by ICA do not always hold. Therefore researchers have started to deal with a few of the limitations of ICA.

For the applications where the propagation delays are negligible (such as in the case of EEG/ERPs/EPs signals), the instantaneous mixing model may be appropriate. However, in some other environments substantial time-delays may occur and an architecture and algorithm is needed to account for the mixing of time-delayed sources and convolved sources.

**Table 2.1 Part B**

Methods	Comments	Authors associated with the method.
Time-delayed decorrelations	The approach reduces the determination of the mixing coefficients to an Eigenvalue problem which involves simultaneous diagonalisation of matrices whose elements are measurable time-delayed correlation functions [2.42]. This approach allows to separate non-linear mixtures [2.43].	[2.42] [2.43]
Multichannel blind source separation	The problem was addressed using learning rules based on fourth-order cumulants criteria[2.44][2.45]. It was also addressed generalising the notion of SSS/ICA to the notion of multidimensional ICA (MICA) [2.46] and was applied to ECG multichannel decomposition.	[2.44] to [2.46]
Time-delayed and convolved sources approach for infomax.	An extension to time-delays and convolved sources from the infomax viewpoint using a feedback architecture was developed [2.47]. The blind source separation problem was extended to a full feedback system and a full feedforward system[2.48]. The feedforward architecture allows the inversion of non-minimum phase systems. In addition, the rules are extended using polynomial filter matrix algebra in the frequency domain described in [2.38]. The proposed method can successfully separate voices and music recorded in a real environment. It was shown that the recognition rate of an automatic speech recognition system is increased after separating the speech signals [2.49].	[2.47] to [2.49]
Adaptive learning algorithms	A family of adaptive learning rules [2.51] based on natural gradient with equivariant property was derived for both feedforward and recurrent network models [2.50]. Necessary and sufficient conditions for their local stability were proven[2.52]. A new universal algorithm was proposed which provides stability for any distribution of signals [2.53][2.54].	[2.50] to [2.55]

Researchers have very recently started addressing the ICA formulation to nonlinear mixing models. The proposed nonlinear ICA methods can be roughly divided in two classes of approaches.

**Table 2.1 Part C**

Methods	Comments	Authors associated With the method.
Non-linear mixing condition of ICA	<p>The first class of methods uses self-organising-maps (SOM) to extract nonlinear features in the data ([2.56] to [2.59]). Their approach is flexible to some extent and parameter-free, which allows greater freedom of nonlinear representation. However although simple and attractive, these methods are far from being generally applicable. They require a huge number of neurons for good accuracy and are restricted to sources having probability density functions with bounded supports.</p> <p>The second class of methods is a more direct extension of the linear ICA model where nonlinear mixing models are added to the linear model and the task is to find the inverse of the linear model as well as the inverse of the nonlinear model ([2.60] to [2.63]). The nonlinearities are often parameterised allowing limited flexibility. More recently there have also been discussions on using neural networks to separate the nonlinear blind mixtures and a low complexity coding and decoding approaches for nonlinear ICA has been proposed [2.64].</p> <p>The latest advances in the field of nonlinear ICA have involved developing more realistic models through a post-nonlinear mixing (PNL) problem ([2.65] to [2.68]). The PNL mixtures are constituted by a linear instantaneous mixtures followed by an unknown and invertible nonlinear distortion. The learning rule of the PNL algorithm is derived through the information-theoretic principle.</p>	<p>[2.56] to [2.59]</p> <p>[2.60] to [2.64]</p> <p>[2.65] to [2.68]</p>

An extension of current ICA models was investigated in order to deal with the case where the source signals are non-stationary.

**Table 2.1 Part D**

Method	Comments	Authors associated with the method.
Non-Stationarity condition of ICA	<p>An approach was suggested, that specifies a set of second order conditions for non-stationary signals that uniquely determines the parameters <math>A</math> (coefficients of the mixing channels) [2.69]. This idea was used in the case of broad-band signals. No algorithm or results were reported on this approach.</p> <p>An alternative approach to the statistical independence condition was proposed. It exploited the additional second order information provided by non-stationary signals [2.70]. They demonstrated that while it is true that diagonalisation of single cross-correlation (or cross-power spectrum) is not sufficient, additional information is obtained if one considers second order statistic at multiple times. They applied this idea in the instantaneous case of mixtures. A Souloumiac et. al. used the same idea in the equivalent problem of convolutive mixtures of narrow-band signals [2.71].</p> <p>Recently it was proposed a related algorithm that attempts to solve for the frequency components of <math>A</math> by extending prior work of Molgedey and Schuster [2.42] on instantaneous mixtures into the frequency domain [2.72]. However they mistakenly confused this idea with simple decorrelation of multiple taps in the time domain which had been demonstrated by R.L.L. Tong <i>et al.</i> [2.71] to be insufficient.</p> <p>It was suggested a similar multiple decorrelation approach for the time domain ([2.74][2.75]) and for the frequency domain ([2.76][2.77]).</p> <p>More recently Parra and Spence [2.78] and a number of other authors ([2.79] [2.80] [2.81]) exploited the nonstationary properties of the source signals. Parra and Spence uses the idea that the changing cross-correlations at multiple times (multiple decorrelation approach) give a sufficient set of constraints for the unknown variables (source signals) and proposed a least-squares optimisation approach which allows to estimate a forward model (<math>A</math>). In the same manner they found a backward model (<math>W</math>) which generated the separated model source signals. They showed good performance in real room environments and demonstrated the algorithms utility for automatic speech recognition. An investigation of the performance of non-stationarity model for source separation problem is carried out by Cardoso in [2.82]. He reveals how non-stationarity and non-Gaussianity jointly govern the achievable performance, by exploiting variation in the distribution of the signals to achieve separation.</p>	<p>[2.69]</p> <p>[2.70] [2.71]</p> <p>[2.72] [2.73]</p> <p>[2.74] to [2.77]</p> <p>[2.78] to [2.82]</p>

Another issue of research concerns is the case where there is unequal number of sources and mixtures. Limitations such as the under-determined problem, i.e. having less sensors than sources, and noise models in the ICA formulation are subject to current research efforts. The overcomplete ICA problem, i.e. where the number of mixtures (observations) is larger than the number of sources, is of theoretical and practical interest.

**Table 2.1 Part E**

<p>Unequal number of mixtures and sources in ICA</p>	<p>Hyvarinen and Oja ([2.33] [2.37]) have recently developed separating algorithms which estimate one source at a time. However, the sources are extracted in somewhat arbitrary order depending on the initial values etc., though the first few separated components are usually among the most powerful ones. Instead of neural gradient rules which converge somewhat slowly and may not be applicable to high-dimensional problems, Hyvarinen ([2.34] [2.35]) use semi-neural fixed-point algorithms for separating sources.</p>	<p>[2.33] [2.34] [2.35] [2.37]</p>
	<p>Porrill and Stone have modified the ICA algorithm, so that one can specify in advance the number of signals to extract [2.83]. They introduced an undercomplete independent component analysis algorithm [2.83]. They demonstrated that using an undercomplete basis set to extract independent components is useful when the number of signal mixtures <math>m</math> is larger than the number of source signals <math>n</math>. They showed that <math>k &lt; n</math> signals could be extracted using a <math>k \times m</math> rectangular unmixing matrix <math>W</math> by maximising the joint entropy of <math>k</math> whitened, unmixed signals.</p>	<p>[2.83]</p>
	<p>An extension of the method in [2.83] was reported by Porrill and Stone [2.84] and used to for a step-wise extraction of each of <math>n</math> source signals from a set of <math>m &gt; n</math> signal mixtures rather than extracting <math>k &lt; n</math> signals simultaneously. They use a step-wise procedure in which each step consists of extracting <math>k=1</math> source signal, and then subtracting the signal from the signal mixtures.</p>	<p>[2.84]</p>
	<p>S.J.Roberts [2.85] presented a method of independent component analysis which assesses the most probable number of sources sequences from a larger number of observed sequences and estimates the unknown sources sequences and mixing matrix. The estimation of the number of sources is regarded as a model-order estimation problem and is tackled under a Bayesian paradigm.</p>	<p>[2.85]</p>
	<p>Cichoki et. al. ([2.86] [2.87]) proposed various neural network architectures and discussed associated adaptive learning algorithms for handling the cases where the number of sources is not known in advance. These techniques include estimation of the number of sources, redundancy removal among the outputs of the networks, and extraction of the sources one at a time. Other authors have tackled sequential extraction of sources [2.88][2.89].</p>	<p>[2.86] [2.89]</p>
	<p>The latest work carried out in the field of unequal number sources and mixtures is mostly towards solving the overcomplete (underdetermined) problem, i.e. where the number of sources is greater than the number of sensors observations ([2.90] to [2.94]). The case of overdetermined mixtures (more sensors than sources) has nonetheless been considered [2.95].</p>	<p>[2.90] to [2.95]</p>

Part of this review was obtained from the independent component analysis (ICA) book [2.96]. For more details on ICA, the reader may refer to the three recently published books by Lee [2.96], Hyvarinen, Karhunen and Oja [2.97].

## 2.4 A brief review of the Principal Component Analysis (PCA)

Principal component analysis (PCA) [1.12] is a multivariate data analysis procedure that transforms a set of  $n$  correlated variables,  $X = \{x_1, \dots, x_n\}$ , into a set of uncorrelated variables called principal components  $U = \{u_1, u_2, \dots, u_n\}$ . Each variable  $x_i$  and  $u_i$  contains  $N$  time-points. The method is implemented using a technique called singular value decomposition (SVD) [2.98] that finds orthogonal directions of greatest variance in the data set (more details on the principle of SVD are given in the next paragraph). The first principal component accounts for most of the variability in the data while each of the succeeding components in turn account for the highest amount of the remaining variability.

SVD is usually used as a method to principal component analysis of the EEG. SVD may be used to express any  $n \times N$  matrix  $X$  as a product of three matrices by the equations  $X = P\lambda M^T$ , where  $P$  is a  $n \times N$  matrix such that  $P^T P = 1$ ,  $\lambda$  is an  $n \times n$  diagonal matrix, and  $M$  is an  $n \times n$  matrix such that  $M^T M = M M^T = 1$ . If  $X$  is an epoch of EEG data (with  $n$  channels and  $N$  time points),  $P$  will contain the  $n$  normalised (with no amplitude information) principal component waveforms of the EEG, that is  $n$  decorrelated waveforms or features that can be combined to reconstruct the original EEG. Decorrelated means that the correlation between any two waveforms in  $P$  is zero, that is the waveforms are non-correlated in time as well as in their spatial distribution.  $\lambda$  will contain  $n$  ordered eigenvalues (or amplitudes) that apply to the  $n$  normalised principal component waveforms.  $M$  is a matrix that contain the corresponding eigen-vectors or mapping matrix (set of linear weighting factors) that is used to combine the  $n$  component waveforms. Each eigen-value in  $\lambda$  specifies the amount of data variance associated with the direction defined by a corresponding eigen-vector.  $M$  can be displayed as a topographic map or as a histogram;  $M_{ij}$  is the contribution of  $j$ th principal component waveform to the  $i$ th EEG channel. With the definition  $L = P\lambda$  (the  $n$  non-normalised principal component waveforms of the EEG, which can be displayed as multichannel waveforms),  $X$  can be expressed as  $X = LM^T$ . Each principal component is a linear combination of the variables  $X$ . The  $i$ th principal

component  $y_i$  can thus be expressed as,  $y_i = M_i^T X$  where,  $M_i$  is the  $i$ th eigen-vector of the covariance matrix  $R_x$  of  $X$  ( $M_i^T$  is the transpose of  $M_i$ ). Note that the dimension of  $y_i$  is  $1 \times N$ , that of  $M_i^T$  is  $1 \times N$  and that of  $X$  is  $n \times N$ .

The SVD method is based on second order covariance matrix. SVD identifies components by a systematic approach that analyses the variations in all the waveforms in  $X$ . This analysis starts by computing the correlations (or covariance),  $R_x = E[XX^T]$ , of each of the time points with each of the other time points across all waveforms in the data set  $X$ . In SVD the eigen-vectors of the signal covariance matrix gives the directions of greater variance on the input data  $X$ . The structure is computed from these correlations, with the key idea that variables (time-points) that are correlated belong to the same underlying component. SVD finds an orthogonal basis for its given data set  $X$ , and therefore the principal components found by projecting  $X$  onto those perpendicular basis vectors are uncorrelated, and their directions orthogonal.

## 2.5 A brief overview of the Non-linear PCA (NLPCA) Approach

A recursive least square (RLS) algorithm for adaptive tracking of signal subspaces was reported by Yang [2.27]. The algorithm is derived from the cost function,

$$J_2(W) = E[\|X - W W^T X\|^2] \quad (2.5)$$

where  $X = \{x_1, \dots, x_n\}$  is the matrix of signal mixtures,  $n$  is the number of mixtures,  $W$  is an  $n \times n$  weight matrix ( $n$  is the number of sources and is assumed to be equal to the number of mixtures as described in section 2.2, Fig.2.1),  $^T$  represents the transpose and  $E[\cdot]$  the expectation operations. The minimum of the cost function in (2.5) is provided by any orthogonal matrix  $W$  whose columns span the PCA subspace defined by the principal eigen-vectors of the covariance matrix of  $X$ . The method is recursive in the sense that starting from some initial (arbitrary) value for the weight vector, it improves with the increased number of iterations.

Karhunen and Pajunen [1.11] have extended Yang's RLS algorithm so that it can be used for minimising the nonlinear cost function reported in [2.26] given as,

$$J_2(\mathbf{W}) = E[\|X - \mathbf{W}g(\mathbf{W}^T X)\|^2] \quad (2.6)$$

where  $g(\cdot)$  is a non-linear transfer function. This transfer function enables the method to deal with the higher-order (higher than second order) statistics of the data. This means that the method of NLPCA will not only decorrelate the data but will also attempt to deal with higher-order dependencies and can therefore be applied to perform blind source separation.

This resulted in an adaptive learning algorithm described by the following steps.

$$\begin{aligned} y(t) &= g(\mathbf{W}^T(t-1) \mathbf{v}(t)) = g(\mathbf{U}(t)), \\ h(t) &= \mathbf{Q}(t-1)y(t), \\ m(t) &= h(t) / (\beta + y^T(t)h(t)), \\ \mathbf{Q}(t) &= \frac{1}{\beta} \text{Tri}[\mathbf{Q}(t-1) - m(t)h^T(t)], \\ e(t) &= \mathbf{v}(t) - \mathbf{W}(t-1)y(t), \\ \mathbf{W}(t) &= \mathbf{W}(t-1) + e(t) m^T(t). \end{aligned} \quad (2.7)$$

where  $e(t)$  is the training error,  $\mathbf{U}(t)$  is an estimate of the underlying source signals and  $y(t)$  is the output of the nonlinear transfer function  $g(\cdot)$ . The matrix  $\mathbf{v}(t)$  is the input to the algorithm and is produced by whitening the mixtures  $X(t)$ . The whitening matrix is chosen so that the covariance of the whitened vectors  $\mathbf{v}(t)$  expressed as  $E[\mathbf{v}(t) \mathbf{v}(t)^T]$  is equal to the identity matrix,  $\mathbf{I}$ . Prewhitening is performed on the data  $X(t)$  by  $\mathbf{v}(t) = \mathbf{O}_x(t)X(t)$ , in order to help the separation process by decorrelating the data. Decorrelation is a necessary prerequisite of independence. The algorithm is implemented using the RLS scheme described in [2.99] for solving the weight matrix  $\mathbf{W}$  iteratively. The constant  $0 < \beta \leq 1$  is a forgetting term which is normally set close to 1 because the source signals are assumed nonstationary. The use of the weighting factor in general is intended to ensure that data in the distant past are ‘forgotten’ in order to afford the possibility of following the statistical variations of the observable data when the filter operates in a nonstationary environment.  $\mathbf{Q}(t)$  is referred to as the inverse correlation matrix of the input signals weighted by  $\beta$ , and  $\mathbf{Q}(t-1)$  is the ‘old’ value of the correlation matrix.  $\mathbf{Q}(t)$  is a symmetrical matrix where its upper triangular part is computed by operation *Tri* and its transpose is copied to the lower triangular part. In (2.7) variables  $h(t)$  and  $m(t)$  are intermediate variables used for computational purposes when implementing the matrix inversion *lemma* described in [2.99] for computing the least-square solution for the weight matrix  $\mathbf{W}$ .

The algorithm reported in [1.11] may be regarded either as a neural network learning algorithm or adaptive signal processing algorithm. The algorithm is implemented within a two-layer network structure with weight matrices  $O_x$  and  $W$ . A block diagram that illustrates the NLPCA algorithm operation when applied to 2 sources is shown in Fig.2.2.

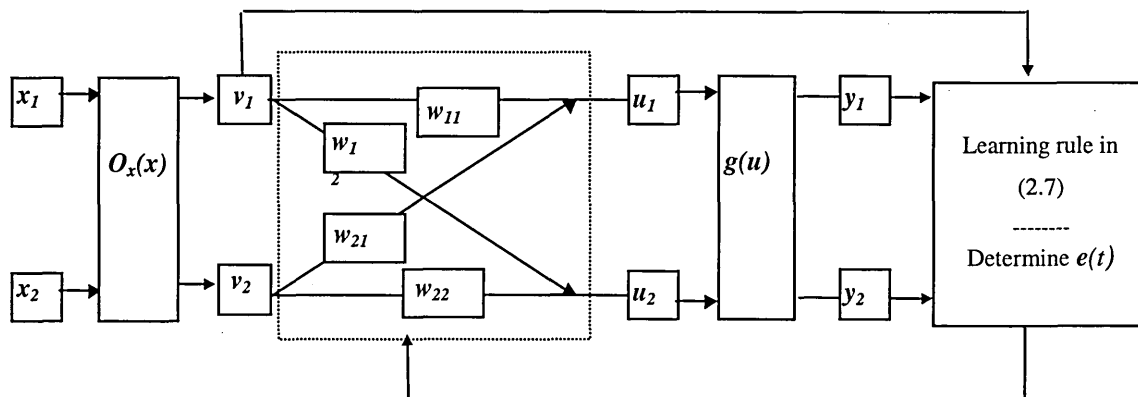


**Fig.2.2** Block diagram of the operation of NLPCA when applied to 2 sources;  $O_x(\cdot)$  is the whitening process of the mixtures.

## 2.6 Independent Component Analysis of Bell and Sejnowski (BS\_ICA)

The independent component analysis of Bell and Sejnowski (BS\_ICA) can be viewed as an extension of PCA that not only decorrelates the data but also reduces higher order dependencies (up to fourth-order moments). BS\_ICA and PCA have two different goals. Indeed whereas the aim of PCA aim is to summarise Gaussian data in as few principal (uncorrelated) components as possible, BS\_ICA on the other hand tries to find as many statistically independent components as possible within non-Gaussian data. This means that the value of any one of the components gives no information on the values of the other components.

### 2.6.1 Assumptions and general principle

BS\_ICA technique is a mathematically rigorous method based on statistical principle used in signal processing to perform blind signal source separation (BSS) of independent components from within linear mixtures of them. The goal of the BS\_ICA technique is to recover the independent sources given only sensor observations that are unknown linear mixtures of the unobserved source signals.

The BS\_ICA technique relies on a number of fundamental assumptions. BS\_ICA assumes that:

- different physical processes tend to generate statistically independent signals,
- the physical processes responsible for mixing the sources are linear,
- the probability distribution function of independent signals has a non-Gaussian (i.e. uniform) distribution whereas the distribution of a mixture of them has a Gaussian distribution,
- the joint distribution of non-Gaussian distribution of the independent sources has maximum Entropy,
- the sources signals are at each instant mutually independent,
- at most one source is normally distributed,
- instantaneous mixing is assumed: in EEG analysis, the propagation of the signals is considered immediate as the electrodes on the scalp are placed close to each other (about a centimetre apart) over the entire surface of the scalp. It takes a short time (typically less than 10 milliseconds) for a signal to propagate across the scalp. Consequently, it is assumed that no significant time-delays are introduced in the mixing and that the mixing transformation is instantaneous. Moreover, as shown in Fig.1.1, the latency of the signal of interest in this study (i.e. the lambda wave) typically lies within a 500 ms time window from the onset of the stimulus. The sampling rate being 250Hz (i.e. 4 ms per time-point), instantaneous mixing is considered appropriate.
- no sensor noise or only low additive noise signals is permitted.

## 2.6.2 The information theoretic principle

The ICA algorithm of Bell and Sejnowski [1.9] (the algorithm used in this study) is based on the information theoretic principle. This principle can be described as follows. Let  $p_x$  be the distribution of any signal in mixtures matrix  $X$ . The mixtures matrix  $X$  is such that  $X = AS$  where  $S$  contains  $n$  independent source signals and  $A$  is a linear mixing of the sources  $S$ . Each source signal in  $S$  has a distribution  $p_s$ . There exists a linear unmixing transformation  $W$  followed by a non-linear transformation  $p(\cdot)$ , such that the resultant distribution,  $Y = p(WX)$ , has maximum entropy and  $p(WX) = p(S)$ . This can be used to recover the original sources  $S$  by defining a plausible distribution (i.e. non-Gaussian), and then finding an unmixing matrix  $W$  that maximises the entropy of  $Y = p(U)$  thus making the

outputs  $U = WX$  as independent as possible. If a set of signals that have a non-Gaussian distribution can be extracted from a set of signal mixtures, then these extracted signals are likely to be the original source signals; those signals are mutually independent and the mutual information (MI) between them is equal to zero. The information theoretic principle is illustrated in Fig.2.3.

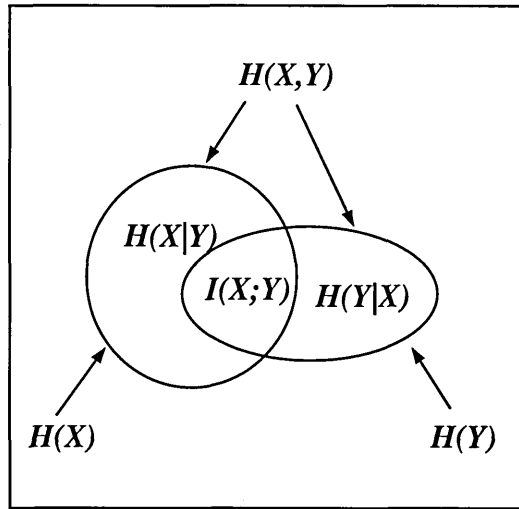


**Fig.2.3** The information theoretic principle

In Fig.2.3,  $I(X;Y)$  is the mutual information between variables  $X$  and  $Y$ , i.e. a measure of the amount of information that a variable  $X$  contains about another variable  $Y$ .  $H(X,Y)$  represents the joint entropy between variables  $X$  and  $Y$ .  $H(X|Y)$  and  $H(Y|X)$  are the conditional entropies between the two variables and  $H(Y)$  and  $H(X)$  are their marginal entropies [2.100].

The entropy  $H(X)$  of a variable  $X = \{x_1, \dots, x_n\}$  with probability distribution  $p(x_i)$  is defined as,

$$H(X) = -\sum_{i=1}^n p(x_i) \ln(p(x_i)) \quad (2.8)$$

$H(X)$  is a measure of variability of the variable  $X$  [2.100].

The joint entropy  $H(X,Y)$  of a pair of variables with a joint distribution  $p(x_i, y_i)$  where  $x_i = \{x_1, x_2, \dots, x_n\}$  and  $y_i = \{y_1, y_2, \dots, y_n\}$ , is defined as,

$$H(X,Y) = -\sum_{i=1}^n p(x_i, y_i) \ln(p(x_i, y_i)) \quad (2.9)$$

which can also be expressed as,

$$H(X, Y) = -E[\ln(p(X, Y))] \quad (2.10)$$

where  $E[\cdot]$  is the expectation operation. The relative entropy is also known as the *Kullback Leibler distance* [2.100] between two probability distributions. Let  $p_1(x_i)$  and  $p_2(x_i)$  be two probability distributions of variable  $x_i = \{x_1, x_2, \dots, x_n\}$ . The *Kullback Leibler distance* is defined as,

$$\begin{aligned} D(p_1(x_i) || p_2(x_i)) &= \sum_{x=1}^n p_1(x_i) \ln \left( \frac{p_1(x_i)}{p_2(x_i)} \right) \\ &= E_p \left[ \ln \left( \frac{p_1(X)}{p_2(X)} \right) \right] \end{aligned} \quad (2.11)$$

Consider the two variables  $X$  and  $Y$  with a joint distribution  $p(x_i, y_i)$ , and probability distributions  $p(x_i)$  and  $p(y_i)$ . It can be shown that the mutual information  $I(X; Y)$  is the relative entropy between the joint distribution  $p(x_i, y_i)$  and the product distribution  $p(x_i)p(y_i)$  [2.100], giving,

$$\begin{aligned} I(X; Y) &= \sum_{i=1}^n p(x_i, y_i) \ln \left( \frac{p(x_i, y_i)}{p(x_i)p(y_i)} \right) \\ &= D(p(x_i, y_i) || p(x_i)p(y_i)) \\ &= E_{p(x_i, y_i)} \left[ \ln \left( \frac{p(X, Y)}{p(X)p(Y)} \right) \right] \end{aligned} \quad (2.12)$$

From (2.12), it can be shown that  $I(X; Y)$  is the reduction of uncertainty of  $X$  due to the knowledge of  $Y$  [2.100].

$$\begin{aligned} I(X; Y) &= \sum_{i=1}^n p(x_i, y_i) \ln \left( \frac{p(x_i, y_i)}{p(x_i)p(y_i)} \right) \\ &= \sum_{i=1}^n p(x_i, y_i) \ln \left( \frac{p(x_i | y_i)}{p(x_i)} \right) \end{aligned}$$

$$\begin{aligned}
&= -\sum_{i=1}^n p(x_i, y_i) \ln(p(x_i)) + \sum_{i=1}^n p(x_i, y_i) \ln(p(x_i | y_i)) \\
&= -\sum_{i=1}^n p(x_i) \ln(p(x_i)) - \left( -\sum_{i=1}^n p(x_i, y_i) \ln(p(x_i | y_i)) \right) \\
&= H(X) - H(X|Y)
\end{aligned} \tag{2.13}$$

According to Fig.2.3,  $I(X,Y)$  is the intersection between the information in  $X$  and the information in  $Y$ , giving,

$$\begin{aligned}
I(X;Y) &= H(X) - H(X|Y) \\
&= H(Y) - H(Y|X)
\end{aligned} \tag{2.14}$$

where  $H(Y|X)$  is whatever information the output  $Y$  has, which did not come from the input  $X$ . Note that in the low-noise case, i.e. where little to no noise is assumed in the generative model of the BS\_ICA algorithm (see BS\_ICA assumptions in section 2.6.1), this  $H(Y|X)$  term can be neglected.

### 2.6.3 A neural network implementation of BS\_ICA

Bell and Sejnowski have proposed an unsupervised neural network algorithm based on the information theoretic principle [1.9].

Artificial neural networks are computer programs that are inspired from the biological learning systems to model the learning function in neurons. A neural network is characterised by three specifications: the architecture, the activation function and the learning rule. The architecture specifies the variables involved in the model and the topological relationship between them, the variables being the weights of the connections between neurons and the activities of the neurons. The activation function specifies the dynamics between the input and output of the network. The learning rule specifies the way in which the neural network's weights changes with time. When the learning process depends solely on the unlabeled data and objective functions, then the learning process is unsupervised. The purpose of unsupervised learning rule is to discover significant pattern or features in the data. During the training, the algorithm adjusts the weights in such a way as to minimise the objective function. Rather than minimising the function, some

unsupervised algorithm learning rules make use of the gradient of the objective function with respect to the weights.

### 2.6.3.1 Principle of maximum entropy preservation (infomax)

Bell and Sejnowski showed that maximising the joint entropy  $H(y_1, \dots, y_n)$  of the output of a neural network processor can approximately minimise the mutual information among the outputs signal components  $Y = g(U)$  [1.9], where  $g(\cdot)$  is an invertible monotonic non-linear transfer function and  $U=WX$ .

The joint entropy of the outputs of a neural network is,

$$H(y_1, \dots, y_n) = H(y_1) + \dots + H(y_n) - I(y_1, \dots, y_n) \quad (2.15)$$

Where  $H(y_i)$  are the marginal entropies of the outputs and  $I(y_1, \dots, y_n)$  is their mutual information. Maximising  $H(y_1, \dots, y_n)$  consists of maximising the marginal entropies and minimising the mutual information. The output  $y_i$  are amplitude-bounded random variables and therefore the marginal entropies are maximum for a uniform distribution of  $y_i$ . Maximising the joint entropy will also decrease  $I(y_1, \dots, y_n)$  since the mutual information is always positive. For  $I(y_1, \dots, y_n) = 0$  the joint entropy is the sum of the marginal entropies.

$$H(y_1, \dots, y_n) = H(y_1) + \dots + H(y_n) \quad (2.16)$$

The maximal value for  $H(y_1, \dots, y_n)$  is achieved when the mutual information among the bounded random variables  $\{y_1, \dots, y_n\}$  is zero and their marginal distribution is uniform.

### 2.6.3.2 The BS\_ICA learning rule

Using the infomax principle described in section 2.6.3.1, the learning rule of the neural network can be derived from equation (2.14), by considering the gradient of information theoretic quantities with respect to some parameter  $W$  in the network as,

$$\frac{\partial I(Y,X)}{\partial W} = \frac{\partial H(Y)}{\partial W} \quad (2.17)$$

The mutual information equation can be therefore differentiated with respect to the learning parameter  $W$  involved in the mapping from  $X$  to  $Y$ . Moreover, Nardal et Parda showed that maximisation of the mutual information  $I(Y;X)$  between the input  $X$  and output  $Y$  of a neural network is equivalent to maximisation of the output entropy  $H(Y)$  as the  $H(Y|X)$  quantity is considered as additive noise which does not vary with respect to  $W$  and can therefore be neglected [2.13]. This is only true in the low-noise case [2.13], as previously described in equation (2.14). The learning rule is derived by maximising output entropy  $H(Y)$  with respect to the weights matrix  $W$  giving,

$$\Delta W \propto \frac{\partial H(Y)}{\partial W} \quad (2.18)$$

This implies that the non-linearity  $g(.)$  has the form of the distribution of the true original signal distribution  $s_i$ . The choice of the non-linear function of the neural network usually depends on the type of transformation required between input and output of the network. Here, the aim is to find an invertible non-linear squashing transformation capable of transforming a highly Gaussian input distribution (of the mixtures) into a nearly-flat uniform output distribution of the extracted independent sources. Independent source signals have marginal distributions with different means. As a result, the joint distribution of a large number of independent source signals will tend to a near-to-flat uniform distribution.

In practice, a logistic transfer function sigmoid, shown in Fig.2.4, is used. It has a non-linear sigmoidal shape which fits the previous requirement.

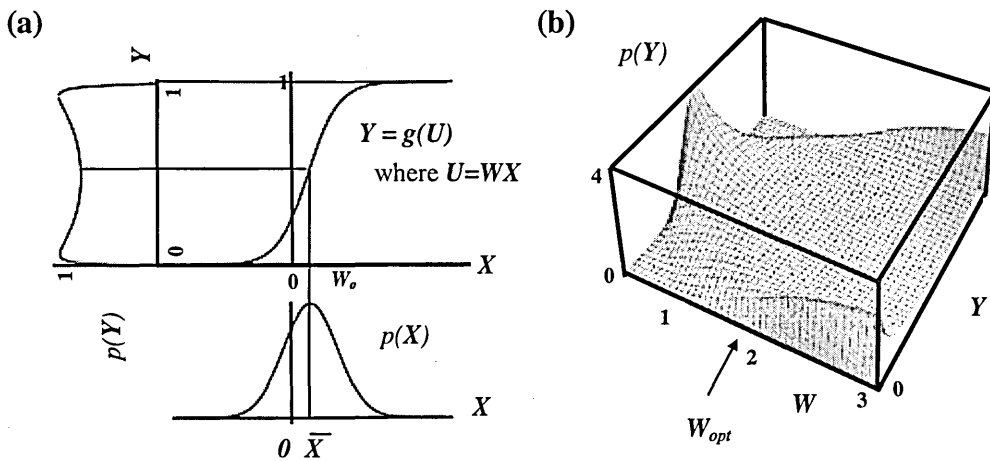


Fig.2.4 Optimal information flow in sigmoidal neurons [1.9]

(a) The Gaussian  $p(X)$  is passed through the sigmoid non-linear function. The information in the resulting density  $p(Y)$  is obtained by matching the mean and variance of  $X$  to the threshold  $W_0$  and slope  $W$  of the sigmoid. This is done by adjusting the weights  $W$  of the neural network.

(b)  $W$  is optimum when  $p(Y)$  has a near-flat shaped distribution. The entropy  $H(Y)$  of the output  $Y$  is maximised when the high density parts of the distribution of  $X$  is aligned with the highly sloping parts of the function sigmoid. This is the idea of matching a neuron's input-output function to the expected distribution of signals.

#### 2.6.4 Mathematical Analysis and derivation of the BS\_ICA learning rule

Suppose the output sensors  $X = \{x_1, \dots, x_n\}$  of  $n$  measurement devices are a linear mixture of  $n$  independent signal sources  $S = \{s_1, \dots, s_n\}$ , such that  $X = AS$ , where  $A$  is an  $n \times n$  matrix. We wish to find an  $n \times n$  unmixing matrix  $W$  such that each of the  $n$  components recovered by  $U = WX$  is one of the original signals  $S$ .

As discussed in section 2.6.2, an unmixing matrix  $W$  can be found by maximising the joint entropy  $H(y_1, \dots, y_n)$  of the output signal  $Y=g(U)$  where  $U = WX$ .

Assume, that the learning activation function is a sigmoid function which is monotonically increasing (i.e. has a unique inverse). The BS\_ICA algorithm may be broken down and summarised in five main steps. They are as follows:

**step 1.** The distribution  $p(Y)$  of the output  $Y$ , can be written as a function of the distribution  $p(X)$  of the input  $X$  in the following manner:

$$p(Y) = \frac{p(X)}{|\partial Y / \partial X|} \quad (2.19)$$

where  $|\cdot|$  denotes absolute function.

The transformation of a given data set  $X$  affects the entropy of the transformed data  $Y$  according to the change in the amount of ‘spread’ introduced by the transformation. Given a multidimensional signal  $X$ , if a cluster of points in  $X$  is mapped to a large region in  $Y$ , then the transformation implicitly maps infinitesimal volumes from one space to another. The ‘volumetric mapping’ between spaces is given by the *Jacobian* of the transformation between spaces. The Jacobian  $J$  combines the derivative of each axis in  $X$  with respect to every axis in  $Y$  to form a ratio of infinitesimal volumes in  $X$  and  $Y$ .

Analogously, the multivariate distribution of  $Y$  can be written as follows, where  $J$  is the determinant of the matrix of partial derivatives:

$$p(Y) = \frac{p(X)}{|J|} \quad \text{where} \quad J = \det \begin{bmatrix} \frac{\partial y_1}{\partial x_1} & \cdots & \frac{\partial y_1}{\partial x_n} \\ \vdots & & \vdots \\ \frac{\partial y_n}{\partial x_1} & \cdots & \frac{\partial y_n}{\partial x_n} \end{bmatrix} \quad (2.20)$$

**step 2.** The general expression of the entropy of signal  $Y$  with distribution  $p(Y)$  can be expressed as,

$$H(Y) = - \int_{-\infty}^{\infty} p(Y) \ln(p(Y)) dY = - E[\ln(p(Y))] \quad (2.21)$$

**step 3.** Substituting equation (2.20) into equation (2.21) gives,

$$\begin{aligned} H(Y) &= - E \left[ \ln \frac{p(X)}{|J|} \right] \\ &= - E [ \ln(p(X)) - \ln(|J|) ] \\ &= - E[\ln(p(X))] + E[\ln(|J|)] \\ &= E[\ln(|J|)] - E[\ln(p(X))] \\ &= E[\ln(|J|)] + H(X) \end{aligned} \quad (2.22)$$

where  $H(X)$  is the entropy of the input  $X$ . Considering that  $H(X)$  is constant and therefore not affected by the changes in  $W$  maximising the entropy  $H(Y)$  with respect to  $W$  needs

only maximising the first term of equation (2.22) which is the average logarithm of how the input affects the output, where  $|J| = \left| \frac{\partial Y}{\partial X} \right|$ .

Estimating that  $E[\ln(|J|)] \approx \ln(|J|)$ , the BS\_ICA learning rule can be derived as,

$$\Delta W \propto \frac{\partial H(Y)}{\partial W} = \frac{\partial}{\partial W} \ln \left| \frac{\partial Y}{\partial X} \right| \quad (2.23)$$

Using mathematical derivation rules [2.98], the right hand-side of equation (2.23) can be calculated as follows,

$$\frac{\partial}{\partial W} \ln |K| = (K)^{-1} \quad (2.24)$$

where  $K = \frac{\partial Y}{\partial X}$  and,

$$\frac{\partial}{\partial W} |K| = \frac{\partial}{\partial W} \left| \frac{\partial Y}{\partial X} \right| \quad (2.25)$$

Thus combining equations (2.25) and (2.24) yields,

$$\frac{\partial}{\partial W} \ln \left| \frac{\partial Y}{\partial X} \right| = \left( \left| \frac{\partial Y}{\partial X} \right| \right)^{-1} \frac{\partial}{\partial W} \left( \frac{\partial Y}{\partial X} \right) \quad (2.26)$$

**step 4.** Setting  $Y$  equal to the sigmoid learning activation function gives,

$$Y = \frac{1}{1 + e^{-D}} \quad (2.27)$$

where  $D = WX + W_o$  and  $W_o$  is the bias weight of the learning rule.

The right hand side of equation (2.26) will be derived to provide the update rule for the weight matrix  $W$  of the neural network. This operation will be carried out in 2 stages (a) and (b).

Stage (a) - The first part of the right hand side of (2.26) can be derived as follow,

$$\frac{\partial Y}{\partial X} = \frac{\partial \left( \frac{1}{1 + e^{-(WX+W_0)}} \right)}{\partial X} \quad (2.28)$$

Using the mathematical derivation rule,

$$\frac{\partial \left( \frac{f(X)}{g(X)} \right)}{\partial X} = \frac{\frac{\partial f(X)}{\partial X} g(X) - \frac{\partial g(X)}{\partial X} f(X)}{g(X)^2} \quad (2.29)$$

yields,

$$\frac{\partial Y}{\partial X} = \frac{\partial \left( \frac{1}{1 + e^{-(WX+W_0)}} \right)}{\partial X} = \frac{W e^{-(WX+W_0)}}{\left(1 + e^{-(WX+W_0)}\right)^2} \quad (2.30)$$

Using equation (2.27), the following equalities can be deduced,

$$Y = \frac{1}{1 + e^{-(WX+W_0)}} \text{ gives } 1 + e^{-(WX+W_0)} = \frac{1}{Y} \text{ gives } e^{-(WX+W_0)} = \frac{1}{Y} - 1 \quad (2.31)$$

Substituting equation (2.31) into equation (2.30) gives,

$$\frac{\partial Y}{\partial X} = \frac{W \left( \frac{1}{Y} - 1 \right)}{\frac{1}{Y^2}} \quad (2.32)$$

$$\frac{\partial Y}{\partial X} = W Y (1 - Y) \quad (2.33)$$

Stage (b) - Using equation (2.33), the second part of equation (2.26) can be derived as follow,

$$\frac{\partial}{\partial W} \left( \frac{\partial Y}{\partial X} \right) = \frac{\partial}{\partial W} (WY(I-Y)) \quad (2.34)$$

$$\frac{\partial}{\partial W} \left( \frac{\partial Y}{\partial X} \right) = \frac{\partial}{\partial W} \left( W \left( \frac{I}{I+e^{-(WX+W_0)}} \right) \left( I - \frac{I}{I+e^{-(WX+W_0)}} \right) \right) \quad (2.35)$$

$$\frac{\partial}{\partial W} \left( \frac{\partial Y}{\partial X} \right) = \frac{\partial}{\partial W} \left( W \left( \frac{I}{I+e^{-(WX+W_0)}} \right) - W \left( \frac{I}{I+e^{-(WX+W_0)}} \right) \left( \frac{I}{I+e^{-(WX+W_0)}} \right) \right) \quad (2.36)$$

$$\frac{\partial}{\partial W} \left( \frac{\partial Y}{\partial X} \right) = \frac{\partial}{\partial W} \left( \frac{W}{I+e^{-(WX+W_0)}} - \frac{W}{(I+e^{-(WX+W_0)})^2} \right) \quad (2.37)$$

Deriving equation (2.37) with respect to  $W$  gives,

$$\frac{\partial}{\partial W} \left( \frac{\partial Y}{\partial X} \right) = \frac{(I+e^{-(WX+W_0)}) + WXe^{-(WX+W_0)}}{(I+e^{-(WX+W_0)})^2} - \frac{(I+e^{-(WX+W_0)})^2 + 2WX(I+e^{-(WX+W_0)})(e^{-(WX+W_0)})}{(I+e^{-(WX+W_0)})^4} \quad (2.38)$$

Substituting appropriately equation (2.31) into equation (2.38) yields,

$$\frac{\partial}{\partial W} \left( \frac{\partial Y}{\partial X} \right) = \frac{\frac{I}{Y} + WX \left( \frac{I}{Y} - I \right)}{\left( \frac{I}{Y} \right)^2} - \frac{\left( \frac{I}{Y} \right)^2 + 2WX \left( \frac{I}{Y} \right) \left( \frac{I}{Y} - I \right)}{\left( \frac{I}{Y} \right)^4} \quad (2.39)$$

Multiplying both the numerator and denominator of equation (2.39) by  $Y^2$  yields,

$$\frac{\partial}{\partial W} \left( \frac{\partial Y}{\partial X} \right) = \frac{Y^2}{Y} + Y^2 WX \left( \frac{I}{Y} - I \right) - \frac{Y^4}{Y^2} - 2WXY^4 \left( \frac{I}{Y} \right) \left( \frac{I}{Y} - I \right) \quad (2.40)$$

After simplification, equation (2.40) becomes,

$$\frac{\partial}{\partial W} \left( \frac{\partial Y}{\partial X} \right) = Y + YWX - Y^2WX - Y^2 - 2WXY^4 \left( \frac{1}{Y} \right) \left( \frac{1}{Y} - 1 \right) \quad (2.41)$$

$$\frac{\partial}{\partial W} \left( \frac{\partial Y}{\partial X} \right) = Y + YWX - Y^2WX - Y^2 - 2WXY^2 + 2WXY^3 \quad (2.42)$$

After further simplification and factorisation, (2.42) becomes,

$$\frac{\partial}{\partial W} \left( \frac{\partial Y}{\partial X} \right) = Y(1-Y)(1+WX(1-2Y)) \quad (2.43)$$

Equations (2.43) and (2.33) can be combined to express equation (2.26) as follows,

$$\left( \frac{\partial Y}{\partial X} \right)^{-1} \frac{\partial}{\partial W} \left( \frac{\partial Y}{\partial X} \right) = \frac{Y(1-Y)(1+WX(1-2Y))}{WY(1-Y)} \quad (2.44)$$

$$\left( \frac{\partial Y}{\partial X} \right)^{-1} \frac{\partial}{\partial W} \left( \frac{\partial Y}{\partial X} \right) = \frac{1}{W} + X - 2XY \quad (2.45)$$

The  $\Delta W$  rule which updates the value of the weights matrix  $W$  after each iteration of the neural network training process is given as,

$$\frac{\partial H(Y)}{\partial W} = \left( \frac{\partial Y}{\partial X} \right)^{-1} \frac{\partial}{\partial W} \left( \frac{\partial Y}{\partial X} \right) = [W^T]^{-1} - 2YX^T \quad (2.46)$$

The adaptive learning process can be carried out in small steps by multiplying by a factor value of size  $\eta$  which yields,

$$\frac{\partial H(Y)}{\partial W} = \eta [W^T]^{-1} - 2YX^T \quad (2.47)$$

where  $\eta$  is called the learning rate of the neural network. Additionally, the  $\Delta W$  rule can be multiplied by the  $W^T W$  'natural gradient' of Amari [2.40] to avoid matrix inversion and also to speed up the learning convergence of the neural network yielding,

$$\Delta W \propto \frac{\partial H(Y)}{\partial W} W^T W \quad (2.48)$$

Combining equations (2.47) and (2.48), the following derivation can be carried out,

$$\begin{aligned} \Delta W &= \frac{\partial H(Y)}{\partial W} W^T W = \left( (W^T)^{-1} + (I - 2Y) X^T \right) W^T W \\ &= W + X^T W^T W - 2Y X^T W^T W \\ &= W + U^T W - 2Y U^T W \\ &= [I + (I - 2Y) U^T] W \end{aligned} \quad (2.49)$$

where  $U^T = X^T W^T$ .

The BS\_ICA learning rule can therefore be expressed as,

$$\Delta W \propto \frac{\partial H(Y)}{\partial W} W^T W = \eta [I + (I - 2Y) U^T] W \quad (2.50)$$

**step 5.** A similar operation as in step 4 is carried out in order to obtain the update rule for the bias weights matrix  $W_o$  using the following learning rule,

$$\frac{\partial}{\partial W_o} \ln \left| \frac{\partial Y}{\partial X} \right| = \left( \frac{\partial Y}{\partial X} \right)^{-1} \frac{\partial}{\partial W_o} \left( \frac{\partial Y}{\partial X} \right) \quad (2.51)$$

The first part of the right hand side of equation (2.51) does not vary with respect to  $W_o$ ,

therefore this part remains equal to equation (2.33), i.e.  $\frac{\partial Y}{\partial X} = W Y (I - Y)$ .

The second part of the right hand side of (2.51) can be derived with respect to  $W_0$  as follows,

$$\frac{\partial}{\partial W_0} \left( \frac{\partial Y}{\partial X} \right) = \frac{\partial (WY(1-Y))}{\partial W_0} \quad (2.52)$$

$$\frac{\partial}{\partial W_0} \left( \frac{\partial Y}{\partial X} \right) = \frac{\partial}{\partial W_0} \left( \frac{W}{1+e^{-(WX+W_0)}} - \frac{W}{(1+e^{-(WX+W_0)})^2} \right) \quad (2.53)$$

$$\frac{\partial}{\partial W_0} \left( \frac{\partial Y}{\partial X} \right) = \frac{We^{-(WX+W_0)}}{(1+e^{-(WX+W_0)})^2} - \frac{2W(1+e^{-(WX+W_0)})(e^{-(WX+W_0)})}{(1+e^{-(WX+W_0)})^4} \quad (2.54)$$

Substituting appropriately equation (2.31) into equation (2.54) yields,

$$\frac{\partial}{\partial W_0} \left( \frac{\partial Y}{\partial X} \right) = \frac{W \left( \frac{1}{Y} - 1 \right)}{\left( \frac{1}{Y} \right)^2} - \frac{2W \left( \frac{1}{Y} \right) \left( \frac{1}{Y} - 1 \right)}{\left( \frac{1}{Y} \right)^4} \quad (2.55)$$

$$\frac{\partial}{\partial W_0} \left( \frac{\partial Y}{\partial X} \right) = \frac{Y^2 W}{Y} - WY^2 - \frac{2WY^4}{Y^2} + \frac{2WY^4}{Y} \quad (2.56)$$

After simplification, equation (2.56) becomes,

$$\frac{\partial}{\partial W_0} \left( \frac{\partial Y}{\partial X} \right) = WX(1-Y-2Y+2Y^3) \quad (2.57)$$

$$\frac{\partial}{\partial W_0} \left( \frac{\partial Y}{\partial X} \right) = WX(1-Y)(1-2Y) \quad (2.58)$$

Combining equations (2.58) and (2.33), the following ratio can be expressed,

$$\left(\frac{\partial Y}{\partial X}\right)^{-1} \frac{\partial}{\partial W_o} \left(\frac{\partial Y}{\partial X}\right) = \frac{WX(I-Y)(I-2Y)}{WY(I-Y)} \quad (2.59)$$

Simplification of equation (2.59) yields the learning rule,

$$\Delta W_o \propto \frac{\partial H(Y)}{\partial W_o} = \left(\frac{\partial Y}{\partial X}\right)^{-1} \frac{\partial}{\partial W_o} \left(\frac{\partial Y}{\partial X}\right) = I - 2Y \quad (2.60)$$

Taking small steps of size  $\eta$  yields,

$$\Delta W_o \propto \frac{\partial H(Y)}{\partial W_o} = \eta(I - 2Y) \quad (2.61)$$

As can be shown on Fig.2.4, the effect of these two balanced learning rules is to produce an output distribution  $p(Y)$  that is close to the near-flat distribution.

- the  $\Delta W_o$  rule centres the steepest part of the sigmoid curve to the peak of the distribution  $p(X)$ , matching input density to output slope using equation (2.61).
- the  $\Delta W$  rule then scales the slope of the sigmoid curve to match the variance of the distribution  $p(X)$  using equation (2.50).

### 2.6.5 The extended version of the BS\_ICA learning rule

The ICA algorithm of Bell and Sejnowski [1.9] which uses a sigmoidal activation function is specifically suited to separate signals with super-Gaussian distribution (i.e. positive kurtosis). Lee and Sejnowski [2.24] proposed an extension of the infomax algorithm proposed by Bell and Sejnowski that is able to separate signals with sub- as well as super-Gaussian distributions. This preserves the architecture of Bell and Sejnowski ICA algorithm but it uses a learning rule derived by Girolami and Fyfe [2.23]. It determines the sign changes (positive to negative and vice versus) required by the algorithm to handle both sub- and super-Gaussian distributions. This is achieved by considering the normalised fourth-order kurtosis ( $K_4$ ) of the estimated signal sources. In extended ICA, the amount of change ( $\Delta W$ ) required to update the unmixing weight matrix  $W$  is given by,

$$\Delta W \propto \frac{\partial H(Y)}{\partial W} W^T W = [I - \text{sign}(K_4)(1-2Y)U^T - UU^T] W \quad (2.62)$$

where  $W^T W$  is the *natural gradient* of Amari *et al.* [2.40] used as an optimiser for speeding up the convergence.

A detailed description of BS\_ICA and its extended version are included in the book by Lee [2.96].

### 2.6.6 Mode of operation of BS\_ICA

The concept of BS\_ICA for a situation involving two signal sources ( $S = \begin{bmatrix} s_1 \\ s_2 \end{bmatrix}$ ) is

illustrated in Fig.2.5 The mixtures ( $X = \begin{bmatrix} x_1 \\ x_2 \end{bmatrix}$ ) are generated by the operation,  $X = AS$ ,

where  $A = \begin{bmatrix} a_{11} & a_{12} \\ a_{21} & a_{22} \end{bmatrix}$  is the mixing matrix.

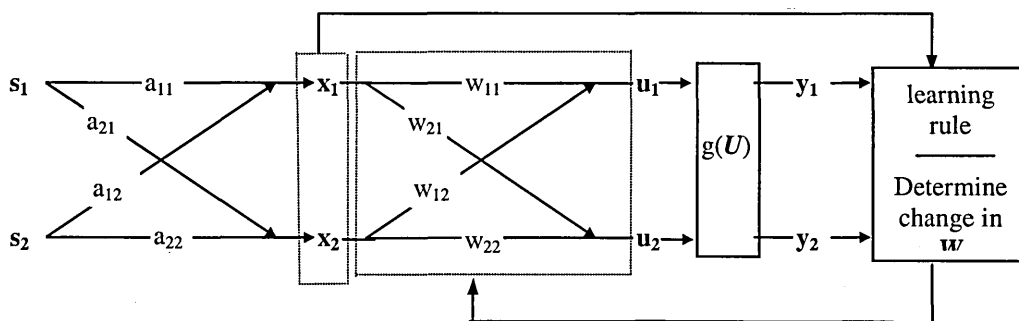


**Fig.2.5** A diagram to illustrate the operation of BS\_ICA.

The aim is to estimate an unmixing matrix  $W = \begin{bmatrix} w_{11} & w_{12} \\ w_{21} & w_{22} \end{bmatrix}$  which in turn enables an

estimate of the signal sources  $U = \begin{bmatrix} u_1 \\ u_2 \end{bmatrix}$  to be obtained by  $U = W X$ .

## 2.7 ICA using the Joint Diagonalisation of Eigen Matrices (JADE)

### 2.7.1 Definition and assumptions

In this signal source separation technique called the Joint Approximation Diagonalisation of eigen-matrices (JADE) algorithm [1.10], the key assumption blind identification relies on is the statistical independence of the sources, which is exploited using a family of fourth-order cumulant-based criteria for blind source separation so as to separate statistically independent signals in a mixture. These criteria involve a set of cumulant matrices, whose joint diagonalisation is equivalent to criterion optimisation.

Contrary to some other ICA algorithms, JADE does not operate on the data themselves but on a statistical representation of them which is a set of fourth-order cumulants  $C_x$  of the array output. For  $X$  a complex  $n$ -dimensional random vector with coordinates  $X=\{x_1, \dots, x_n\}$  and finite fourth-order cumulants, it can be defined a cumulant set denoted  $C_x$  as,

$$C_x = \{ Cum^{(4)}(x_i) \mid 1 \leq i_1 \leq n \} \quad (2.63)$$

The process  $x(t)$  is assumed stationary therefore does not depend on  $t$ ; so  $C_x(t)$  is denoted  $C_x$ . The JADE technique relies on a number of assumptions for its algorithm to hold. They are,

$A_0$  - The source signals and noise are assumed jointly stationary.

$A_1$  - A source is said to be kurtic if it has a non-zero kurtosis. In JADE, the case is restricted where there is at most one non-kurtic source.

The key assumptions that the blind identification relies on are related to independence, and is exploited in this algorithm by assuming non-Gaussian signals. More specifically, it assumes that,

$A_2$  - The vectors  $A = \{a_1, \dots, a_n\}$  of the mixing process are linearly independent but otherwise arbitrary.

$A_3$  - The sources signals  $S = \{s_1(t), \dots, s_n(t)\}$  are statistically independent for each  $t$ .

It is further assumed that,

$A_4$  - There exist consistent estimate of  $C_x$  and  $R_x$  where  $C_x$  and  $R_x$  is the cumulant matrix and the correlation matrix respectively of the mixture signals.

A<sub>5</sub> - The additive noise  $N(t)$  is normally distributed and independent from the sources.

An estimate of the cumulant matrix of the mixtures is then an estimate of  $C_x$  since the cumulants are additive for independent variables and since higher-order cumulants are zero for normally distributed variables.

A<sub>6</sub> - The additive noise is spatially white with unknown variance. Therefore, an estimate of  $R_y$  (i.e. the correlation matrix of the output  $Y(t) = X(t) + N(t)$ ) can be constructed from the eigen decomposition of an estimate of  $R_x$ .

## 2.7.2 JADE principle and mathematical analysis

### 2.7.2.1 Concept

The JADE algorithm transforms the identification problem into a diagonalisation problem. The fourth-order cumulants of the received signals  $X$  (observed mixtures) are exploited to recover the source signals which are assumed statistically independent and non-normally distributed. JADE tests this independent with respect to higher-order statistics by using the cumulants as a criteria. According to the theory of separation described in [1.10], the second-order cross cumulant of two random (Gaussian) signals equals the covariance of the two signals when they are independent, the covariance being equal to zero. Therefore JADE cost function separates prewhitened (decorrelated) sources by optimising the sum of fourth-order cumulants (also called kurtosis) of the signals. The kurtosis of the  $i$ th signals  $x_i$  is defined as,

$$K_4 = Cum^{(4)}(x_i) = E[x_i^4] - 3[E[x_i^2]]^2 \quad (2.64)$$

Due to prewhitening,  $E[x_i^2] = 1$ , and it suffices to consider the sum of fourth-order moments of the signals. Generally, this criterion is minimised for sub-Gaussian sources (for which the kurtosis is negative), and maximised for super-Gaussian sources (having a positive kurtosis value). For Gaussian sources, the kurtosis is zero. It has been reported that the sources are perfectly recovered but subject to a permutation change (i.e. signals are recovered in the incorrect channel) and subject to a scale change (i.e. signals are recovered without the right amplitude information) [2.101]. The scale change of the recovered signals is due to the fact that the measured mixtures are whitened as a pre-processing step to signal source separation (see section 2.7.2.2 for more details on whitening), thus normalising their

variance to unity. It is therefore assumed that the sources are normalised up to the unit variance (i.e.  $E[|s_i(t)|^2] = 1; 1 < i < n$ ) and that the amplitude information of the sources is contained in the corresponding column of the mixing matrix  $A$ . For independent sources, this gives,

$$R_s = E[s(t)s(t)^T] = \text{Cov}(s(t)s(t)^T) = I_n \quad (2.65)$$

Where  $\text{Cov}(\cdot)$  is the covariance operation and  $I_n$  is the identity matrix, so that

$$R_x = AA^H \quad (2.66)$$

where  $R_s$  and  $R_x$  are spatial covariance operator,  $A^\# = (A^H A)^{-1} A^H$  is the pseudo-inverse of  $A$  where  $^H$  stands for Hermitian adjoint or component-wise-conjugate transpose of  $A$  (also  $A^H = \overline{A}^T$ ).

JADE algorithm uses a whitening operation to simplify the BSS problem. Whitening makes use of the previously mentioned second-order information in the form of the estimate of  $R_x$  so as to reduce the determination of the  $n$ -by- $n$  mixing matrix  $A$  to the determination of a unitary  $n$ -by- $n$  matrix  $Z$ . This is only possible because the sources have been normalised to the unit variance so that their amplitude information is accounted for in the mixing matrix  $A$ , yielding  $R_x = AA^H$ .

### 2.7.2.2 Whitening

The whitening process consists of making the observed mixture vector  $X(t)$  spatially white. This means that it is linearly transformed so that the resulting vector has decorrelated components. Furthermore the variance of each component is normalised to unity. Formally, a whitening transform  $\hat{O}_x$  is such that the whitened vector,

$$V = \hat{O}_x X \quad (2.67)$$

has its correlation (covariance) matrix  $R_v = E[VV^T] = I_n$ , where  $I_n$  is the identity matrix.

Using this notation, the estimate of the sources vector becomes,

$$U = Z^T V = Z^T \hat{O}_x X \quad (2.68)$$

where  $Z^T \hat{O}_x$  is the separating matrix or unmixing matrix, and  $X$  the observed mixtures vector.

It can be shown that the separating matrix of the pre-whitened vector  $V$ , i.e. vector with zero mean and unit variance, is orthogonal. Indeed, the correlation matrix of the output vector  $U$  is equal to,

$$R_U = E [Z^T V V^T Z] \quad (2.69)$$

$$R_U = E [Z^T Z] E [V V^T] \quad (2.70)$$

$$R_U = E [Z^T Z] R_v \quad (2.71)$$

since  $R_U = E [V V^T] = I_n$ , this yields,

$$R_U = Z^T Z = I_n \quad (2.72)$$

The last equality means that  $Z$  is orthogonal as a matrix  $Z$  is said to be orthogonal if  $Z^T Z = I_n$ . Therefore when pre-whitening is used, it is sufficient to find an orthogonal matrix  $Z$  (as the sources can be assumed to have unit variance). From there, the whiteness condition (i.e.  $R_v = I_n$ ) can be expressed as follows,

$$I_n = E [(\hat{O}_x X) (\hat{O}_x X)^T] \quad (2.73)$$

$$I_n = E [\hat{O}_x X X^T \hat{O}_x^T] \quad (2.74)$$

$$I_n = E [\hat{O}_x^T \hat{O}_x] E [X X^T] \quad (2.75)$$

$$I_n = \hat{O}_x^T \hat{O}_x R_x \quad (2.76)$$

$$I_n = \hat{O}_x^T \hat{O}_x A A^T \quad (\text{use of second-order information in 2.66}) \quad (2.77)$$

$$I_n = \hat{O}_x A A^T \hat{O}_x^T \quad (2.78)$$

The last equation means that  $\hat{O}_x A$  is a unitary matrix.

### 2.7.2.3 Simplification of the SSS problem

This last equation implies that for any whitening matrix  $\hat{O}_x$ , it then exists a unitary matrix  $Z$  such that  $\hat{O}_x A = Z$ . As a consequence, matrix  $A$  can be factorised as:

$$A = \hat{O}_x^\# Z = \hat{O}_x^\# [Z_1, \dots, Z_n] \quad (2.79)$$

where  $\hat{O}_x^\#$  is the pseudo-inverse of  $\hat{O}_x$ . The use of the second order information, in the form of the estimate of  $R_x$  which is used to solve for  $\hat{O}_x$ , has reduced the determination of the  $n$ -by- $n$  mixing matrix  $A$  to the determination of a  $n$ -by- $n$  unitary matrix  $Z$ .

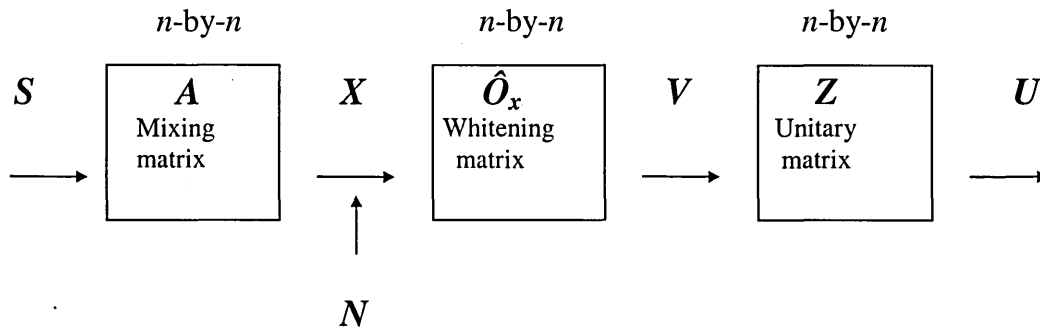


**Fig.2.6** A diagram to illustrate the operation of JADE: inverting  $A$  by chaining a whitener and a unitary matrix.

As shown in Fig.2.6,  $W = \hat{O}_x Z$  is the separating matrix. Discarding the additive noise, the whitened process  $V = \hat{O}_x X$  still obeys the linear model shown in Fig.2.6 according to:

$$V = \hat{O}_x X = \hat{O}_x A S = Z S \quad (2.80)$$

The signal part of the whitened process now is a unitary mixture of the source signals.

### 2.7.2.4 Determining the unitary matrix through joint-diagonalisation

In the case of JADE algorithm, the approach obtains an estimate of  $Z$  as the optimiser of some identification criterion  $C(Z)$  which is a function of the whole cumulant set  $C_x$  previously described.  $C(Z)$  is defined as follows,

$$C(\mathbf{Z}) = \sum_{i=1,n} |Cum^{(4)}(x_i)|^2 \quad (2.81)$$

The main reason for considering this criterion is its link to underlying eigen-structures, which allows for an efficient optimisation of it by the mean of joint-diagonalisation.

The link between optimisation-based and eigen-based blind identification techniques is established by considering the joint diagonalisation of several cumulant matrices. The joint diagonalisation of a set of square matrices consists of finding the orthonormal change of basis which makes the matrices as diagonal as possible. Joint diagonalisation of a set  $\mathbf{B}$  of  $m$  matrices with common size  $n$ -by- $n$  is defined as the unitary diagonaliser of the criterion,

$$C(\mathbf{Z}, \mathbf{B}) = \sum_{r=1,m} |diag(\mathbf{Z}^H \mathbf{B}_r \mathbf{Z})|^2 \quad \text{with } \mathbf{B} = \{ \mathbf{B}_r \mid 1 \leq r \leq m \} \quad (2.82)$$

where  $|diag(\cdot)|$  is the norm of the vector build from the diagonal of the matrix argument. The Jacobi technique [2.102] for diagonalising a unique Hermitian matrix is extended for a joint approximate diagonalisation of a set  $\mathbf{B}$  of arbitrary matrices. It consists in maximising the diagonalisation criterion by successive Givens rotations. When the set  $\mathbf{B}$  contains only one Hermitian matrix ( $\mathbf{B}_i = \mathbf{B}_i^H$ ), joint diagonalisation is equivalent to unitary diagonalisation; this extension offers a computational cost-efficiency which is roughly  $m$  times the cost-efficiency of diagonalising a single matrix. If the set  $\mathbf{B}$  cannot be exactly jointly diagonalised (this is the case when sample cumulants are processed), the unitary maximisation of the above criterion defines a joint approximate diagonalisation. Blind identifiability via joint unitary diagonalisation is possible with assumptions  $A_0$ - $A_3$ .

The fourth-order cumulants can be represented by eigen-matrices. Indeed, the joint diagonalisation computational efficiency can be further increased by downsizing  $\mathbf{B}$  to a smaller set made of the significant eigen-matrices. For any  $n$ -dimensional complex random vector  $\mathbf{x}$  with fourth-order cumulants, there exists  $n^2$  real numbers  $\lambda_1, \dots, \lambda_{n^2}$  and  $n^2$  called eigen-values, where  $\mathbf{M}_1, \dots, \mathbf{M}_{n^2}$  are the eigen-matrices, verifying,

$$C(M_r) = \lambda_r M_r \quad 1 \leq r \leq n^2 \quad (2.83)$$

where  $C(\cdot)$  is the *quadrivariance* associated with any  $n$ -dimensional complex random vector  $\mathbf{x}$  with fourth-order cumulants; it is defined by a linear matrix-to-matrix mapping  $M \rightarrow B = C(M)$ , where  $M$  and  $B$  are  $n$ -by- $n$  matrices with entries  $M_{kl}$  and  $B_{ij}$  related by,

$$B_{ij} = \sum_{k,l=1,n} \text{Cum}^{(4)}(\mathbf{x}_i) M_{kl} \quad 1 \leq i, j \leq n \quad (2.84)$$

The algorithm produces  $n$  eigen-values equal to the kurtosis of the sources. An orthonormal set of eigen-matrices provides an alternate way of representing the set of all possible fourth-order cumulants of a random variable  $n$ -vector  $\mathbf{x}$ . The advantage of this approach lies in the data reduction: the quadrivariance of  $\mathbf{x}$  has exactly rank  $n$  so that only  $n$  out of  $n^2$  eigen-values are non-zero. As a consequence, the whole fourth-order cumulant information is actually contained in a set of  $n$  eigen-pairs ( $\lambda_r M_r \mid r = 1, n$ ) where the convention is taken to number from 1 to  $n$  the eigen-values associated with non-zero eigen-values. The eigen-values are ordered by decreasing order of magnitude and form an eigen-reference of the cumulant matrix which contains the relevant fourth-order information. This reduced set of  $n$  matrices (rather than  $n^2$ ) together with the extended Jacobi technique makes the maximisation of  $C(\mathbf{Z})$  computationally efficient.

### 2.7.2.5 Summary of the main steps of the JADE algorithm

The operation of the JADE algorithm can be summarised through the four main steps outlined below.

- i) The covariance matrix ( $\hat{R}_x$ ) of the mixtures is obtained. The whitening matrix  $\hat{O}_x$  is computed by considering the whitening condition  $I = \hat{O}_x \hat{R}_x \hat{O}_x^H$ . Replacing  $\hat{R}_x$  gives  $I = \hat{O}_x A A^H \hat{O}_x^H$ , where  $I$  is the identity matrix. This implies that  $\hat{O}_x A$  is a unitary matrix ( $Z$ ) and therefore  $A$  can be factorised as  $A = \hat{O}_x^{\#} Z$ .

- ii) The mixtures are then whitened according to  $\hat{V} = \hat{O}_x \hat{X}$ . The operation involves computing the estimate of the covariance matrix ( $\hat{R}_x$ ) of the mixtures ( $X$ ). The whitening matrix ( $\hat{O}_x$ ) is computed by considering the whitening condition  $I = \hat{O}_x \hat{R}_x \hat{O}_x^H$ , where  $\hat{O}_x^H$  is the Hermitian matrix of  $\hat{O}_x$  and  $I$  is the identity matrix. The whitened mixtures ( $\hat{V}$ ) are obtained by  $\hat{V} = \hat{O}_x \hat{X}$ . The whitened mixtures ( $\hat{V}$ ) obey the linear model  $\hat{V} = \hat{O}_x A S$ . Substituting for  $A$  gives  $\hat{V} = \hat{O}_x \hat{O}_x^H Z S = Z S$ .
- iii) In order to determine the unitary matrix  $Z$ , the fourth-order cumulants of the whitened mixtures are computed. Their  $n$  most significant eigen-values ( $\lambda_i$ ) and their corresponding eigen-matrices ( $M_i$ ) are determined. An estimate of the unitary matrix ( $\hat{Z}$ ) is obtained by maximising the criteria  $B = \lambda_i M_i$  by means of joint diagonalisation.
- iv) An estimate of the unmixing matrix ( $\hat{W}$ ) is obtained by  $\hat{W} = \hat{O}_x \hat{Z}$ . This is then used to compute an estimate of the original signal sources  $\hat{U} = \hat{Z} \hat{V}$ .

## 2.8 Conclusion

An overview of the signal source separation (SSS) techniques used in this study has been provided. A second-order statistics methods, namely PCA, is briefly described. The ability of SSS approaches to deal with higher-order dependencies is introduced. The ICA-based signal source separation techniques of the NLPCA algorithm, the ICA algorithm of Bell and Sejnowski and the JADE algorithm of Cardoso are discussed, and their ability to deal with higher-order dependencies of the signals is outlined.

## **Chapter 3. Description of Signals Processed in the Study**

### **3.1 Chapter Summary**

This chapter provides an overview of the signals processed in this study. Firstly, it describes the electroencephalogram (EEG) and electrooculogram (EOG), and the method used to record them. Then, properties and characteristics of evoked potentials (EPs) and event-related potentials (ERPs) are outlined and factors that need to be considered during their recording are discussed. Finally, a description of the type of signals used in this study, namely saccade-related evoked potentials is provided and their clinical interest is highlighted. An analysis methodology to extract the EPs of interest from the EEG mixtures is discussed.

### **3.2 Electroencephalogram (EEG)**

The Electroencephalogram (EEG) is the measurement of the ongoing electrical activity generated by a large number of brain neurons, usually recorded from surface electrodes on the scalp. Specifically, it is a measure of the extracellular current flow associated with the summed activity of many individual neurons [3.1]. Surface recorded potentials reflect predominantly the activity of cortical neurons in the area underlying the EEG electrode. This activity is defined by frequency and amplitude of electrical signals. The study of electrical activity of the brain (EEG) is a tool which gives an insight into the brain and its abnormalities. Because it is noninvasive, the EEG is important in the clinical assessment of cortical function. For example, it provides important indices for studying certain normal behavioural states such as arousal, wakefulness, sleep and dreaming and for diagnosing certain disease states such as epilepsy and coma.

The first reported observation of EEG was made by [3.2]. Berger was the first to observe EEG in human subjects by putting electrodes on the scalp [3.3]. Since then there have been significant advances in both recording and interpretation of EEG waveforms. The EEG is a record of the electrical activity of the brain while the subject is sitting quietly or sleeping. The EEG is also recorded during specific repetitive natural sensory simulation (such as a tap on the skin, presentation of a flash of light or a tone) and thus can be made to be time-

locked to the occurrence of discrete stimuli (events). The stimuli can be visual, auditory or cognitive processes, triggered by external sources to activate sensory receptors. They cause voltage fluctuations within the EEG that are known as sensory evoked potential or event-related potential. These components are described in the next section.

Electroencephalograms are analysed in the temporal, frequency and spatial domains. The frequencies of the potentials recorded from the surface of the scalp of a normal human typically vary from 1-30Hz, and the amplitudes typically range from 20-100 $\mu$ V.

A computer samples the EEG for a brief period before and after the stimulus and the sample data are averaged to enhance the signal-to-noise ratio.

### **3.3 Evoked Potentials (EPs) and Event Related Potentials (ERPs)**

#### **3.3.1 EPs/ERPs characteristics**

Evoked potentials (EPs) are very small voltage deviations (usually in the range of 4 to 30 $\mu$ V) in the EEG generated in the brain structures in response to specific events or stimuli. These stimuli time-locked potentials are selected from the ongoing EEG activity by averaging epochs of EEG following repeated sensory stimuli such as series of clicks (auditory stimuli) or flashes of light (visual stimuli) [3.4]. ERPs and the way they change under various recording conditions are a powerful, non-invasive and relatively simple means of relating psychopathology to underlying physiology, and by comparing ERPs with imaging data, it should be possible to compare electrical activity with changes in brain structure and blood flow in different disease states.

It takes about 20 to 30 ms for information to reach the cortex from a peripheral sense organ, so early-ERPs generated within this time mainly reflect neuronal activity in the sensory organ itself and in the afferent pathways of the brain-stem [3.4]. These early responses are termed 'exogenous' because they are generated regardless of what the subject is thinking, and they are quite independent of any response the subject may subsequently make to the stimulus. They are very useful clinically for detecting disorders of sensory end organs and the brain-stem.

In contrast to these exogenous potentials, ERPs generated after about 70 ms often reflect the manner in which a stimulus is evaluated by the subject. These later components are termed 'cognitive' or 'endogenous' ERPs because their amplitudes and latency may depend on the motivation of the subject and the cognitive, affective or motor response to that particular stimulus. It is therefore valuable to record these late endogenous ERPs in psychiatric patients with conditions such as dementia, depression and schizophrenia (ERPs have been extensively studied in order to improve the understanding of sensory organs and to diagnose a number of brain related disorders including schizophrenia ([3.5] [3.6]), which are associated with disordered attention since ERPs might contribute to diagnosis and provide a method for monitoring cognitive change in response to specific treatments. For example, all three subject groups, Huntington's, Parkinson's and schizophrenia's demented groups, were differentiated with reasonable accuracy on the basis of ERPs (related articles includes [3.5] [3.7]). Various factors such as age and sex are known to affect the characteristics of ERPs. When using ERPs to investigate brain functions/dysfunctions, the subjects/patients participating in the experiment are usually matched with each other in terms of these contributing parameters.

In the category of 'exogenous' processes are the sensory EPs which represent the summated electric fields from the synchronous activation of neuronal populations by an external stimulus event. Because the sensory EPs reflect the processing of the physical characteristics of the stimulus, they are clinically useful for assessing the functions of sensory systems. Sensory EPs, which are by definition, rather not easily influenced by variations of the psychological state of the observer, are distinguished from ERPs which are dependent on the context in which the stimulus is presented such as whether the stimulus is expected or a surprise. These ERPs form the class of 'endogenous' ERPs which are coupled with perceptual, cognitive (include decision making, recognition, memory, concentration, attention, motivation), affective, sensory and motor (it is the cortical activity preceding and accompanying voluntary movements) processes in the brain.

### **3.3.2 EP/ERP analysis**

The conventional methods for extracting the EPs/ERPs from the ongoing EEG involves computer averaging procedures where, the background EEG waves considered as "noise" in most EP/ERP experiments, are typically larger than the waves of interest. This technique

requires that both the wave shape of the EP/ERP and its temporal relationship to the time locking reference event (stimulus) remain constant from one occurrence to the next. Since the background EEG fluctuations are not time-locked to the reference event, they will average out toward zero when the EPs/ERPs from the successive trials are added together by the computer, thus improving the signal-to-noise ratio (SNR). Following the SNR improvement techniques, EPs/ERPs are typically characterised using peak polarity, amplitude and latency (usually with respect to the stimulus onset) measures.

### **3.3.3 Clinical and other applications of ERPs**

An understanding of the genesis and working of ERPs leads to increased knowledge of the complex system associated with the brain. This knowledge has application in a number of areas. Most importantly, in understanding the working of the brain, mental disorders including schizophrenia and epilepsy can be better understood and perhaps treated more efficiently. This knowledge also allows modelling of the brain and hence the ability to produce improved artificially intelligent systems. The application of such systems is widespread and is likely to change the way in which computers operate. For example artificial neural network chips could be integrated into computer systems to allow computers to converge to a solution to a problem through a process of adaptive learning (i.e. learning from experience) in a similar way as the human brain operates. The intermediate ground is in the area of human computer interfacing. Recent reports show that control of computers by severely disabled people will be possible in the future [3.8].

## **3.4 Electrooculogram (EOG)**

EEG can be contaminated by a number of electrophysiological signals, the largest of which is the electrooculogram (EOG).

### **3.4.1 EOG characteristics**

The human eye contains an electrical dipole caused by a positive cornea and negative retina. When the eyes move (i.e. eye movements and blinks), the electrical dipole changes orientation thus causing an electrical signal known as EOG. The shape of the EOG

waveform depends on factors such as the direction of eye movements. There are several types of ocular movements ([3.9] [3.10]), of which the more relevant to EEG work are described in this section.

Blinks (Fig.3.1) are characterised by a brief artefact potential of between 0.2 to 0.4 secs in duration and occur at intervals of 1-10 secs. Barry and Jones [3.11] and Matsuo et al. [3.12] showed that blinks were attributable to the eyelid moving over the cornea. Ocular artefact (OA) is a collective name given to the electrical contaminants of EEG caused by eye movements and blinks [3.13]. OA due to blinks is always of concern in any experiment in which the eyes are open. Electrical signals produced by blinks (i.e. by the eyelid moving up and down) cause spike-shaped waveform as shown in Fig.3.1.

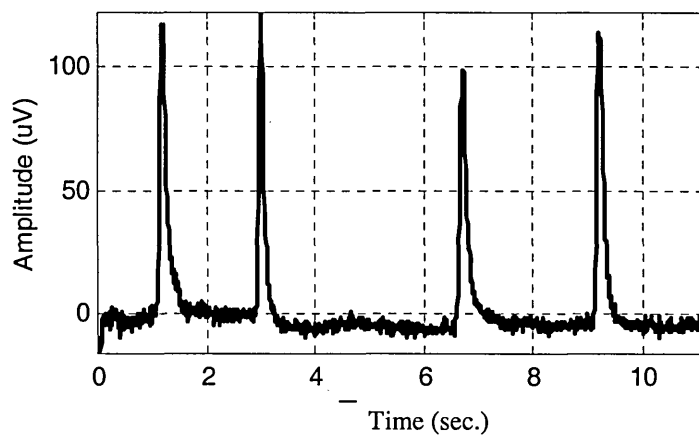


**Fig.3.1** Spike-shaped EOG waveform caused by blinks

Saccadic eye movements (Fig.3.2) are rapid conjugate movements of speeds between 100 and 500 degrees per second. Normal every day movements of the eye from one fixation point to another (e.g. when reading or scanning a visual field) come under this category. Vertical and horizontal eye movements (eyes moving up, down, left and right from the centre and vice versa) produce a square-like EOG waveform as shown in Fig.3.2.

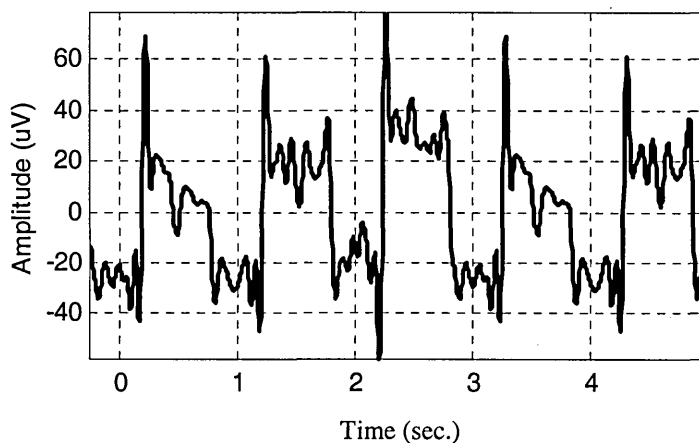


**Fig.3.2** Square-like waveforms caused by saccadic eye movements.

### 3.4.2. EOG filtering

A fraction of the EOG spreads across the scalp and it is superimposed on the EEG. This presents serious problems for EEG interpretation and analysis. In order for the EEG to be interpreted for clinical use, EOG contamination needs to be removed (filtered) from the EEG. Analogue and digital filters are not effective for this purpose as EEG and EOG signals occupy similar frequency band (covering a range close to DC to about 100 Hz). Conventional methods of EP/ERP averaging may not cancel all artefacts induced by eye movement or blinks as they are time-locked to experimental events. Often all epochs contaminated by large eye artefacts, usually larger than some arbitrarily selected EEG voltage value, are rejected as unusable, though this may prove unacceptable when blinks and eye movements occur frequently and when limited data are available. Frontal channels are also often used as reference signals to regress out eye artefacts, but inevitably portions of relevant EEG signals also appearing in EOG channels are thereby eliminated or mixed into other scalp channels.

## 3.5 Saccade-Related Evoked Potentials

Saccades are rapid changes in the orientation of the eyes for realigning the visual axes on objects of interest. Dysfunction in this system may affect various visual functions such as depth perception and reading [3.14]. The study of the saccade-related EPs provides

valuable information about how the brain deals with vision when eye movements are performed.

### 3.5.1 Types of saccade-related EPs

Saccadic eye movements influence the electrical brain activity. The literature on the neuronal mechanisms of eye movements in humans illustrates that electrical brain activity can be obtained with three different experimental paradigms analysing: (1) motor activity – related neuronal correlates of eye movements; (2) lambda waves of the EEG following eye movements; and (3) evoked cortical activity modulated by the occurrence of saccades. The present study will focus on the two former [1.7].

*motor activity – related neuronal correlates of eye movements:* In all motor activities, the planning and execution of saccades is preceded by a ‘readiness’ potential as well as by the neuronal activation of specific areas of the motor cortex [3.14]. This potential appears to be identical to what has been termed presaccadic negativity which in part originates in the supplementary motor area that is crucial for the control of self-initiated movements ([3.15] [3.16]). In addition, the initiation of saccades is paralleled by activity of neurons in the frontal and supplementary eye fields that has been recorded in animals before and during saccadic eye movements [3.17] [3.18] as well as in humans [3.19]. This activity is independent of the so-called spike potential which originates in the eye-muscles at the beginning of the saccades [3.20].

*lambda waves of the EEG following eye movements:* following rapid eye movements the spontaneous EEG displays so-called lambda waves that have been reported to originate in the parieto-occipital area (back of the head) of the cerebral cortex ([1.6] [3.21]). Lambda waves are believed to be related to visual information processing triggered by the relative movement of visual features of the visual field across the retina (e.g. [1.4]), and thus, their appearance has first been paralleled to the conventional visually evoked potential. However, a more recent study has shown that such components are involved in a special kind of visual processing reflecting the functional combination of corollary neuronal activity from motor areas involved in the planning and execution of saccades with primarily sensory brain activity elicited by stimulus occurrence, which appears to be independent from incoming visual information and thus is not influenced by the variation

of physical stimulus parameters [1.7]. The lambda wave is a saccade-related EP which provides a means of studying the neuronal mechanisms involved in saccade performance. Studies have reported that it could be observed in EEG recordings with eyes open but it was found to be inhibited during steady fixation or in the absence of a contrast (e.g. a black and white checkerboard pattern) ([3.22] [3.23]). The lambda wave has a number of sub-components, which are time-locked to the saccade onset (i.e. initiation of the eye-movement) and offset (i.e. termination of the eye-movement) [1.5]. These sub-components include a pronounced positive peak which appears within a 200 ms period after the saccade offset [1.5].

### **3.5.2 Saccade-related EP/ERP model**

The electrical activity recorded on the surface of the scalp can be assumed to be the sum of a number of signal sources from the cortex. Large numbers of functional imaging reports of the brain have showed that performance of particular tasks increases blood flow within small (of the order of several cubic centimetres) discrete regions [3.24]. The time course of these activations suggests the hypothesis that spatially independent groups of neurons are recruited to accomplish a given task. Furthermore, different regions of the brain are known to be responsible for given tasks, i.e. visual and motor cortex. In trying to understand the functionality of the brain several models have been suggested [3.25]. Most models are based on a grouping of a number of neurons into a single source or generator of electrical activity. The way in which the models differ is related to the constraints that are placed on the sources. In particular the types of signal or activity they produce. Each signal source can be considered to be an oscillator which has analogies in both electrical and mechanical engineering [3.26]. An oscillator has a number of parameters which alter its characteristics. These are amplitude, frequency and phase of the signal's oscillation.

When BS\_ICA is applied to the EEG waveforms, the source signals are considered to be concurrent electromagnetic activities that are temporally independent of each other and that are generated by spatially fixed sources [3.27]. These signals are mixed as they propagate from their sources to the electrode locations on the scalp. Networks producing such concurrent activity are defined not by compact spatial distributions in the brain but by the covarying field measurements they produce at the scalp sensors. In general "sources" of BS\_ICA components may be distributed brain networks rather than "physically compact

active brain regions”. These networks may be functionally linked, forming larger networks. Rather than thinking about the brain as being a collection of physically discrete neural networks which pass information to each other by impulses as we send letters or emails to each other (viewpoint of classical anatomy and physiology), BS\_ICA treats the brain as being a dynamically shifting collection of interpenetrating, distributed and possibly transient neural networks that communicate via some form(s) of mass action (viewpoint of a slowly emerging dynamic systems perspective on neuroscience) [3.27]. Brain networks are most probably not physically wholly isolated from one another, nor do they act wholly independently. The two viewpoints are complementary, hence the answers they produce may be complementary parts of the functioning of the brain.

BS\_ICA can only successfully separate “BS\_ICA-relevant” processes, i.e. processes whose activities satisfy several assumptions used in BS\_ICA (see section 2.6.1 in chapter 2). BS\_ICA analysis of ERP data must therefore be viewed as explanatory and care must be taken to test the functional distinctness of the resulting BS\_ICA components. Simply demonstrating their replicability across subjects and experimental conditions is not sufficient to ensure their physiological unity. One must attempt to establish relationships between component activations and independent variables such as subject performance and behaviour as well as considering their physiological plausibility.

### **3.6 Analysis of the data considered in this study**

The EEG waveforms recorded from the scalp during a saccade-related performance are signal mixtures consisting of the following: (i) Saccade-related EP components. These overlap in time and may also have overlapping spatial topographies. (ii) The obscuring non-saccade-related EEG components, i.e. the background EEG and EPs that are not related to the saccade. (iii) The contaminating electrophysiological signal artefacts such as the electrooculogram (EOG) generated by the eyes and the electromyogram (EMG) caused by muscle activity. (iv) Non-electrophysiological (external) sources of contamination, for example the mains interference.

Different neural signal components are involved in preparation and execution of saccadic eye movements. One of these is described as a frontal pre-saccadic potential related to

motor commands for saccade generation preceding voluntary saccades [3.28]. Others, such as efferent feedback from saccade generating centres to visual cortex are believed to provide visual stability of the surrounding world across the eye movements. The saccadic movement is accompanied by an EEG signal associated with visual information processing called the lambda-wave [1.5]. The extraction of these components will be useful for providing information about how the brain deals with the problem of vision with moving eyes.

### **3.7 Conclusion**

The study of saccade-related EP components will be useful as it provides information about how the brain deals with the problem of vision with moving eyes. The EEG waveforms recorded from the scalp during a saccade-related performance are mixtures of a number of different signals. Conventional EP/ERP averaging methods are useful for reducing the obscuring background EEG. However this method cannot separate the electrooculogram (EOG) signal caused by eye movements from the saccade components of interest. A signal source separation based methodology such as BS\_ICA is valuable in order to filter the EOG signals from the EEG signals and to extract saccade-related components from the EEG mixtures and identify the brain regions responsible for their generation.

## **Chapter 4. Data Recording Experimental Methodology**

### **4.1 Chapter Summary**

This chapter is concerned with technical aspects of recording. It describes the experimental procedures and methodology utilised to record the data used in this study. This includes a description of the data recording system and set-up utilised to record the waveforms and the design and implementation of the clinical experiments carried out by the subjects.

### **4.2 Data Recording System Set-Up**

In order to establish and run an EEG laboratory to satisfactory standards, it is necessary to be able to record the EEG signals faithfully and with minimal distortion. Only then one is in a position to comment on its clinical significance. Sensitive amplifying and filtering equipments are required to enhance potentials picked up from skin electrodes, which are inevitably situated at a considerable distance from the generator source, and to discriminate between the evoked responses and other usually larger potentials of physiological and extrinsic origin with which it is intermixed.

To record the EEG at least two electrodes are used. An 'active electrode' is placed over a site of neuronal activity, and an 'indifferent electrode' is placed at some distance from this site. In clinical EEG recordings numerous active electrodes are situated over different parts of the head. All recordings however, measure the potential difference between two electrodes, either between the active and indifferent electrode or between two active electrodes. The recording electrodes are usually placed over the frontal, parietal, occipital, and temporal lobes on the left and right hemispheres of the scalp, symmetrically distributed with respect to the nasion-inion line and the pre-auricular line ( $A_1-A_2$ ), according to a conventional scheme shown in Fig.4.1. The nasion and the inion lines cross on the scalp at a point called the Vertex (denoted by  $C_z$  in Fig.4.1). When recording all types of brain electrical signal, it is common practice to place electrodes at or near sites determined by the 10-20 system of electrode location. This system was originally designed to standardised placement of electrodes for recording EEGs and makes use of percentage

distances (mostly 10 and 20%) to compensate for different head sizes and shapes [4.1], as shown in Fig.4.1.

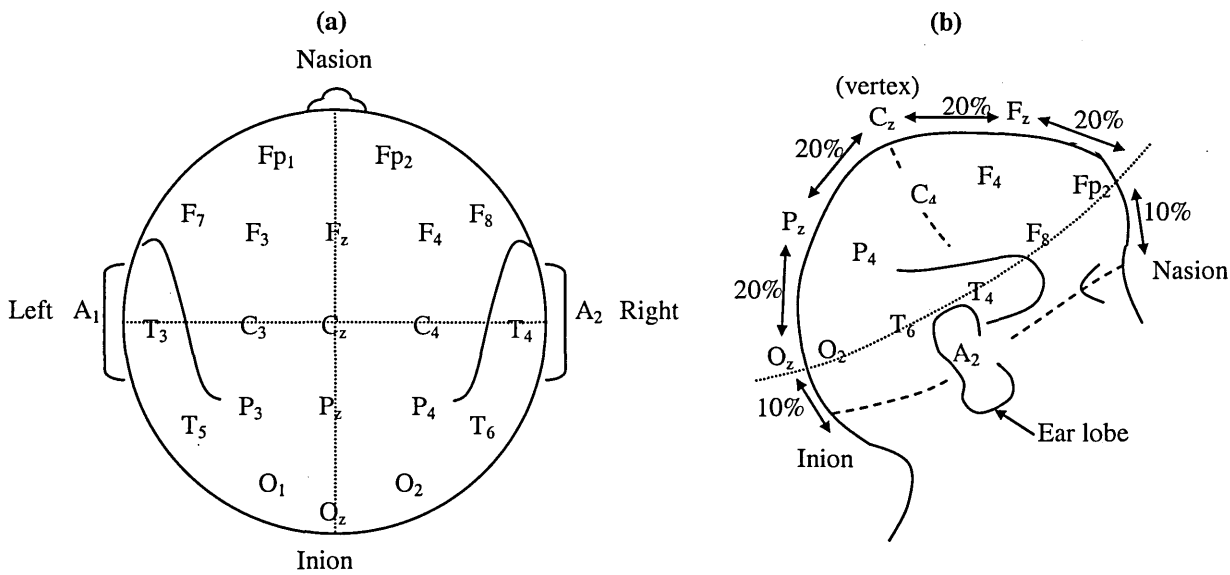


**Fig.4.1** The international 10-20 system of electrode placement: (a) top view and (b) side view of the head with the alpha-numeric designation of electrodes placement on the scalp for the EEG recordings.

The international 10-20 system of electrode placement utilised an alpha-numeric designation of electrodes placement on the scalp for the EEG recordings. Abbreviations for multiple electrodes are: A, auricle; C, central; Cz, vertex; F, frontal; Fp, frontal pole; O, occipital; P, parietal; T, temporal. The multiple electrodes placements overlying a given area (e.g. temporal) are indicated by numerical subscripts.

A major problem with the 10-20 system of electrode placement for recording EPs and ERPs is that the sites and spacing of electrodes are not optimal for displaying all types of responses. A modification of the 10-20 system was implemented by the Electrical Geodesics Inc. (EGI) [4.2] to allow for the positions of more closely spaced electrodes to be specified. A more detailed description of the EGI EEG recording system is provided in section 4.3.

A satisfactory environment for both the subjects and equipment must be ensured. The subject is usually conformably sited on a chair, in a room isolated from external noises

and disturbances, and the network of electrodes is carefully adjusted on the subject's scalp before beginning the experiment.

The raw EEG signals waveforms picked up by all electrodes are recorded during the experiment and the data acquired are stored on the computer drive for offline use, processing and analysis. Information about the subjects (this includes details such as their name, age, sex, medical history, etc.), recording settings and stimulus parameters are also carefully stored in order to facilitate later retrieval and manipulation of the data.

### 4.3 Electrical Geodesic Inc. (EGI) EEG Recording System

The EGI EEG recording system includes a Geodesic Sensor Net (GSN), an amplifier unit (Net Amps) and a Data acquisition computer (DAC) running EGI Net Station software.

A functional diagram of the EGI System is shown in Fig.4.2.

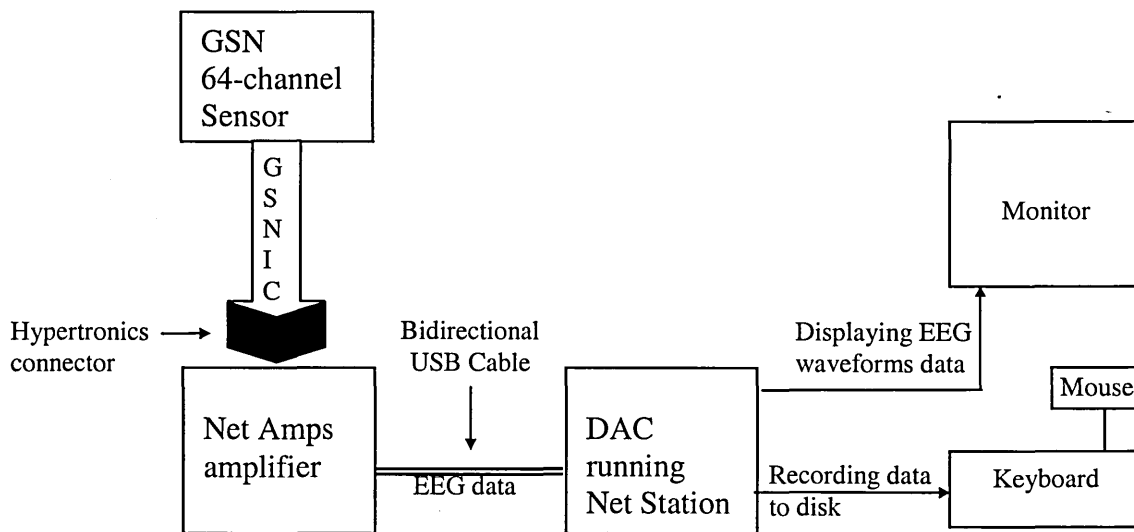
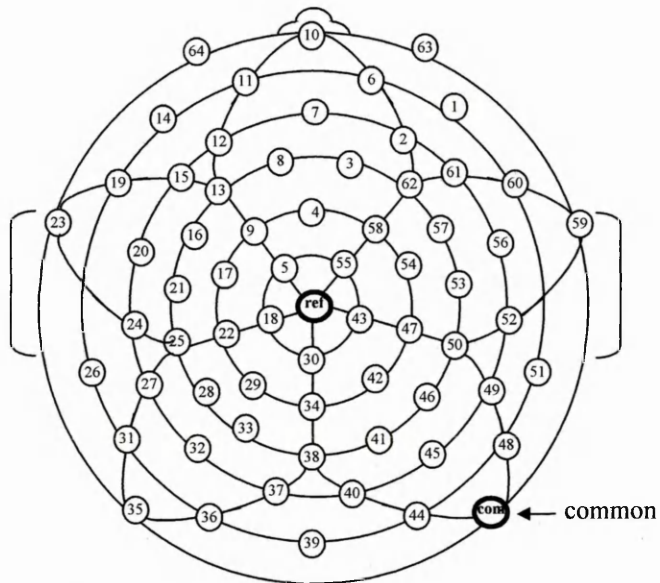


Fig.4.2 The Electrical Geodesics Inc. (EGI) system

#### 4.3.1 The Geodesic Sensor Net (GSN)

During EEG recordings, subjects wear a Geodesic sensor net (GSN). It consists of an array of 64 sensors, together with a reference and isolated common sensors. A diagram of the GSN is shown in Fig.4.3.

Geodesic Sensor Network  
64 Channels



**Fig.4.3** The Electrical Geodesics sensor network (GSN) of 64 electrodes

The network of 64 silver-silver chloride (Ag/AgCl) electrodes rest against the head of the subject and covers the surface of the scalp. A subject wearing a 64-channel adult-sized GSN is shown in Fig.4.4.

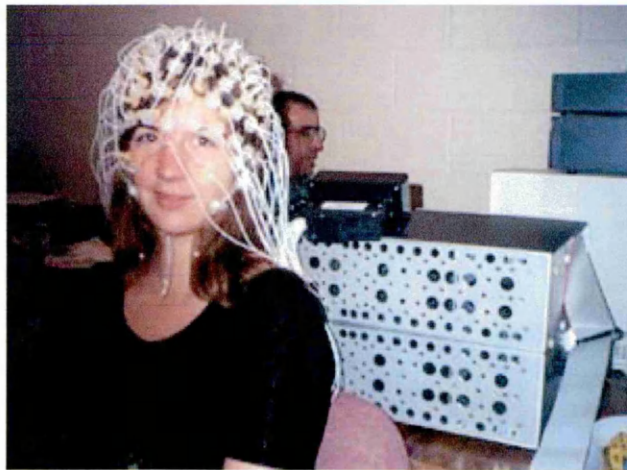


**Fig.4.4** Subject wearing the 64-channel GSN.

The GSN features EGI's patented dense array of EEG sensors held in a tension structure that stretches over the subject's head. The sensors' contact with the surface of the head is achieved using electrolyte-wetted sponges, and without abrasion of the subject's scalp.

The 64-channel GSN sensors pick up changes in voltage originating at the surface of the subject's head (the EEG), along with a certain amount of electrical noise originating in the room environment. Physically, the GSN is connected to the amplifier unit via the Geodesic Sensor Net Interface Cable (GSNIC).

#### **4.3.2 The Geodesic Sensor Net Interface Cable (GSNIC)**

The GSNIC allows the subject to be positioned conveniently within a meter or two of the amplifier unit. Each sensor in the GSN is wired via the GSNIC to an individual pin on a multi-pin receptacle called an Hypertronics connector located on the front of the amplifier unit as shown in Fig.4.2.

#### **4.3.3. The Net Amps Amplifier Unit**

The Net Amps amplifier unit inputs are differential, i.e. the voltage measured at every channel is the difference in voltage between the reference (vertex) sensor and the channel sensor. There is no ground sensor *per se*, i.e. the subject is never connected to earth ground. This would make the subject vulnerable to electrical hazard, just as standing in water makes one vulnerable to electric shock. The ground sensor on the GSN is actually an isolated common, which means it is tied to the zero level or common the isolated amplifier circuit's power supply. This supply is isolated, so it is not connected to earth, the computer, or anything else. Thus an electrical hazard would not make a dangerous loop with the isolated common.

Electrophysiological amplifier arrays, such as the Net Amps, take low-level, microvolt signals and amplify them to a level that conventional electronics can manipulate. With the Net Amps, each channel's amplification factor, or *Nominal Gain*, is approximately 1000 (meaning that the amplifier output signal is 1000 times greater than the input).

Electrical signals from all the sensors of the GSN are received simultaneously by the amplifier unit where they are measured, amplified, filtered, sampled at millisecond intervals and digitized.

As quickly as the samples are acquired they are packaged and sent out to the data acquisition computer (DAC) along the universal serial bus (USB) cable that connects the amplifier and the DAC. The digitized samples are transferred to the DAC in real time.

#### **4.3.4. The Data Acquisition Computer (DAC)**

Once the packets of data containing digitized EEG samples are received by the DAC, the Net Station software can collect them for display and storage to disk. Since the USB cable is bidirectional, Net Station software can send queries and commands to the amplifier unit as well as receive data from it.

#### **4.3.5. The Net Station software**

Net Station resides on the DAC, where it is capable of continuously collecting dense array EEG data from the amplifier unit. In Net Station, users can display EEG data in a variety of ways and record them to permanent computer files. The data of each sensor are segregated into their own channels. As the samples stream into the DAC over the USB cable, Net Station gathers, organizes, and displays each channel's EEG data in the manner of a traditional chart recorder. When Net Station is instructed by the user (via mouse and keyboard) to record the data to a file, the chart recorder display continues on the monitor without interruption while the data are being written to disk.

A maximum sample rate of 1000 samples per second stream continuously into Net Station's buffers. Users can observe the waveforms of each channel in groups limited only by the size of the computer monitor, even as the data are written to disk.

Users access the settings of the Net Amps (amplifier unit) using the Net Station software. Net Station monitors, calibrates, and controls the amplifier channels, and acquires EEG data from the Net Amps. In addition to Net Amps calibration and channel impedance measurements, Net Station's Net Amps controls panel allows modification of the following amplifier settings:

- Sampling rate (50-1000 samples per second)

- Lowpass hardware filter cutoff (0.0-400.0 Hz)
- Bessel versus elliptical hardware filter type
- Option to auto set filter cutoff to Nyquist frequency
- Highpass hardware filter cutoff

Hardware filters (also described as “analog signal filtering”) integrate with each discrete amplifier to form an amplifier/filtering unit with sample and hold. After amplification, filtering, and sampling, the EEG signals are digitized by a 16-bit analog-to-digital converter.

## **4.4 Data Recording Procedure**

Two sets of data were used in the study. The first set of data consisted of EEG and EOG waveforms recorded from an experiment where subjects were relaxed and fixating at a white board. The second set of data consisted of saccade-related waveforms recorded from an experiment where subjects followed with gaze a red square stimulus that changes location on a checkerboard pattern screen display. For the second set of experiments, subjects were asked to avoid blinking and body movements, in order to limit the contamination of the data by ocular and muscle artefacts. In both experiments, the signals were recorded using electrodes placed on the subjects scalp.

### **4.4.1. First set of experimental data: EOG filtering from the EEG waveforms**

The data collected in the first experiment was used to quantify the effectiveness of a number of OA removal methods. The operation required the availability of the EEG waveforms before and after OA contamination so that the recovered EEG waveforms could be compared with the original (uncontaminated) EEG. Furthermore, the OA removal used required the original signal sources to be independent.

The EEG and EOG data were recorded in an EEG data recording room with subjects relaxed and fixating at a white board. Four sets of EEG waveforms were recorded from four subjects (2 males, 2 females), mean-age 32 years (standard deviation 9). Each set consisted of thirty-two waveforms. By recording each EEG data set from a different

subject, the condition for independence of the signal sources was conformed. Thirty-two EOG waveforms were recorded from another subject. The subject was asked to make eye movements and blinks (in random order) at a rate of about one every second during each EOG recording so as to record OA electrical activity. By recording the EOG data from a separate subject it was ensured that they had not contaminated any of the EEG data sets.

EEG data were recorded from the scalp (location CZ in accordance with the 10-20 standard electrode positions). EOG data were recorded using a pair of electrodes placed adjacent to the right eye. The reference for both EEG and EOG recordings was a pair of joined electrodes placed on the ear lobes. Silver-silver chloride electrodes were used for all recordings. The sampling rate was 125 Hz and the signals were band limited to 30 Hz. Each waveform contained 1500 data points (i.e. about 12 seconds).

#### **4.4.2. Second set of experimental data: Saccade-related EEG and EOG waveforms**

The second set of data was recorded in order to study the electrical brain activity that is generated during the performance of saccadic eye movements. Seven healthy adults (3 males, 4 females) mean age 27 years (standard deviation 6) with normal or corrected-to-normal vision participated in the study. The subjects had no history of a neurological or ophthalmologic disease and were all right-handed. They were seated in an EEG recording laboratory at about 60 cms from a computer that displayed a black and white checkerboard pattern background.

A red square visual target stimulus (hereafter referred to as the stimulus) appeared on a computer screen at one of five predefined checkerboard locations: centre, left, right, up and down as shown in Fig.4.5. The sequence of the stimulus appearance on the checkerboard was random to reduce the effect of expectancy.

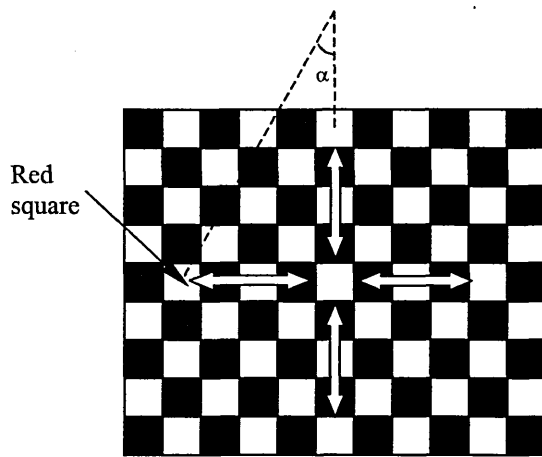


**Fig.4.5** A representation of the checkerboard showing the directions of saccade and the viewing angle.

The subjects were instructed to visually follow the stimulus as fast as possible. They were also asked to avoid head movements and minimise blinks in order to limit to a minimum the contamination of the EEG by ocular and muscle artefacts. The viewing angle ( $\alpha$ , shown in Fig.4.5) of the peripheral positions from the centre was about 10 degrees. This value was also used in one of the saccade experiments reported in [1.5]. This made it possible to compare the lambda waves observed in both studies. There were 8 directions of saccade and a fixation. These were: 4 centre-to-peripherals, 4 peripherals-to-centre and a centre-to-centre (i.e. no eye-movement) as indicated in Fig.4.5.

In order to avoid the effect of anticipating the onset of the stimulus, the 'pre-stimulus period' was varied randomly (between 850ms to 1500 ms). The 'response period' is the time it takes for a subject to initiate the eye-movement after the onset of stimulus (i.e. after the red-square appears at a new location). The 'post-response period' consists of the time it takes for the subject to visually re-orientate his/her visual axis to a new stimulus location (i.e. saccade duration) and the time duration that the subject fixates the stimulus at one of the five predefined checkerboard locations (i.e. fixation time). The composition of the trials is shown in Fig.4.6.

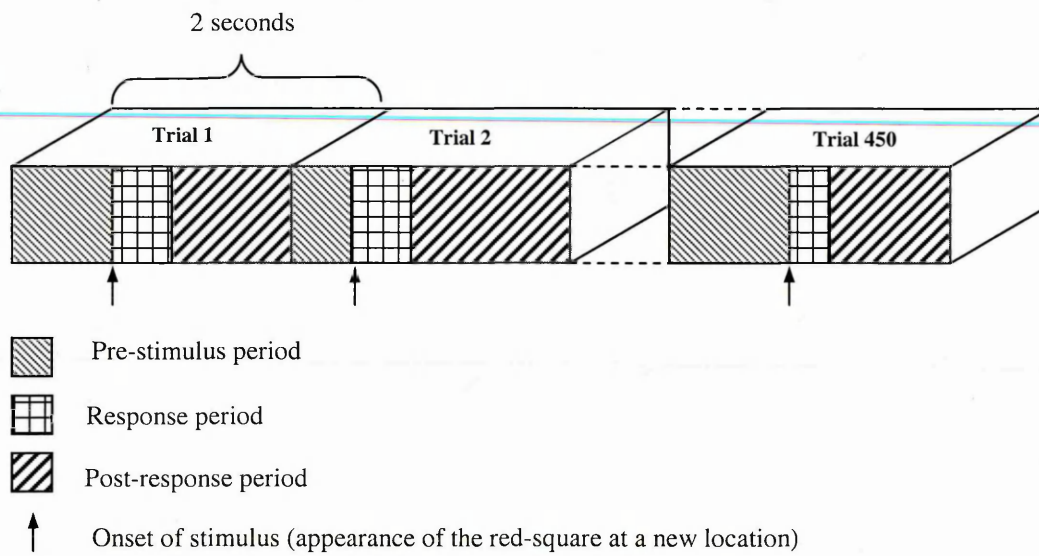


**Fig.4.6** Composition of the recorded trials.

The EEG and EOG data were recorded using a network of 64 silver-silver chloride electrodes. The type of EEG recording machine was the Electrical Geodesics. Its features together with the details of the electrode locations on the subject's scalp can be found at reference [4.2]. The structure and operation of the EGI data recording system are described in section 4.3. The EOG data were recorded so that the eye-movements can be monitored. All channels (EEG and EOG) were referred to the vertex ( $C_z$ ) electrode. The recording system band-pass filter had a frequency range of 0.01 to 100 Hz. The digitisation sampling rate was 250 Hz. The term recorded-waveform is used (in this thesis) to refer to a waveform recorded from an electrode site. A collection of the recorded-waveforms from the 64 electrode sites when performing a single saccade is referred to as one trial. Up to fifty trials were recorded per saccade direction. Each trial lasted about 2 seconds, however the lambda wave was contained within a one-second window of each trial. This one-second window was selected and processed in the analysis performed in the study. A collection of 50 trials is referred to as an event. The total number of recorded trials per subject was up to 450 (i.e. 50 trials  $\times$  (8 directions of saccade + 1 fixation)).

## 4.5 Conclusion

In this chapter, a description of the data recording system and set-up utilised to record the signal waveforms and the design and implementation of the two clinical experiments carried out, was provided. The data collected in the first experiment was used to quantify

the effectiveness of a number of ocular artefact (OA) removal methods which required the availability of the EEG waveforms before and after OA contamination. The second set of data was recorded in order to study the electrical brain activity that is generated during the performance of saccadic eye movements by the subjects when visually following a red square target on a checkerboard pattern background. The signals were recorded using electrodes placed on the subjects scalp.

# Chapter 5. Analysis of Conventional and Signal Source Separation Approaches for Removing Ocular Artefact from the EEG

## 5.1. Chapter Summary

A procedure for quantifying the effectiveness of an algorithm for removing ocular artefact (OA) from the EEG was devised. A comparative investigation of four methods for OA removal was carried out. Procedures to overcome some of the limitations of two ICA-based OA removal methods were implemented. The experimentation details are provided and the results obtained are discussed.

## 5.2. Introduction

The human eye contains an electrical dipole which is caused by a positive cornea and negative retina [5.1]. Eye movements and blinks change the dipole causing an electrical signal known as the electrooculogram (EOG). A fraction of the EOG spreads across the scalp and it is superimposed on the EEG. In order for the EEG to be interpreted for clinical use, the EOG needs to be removed (filtered) from the EEG. Analogue and digital filters are not effective for this purpose as EEG and EOG signals occupy similar frequency band (covering a range close to DC to about 100 Hz).

One of the earliest methods for OA removal was based on the use of potentiometers to balance out the effect of vertical and horizontal eye movements [5.2]. The required adjustments were made manually by monitoring the EEG and thus they were subjective. A software-based OA removal method was proposed by Quilter *et. al.* [1.13]. The method, known as EOG subtraction, involves subtracting a fraction of the EOG from the contaminated EEG. Its operation is based on the assumptions that: (i) the recorded (contaminated) EEG is a linear combination of the original (i.e. uncontaminated) EEG and OA, (ii) the contaminating OA can be estimated from the EOG, (iii) there is no correlation between the original EEG and the EOG signals. The method can easily be implemented but it causes distortion of the

recovered EEG. This is because a fraction of the EEG also contaminates the EOG and thus the subtraction process causes part of the desired EEG to be removed.

---

In order to improve the performance of the EOG subtraction method, a technique referred to as “multiple source eye correction” was developed by Berg and Scherg [5.3]. They estimated the component of the recorded EOG which was not contaminated by the EEG. A fraction of this component was then subtracted from the recorded EEG. The method however, required an accurate modelling of propagation paths for the signals involved.

Adaptive digital filters have also been used for OA removal. For example, Rao and Reddy [5.4] developed an on-line method of OA removal system based on this approach. They used a non-linear recursive least square algorithm to train an adaptive digital filter. The main limitation of the method was the need for a suitable EOG reference model for adapting (training) the filter.

Principal component analysis (PCA) [1.12] is a well known decorrelation technique and has provided another approach for OA removal from the EEG. PCA enables an epoch of multi-channel EEG to be decomposed into linearly uncorrelated components on the basis of their spatial distribution across channels. By omitting unwanted components (such as OA) from the linear combination, a less contaminated EEG can then be reconstructed. Lagerlund, *et al.* [2.10] developed a variation of this technique in which the PCA coefficients were stored in a single matrix. This allowed the matrix to be calculated on the basis of one representative epoch that contained the artefacts to be removed. The matrix was then applied to the subsequent EEG epochs, without repeating the PCA operation. The limitations of the PCA approach are that: (i) it is unable to completely separate the OA from the EEG, specially when both waveforms have similar voltage magnitudes, (ii) it requires the distribution of the signal sources to be orthogonal, (iii) its effectiveness is limited to decorrelating signals and thus it cannot deal with higher-order (i.e. greater than second order) statistical dependencies.

In order to overcome the limitations of PCA, Makeig *et al.* [5.5] applied independent components analysis of Bell and Sejnowski (BS\_ICA) for removing artefacts from the EEG. BS\_ICA is an extension of the PCA which not only decorrelates but can also deal with higher-order statistical dependencies. Bell and Sejnowski proposed an information-theoretic based BS\_ICA algorithm that uses an unsupervised learning rule [1.9]. It finds a linear

transformation within the data to make the separated signal components as statistically “independent” as possible. The technique does not need *a priori* knowledge of the physical location or the configuration of the sources and unlike PCA, it does not require the distribution of the signals sources to be orthogonal. However for it to function correctly, the signal sources must be statistically independent and the distribution of not more than one source can be Gaussian. The EEG signal sources represent the signals produced by the various signal generators of the brain and not the recorded EEG signals that represent a mixture of brain electrical activities from many sources. The BS\_ICA algorithm applied by Makeig *et. al.* [5.5] is suitable for sources with super-Gaussian distribution (i.e. irregularly occurring signals with sharply peaked distributions and positive kurtosis). Lee and Sejnowski [2.24] extended the BS\_ICA algorithm to make it also suitable for signal sources with sub-Gaussian distribution (i.e. signals with negative kurtosis). Jung *et. al.* [5.6] applied the extended version of the BS\_ICA algorithm to isolate and remove a variety of EEG contaminating artefacts.

Another ICA algorithm for signal source separation was proposed by Cardoso [1.10]. The method is based on the joint approximate diagonalisation of eigen-matrices (JADE). It operates by exploiting the higher-order statistical properties of the signals based on their fourth-order cumulants. Like the ICA algorithm of Bell and Sejnowski [1.9], this algorithm also requires the sources to be statistically independent and at most the distribution of one source can be Gaussian [5.7].

In the study presented in this chapter, a method to quantitatively evaluate the effectiveness of an algorithm for OA removal from EEG waveforms was devised. The method was used to evaluate and compare the performance of two ICA-based approaches, namely the extended version of the ICA algorithm of Bell and Sejnowski (hereafter referred to as extended-ICA) [1.9] and the ICA algorithm of Cardoso (hereafter referred to as JADE) [1.10] to that of two decorrelation-based methods, namely PCA [1.12] and EOG subtraction [1.13] methods, for removing the OA from the EEG. EOG subtraction method was included because it is one of the conventional methods for performing OA removal from the EEG. PCA was included in order to investigate the need for considering the higher statistical dependencies in OA removal process. Extended-ICA and JADE were included as they are well-established ICA-based signal source separation techniques. Both extended-ICA and JADE are based on information theoretic principles, however the extended-ICA algorithm of Bell and Sejnowski uses entropy while the JADE algorithm of Cardoso exploits the fourth-order cumulants of the data.

A review of the most relevant work in the area of EOG removal over the past 20 years is provided in Table 5.1.

**Table 5.1** A review of reported work on ocular artefact removal over the past 20 years.

Method	Principle	Comments on the method	Authors associated with the method
<b>Regression in time domain / in frequency domain methods</b>	Both time and frequency regression methods depend on having a good regressing channel. It was shown that relevant EEG contained in the EOG channel is cancelled out along with OA as spread of excitation from OAs and EEGs is bi-directional.	- time-domain regression tends to overcompensate for blinks artefacts. - frequency-domain regression is a causal and thus unsuitable for real-time applications.	[5.9] [5.10] [5.11] [5.12]
<b>A simple on-line technique</b>	Based on the use of potentiometers to balance out the effects of vertical and horizontal eye movements.	- these adjustments are normally made whilst visually observing the EEG signal and thus are subjective.	[5.2]
<b>Rejection method</b>	Based on discarding portions of EEG that correspond to EOG channel(s) containing attributes that exceed a determined criterion threshold.	- may lead to a significant loss of data. - inability to identify all eye artefacts but only part of it which may leads to artefact-reduced instead of artefact-free EEGs. - has shown not to perform well the OA removal.	[5.13] [5.14]
<b>Spatio-temporal dipoles model method</b>	Requires <i>a priori</i> assumptions about the number of dipoles for EOGs and assumes that they have a simple dipolar structure.		[5.15]
<b>Eye-fixation method</b>	So as to reduce the presence of eye activity in EEGs the subject is asked to avoid blinking by fixing the eyes on a target.	- the subjects might not always be fully co-operative leading to collection of insufficient amount of data. - this secondary task may have effects on the signal of interest.	[5.16] [5.17]
<b>Subtraction method</b>	Based on correlation technique, it assumes that measured EEG is a linear combination of true EEG and OA; correction is achieved by subtraction of regressed portion of OA from the contaminated EEG.	- assumes that the OA can be estimated from the EOG data and that there is no correlation between the true EEG and EOG signals. - subtraction distorts the shape of EEG responses as EOG contains a certain amount of brain activity.	[5.2] [5.8] [5.18] [1.13] [5.19]
<b>MSEC (multiple source eye correction)</b>	Subtracts source waveforms defined by eye activity rather than proportions of the resulting EOG signal; original sources are computed from EEG and topographic estimation of propagation path of EOGs.	- function of location and orientation of each sources and some head parameters. - requires a set of calibrating data which goes well above the background signal (EEG). - assumes orthogonality of the sources vectors.	[5.3]
<b>Signal-space projection method</b>	Based on a parameterised modelling of propagation path of eye activity throughout the head.	- requires a prior modelling of the production of the artefacts. - requires a considerable amount of data where OA amplitude is much higher than that of the background EEG.	[5.20]
<b>Non-linear on-line method</b>	Enhances EEG signals in the presence of OAs. Uses the recursive least squares based on second-order Volterra filter.	- has shown good performance but - its second order (variances and covariances) non-linearity is too limited.	[5.4]

Table 5.1 (continued)

Method	Principle	Comments on the method	Authors associated with the method
<b>Principal Component Analysis (PCA)</b>	Using the second order covariance matrix of the observations (data), PCA finds orthogonal directions of greatest variance in the data with the key idea that variables (time points) that are correlated belong to the same underlying component.	<ul style="list-style-type: none"> <li>- assumes orthogonality of the components distributions</li> <li>- only removes up to second order statistics dependencies.</li> <li>- is not suitable for dealing with non-Gaussian data.</li> <li>- cannot completely separate out OAs from EEGs when they have comparable amplitude.</li> </ul>	[2.10]
<b>Independent component analysis (ICA) / Extended -ICA methods</b>	Assumes that the OAs and EEGs are physiological separate processes and that their independence is reflected in the statistical relation (based on information-theoretic principle) between the signals. Performs a blind separation of the signals as no <i>a priori</i> knowledge of the sources or information on the channel characteristics is required.	<ul style="list-style-type: none"> <li>- not only decorrelates the signals (removing second order statistics) but also reduces higher-order dependencies.</li> <li>- does not require orthogonality of the components distributions (the brain is not orthogonal).</li> <li>- requires appropriate non-Gaussian distribution of the components and assumes linear mixing of the signals.</li> </ul>	[5.5] [5.21] [5.22] [5.6] [5.23]

As reported in Table 5.1, EOG subtraction, PCA and the extended-ICA have all been previously applied to the problem of OA removal, however the aim of this part of the study is to extend the information available by providing a quantitative evaluation and comparison of their performance based on a series of statistical tests.

From the OA removal studies reported in Table 5.1, it was deduced that an efficient technique for performing the removal of ocular artefacts from the background EEG was Extended-ICA. This method is based on the key assumption of statistical independence between the brain and the artefacts waveforms. This independency between the components is assessed through a measure of similarity between their joint amplitude distribution using a principle of information theory called entropy. The technique appears to be an improvement from the traditional artefact cancelling methods and seems to be a generally applicable and effective method for removing a variety of artefacts from EEG recordings, since their time-courses are generally temporally independent, and differently distributed than sources of cerebral activity.

From the literature review outlined in Table 5.1, the advantages of the extended-ICA method over the more conventional OA removal methods were identified as follows: (1) It is generally applicable to remove a wide variety of EEG artefacts. (2) Separate analyses are not required to remove different classes of artefacts. (3) A single analysis simultaneously separates both the EEG and its artefacts into independent components based on the statistics of the data, without relying on the availability of 'clean' reference channels. This avoids the problem of mutual contamination between regressing and regressed channels. Moreover no arbitrary threshold (variable across sessions) are needed to determine when regression should be performed. (4) Once the training is complete, the artefacts-free EEG records can then be derived by eliminating the contributions of the artefactual sources. (5) In most cases, extended-ICA preserves the recovered brain electrical activity more accurately when compared with PCA in decomposing EEG data. (6) The extended-ICA algorithm is computationally more efficient than BS\_ICA algorithm as it speeds up convergence [2.40].

In most cases this independence is verified due to the differences in physiological origins of those signals. In experimental data, extended-ICA was able to extract the eye-information present in the EOG signals, and use this information in the removal of this type of artefact, rather than the complete EOG (that still has some remaining brain activity).

The effectiveness of other types of algorithm such as for instance the ‘non-neural’ JADE algorithm developed by Cardoso and Souloumiac [2.16] which is an ICA method that exploits the higher order statistics fourth-order cumulants of the data should be investigated and their performance in performing OA removal from the EEG compared with the extended-ICA algorithm.

As the operations of both ICA algorithms of Cardoso and Bell and Sejnowski are subject to amplitude scaling and channel permutation, procedures were incorporated as part of these two methods to estimate the amplitude of the separated signals and to allocate them to the correct channels. A description of the theory of the signal separation methods (JADE, extended-ICA and PCA) is provided in chapter 2. A brief description of the EOG subtraction method is provided in section 5.3. Then the experimental procedures are outlined and the results obtained are discussed.

### 5.3. A brief overview of the EOG Subtraction method

The operation of EOG subtraction [1.13] method for removing OA from an EEG waveform consisting of  $N$  data points is outlined below. The contaminated EEG waveform ( $EEG_c$ ) can be expressed as the sum of the original EEG ( $EEG_o$ ) and a fraction ( $\hat{\theta}$ ) of the EOG waveform, i.e.

$$EEG_c(i) = EEG_o(i) + \hat{\theta} EOG(i) \quad i=1, 2, \dots, N \quad (5.1)$$

The correlation (at zero lag) between the EOG and contaminated EEG waveforms is given by,

$$Correlation = \sum_{i=1}^N EEG_c(i) EOG(i) \quad (5.2)$$

Substituting  $EEG_c$  from equation (5.1) into equation (5.2) results,

$$Correlation = \sum_{i=1}^N EEG_o(i) EOG(i) + \hat{\theta} \sum_{i=1}^N EOG(i)^2 \quad (5.3)$$

Equating equations (5.2) and (5.3) provides,

$$\sum_{i=1}^N EEG_c(i) EOG(i) = \sum_{i=1}^N EEG_o(i) EOG(i) + \hat{\theta} \sum_{i=1}^N EOG(i)^2 \quad (5.4)$$

However in this method it is assumed that there is no correlation between the original EEG and EOG therefore,

$$\sum_{i=1}^N EEG_o(i) EOG(i) = 0 \quad (5.5)$$

Substituting equation (5.5) into equation (5.4) simplifies equation (5.4) and from it the value of  $\hat{\theta}$  can be determined by,

$$\hat{\theta} = \frac{\sum_{i=1}^N EEG_c(i) EOG(i)}{\sum_{i=1}^N EOG(i)^2} \quad (5.6)$$

The original EEG waveform can be obtained by using  $\hat{\theta}$  in equation (5.1). Therefore,

$$EEG_o(i) = EEG_c(i) - \hat{\theta} EOG(i) \quad i=1,2, \dots, N \quad (5.7)$$

As described in section 5.2, the method of EOG subtraction involves subtracting a fraction ( $\hat{\theta}$ ) of the EOG from the contaminated EEG. However, because the algorithm assumes that there is no correlation between the original EEG and the EOG signals, the method causes an estimation error to be introduced at two levels: (1) the estimation of  $\hat{\theta}$  will be erroneous since the EOG channel is not pure and contains some EEG signal and, (2) the recovered EEG will be distorted since the fraction of the EEG that has contaminated the EOG will be removed from the desired EEG signal during the subtraction process.

## 5.4. Experimental procedures

### 5.4.1. Experimental methods

In order to quantify the effectiveness of each OA removal method, the recovered EEG waveforms were compared with the original (uncontaminated) EEG. A measure of similarity indicated how well the OA removal method had performed. The operation required the availability of the EEG waveforms before and after OA contamination. Furthermore,

extended-ICA and JADE required the original signal sources to be independent. The steps for satisfying these requirements are described as part of the overall experimental method. The experiments consisted of: (i) comparison of the four OA removal methods based on single EEG and EOG channels, (ii) analysis of the effect of mixing matrix values on the recovered (separated) EEG waveforms, (iii) analysis of the effect of additive Gaussian noise on the operation of the four OA removal methods. (iv) comparison of the two ICA algorithms of JADE and extended-ICA, based on multiple EEG and EOG channels.

Further details on the data recording procedures used to record the EEG and EOG data are provided in section 4.4.1. of Chapter 4.

#### 5.4.2. Source signals and mixtures generation

In order to carry out the analysis based on single EEG and EOG channels, 32 pairs of EEG and EOG mixtures were generated using the mixing matrix  $A = \begin{bmatrix} 0.8 & 0.2 \\ 0.2 & 0.8 \end{bmatrix}$ . The mixing

operation was carried out by performing  $\begin{bmatrix} EEG_c \\ EOG_c \end{bmatrix} = A \begin{bmatrix} EEG_o \\ EOG_o \end{bmatrix}$ , where  $EEG_o$  and  $EOG_o$  were

the original EEG and EOG respectively and  $EEG_c$  and  $EOG_c$  were the resulting contaminated mixtures. The operation caused the original EEG waveforms to be contaminated by  $\frac{1}{5}$  of the EOG (and vice versa). This mixing matrix was considered appropriate as only a

fraction of the EOG and EEG can contaminate each other. The mixing operation resulted in 32 pairs of contaminated EEG and EOG mixtures.

The distribution of the EEG and EOG waveforms was tested by the Univariate procedure using Statistical Analysis System [5.24]. This indicated that the EEG waveforms had a Gaussian distribution while the EOG were not Gaussian. Therefore, the requirement for both JADE and extended-ICA where not more than one source can be Gaussian was not breached.

The 32 pairs of EEG and EOG mixtures generated using the mixing matrix  $A = \begin{bmatrix} 0.8 & 0.2 \\ 0.2 & 0.8 \end{bmatrix}$

were also used to investigate the effect of additive Gaussian noise on the operation of the four OA removal algorithms. Gaussian noise (band limited to 50 Hz) were added to the 32 pairs of

mixtures and then the four methods for OA removal were applied to recover the EEG waveforms. Statistical parameters (described in section 5.4.3) were calculated to determine the ability of each method in recovering the EEG when contaminated by additive Gaussian noise. For each test, the 32 recovered EEG waveforms were averaged to produce a single representative EEG waveform. The experiment was repeated for different amounts of noise. The signal-to-noise ratio (SNR) values represented the signal power (before addition of the noise) to the noise power.

The mixing matrix  $A$  used in the above analysis conformed to a unity value for the sum of elements in its columns. In order to investigate the effect of not conforming to this condition, the experiment for the recovery of EEG waveforms was repeated using the mixing matrix

$$A = \begin{bmatrix} 0.5 & 0.2 \\ 0.3 & 0.5 \end{bmatrix}.$$

The analysis based on multiple EEG and EOG channels was carried out by using the four EEG and EOG data sets. The condition for independence of sources was ensured as each of the four EEG data sets had been recorded from a different subject. The Univariate statistical procedure was used to test the EEG and EOG distribution. This indicated that while the EOG data were not Gaussian, the EEG data had a Gaussian distribution and therefore they could not be considered as valid signal sources for extended-ICA and JADE algorithms. The required EEG signal sources were obtained by transforming the recorded EEG data. The transformation involved the following steps: i) a DC offset was added to the EEG signals so that their minimum values became zero, ii) they were squared and their mean values were removed, iii) the resulting signals were re-scaled to the original amplitude ranges, iv) the Univariate statistical procedure was applied to the transformed EEG waveforms to ensure they had the required non-Gaussian distribution. Typical distributions of transformed EEG waveform are shown in Fig.5.1. This transformation of the EEG waveforms prior to carrying out the mixing of the waveforms was required in order to simulate a situation where the original brain signals in the mixtures are independent of each other and have non-Gaussian distributions.

Regarding the EEG waveforms transformation procedure, the following comments can be made. In step ii), the waveforms were squared. Although they were re-scaled to their original amplitude range as described in step iii) (so as to simulate a situation where the EEG

waveforms have a typical EEG amplitude range), the values remain in  $\mu V^2$  unit. A way to get back the  $\mu V$  unit may have been to square-root the waveforms. Other types of transformations (such as  $x^3$ ,  $\tanh(x)$ ,  $1/x$ ) were also investigated. However, best results (i.e. least Gaussian distribution) were obtained for the  $x^2$  transformation described in steps i) to iv).

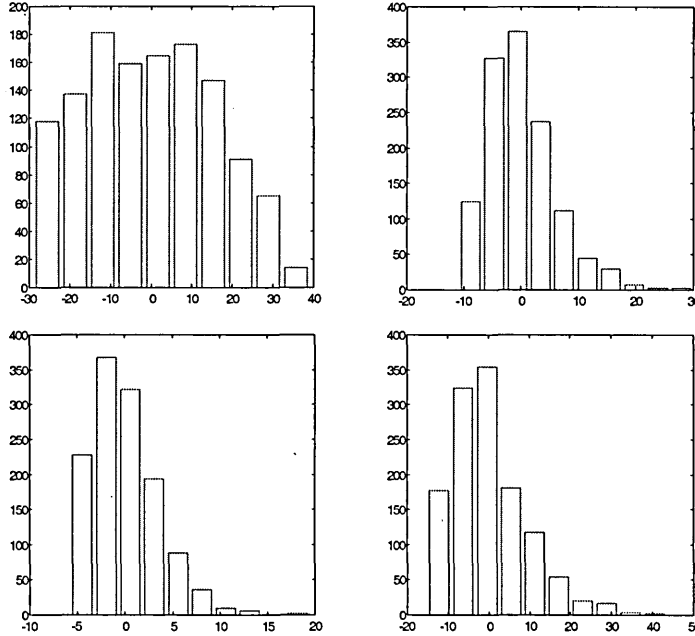


**Fig.5.1** Typical distributions of transformed EEG waveforms (the horizontal axis is amplitude in  $\mu V^2$  and the vertical axis is frequency of occurrence for an amplitude range).

Thirty two sets, each consisting of five signal mixtures were generated by carrying out the mixing operation,

$$\begin{bmatrix} EEG_{1c} \\ EEG_{2c} \\ EEG_{3c} \\ EEG_{4c} \\ EOG_c \end{bmatrix} = A \begin{bmatrix} EEG_{1t} \\ EEG_{2t} \\ EEG_{3t} \\ EEG_{4t} \\ EOG_o \end{bmatrix},$$

where  $EEG_{1c}$  to  $EEG_{4c}$  were the contaminated EEG signals and the  $EOG_c$  was the contaminated EOG.  $EEG_{1t}$  to  $EEG_{4t}$  were the transformed EEG signals and  $EOG_o$  was the original EOG waveform. The values of the mixing coefficients in matrix  $A$  was chosen arbitrarily. A contamination by 0.125 of each contaminating signal was considered appropriate as only a fraction of the EOG and EEGs can contaminate each other. The mixing matrix  $A$  was given by,

$$A = \begin{bmatrix} 0.5 & 0.125 & 0.125 & 0.125 & 0.125 \\ 0.125 & 0.5 & 0.125 & 0.125 & 0.125 \\ 0.125 & 0.125 & 0.5 & 0.125 & 0.125 \\ 0.125 & 0.125 & 0.125 & 0.5 & 0.125 \\ 0.125 & 0.125 & 0.125 & 0.125 & 0.5 \end{bmatrix}.$$

### 5.4.3. Procedures to Enable JADE and Extended-ICA Deal with the Problems of Amplitude Scaling and Channel Permutation

JADE and extended-ICA scale and may invert the recovered signals. Furthermore, the recovered signals may not appear in the correct channels (channel permutation). In order to deal with the channel permutation problem, each recovered signal was compared with each mixture and their correlation coefficient was calculated. A recovered signal was then allocated to the channel which corresponded to the highest correlation coefficient value. The operation assumed that each mixture contained a larger contribution from the original signal source than from the contaminating source. The possible sign change (i.e. signal inversion) was corrected by considering the sign of the correlation coefficient.

In order to estimate the amplitude of the recovered signals for both JADE and extended-ICA, a modified version of a procedure proposed by Cardoso [5.25] was implemented. The steps are outlined below for a case involving two signal sources, however the method can be extended to situations involving more than two sources. The original Cardoso's Algorithm involved the following steps:

- i) The inverse of the unmixing matrix  $W^{-1} = \begin{bmatrix} w_{11} & w_{12} \\ w_{21} & w_{22} \end{bmatrix}$  was obtained. This provided an estimate of the mixing matrix.
- ii) The total contribution of each original signal source to the mixtures was estimated from  $W^{-1}$ . This required summing the squared elements in each of its columns. The resulting sums were square rooted. The squaring of the elements was necessary to ensure negative values did not cancel positive values during the summing process.

The modification to Cardoso's procedure consisted in multiplying the resulting square-rooted sums by a scaling factor ( $k_j$ ). This produced a row vector,

$\mathbf{p} = [k_1 \sqrt{(w_{11}^2 + w_{21}^2)}, k_2 \sqrt{(w_{12}^2 + w_{22}^2)}]$ . The scaling factor  $k_1$  and  $k_2$  were required to deal with for the mathematical inequality that for any two values (x and y),  $|x| + |y| \neq \sqrt{x^2 + y^2}$ . The expression for  $k_j$  ( $j=1,2$ ) is given by,

$$k_j = \frac{\sum_{i=1}^2 |w_{ij}|}{\sqrt{\sum_{i=1}^2 (w_{ij})^2}} \quad (5.8)$$

where  $w_{ij}$  represents an element (in the  $i$ th row and  $j$ th column) of the matrix  $\mathbf{W}^{-1}$ . It was observed that with the modification  $k_j$  included,  $\mathbf{p}$  could be computed by a simple addition operation  $\mathbf{p} = [ |w_{11}| + |w_{21}|, |w_{12}| + |w_{22}| ]$ . The unmixing matrix  $\mathbf{W}$  was then re-scaled by multiplying its columns by the corresponding columns of the row vector,  $\mathbf{p}$ .

The reason behind the modification of Cardoso's procedure through the use of a factor  $k_j$  was that the Cardoso's procedure obtained a measure of energy, whereas a measure of amplitude was required to estimate the amplitude of the recovered signals.

#### 5.4.3. Parameters for Evaluating the OA Removal Methods

In order to assess the performance of each OA removal method, the similarity between the original and recovered EEG waveforms was measured. This required quantifying any change in the amplitude and shape of the waveforms. The required measurements were carried out by using the correlation coefficient, standard deviation and Euclidean distance parameters. The justification for using these parameters is provided below.

- i) *Correlation coefficient*. This provided a measure of the similarity in shape for the recovered and original EEG waveforms. A value with magnitude of 1 indicated that the recovered and original waveforms had exactly the same shape. However, this parameter did not provide any information about amplitude changes.
- ii) *Standard deviation ratio*. This was the ratio of the original EEG standard deviation to that of the recovered EEG. A value of 1 indicated that the original and recovered signals had the same power. A value more than 1 indicated a loss in the recovered signal power. As both extended-ICA and JADE scale the amplitude of the recovered signals, this parameter

indicated how well (for a particular mixing matrix) the Cardoso's amplitude estimation operates as part of JADE and extended-ICA algorithms.

iii) *Euclidean distance*. This provided a measure of similarity in both shape and amplitude. The Euclidean distance between two signals ( $x$  and  $y$ ) of length  $N$  can be expressed as [5.26],

$$\text{Euclidean distance} = \sqrt{\sum_{i=1}^N (x_i - y_i)^2} \quad (5.9)$$

#### 5.4.5 Statistical Tests for Determining the Significance of Differences

In order to determine the significance of the differences between the performance of the four OA removal methods, a number of tests were carried out using the Statistical Analysis System [5.24] package. The tests were based on the analysis-of-variance (ANOVA) technique. This enabled the F-statistic test [5.27] to be carried out on the mean values (over thirty two trials) for each the three parameters (correlation coefficient, Euclidean distance and standard deviation ratio) across the four OA removal methods. The F-statistic was suitable because it tested the null hypothesis that a significant difference did not exist between the means for a given parameter. An F value close to 1 resulted in accepting the null hypothesis, otherwise it was rejected.

Although the F-statistic indicated whether means were significantly different across the four OA removal methods, it did not however indicate which mean differed significantly from the other means. In order for this to be determined, Tukey's studentised range test [5.24] was performed. This test was based on analysing the pair-wise differences between the means.

### 5.5. Results and Discussion

The results obtained for JADE and extended-ICA were computed after incorporating the amplitude estimation procedure as part of their algorithms. The mixtures were processed by the four OA removal methods in order to recover the original EEG waveforms. The results are described in the following sections.

### 5.5.1. Single EEG and EOG Data Set Analysis

This investigation used the signals generated with the mixing matrix  $A = \begin{bmatrix} 0.8 & 0.2 \\ 0.2 & 0.8 \end{bmatrix}$ . Typical

plots for one pair of original EEG and EOG waveforms, their mixtures and the recovered EEG waveforms following the application of the four OA removal algorithms are shown in Figs.5.2a-h.

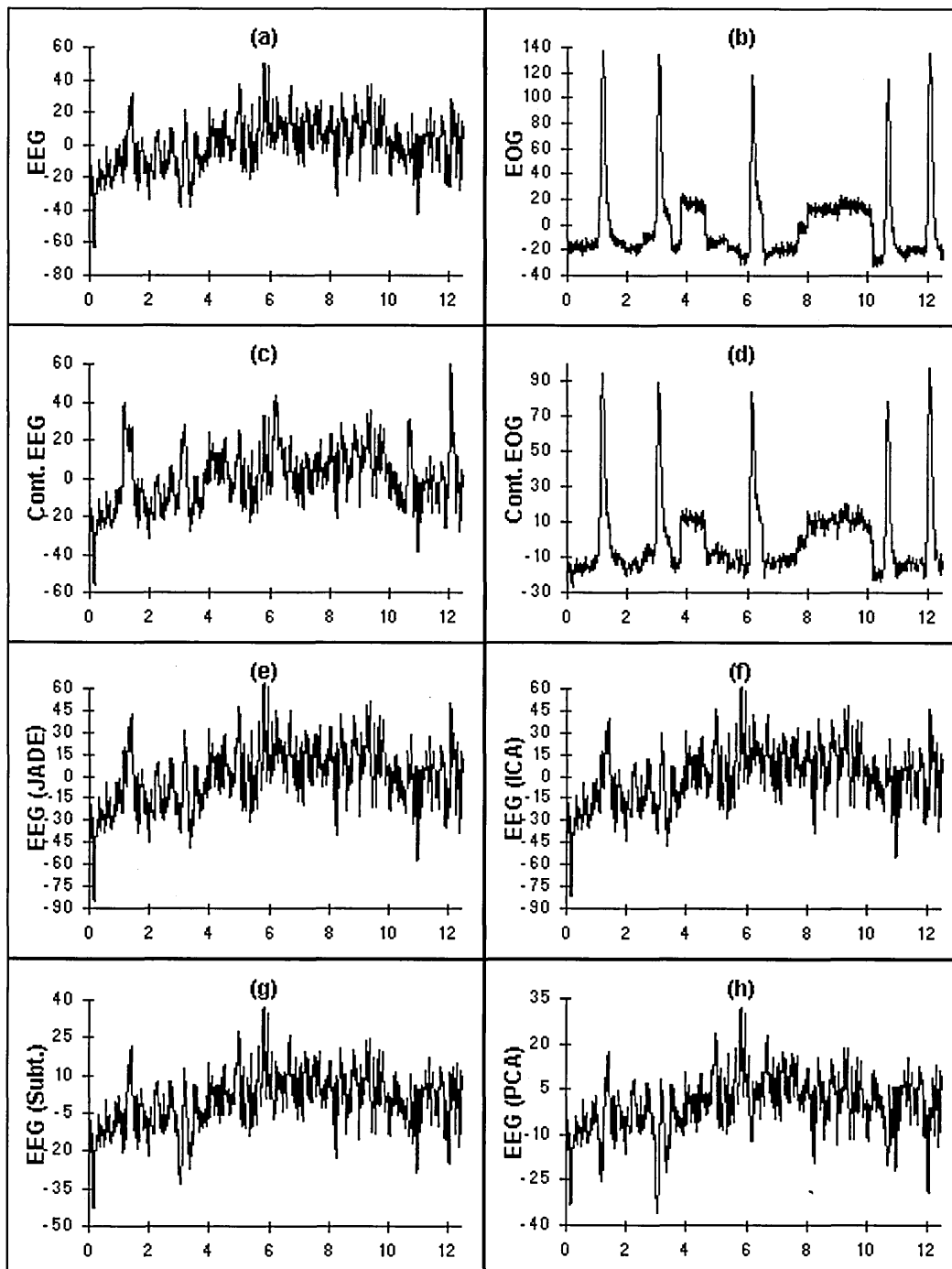


**Fig.5.2** Typical plots of original EEG (a), EOG (b), contaminated EEG (c), contaminated EOG (d), recovered EEG waveforms using JADE (e), extended-ICA (f), EOG subtraction (g) and PCA (h). The vertical axis is amplitude in  $\mu V$  and horizontal axis is time in seconds.

The standard deviation ratio, Euclidean distance and correlation coefficient values were computed for the EEG signals. Plots of these for the 32 trials are shown in Figs.5.3a-l.

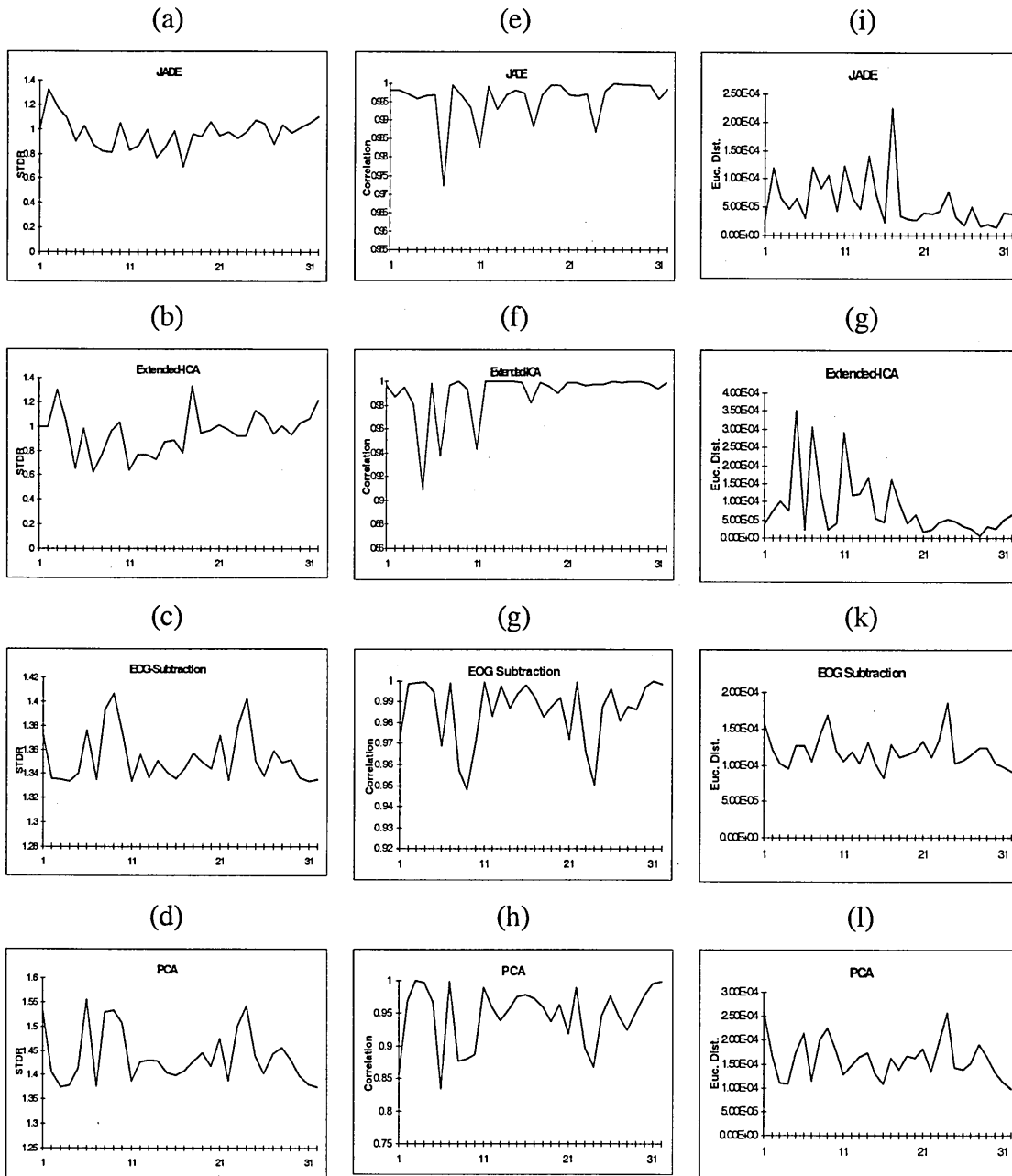


**Fig.5.3** Plots of standard deviation ratio (STDR) (a-d), correlation coefficient (e-h) and Euclidean distance (i-l) parameters for JADE, extended-ICA, EOG subtraction and PCA algorithms. The horizontal axis is trial number for all plots.

The corresponding means and variances are provided in Table 5.2.

**Table 5.2** Means and variances for the three parameters over 32 trials.

Methods	Standard deviation ratio		Correlation coefficient		Euclidean distance	
	Mean	Variance ( $\times 10^{-3}$ )	Mean	Variance ( $\times 10^{-3}$ )	Mean ( $10^{-4}$ )	Variance ( $\times 10^{-9}$ )
PCA	1.45	3.0	0.95	2.2	1.59	1.7
Extended-ICA	0.95	29.4	0.99	0.43	0.85	7.4
JADE	0.97	15.9	1.00	0.034	0.60	2.1
EOG subtraction	1.35	0.4	0.99	0.23	1.18	0.48

The following observations were made for the standard deviation ratio parameter. EOG subtraction method provided smallest variance and thus the highest consistency. However, it was always larger than 1 indicating a loss of amplitude in the recovered EEG. This confirmed the limitation of EOG subtraction method in which the part of the EEG which contaminates the EOG is also subtracted from the recovered EEG resulting in a loss of its amplitude (this was first referred to in the introduction section). PCA technique also reduced the amplitude of the recovered EEG. This indicated that PCA could not completely separate the mixtures. This may be because PCA is unable to deal with higher-order statistical dependencies. For extended-ICA and JADE, the standard deviation ratio parameter assessed not only their ability to separate the signal components in the mixtures, but also the ability of the Cardoso's amplitude estimation in re-scaling the separated signals. The results show that JADE and extended-ICA together with the Cardoso's amplitude estimation procedure have provided an accurate recovery of the original EEG waveforms.

JADE provided a correlation coefficient closest to 1 and an Euclidean distance value closest to 0. It was also most consistent (i.e., smallest variance) for these two parameters.

In order to determine the significance of the difference between the observed means two statistical tests were carried out by using the analysis of variance (ANOVA) technique [5.24]. These were F-statistics and Tukey's studentised range test.

The F-statistic test was performed for each measured parameter (standard deviation ratio, correlation coefficient and Euclidean distance) across the four OA removal methods. This

indicated that significant differences ( $p < 0.0001$ ) existed between the means for each of the three parameters across the four methods.

The Tukey's studentised range test was then performed to determine the sign (positive or negative) of the pair-wise differences between the means. This indicated whether a mean was significantly smaller or larger than another mean. The results are shown in Table 5.3.

**Table 5.3** Tukey's test (at level of significance 0.05) for pair-wise differences between algorithms.

Pair-wise differences between the algorithms		Standard deviation ratio	Correlation coefficient	Euclidean distance
PCA-	EOG Subt.	s (+)	s (-)	s (+)
	JADE	s (+)	s (-)	s (+)
	Ext. ICA	s (+)	s (-)	s (+)
EOG Subt. -	PCA	s (-)	s (+)	s (-)
	JADE	s (+)	ns (-)	s (+)
	Ext. ICA	s (+)	ns (-)	s (+)
JADE -	PCA	s (-)	s (+)	s (-)
	EOG Subt.	s (-)	ns (+)	s (-)
	Ext. ICA	ns (+)	ns (+)	ns (+)
Ext. ICA -	PCA	s (-)	s (+)	s (-)
	EOG Subt.	s (-)	ns (+)	s (-)
	JADE	ns (-)	ns (-)	ns (-)

**key:** s = significant, ns = not significant

Considering the standard deviation ratio parameter, the performance of PCA and EOG subtraction was significantly different from JADE and extended-ICA. The performance of Extended-ICA and JADE were not found to be significantly different.

Considering the correlation coefficient parameter, the performance of PCA was significantly different (smaller mean) from the other three algorithms. The latter did not show significant differences between their performances. This parameter indicated that PCA was least effective in preserving the shape of the recovered EEG waveforms.

Considering the results for Euclidean distance parameter, JADE and extended-ICA differed significantly from PCA and EOG subtraction, however they did not differ significantly from each other.

### 5.5.2. Analysis to Determine the Effect of Mixing Matrix

The results shown in Table 5.2 were obtained using a mixing matrix that conformed to unity for the sum of elements in its columns. In order to investigate the effect of not conforming to

this condition, the experiment was repeated using the mixing matrix  $A = \begin{bmatrix} 0.5 & 0.2 \\ 0.3 & 0.5 \end{bmatrix}$ . The

results are shown in Table 5.4.

**Table 5.4** Performance evaluation results when the mixing matrix

$$A = \begin{bmatrix} 0.5 & 0.2 \\ 0.3 & 0.5 \end{bmatrix}$$

Methods	Standard deviation ratio	Correlation coefficient	Euclidean distance ( $\times 10^{-4}$ )
PCA	3.15	0.89	2.93
Extended-ICA	1.23	0.98	1.06
JADE	1.27	0.99	0.87
EOG subtraction	2.77	0.95	2.68

The results for standard deviation ratio (from Table 5.4) indicated that JADE and extended-ICA performed better than PCA and EOG subtraction. Values close to 1.2 signified that little amplitude difference (i.e. a small fraction (0.2) of original waveforms) between original and recovered waveforms was observed for the ICA-based technique. However with values close to 3 (i.e. 3 times the amplitude range of original waveforms) both PCA and EOG subtraction methods resulted in a significant loss in the recovered EEG amplitude. The result also showed that the performance of the amplitude estimation procedure was affected by the mixing matrix values. The results for correlation coefficients were all still close to 1 indicating that the values associated with the mixing matrix do not affect the recovered signals shape. The experiment was repeated with several other mixing matrices. The results were consistent with the above observations.

### 5.5.3. Effect of Additive Gaussian Noise

The effect of additive Gaussian noise on the performance of the four OA removal methods was also investigated. The plots for the observations are shown in Figs.5.4a-c.

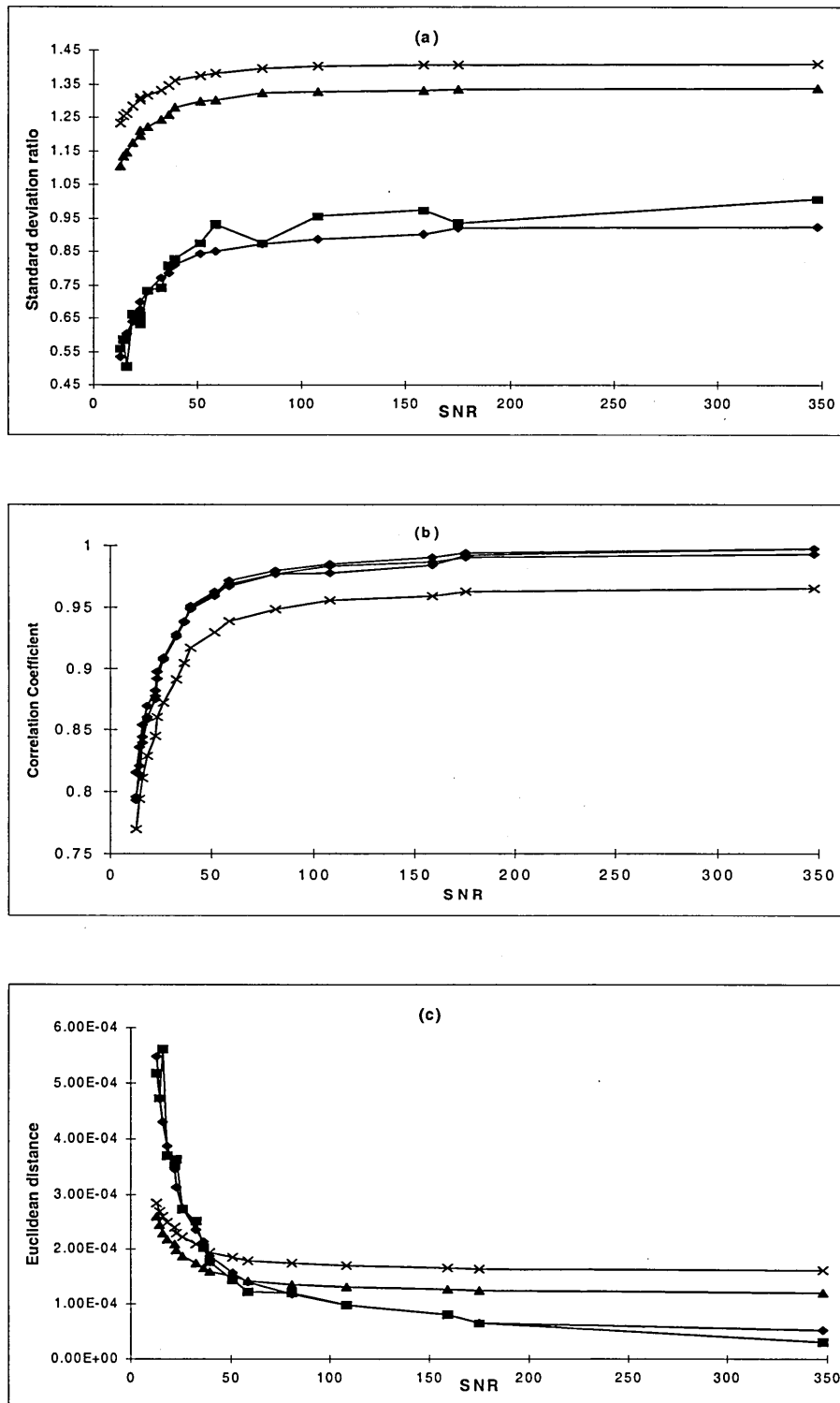


**Fig.5.4** Plots to demonstrate the effect of noise on the performances of extended-ICA (■), JADE (◆), PCA (×) and EOG subtraction (▲). The horizontal axis is linear signal-to-noise ratio (SNR).

On Fig.5.4, the signal-to-noise ratio (SNR) is linear and is defined as the ratio of the signal power over the noise power. The results indicated that the performances of all four algorithms for OA removal degrade rapidly for signal-to-noise ratios below 50.

#### 5.5.4. Multiple EEG Channels Analysis

The results obtained for the data consisting of four sets of thirty two transformed EEG waveforms ( $EEG_{1t}$  to  $EEG_{4t}$ ) are presented in Table 5.5.

**Table 5.5** Results obtained when the algorithms were applied to four transformed EEG sources.

Transformed EEG Data	Standard deviation ratio		Correlation coefficient means		Euclidean distance means ( $\times 10^{-5}$ )	
	JADE	Ext. ICA	JADE	Ext. ICA	JADE	Ext. ICA
$EEG_{1t}$	1.04	1.08	0.95	0.95	11.75	11.48
$EEG_{2t}$	1.15	1.10	0.95	0.96	8.00	7.80
$EEG_{3t}$	1.00	0.97	0.96	0.96	6.28	7.62
$EEG_{4t}$	1.05	1.02	0.98	0.97	7.87	9.31

The mean value for each parameter was obtained by averaging the results over thirty two waveforms. The results obtained were consistent with those obtained involving one set of EEG waveforms. Only JADE and extended-ICA were included in this analysis because they had performed significantly better than PCA and EOG subtraction methods when analysing one set of EEG and EOG channels.

#### 5.6. Key Observations of this Part of the Study

The key observations of the study reported in this chapter were:

- The devised procedures made it possible for the performances of the four algorithms for OA removal to be quantified and compared.
- However, although the transformation of the waveforms highlighted in section 5.4.2 was carried out purely for generating non-normally distributed source signals, one must reflect on the validity of performing such a transformation. Indeed such a situation cannot be applied to real-life signals as the original signal sources are not accessible in the real-life

situation. However, the aim was not to simulate a real-life problem, but rather to simulate a situation where four methods could be quantitatively assessed for performing OA removal of the EEG. In order to perform the assessment, the original signal sources needed to be known so that they could be compared to the recovered signals. Nonetheless the main drawback of the procedure was that it was to some extent biased into producing “ICA-friendly” signals. In a situation where the signals sources had Gaussian distribution, decorrelation-based techniques such as PCA may have performed better than ICA-based separation techniques to recover the EEG.

- The amplitude recovery method enabled the amplitude of the recovered EEG to be estimated for both JADE and extended-ICA. However, the results were affected by changing the values of the mixing matrix.
- The proposed correlation based method provided a means for dealing with the problems of channel permutation and sign changes problems associated with JADE and extended-ICA algorithms.
- JADE and extended-ICA performed significantly better than PCA. This could be because PCA only decorrelates signals while JADE and extended-ICA attempt to make the recovered signal components as independent as possible.
- The EOG subtraction attenuated the recovered EEG signals. This is because a fraction of the EEG that contaminates the EOG signal is also subtracted from the recovered EEG component.
- Extended-ICA method required a significantly longer time to carry out the OA removal operation when compared with JADE. This is because extended-ICA is an iterative algorithm which requires a number of passes through its learning algorithm to converge while JADE only requires one pass through its algorithm.
- Statistical tests showed that on average the performances of JADE and extended-ICA for OA removal were not significantly different. However JADE provided a more consistent set of results and both JADE and extended-ICA performed significantly better than PCA and EOG subtraction.
- The performances of the four OA removal methods were not significantly affected by an additive Gaussian noise source for a signal-to-noise ratio above 50.

## 5.7. Conclusion

A procedure for quantifying the effectiveness of an algorithm for removing OA from the EEG was devised. This enabled the similarity between the EEG waveforms before contamination by OA and the contaminated EEG waveforms following their processing by an OA removal method to be measured. Four methods for OA removal were included in the study. These were the two ICA-based algorithms of extended independent component analysis (ICA) and joint approximation diagonalisation of eigen-matrices (JADE), the principal component analysis (PCA) technique and the EOG subtraction method. The operation of JADE and extended-ICA is subject to amplitude scaling and channel permutation. Procedures were incorporated to estimate the amplitude of the recovered EEG waveforms and to allocate them to the correct channels.

It was demonstrated that the signal separation techniques of JADE and extended-ICA were more effective than EOG subtraction and PCA for removing OA from the EEG. EOG subtraction method was shown to cause attenuation of the recovered EEG waveforms. The effect of additive Gaussian noise on the performance of the four OA removal methods was also investigated. This indicated that the performance of the methods was unaffected by an additive Gaussian noise source as long as the signal-to-noise ratio remained above 50.

This part of the study has demonstrated that the ICA-based signal source separation techniques of JADE and extended-ICA are valuable methods for OA removal of the EEG.

However, care must be taken when interpreting the results of the study. The validity of such results can only be appreciated within the context of the procedure developed and used to assess the four methods for performing OA removal of the EEG. In a situation where the source signals had different (i.e. non ICA-friendly) distributions, the ICA-based separation methods may have performed poorly as compared to the decorrelation-based methods.

# **Chapter 6. The Effect of Signal Length on the Performance of Independent Component Analysis for Extracting the Lambda Wave**

## **6.1. Chapter Summary**

The effect of signal length on the performance of a signal source separation method called independent component analysis of Bell and Sejnowski (BS\_ICA) for extracting a visual evoked potential called the lambda wave from saccade-related electroencephalogram (EEG) waveforms was investigated. The methodology and results obtained are discussed in this chapter. An iterative synchronisation procedure was devised to time-synchronise the recorded waveforms across the recorded trials. The implementation details of the devised procedures are provided. Results for both the artificially generated mixtures as well as the recorded EEG and EOG waveforms are provided and compared.

## **6.2. Introduction**

The main saccade-related EEG component of interest in this study is a visual evoked potential (EP) called the lambda wave. An introduction to saccade-related data is provided in chapter 1, section 1.2. A detailed description of the lambda wave EP signal, together with its clinical attributes are provided in chapter 3, section 3.5.

For the EEG to conform to the stationarity requirement of BS\_ICA, the statistical properties of its components should be time invariant. However, EEG signal components (such as EPs) are short-duration (few hundred milliseconds) transient signals and may not fully conform to the stationarity assumption of BS\_ICA. In this chapter, a method is devised which enables the effective length of the recorded EEG traces to be increased prior to processing by BS\_ICA, so as to increase their stationarity pre-requisite. This involves abutting EEG traces from an appropriate number of successive trials (a trial is a set of waveforms recorded from 64 electrode locations in a experiment involving a saccade performance).

BS\_ICA was applied to the saccade-related EEG and electrooculogram (EOG) waveforms recorded from the electrode locations. The performance of BS\_ICA for extracting the lambda wave was assessed for different lengths of EEG waveforms. One spatial and five temporal features of the lambda wave were monitored to assess the performance of BS\_ICA applied to both abutted and not-abutted waveforms. A description of the theory of the ICA algorithm of Bell and Sejnowski (the algorithm used in this part of the study) is provided in chapter 2, section 2.6. The experimental methodologies are outlined and the results obtained are presented.

### **6.3. Experimental Method**

Details of the data recording procedures are provided in chapter 4, section 4.4.2.

#### **6.3.1. Pre-Processing Procedures**

The recorded data were digitally lowpass filtered at 45 Hz in order to remove any 50 Hz mains interference and the unwanted high frequency signal components. The baseline for each waveform was adjusted by calculating the mean of the pre-stimulus section and subtracting it from the whole waveform. The trials were sorted into their respective directions of saccade and time-synchronised using a procedure described in the next section.

#### **6.3.2. Iterative Time-Synchronisation Operation and its Evaluation**

Temporal averaging of the waveforms across trials was carried out to reduce the effect of background EEG before processing by BS\_ICA (this is described in section 6.3.3). The lambda wave is time-locked to the eye-movement EOG waveforms. The initiation of the eye-movement (i.e. the saccade onset time) and its termination (saccade offset time) vary between trials. This means that the lambda waves from different trials are not time-synchronised. Therefore the averaging process would have produced a distorted waveform. In order to overcome this, an algorithm which time-synchronised the trials was devised. The algorithm ensured that the temporal features of the lambda wave from different trials were aligned to a single reference signal prior to averaging. The EOG waveform was chosen as the reference signal for the synchronisation process because the lambda wave

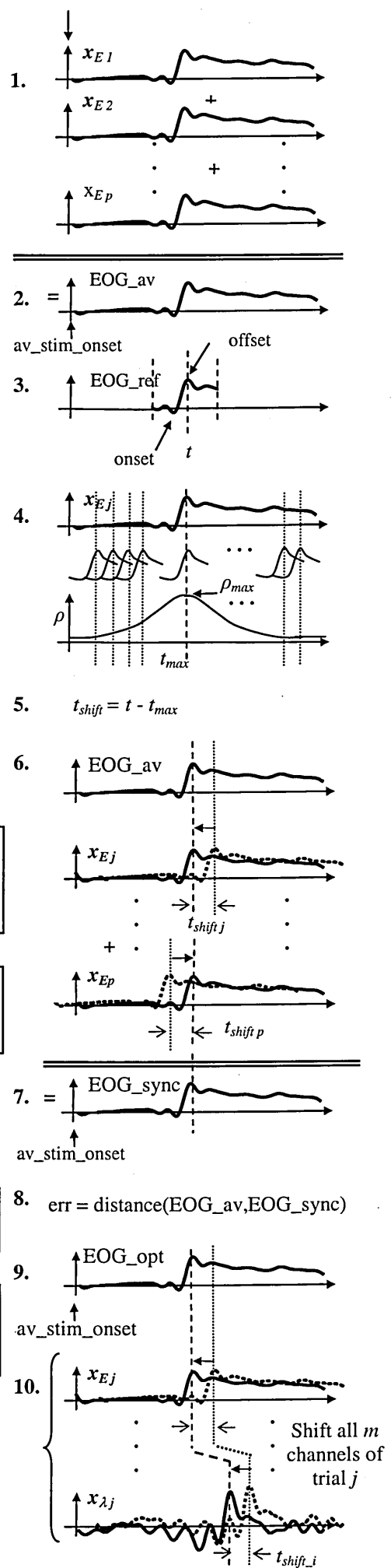
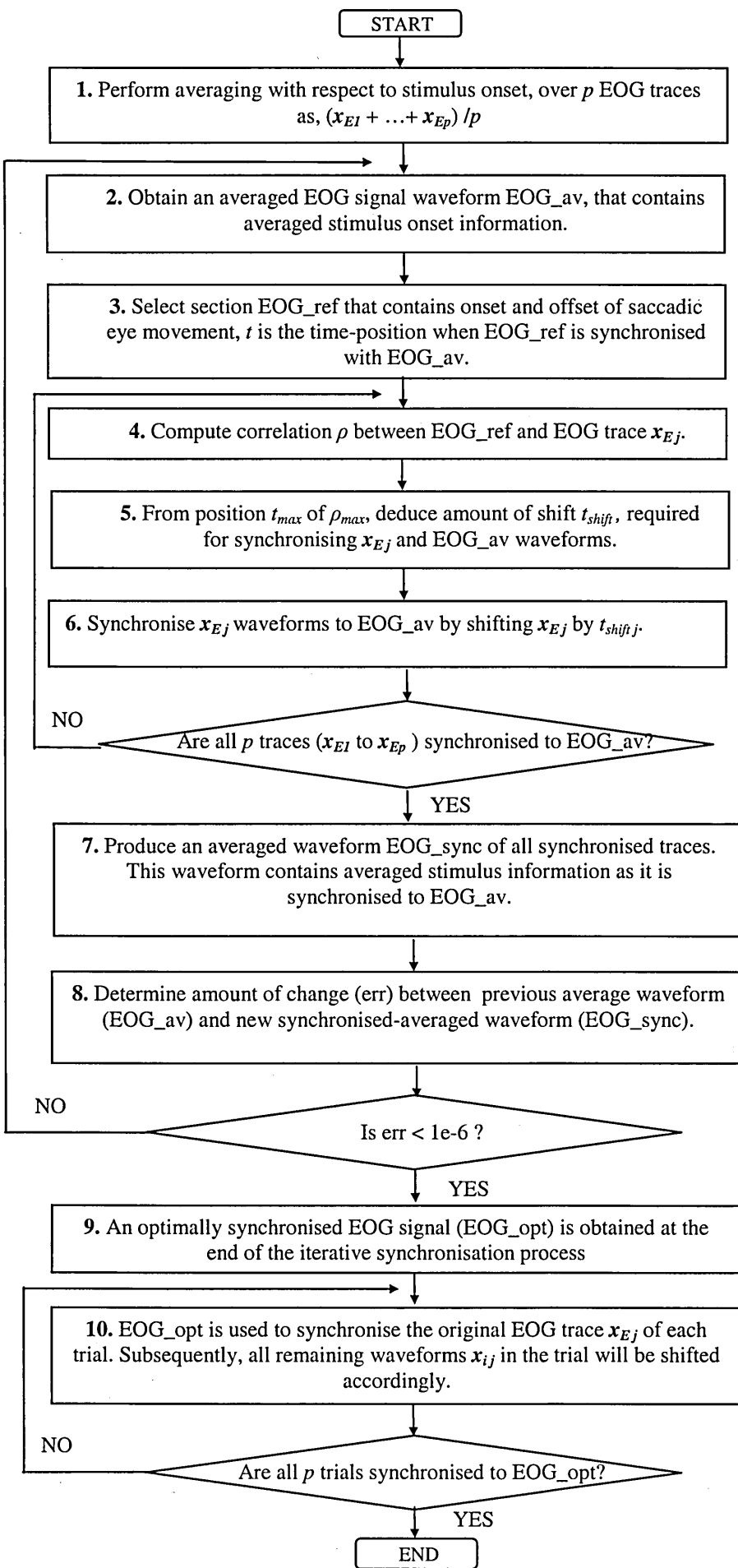
was time-locked to it. The operations involved when performing the time-synchronisation are outlined below.

- i The EOG waveforms across all trials for the desired event were averaged with respect to the stimulus onset. The resulting EOG waveform provided the averaged stimulus onset information.
- ii A section of the averaged EOG waveform which contained both the onset and the offset of the saccade was selected by the software as the reference signal.
- iii The reference signal and the EOG waveform from the trial being synchronised were correlated at each time point (sample value). The maximum correlation coefficient value between the two waveforms indicated the amount of shift required to synchronise the EOG waveform in that trial. This synchronisation was repeated for the EOG waveforms in the remaining trials.
- iv The newly synchronised EOG waveforms from all trials were then averaged. The resulting waveform retained the averaged stimulus onset information. Steps ii-iv (i.e. one iteration) were repeated until the reference signal did not change significantly from one iteration to the next. The changes in the reference signal from one iteration to the next was measured by computing the Euclidean distance between the corresponding waveforms. The synchronisation improved the alignment of EOG waveforms across all trials after each iteration.
- v The last iteration in the above process produced the required reference EOG signal. This signal was then correlated with the original (not synchronised) EOG waveform for each trial and the amount of shift required for their alignment was determined. All 64 waveforms in the corresponding trial were then time-shifted by the calculated amount. The algorithm therefore synchronised all waveforms in all trials to the reference EOG signal.

The iterative time-synchronisation operation is described using a flowchart and explanatory diagrams in Fig. 6.1. Let matrix  $X$  be a  $m \times p$  matrix that contains the recorded data waveforms  $x_{ij}$ , where  $i$  is the channel (electrodes) index, and  $j$  is the index of the trial number for the waveform  $x$ . Matrix  $X$  can therefore be written as,

$$X = \begin{bmatrix} x_{11} & \dots & x_{1j} & \dots & x_{1p} \\ \cdot & & \cdot & & \cdot \\ x_{i1} & \dots & x_{ij} & \dots & x_{ip} \\ \cdot & & \cdot & & \cdot \\ x_{E1} & \dots & x_{Ej} & \dots & x_{Ep} \\ \cdot & & \cdot & & \cdot \\ x_{m1} & \dots & x_{mj} & \dots & x_{mp} \end{bmatrix}, \quad \text{where } 1 < i < m \text{ and } i=E \text{ is the index of an EOG channel.}$$

**Fig. 6.1** Flowchart of the iterative time-synchronisation operation.



The performance of the time-synchronisation procedure was evaluated. This involved plotting the histogram of the saccade offset across the 50 trials for a given subject and experimental event. In order to determine the saccade offset of the EOG waveforms the following procedure was followed.

A visual inspection of the data recorded from the 7 subjects, indicated that it takes about 160 to 200 ms for a subject to start moving his/her eyes in response to the appearance of the stimulus at a new location on the checkerboard. Furthermore, it can be assumed that the saccade is complete within the following 300 ms [6.1]. The saccade offset corresponded to the largest peak in the eye-movement EOG waveform within this 300 ms time interval. In order to locate this peak, the first derivative of the eye-movement EOG waveform was computed as shown in Fig.6.2.

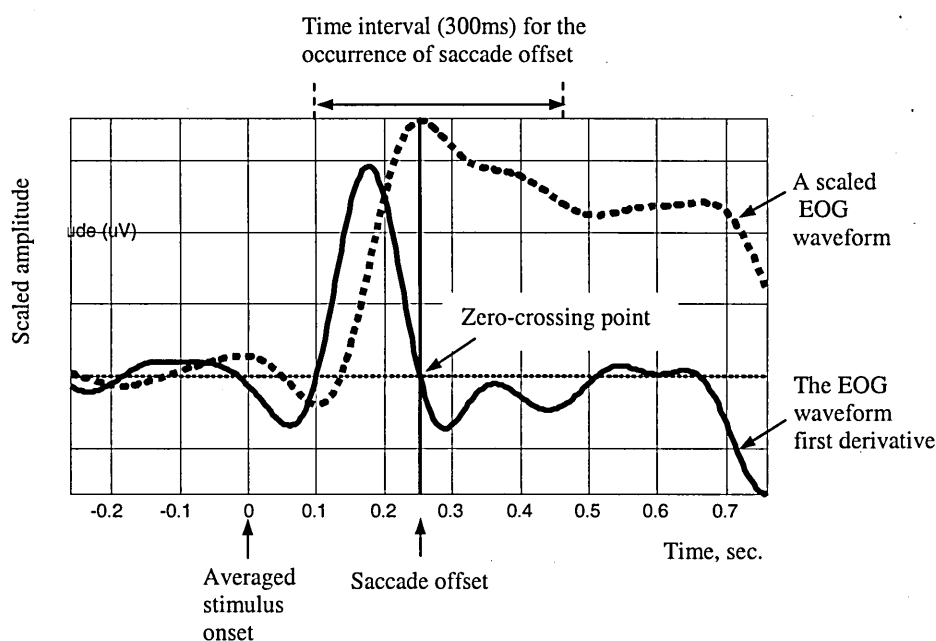


**Fig.6.2** Scaled eye-movement EOG waveform and its first derivative.

The maximum value of the derivative within the 300 ms time window was identified by a computer program. This corresponded to the highest gradient value of the EOG waveform within this time interval. The first zero-crossing after this peak represented the saccade offset for an EOG waveform of a given trial. The statistical distribution (histogram) of the saccade offsets across the 50 trials could then be obtained by repeating the procedure for each trial.

### 6.3.3. Averaging Process

Both spatial and temporal averaging of the waveforms were carried out. A description of each follows.

#### 6.3.3.1 Spatial Averaging

The saccade-related EEG waveforms recorded from the 64 channels were spatially averaged. This operation was carried out so as to reduce their number from 64 to 22 and to further enhance the features of the waveforms to enable the BS\_ICA algorithm to operate more effectively. The operation involved averaging together the waveforms from channels close to the international 10-20 system of electrode site placement as denoted by the regions circles by dashed lines in Fig.6.3a. This operation resulted in 20 EEG waveforms obtained from the 20 locations highlighted by the alpha-numeric numeric designation of electrodes placement in Fig.6.3b, and 2 EOG waveforms ( $EOG_L$  and  $EOG_R$  for the left and right sides respectively) which were then used as input to BS\_ICA. The 22 resulting locations were symmetrically distributed on the left and right hemispheres of the scalp, with respect to the nasion-inion line and the pre-auricular line ( $A_1$ - $A_2$ ), according to the conventional scheme shown in Fig.6.3b. Details of the electrodes placement and designation are provided in chapter 4, section 4.2.

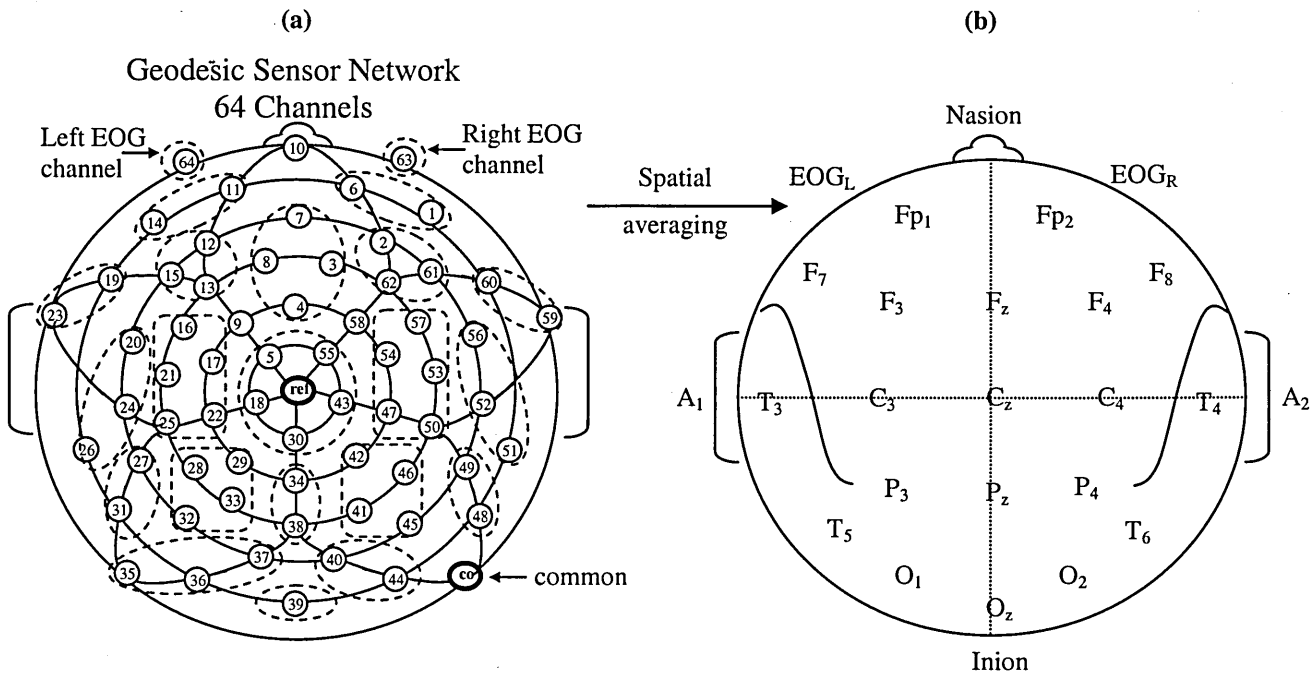


**Fig.6.3** Spatial averaging operation: (a) the Electrical Geodesics sensor network of 64 electrodes and (b) the International 10-20 system of electrode placement with the alpha-numeric designation of electrodes placement on the scalp for the EEG.

### 6.3.3.2 Temporal Averaging

This was performed to reduce the obscuring effect of the background EEG on the EP component of interest (i.e. the lambda wave). For evaluation purposes, temporal averaging was carried out in three forms:

- i) Not-abutted, averaged waveforms without time-synchronisation. This involved obtaining the mean of the waveforms for each channel across the 50 trials.
- ii) Not-abutted, averaged waveforms with time-synchronisation. This was similar to the first form except that the waveforms were time-synchronised prior to averaging.
- iii) Abutted, averaged waveforms with time-synchronisation. This involved abutting time-synchronised waveforms from a suitable number of successive trials and then obtaining the mean. The number of trials abutted were determined experimentally as described in the Analysis Procedure section.

### 6.3.4. Whitening Process and Application of BS\_ICA

The averaged waveforms were whitened. Whitening is a process which makes the mixtures mutually uncorrelated as well as ensuring they have unity variance [6.2]. By decorrelating the data beforehand, BS\_ICA can concentrate on the higher-order statistical dependencies of the waveforms.

BS\_ICA has a number of parameters which need to be initialised. One of these is the learning rate ( $\eta$ , described in chapter 2, section 2.6). It was experimentally found that a value of  $5 \times 10^{-4}$  was an appropriate initial value for this parameter. The value of  $\eta$  was gradually decreased during the learning process until the rate of change was less than  $1 \times 10^{-6}$ . The weight matrix ( $W$ ) was initialised to the identity matrix and then updated during the learning process by the amounts  $\Delta W$  and  $\Delta W_o$  using equations (2.50) and (2.61) respectively. The training of BS\_ICA stopped when the value of  $\Delta W$  became less than a predefined small value ( $1 \times 10^{-9}$ ).

### 6.3.5. Backprojection of the Separated Components

The whitened waveforms were then input into BS\_ICA. The resulting BS\_ICA time series were back-projected to the 22 scalp locations (i.e. the 10-20 international EEG and EOG electrode placement locations) in order to obtain their scalp distributions. This involved multiplying the inverse of the unmixing matrix ( $W$ ) by the BS\_ICA time series to obtain an estimate of the contributions of the separated components at each of the 22 scalp locations.

A procedure was devised to assess the effectiveness of BS\_ICA for determining the scalp distribution of the lambda wave. This estimated the percentage contribution of each BS\_ICA-extracted component to the expected region of the scalp associated with the lambda wave (i.e. parieto-occipital). The procedure used is outlined below.

- i) The estimated contributions of each extracted component to all electrode sites were normalisation between 0 and 1.
- ii) The sum ( $S_t$ ) of the resulting contributions was obtained.
- iii) The sum ( $S_\lambda$ ) of the contributions for the parieto-occipital area of the cerebral cortex (i.e. region defined by the 8 electrodes P<sub>3</sub>, P<sub>4</sub>, P<sub>z</sub>, O<sub>1</sub>, O<sub>2</sub>, O<sub>z</sub>, T<sub>5</sub> and T<sub>6</sub>, as shown in Fig.6.3b) was calculated.
- iv) The required percentage contribution was then determined as  $S = (S_\lambda/S_t) \times 100$ .

### 6.3.6. Analysis Procedure

The analysis was initially carried out on artificially mixed waveforms. This allowed the approaches to be quantitatively assessed. The analysis was then extended to the 22 spatially and temporally averaged waveforms (described in section 6.3.3). The details of these analysis are provided next.

For the artificially mixed signals, the 22 averaged waveforms were visually inspected and two waveforms were selected. These two waveforms were selected from different subjects to ensure their independence. One waveform was an EEG waveform with the temporal features of the lambda wave (as described in the literature such as [1.5]). The other was an eye-movement EOG waveform (recorded from EOG<sub>L</sub> site in Fig. 6.3b). Different lengths of averaged waveforms were produced by abutting successive trials (described in section 6.3.3). The abutted EEG and EOG waveforms for waveform length corresponding to 3 trials are shown in Figs.6.4 and 6.5 respectively. EOG can be hundreds of microvolts in

magnitude and contain the signal components caused by blinks and eye-movements. The EOG waveforms shown in Fig.6.5 are caused by eye movements. The magnitude of this type of EOG is affected by the amount which the eyes are moved when performing saccade (i.e. the viewing angle defined in chapter 4, section 4.4.2 ). The viewing angle of 10 degrees used in this study causes a small deviation of the eyes, thus generating eye-movement waveforms of the range shown in Fig.6.5.

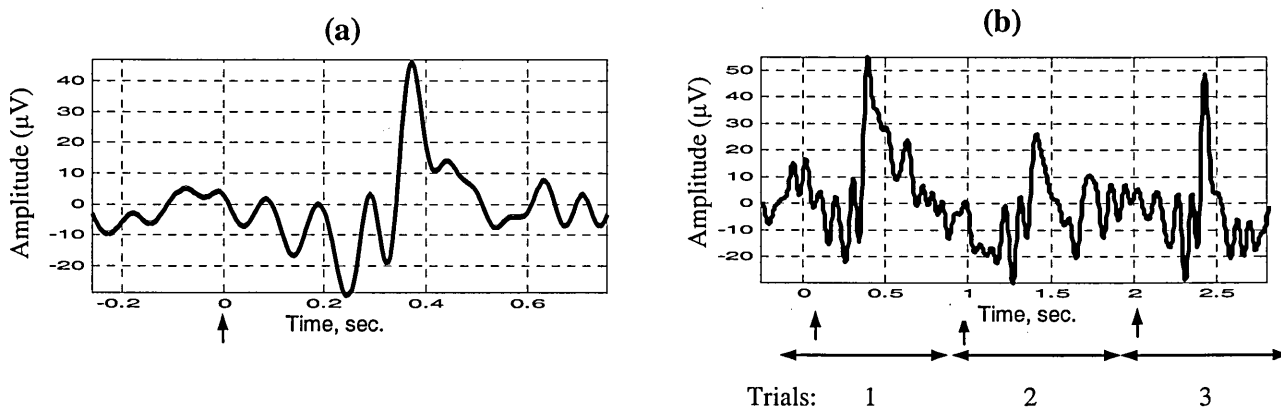


**Fig.6.4** Averaged EEG waveform with lambda wave features: (a) not-abutted, (b) abutted for 3 trials. Vertical arrow indicates the average stimulus onset.

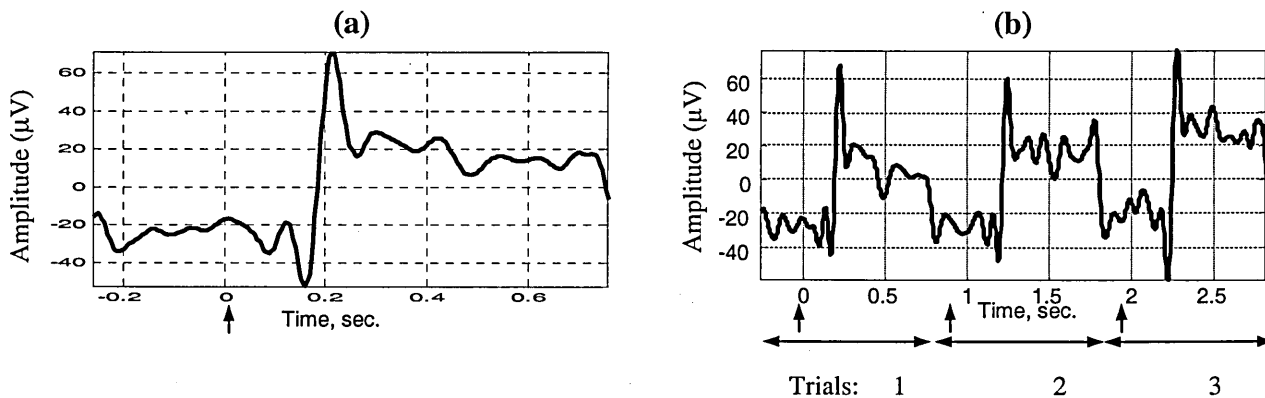


**Fig.6.5** Averaged eye-movement EOG waveform: (a) not-abutted, (b) abutted for 3 trials. Vertical arrow indicates the average stimulus onset.

The Univariate statistical procedure [5.25] was used to test the Gaussianity of the selected EEG and EOG signals. The Univariate procedure tested the null hypothesis that the input data values were a random sample from a normal distribution. In order to decide whether to reject the null hypothesis of the test for normality, it was necessary to examine the probability associated with the test statistic (i.e. the probability value for Shapiro-Wilk statistic). The value obtained was less than 0.05 (i.e. 95% confidence level) for all four

waveforms (the not-abutted and abutted time-synchronised averaged EEG and EOG waveforms). Therefore the null hypothesis was rejected and it was concluded that the four waveforms were not significantly Gaussian.

Artificial mixtures were generated by carrying out the matrix operation,

$$\begin{pmatrix} EEG_m \\ EOG_m \end{pmatrix} = \begin{pmatrix} a_{11} & a_{12} \\ a_{21} & a_{22} \end{pmatrix} \begin{pmatrix} EEG \\ EOG \end{pmatrix} \quad (6.1)$$

Where *EEG* and *EOG* were the original signal sources, *EEG<sub>m</sub>* and *EOG<sub>m</sub>* were the resulting mixtures, and *a<sub>11</sub>* and *a<sub>12</sub>* were the mixing coefficients for the EEG signal, and *a<sub>21</sub>* and *a<sub>22</sub>* were the mixing coefficients for the EOG signal. ICA algorithm of Bell and Sejnowski (BS\_ICA) [1.9] was applied to unmix the mixtures. The effect of signal length on the performance of BS\_ICA was investigated by gradually increasing the length of averaged waveforms from 256 data points (corresponding to 1 trial) to 1536 data points (corresponding to 6 abutted trials). This was carried out for a number of mixing coefficients shown in Table 6.1.

**Table 6.1** The mixing coefficients used to generate the EEG mixtures.

<i>a<sub>11</sub></i>	0.55	0.65	0.75	0.85
<i>a<sub>12</sub></i>	0.45	0.35	0.25	0.15

The EOG mixing coefficients were *a<sub>21</sub>* = 1 - *a<sub>11</sub>* and *a<sub>22</sub>* = 1 - *a<sub>12</sub>*. The gradual increase of the waveforms' length was carried out in such a way that each waveform always contained an integer number of lambda wave section. Indeed, as the lambda wave occurred within the 500 ms time interval following the onset of the stimulus, the abutting process ensured that the end point of the resulting abutted trials did not lie within the this 500 ms window.

The similarity between the original and recovered waveforms was quantified by calculating the following parameters.

- i Correlation coefficient ( $\rho$ ). The value of  $\rho$  is between -1 and 1. Zero indicated no similarity while -1 and 1 indicated 100% similarity in shape (-1 meant an inversion in polarity of the extracted component).

ii Euclidean distance ( $\varepsilon$ ). This provided a measure of similarity in both magnitude and shape of the waveforms and was calculated by,

$$\varepsilon = \sqrt{\sum_{i=1}^L (o(i) - r(i))^2} \quad (6.2)$$

where  $o(i)$  and  $r(i)$  were the original and recovered signals respectively and  $L$  was their length.

### 6.3.7 Summary diagram for the data processing and analysis procedures

A prototype data processing tool was developed and implemented in MATLAB 5.3 software development tool [6.3] for the processing and analysis of the data recorded from the Electrical Geodesic Inc. system [4.2]. The main data processing and analysis procedures operations are outlined in a block diagram in Fig.6.6.

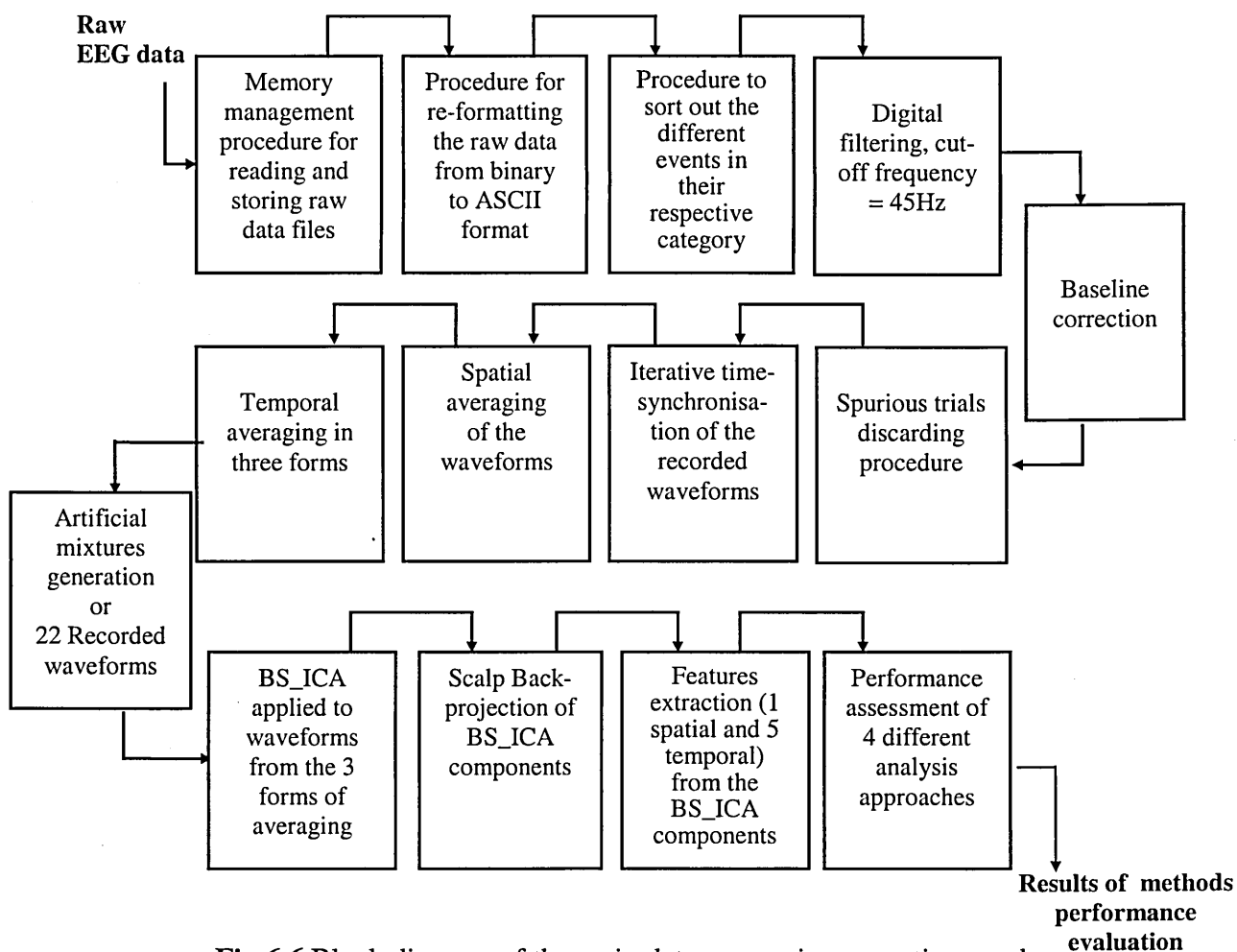
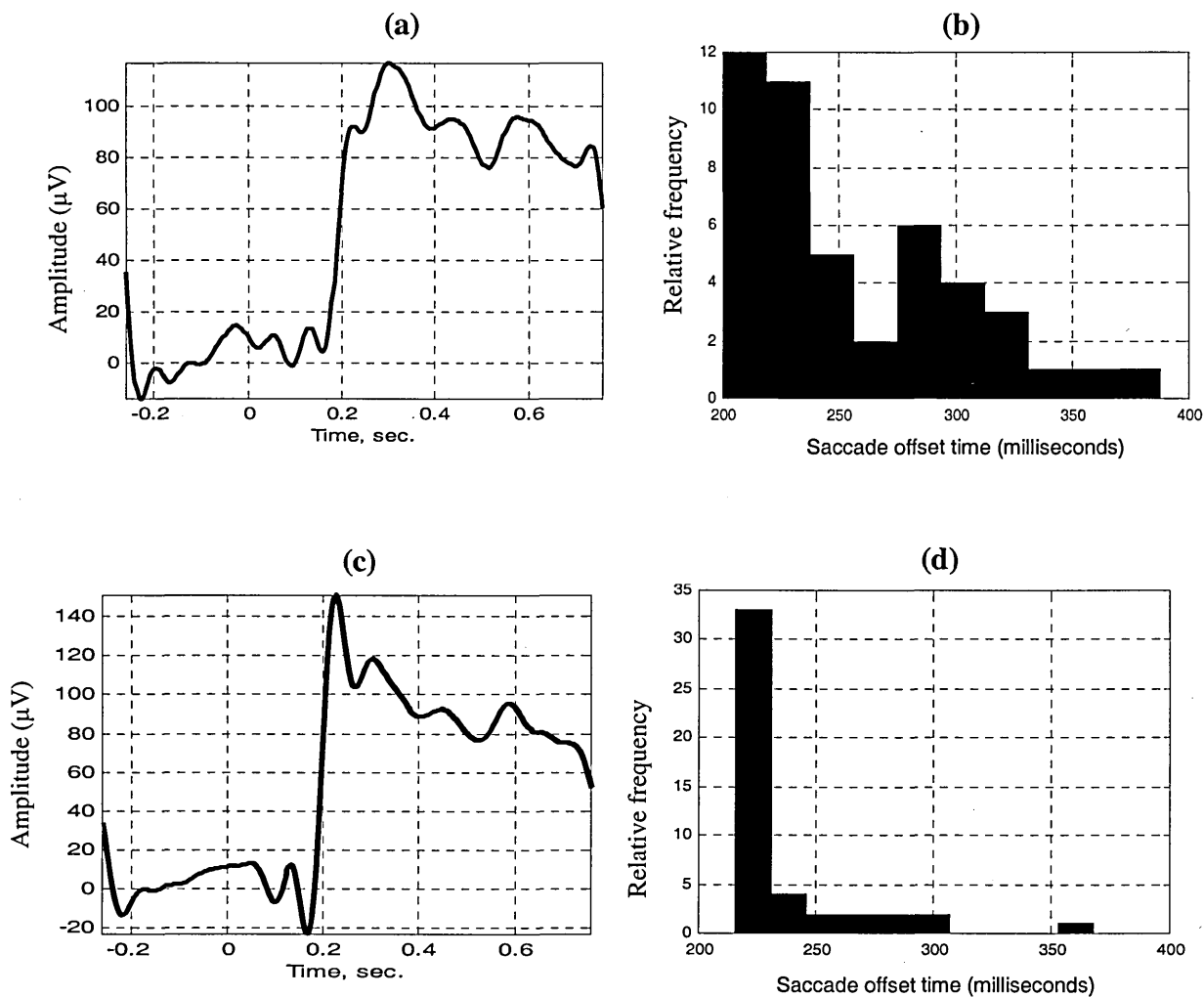


**Fig.6.6** Block diagram of the main data processing operations and analysis procedures.

## 6.4. Results and Discussion

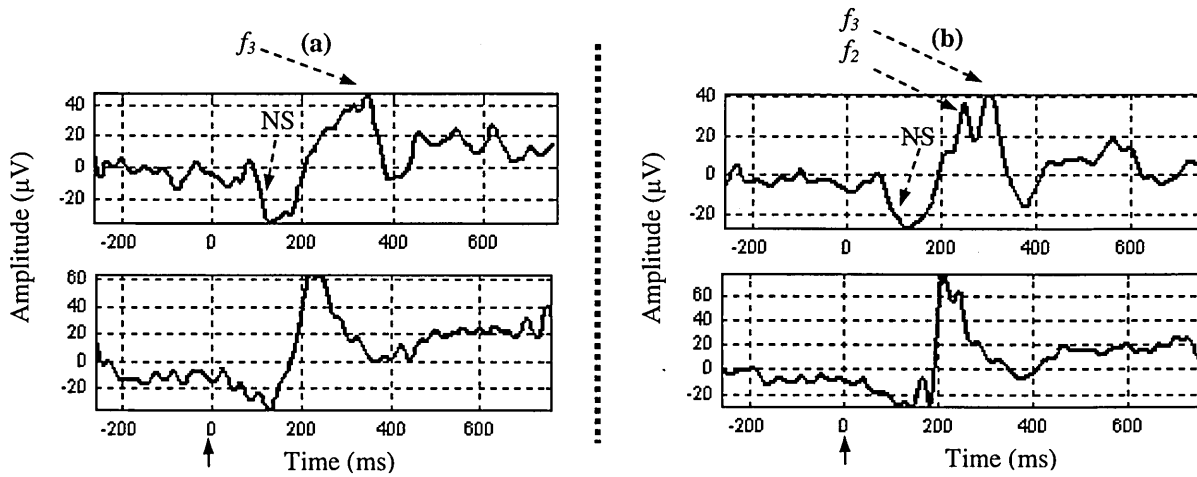
### 6.4.1. Iterative Time-Synchronised Averaging

Fig.6.7a shows an typical average of 50 eye-movement EOG waveforms prior to iterative synchronisation. Fig.6.7b shows the histogram (distribution) of the saccade offsets of the EOG waveforms. The saccade offset of each trial was determined using the procedure described in section 6.3.2. Figs.6.7c and d show the same information once the iterative synchronisation has been performed. It can be observed that the process has reduced the deviation of the saccade offset distribution and thus provided a less distorted averaged EOG waveform.



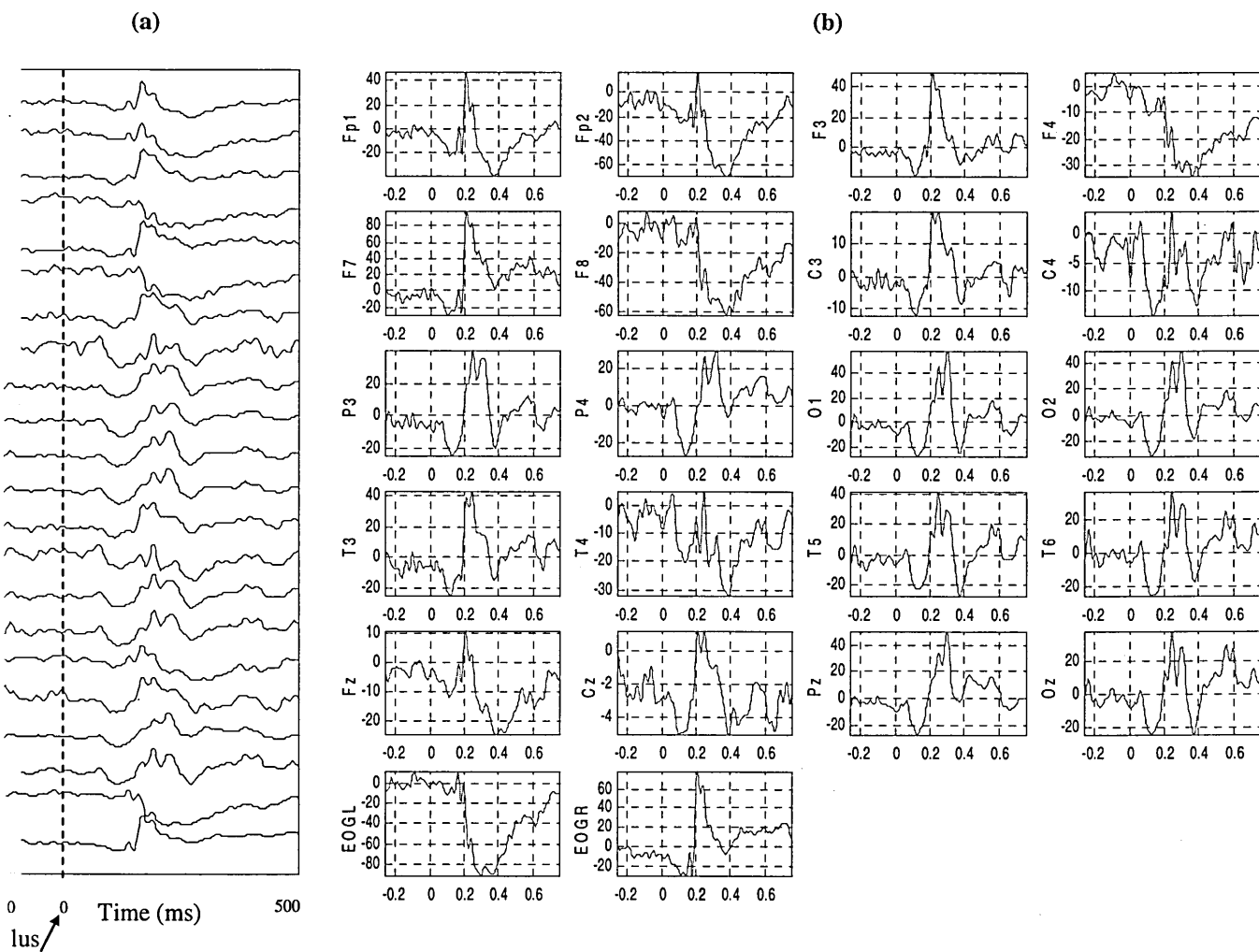
**Fig.6.7** (a) The averaged eye-movement EOG waveform before synchronisation, (b) the saccade offsets distribution. (c) the averaged eye-movement EOG waveform after synchronisation, (d) the saccade offsets distribution.

Fig.6.8a shows the averaged lambda wave (over 50 trials) without time-synchronisation together with its eye-movement EOG waveform. The waveforms following iterative synchronisation are shown in Fig.6.8b. The process of iterative synchronisation resulted in the extraction of the lambda wave feature  $f_2$  which was not visible in the averaged lambda wave without time-synchronisation. The significance of the features  $f_2$ ,  $f_3$  and negative shift (NS) which are shown in Fig.6.8 are outlined in section 6.4.3.



**Fig.6.8** The lambda wave (top) and eye-movement EOG waveform (bottom) obtained by (a) averaging without time-synchronisation, (b) averaging with time-synchronisation. The vertical arrow indicates the average stimulus onset.

Fig.6.9 shows the full set of 22 spatially and temporally time-synchronised averaged waveforms obtained for the 22 electrode locations for a typical subject's event recording. Fig.6.9a shows the waveforms displayed in a clinical format, i.e. normalised waveforms placed on top of each other shown together with their associated electrode name (as described in Fig.6.3b), in order to show the time relation between the waveforms. Fig.6.9b shows the non-normalised waveforms together with their amplitude range (in microvolts) and time course (in second) information. These waveforms are a typical set of waveforms used as input to BS\_ICA signal source separation algorithm.



**Fig.6.9** The 22 averaged waveforms displayed (a) in a clinical format and (b) with their amplitude range and time-course information. In (b), the vertical axis is in microvolts and the horizontal axis is in second.

#### 6.4.2. BS\_ICA Applied to Artificial Mixtures

Figs.6.10a and b show the effect of signal length on BS\_ICA performance when the artificially mixed waveforms were processed. The points on the graphs correspond to the mixing ratios indicated in Table 6.1. The effectiveness of BS\_ICA for extracting the EEG waveform from the mixtures gradually improved (i.e.  $\rho$  closer to 1,  $\varepsilon$  closer to 0) when the signal length was increased (by abutting process) from 256 data points (i.e. 1 trial) to 1024 data points (i.e. 4 trials).

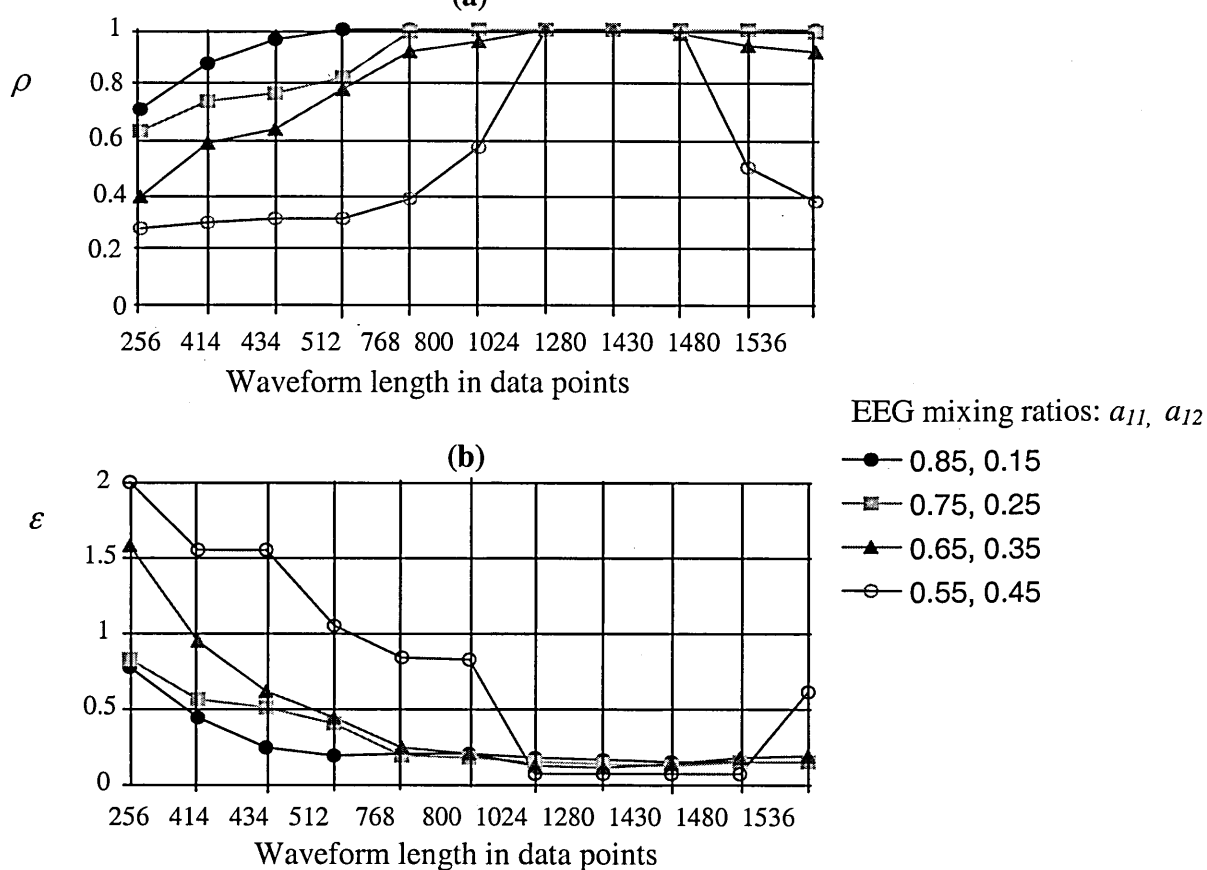


**Fig.6.10 (a)** Correlation coefficient values and **(b)** Euclidean distance values, between the original and recovered EEG waveforms.

The components of the artificially generated signal mixtures (i.e. the EOG waveform and the EEG waveform with main lambda wave characteristics) are short-duration transient signals. The abutting of the waveforms to increase their lengths improved their stationarity. As BS\_ICA relies on the stationarity of the signals, the abutting process therefore provided a means to make the waveforms more suitable for processing by BS\_ICA. For waveforms greater than 1024 data points, no further improvement was observed.

Consistent observations with the above results were made for the extracted eye-movement EOG waveform and the results are summarised in Table 6.2 and Fig.6.11. Correlation coefficient values and Euclidean distance values were obtained for the EOG waveform for the 4 mixing ratios indicated in Table 6.1. However, it was observed that the different mixing ratios did not affect significantly the values of the correlation coefficient and the Euclidean distance obtained for each waveform length. Therefore the mean values across the 4 mixing ratios were obtained at each waveform length for both parameters (correlation and euclidean distance) and the results are summarised in Table 6.2.

**Table 6.2** Mean and standard deviation (std) values (across the four mixing ratios) for  $\rho$  and  $\varepsilon$  (in  $\mu\text{V}$ ) for different lengths of waveforms.

EOG Waveform lengths	Performance Measure			
	$\rho$		$\varepsilon$	
	Mean	Std	Mean	Std
256	0.976	0.020	0.813	0.934
414	0.984	0.022	0.540	0.715
434	0.981	0.018	0.556	0.721
512	0.995	0.005	0.217	0.180
768	0.997	0.004	0.258	0.140
800	0.998	0.002	0.222	0.085
1024	0.997	0.001	0.120	0.045
1280	0.995	0.002	0.120	0.041
1430	0.994	0.005	0.128	0.055
1480	0.997	0.002	0.155	0.074
1536	0.997	0.004	0.183	0.101

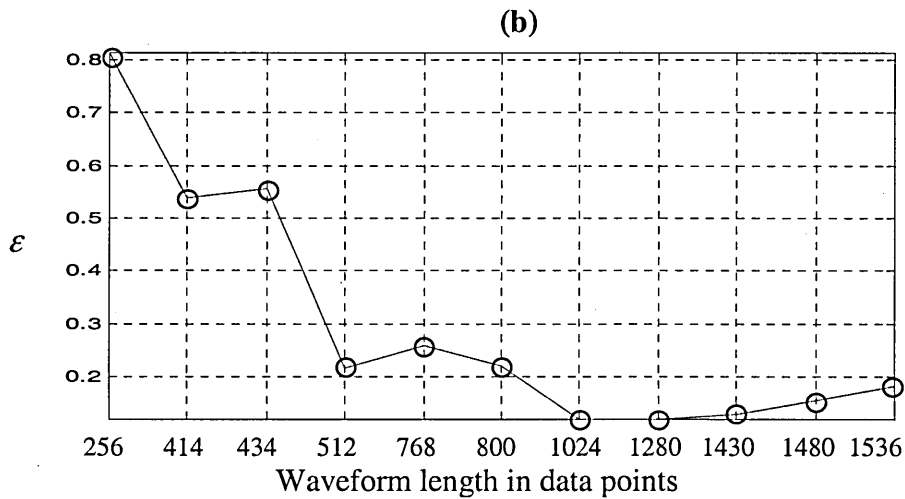
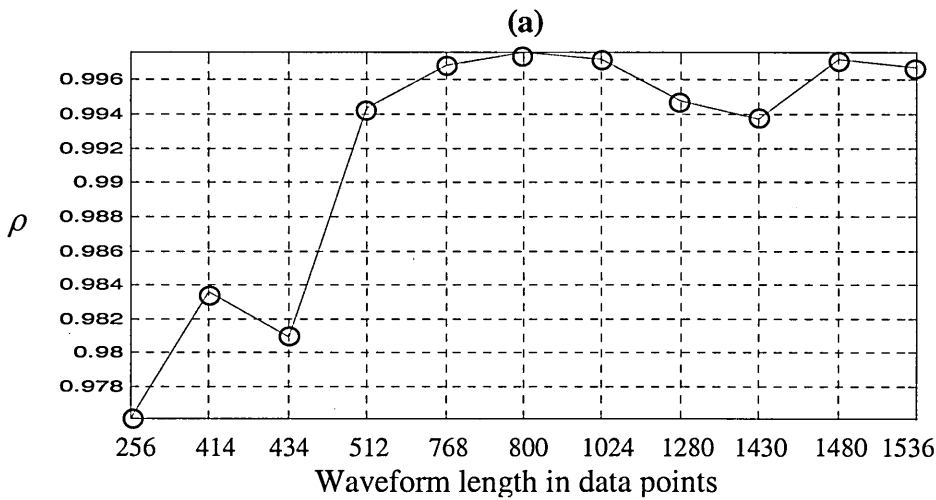


**Fig.6.11** (a) Mean Correlation coefficient values and (b) mean Euclidean distance values, (across the four mixing ratios), between the original and recovered EOG waveforms.

The mean and standard deviation (std) values (across the four mixing ratios) for  $\rho$  and  $\varepsilon$  are given in Table 6.2. Plots of the means (indicated in Table 6.2) are shown in Figs.6.11a and b, for  $\rho$  and  $\varepsilon$  respectively. Figs.6.11a and b indicated that the effectiveness of BS\_ICA for extracting the eye-movement EOG waveform from the mixtures gradually improved (i.e.  $\rho$  closer to 1,  $\varepsilon$  closer to 0) when the signal length was increased (by the abutting process) from 256 data points (i.e. 1 trial) to 1024 data points (i.e. 4 trials).

It was observed that the variation in the mixing ratios affected the recovery of EEG waveform whereas it did not affect the recovery of EOG waveform. Fig 6.10 indicated that the recovery of the EEG waveform was degraded as the contamination of the EEG by the EOG (i.e. larger  $a_{11}$  and smaller  $a_{12}$ ) increased. The recovery of the EOG waveform remained unaffected.

### **6.4.3. BS\_ICA Applied to 22 Spatially and Temporally Averaged Waveforms**

In this section the results of applying the BS\_ICA-based approaches to 22 spatially and temporally averaged waveforms are presented.

#### **6.4.3.1. BS\_ICA extraction of three saccade-related EPs components**

A preliminary study was carried out to investigate the BS\_ICA algorithm when applied to the recorded saccade-related waveforms. In this preliminary study, BS\_ICA was applied to not-abutted time-synchronised averaged waveforms. This enable the extraction of a number of EPs components related to the performance and generation of saccadic eye movements, and their scalp distribution to be obtain. These were: the frontal and occipital pre-saccadic potentials, and the lambda wave.

The results for the centre-to-left saccade event of a typical subject are presented in this section. Figs.6.12-6.16 show the extracted BS\_ICA components for this subject, however similar waveforms were observed in the other subjects. The colour shading reflects the relative strength of an extracted component at various scalp regions.

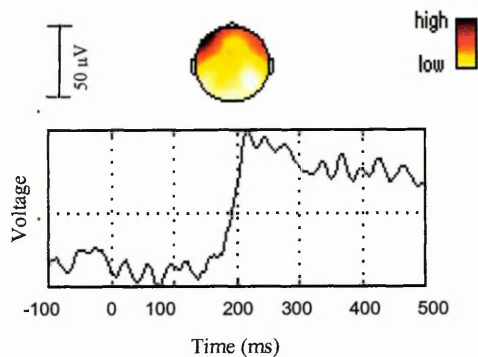


**Fig.6.12** The extracted  $EOG_L$  waveform.

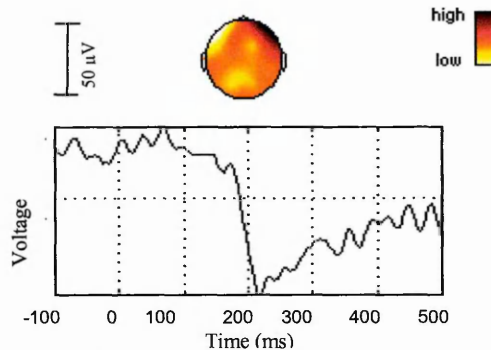


**Fig.6.13** The extracted  $EOG_R$  waveform.

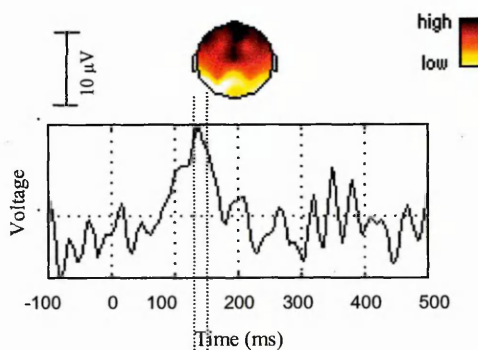


**Fig.6.14** The pre-saccadic potential extracted in the frontal area.

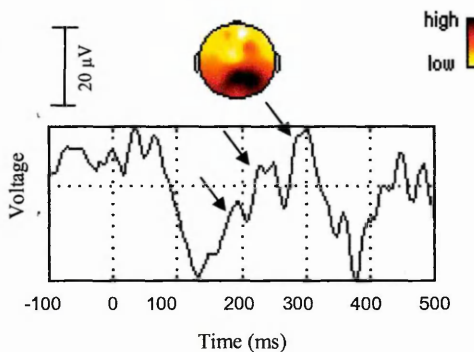


**Fig.6.15** The lambda wave component.

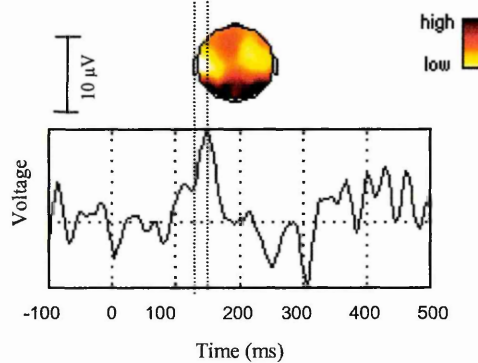


**Fig.6.16** The pre-saccadic potential extracted in the occipital area.

In all figures, the onset of stimulus is shown at 0 ms. Fig.6.12 shows a component with peak activity close to the left eye. It had the characteristics of a saccadic eye movement because of its sharp transition at about 200 ms (saccade onset) after the stimulus onset. A similar component shown in Fig.6.13 was extracted from a region close to the right eye. Waveforms with similar time courses shown in Fig.6.9 are observed in the EOG channels, EOG right (EOG<sub>R</sub>) and EOG left (EOG<sub>L</sub>). The extraction of these components indicated that the method successfully isolated the EOG waveforms caused by eye movements. Fig.6.14 and 6.16 shows two potentials extracted from the frontal (top picture) and occipital (bottom picture) areas. These occurred shortly prior to the saccade onset. The frontal pre-saccadic potential is believed to be related to motor commands preceding voluntary saccades [3.28]. The occipital pre-saccadic potential was found to occur about 30 ms after the frontal one. This finding suggested that the occipital pre-saccadic potential is an efferent feedback or copy from the frontal areas for saccade generation. This is believed to be a prerequisite for visual stability during eye movements [1.7].

Fig.6.16 shows three sub-components (pointed to by arrows) extracted from the occipital area. These appeared immediately after the saccade onset and ended shortly after the saccade offset (about 300 ms after stimulus). These are associated with visual information processing triggered by the relative movement of visual field features across the retina during a saccade [1.5]. The fact that the occipital pre-saccadic potential and the following three sub-components were extracted separately suggested that they were generated by independent neural processes. This could not have been detected without the application of a signal source separation technique. Consistent results were obtained for 7 subjects.

This preliminary study highlighted some of the limitation of BS\_ICA algorithm when applied to EEG and EOG recorded waveforms. It was observed that BS\_ICA is sensitive to large differences in amplitudes ranges between the EEG and the eye-movement EOG signals. To this effect, prior to applying BS\_ICA to the waveforms, the amplitude range of the EOG signals and of the EEG signals recorded from channels close to the EOG electrodes location, were scaled down to the range of the recorded EEG signals (typically – 40 to +40 microvolts) in order to reduce the difference in amplitude between the waveforms. This was considered to be appropriate at this stage as only the time course of the components was of importance and the objective of this preliminary was to extract EPs of very small amplitude (when compared to amplitude of EOG amplitude). The effect of

various scaling range was investigated. It was ensured that the scaling range of the EOG always remained equal or greater than the range of the EEG signals because in a realistic situation, the EOG is seldom smaller in amplitude range than the EEG. Best results were obtained when the EOG were scaled down to the range of the recorded EEG signals.

This preliminary study indicated that the signal source separation of BS\_ICA was a valuable tool for extracting EPs from the recorded saccade-related waveforms. The results of this part of the study revealed valuable information about the brain mechanisms involved in performing saccades. It also highlighted some of the limitation of BS\_ICA algorithm when applied to EEG and EOG recorded waveforms.

#### **6.4.3.2. The effect of signal length on the performance of BS\_ICA for extracting the lambda wave**

In this section, BS\_ICA was applied to the spatially and temporally time-synchronised waveforms but no scaling operation was performed on the waveforms prior to input to BS\_ICA, as such procedure may distort the amplitude relation between the signals.

As a finite number of trials had been recorded (i.e. 50 trials per subject), increasing the number of trials for the abutting process would have resulted in the averaging being carried out over a smaller number of trials, thus reducing the ability to attenuate the background EEG prior to BS\_ICA operation. It was decided to set the length of the abutted waveforms to 3 trials. This was considered to be a reasonable compromise for satisfying these two criteria. Once the components were extracted by BS\_ICA, a further averaging across the trials was carried to produce a single lambda wave.

Fig.6.17 shows typical BS\_ICA-extracted lambda waves (top row) and left-eye eye-movement waveform (bottom row) together with their corresponding scalp distributions, for the not-abutted (a and b) and abutted (c and d) time-synchronised averaged approaches. Similar results were obtained for the other subjects and the results when assessing the methods for all subjects are summarised later in this section.

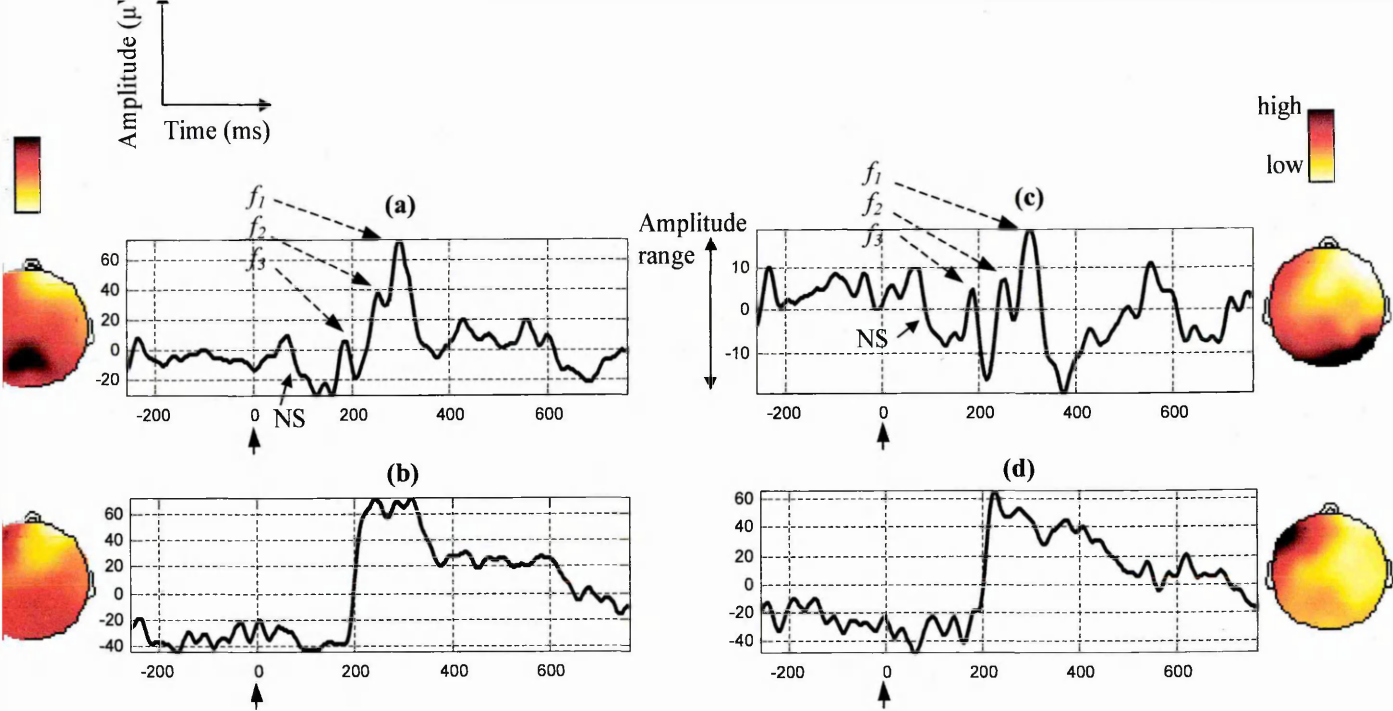


**Fig.6.17** BS\_ICA-extracted lambda waves (top row) and eye-movements (bottom row) together with their respective scalp distributions for ((a), (b)) the not-abutted and ((c), (d)) the abutted approaches. The vertical arrow indicates the average stimulus onset.

The followings are the main observations of this part of the study:

- BS\_ICA managed to extract the lambda wave and the eye-movement waveform when it was applied to both abutted and not-abutted averaged time-synchronised waveforms. However, the features of the lambda wave extracted when BS\_ICA was applied to the abutted waveforms were preserved more accurately. The features considered for this evaluation were  $f_1$ ,  $f_2$  and  $f_3$ , and the pre-saccadic negative shift (NS) (negative shift in the EEG which appears from the onset of the stimulus and ends once the saccade is performed). The features  $f_1$ ,  $f_2$  and  $f_3$  are believed to be related to the movement of the visual field across the retina [1.5]. The features  $f_1$  and  $f_2$  were reported to be time-locked to the onset of the saccade and the feature  $f_3$  to be time-locked to the offset of the saccade [1.5]. The characteristics of these features depend on factors such as the saccade duration or the viewing angle ( $\alpha$ , shown in Fig.4.5 in chapter 4). In our study, where a short duration of saccade (about 20 ms) was used, we did not observed the feature  $f_1$  in either time-synchronised or not time-synchronised averaged lambda waves (see Fig.6.8b). This was in accordance with the observations made in [1.5]. However, in our study this feature became visible when BS\_ICA was applied to either not-abutted or abutted time-synchronised averaged waveforms. The feature  $f_1$  was observed

by [1.5] only in the averaged EEG waveform of a subject for a longer duration of saccade (75 ms to 100 ms).

- Table 6.3 contains a summary of the analysis results across the 7 subjects for the temporal features NS,  $f_1$ ,  $f_2$  and  $f_3$  when assessing the methods to recover the lambda wave component.

**Table 6.3** Summary of the analysis results for the temporal features of the lambda wave when assessing four methods to recover the lambda wave component.

Methods	Lambda wave temporal feature			
	NS	$f_1$	$f_2$	$f_3$
Not-abutted, averaged waveforms without time-synchronisation	7	1	1	1
Not-abutted, averaged waveforms with time-synchronisation	7	2	5	4
BS_ICA applied to not-abutted, averaged waveforms with time-synchronisation	7	4	6	6
BS_ICA applied to abutted, averaged waveforms with time-synchronisation	7	7	7	7

The methods were:

- Not-abutted, averaged waveforms without time-synchronisation.
- Not-abutted, averaged waveforms with time-synchronisation.
- BS\_ICA applied to not-abutted, averaged waveforms with time-synchronisation.
- BS\_ICA applied to abutted, averaged waveforms with time-synchronisation.

An expert familiar with the features of the lambda wave inspected the recovered lambda waves for each method. Four features of the recovered lambda waves (NS,  $f_1$ ,  $f_2$  and  $f_3$ ) were monitored for their visibility. Table 6.3 contains the number of subjects in which each feature was observed for each method. The NS feature was observed in all 7 subjects for all 4 methods. The averaging method without time-synchronisation was least effective, as with this method, each one of the features  $f_1$ ,  $f_2$  and  $f_3$  were observed only once across the 7 subjects. Averaging with time-synchronisation was more effective than averaging without synchronisation, as the method managed to preserve features  $f_1$ ,  $f_2$  and  $f_3$  in 2, 5 and 4 subjects respectively. The results were further improved when BS\_ICA was applied to not-abutted time-synchronised averaged waveforms. The method successfully extracted features  $f_1$ ,  $f_2$  and  $f_3$  in 4, 6 and 6

subjects respectively. The best performance was achieved when BS\_ICA was applied to the abutted time-synchronised averaged waveforms as the features  $f_1$ ,  $f_2$  and  $f_3$  were visible in all 7 subjects.

- Table 6.4 contains a summary of the analysis results across the 7 subjects for the scalp distribution (spatial feature) and the amplitude range when assessing the four methods to recover the lambda wave.

**Table 6.4** Summary of the analysis results for the scalp distribution and amplitude range features when assessing four methods to recover the lambda wave component (std = standard deviation).

Methods	Percentage Scalp distribution (%)		Amplitude Range ( $\mu$ V)	
	mean	std	mean	std
Not-abutted, averaged waveforms without time-synchronisation	--	--	48	13
Not-abutted, averaged waveforms with time-synchronisation	--	--	48	18
BS_ICA applied to not-abutted, averaged waveforms with time-synchronisation	55	9	97	25
BS_ICA applied to abutted, averaged waveforms with time-synchronisation	73	11	29	7

The amplitude range represents the peak-to-peak magnitude of the lambda wave as previously indicated in Fig.6.17. The table provides both the mean and standard deviation values for each of the two parameters across the 7 subjects. Neither averaging methods (i.e. with and without time-synchronisation) provided the scalp distribution of the recovered lambda wave. When using BS\_ICA, the backprojection method described in section 6.3.5, was applied to obtain an estimate of the amplitude ranges. In the same section, the procedure used to estimate the percentage contribution of the BS\_ICA-extracted components to the parieto-occipital region of the cerebral cortex is provided.

When BS\_ICA was applied to the abutted averaged time-synchronised waveforms the contribution of the extracted lambda wave component to the parieto-occipital region of the cerebral cortex (back of the head) was estimated to be 73%. When BS\_ICA was applied to not-abutted averaged time-synchronised waveforms, the contribution was 55%. Therefore, the abutting process improved the spatial resolution of the extracted

lambda wave. With their ability to obtain the scalp distribution of each extracted component, BS\_ICA-based approaches provided a more accurate identification of the area of the cerebral cortex concerned with the lambda wave electrical activity, as compared to the averaging method which did not allow for the spatial resolution of the waveforms to be obtained..

When considering the amplitude range feature, the averaging methods with and without time-synchronisation provided mean values of 48  $\mu\text{V}$ . BS\_ICA applied to the abutted averaged time-synchronised waveforms provided a mean value of 29  $\mu\text{V}$  for the amplitude range while that for BS\_ICA applied to the not-abutted averaged time-synchronised waveforms was 97  $\mu\text{V}$ . The former range is closer to the previously reported lambda wave amplitude range of about 30  $\mu\text{V}$  [1.5]. A smaller standard deviation value of 7  $\mu\text{V}$  across subjects indicated that BS\_ICA applied to the abutted waveforms resulted in more consistent results than that obtained when BS\_ICA applied to the not-abutted waveforms which provided a standard deviation value of 25  $\mu\text{V}$ .

In summary, the four approaches reported in this study were ranked in the following order of decreasing effectiveness for extracting the lambda wave.

- i) BS\_ICA applied to abutted, averaged waveforms with time-synchronisation.
- ii) BS\_ICA applied to not-abutted, averaged waveforms with time-synchronisation .
- iii) Not-abutted, averaged waveforms with time-synchronisation.
- iv) Not-abutted, averaged waveforms without time-synchronisation.

## 6.5. Conclusion

Novel procedures were developed in order to improve the extraction of saccade-related EP components from the recorded EEG and EOG mixtures.

An BS\_ICA-based methodology which enabled three saccade-related EPs components to be successfully extracted from the EEG and EOG recorded waveforms and their scalp distribution to be obtained, was described. The components of interest were: the frontal and occipital pre-saccadic potentials, and the lambda wave. This part of the study demonstrated the usefulness of a signal source separation method (such as BS\_ICA) for analysing

saccade-related EEG waveforms and revealed valuable information about the brain mechanisms involved in performing saccades.

An iterative time-synchronisation procedure was devised to time-synchronise the recorded waveforms across trials. This ensured that the time features of the lambda wave were preserved during the subsequent averaging operation used to reduce the effect of background EEG.

The effect of waveform length on the performance of independent component analysis (BS\_ICA) for extracting a visual evoked potential called the lambda wave from saccade-related EEG waveform was investigated. Experiments were carried out using both artificially generated mixtures as well as the recorded EEG and EOG waveforms. The length of the waveforms were varied by a process which involved abutting successive trials. The study demonstrated that increasing the length of the waveforms improved the performance of BS\_ICA in extracting both the temporal and spatial characteristic features of the components from the recorded electroencephalogram (EEG) mixtures. The reason for this improvement was considered to be due to an improvement to the stationarity of the signals thus making them more suitable for processing by BS\_ICA. This section of the study demonstrated that the abutting of the trials is a valuable mechanism for improving the performance of BS\_ICA in extracting evoked potentials from the recorded EEG waveforms.

# Chapter 7. Model-Based Independent Component Analysis for Extracting the Lambda Wave

## 7.1 Chapter Summary

In this chapter, an approach for incorporating the signal model into independent component analysis of Bell and Sejnowski (BS\_ICA) was developed. The effectiveness of this model-based BS\_ICA was both quantitatively and visually assessed and compared with the same BS\_ICA algorithm without the model. The methodology and results obtained are discussed and details of the implementation is provided. The results for both simulated signal waveforms as well as the recorded EEG and EOG waveforms are provided and discussed.

## 7.2 Introduction

As described in chapter 2, section 2.6, the operation of BS\_ICA requires:

- The number of sources and available (recorded) mixtures to be equal.
- The source signals to be stationary.
- The mixing process to be linear.
- Not more than one source signal to be Gaussian.

However, the above requirements do not fully conform with the components of the EEG signal. For example EPs are short duration transient signals which might not be stationary.

To this effect, a novel method was presented in chapter 6 in order to increase the stationarity pre-requisite of the EEG waveforms prior to BS\_ICA operation. Another particularity of EPs is that they may have multi-modal type distributions. This mismatch between BS\_ICA assumptions and EPs properties may cause distortion of the components extracted by the BS\_ICA algorithm. Therefore, procedures to aid the BS\_ICA algorithm to extract EPs from the recorded EEG mixtures of interest may be valuable. In this chapter, an approach to improve the performance of BS\_ICA for extracting the lambda wave from saccade-related EEG waveforms is presented. The developed method consists of utilising prior information about the time characteristic features of the lambda wave as part of the BS\_ICA signal source separation operation, in order to guide the algorithm for extracting the EP component of

interest (the lambda wave). The performance of the new BS\_ICA-based approach was assessed both quantitatively and visually, and its effectiveness was compared to that of the conventional (without prior information) BS\_ICA algorithm. A description of the developed model-based (with prior information) BS\_ICA approach is provided in section 7.3.2.

## **7.3 Experimental Procedure**

Details of the data recording procedure are provided in chapter 4, section 4.4.2.

### **7.3.1 Outline of the Procedure for Extracting the Lambda Wave**

The operations to extract the lambda wave consisted of the following:

- i) Pre-processing
- ii) Iterative Time-Synchronisation
- iii) Time and Spatial Averaging
- iv) Whitening
- v) Application of either BS\_ICA (without model) or the model-based BS\_ICA
- vi) Back-projection of the separated components to the electrode sites on the scalp.

Operations i) to iv) and vi) are described in more details in chapter 6, sections 6.3.1 to 6.3.4 and 6.3.5 respectively.

In chapter 6, section 6.3.4, the appropriate initial value for the learning rate parameter of the BS\_ICA algorithm was heuristically found to be  $75 \times 10^{-4}$ . This initial value was used in both BS\_ICA-based approaches (with and without model).

Details of operation v) are provided in the following sections.

### **7.3.2 Design of the Model-Based BS\_ICA for the Lambda Wave Extraction**

The design of the model-based BS\_ICA involved the following steps:

- Development of a model for the lambda wave.
- Development of a suitable cost-function.

- Development of a model tracking algorithm.
- Integration of the model into the BS\_ICA algorithm.

The details of these steps are provided next.

### 7.3.2.1 Development of a Model for the Lambda Wave

The function of the model was to represent the lambda wave. This had to be sufficiently flexible to accommodate the variations in the time characteristics of the lambda wave. A model which satisfied these requirements was designed by considering the general trend of the temporal response of the lambda wave. The model consisted of three straight line sections characterised by their gradients ( $m_1$ ,  $m_2$  and  $m_3$ ) and their respective starting and end time points. The three sections of the model are shown in Fig.7.1.

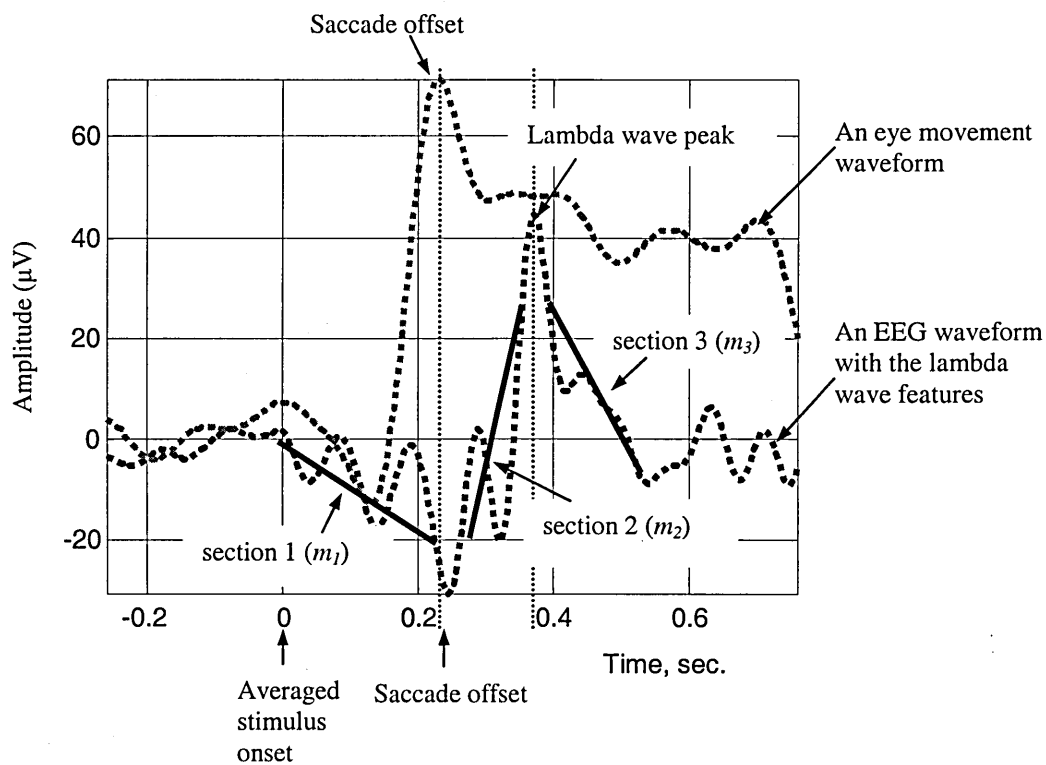


**Fig.7.1** A model of the lambda wave represented by three straight lines.

### *The parameters of section 1*

The lambda wave has a negative shift (NS) starting from the averaged stimulus onset. This was the starting point of section 1 of the model. The end point of this section was chosen to be the saccade offset because the (positive) peak of the lambda wave is time-locked to this offset. Furthermore this negative shift ends around the saccade offset point. The procedure for determining the saccade offset is described in chapter 6, section 6.3.2. The statistical distribution of the saccade offset across subjects was obtained by repeating the procedure for all subjects. The saccade offset distribution was heuristically found to have a mean of 260 ms and a standard deviation of about 30 ms. The peak of the distribution represented the mean offset time for the saccade across all subjects.

### *The parameters of section 2*

The starting point for the second section of the model was the mean saccade offset determined in section 1. The lambda wave has then a positive shift which ends around the peak of the lambda wave. Therefore the end of the second section was chosen to correspond to this peak. In order to determine the time corresponding to the peak of the lambda wave the following procedure was followed. The peak of the lambda wave is time locked to the saccade offset and was experimentally determined (across all subjects) to occur within 200 ms ( $\pm 30$ ms) from the saccade offset. Therefore, the time of occurrence of the peak of the lambda wave corresponded to its maximum amplitude within this region.

### *The parameters of section 3*

The starting point for the third section of the model corresponded to the end point of the second section. After this point the lambda wave has a negative shift. The point of this negative shift was experimentally determined (across all subjects) to be around 500 ms from the averaged stimulus onset. This time point was chosen to be the end of this section of the model.

Once the starting and end points of the three sections were determined, a straight line was fitted into the points in each section by using the least-mean-square technique [7.1] and their corresponding gradients ( $m_1$ ,  $m_2$  and  $m_3$ ) were obtained.

### 7.3.2.2 Development of a Suitable Cost-Function

The purpose of the cost-function ( $\phi$ ) was to provide a measure of closeness between each BS\_ICA (extracted) component and the devised model of the lambda wave. The cost-function used was,

$$\phi = \sqrt{(m_{1m} - m_{1i})^2 + (m_{2m} - m_{2i})^2 + (m_{3m} - m_{3i})^2} \quad (7.1)$$

where  $m_{1m}$ ,  $m_{2m}$  and  $m_{3m}$  are the three gradients obtained (using the procedure described in the previous section) from an averaged saccade-related EEG waveform that contained the broad (coarse) time characteristics (the three voltage shifts described in section 7.3.2.1 ) of the lambda wave. The broad time features of the lambda wave were visible in the averaged EEG waveforms. The gradients  $m_{1i}$ ,  $m_{2i}$  and  $m_{3i}$  were obtained for each extracted BS\_ICA component.

### 7.3.2.3 Development of a Model Tracking Algorithm

The purpose of this algorithm was to identify which BS\_ICA component most closely matched the model of the lambda wave. The smallest cost-function value ( $\phi_s$ ) was identified and the BS\_ICA component which corresponded to it was selected.

### 7.3.2.4 Integration of the Model into the BS\_ICA algorithm

The amount of change ( $\Delta W$ ) for the unmixing weight matrix ( $W$ ) at each iteration of the learning rate for BS\_ICA without model was based on equation (2.50). However, for the model-based BS\_ICA, this equation was modified to,

$$\Delta W = \eta \left[ I + (1-2Y)U^T \right] W \quad \eta = \begin{cases} \eta_1 & \text{for the selected ICA component} \\ \eta_2 & \text{for all other ICA components} \end{cases} \quad (7.2)$$

With this modification, this equation can be rewritten as,

$$\Delta W = \left[ I + (I - 2Y)U^T \right] \begin{pmatrix} \eta_2 w_{11} & \eta_2 w_{12} & \eta_2 w_{13} & \cdots & \eta_2 w_{1n} \\ \eta_2 w_{21} & \eta_2 w_{22} & \eta_2 w_{23} & \cdots & \eta_2 w_{2n} \\ \cdot & \cdot & \cdot & \cdot & \cdot \\ \eta_1 w_{m1} & \eta_1 w_{m2} & \eta_1 w_{m3} & \cdots & \eta_1 w_{mn} \\ \cdot & \cdot & \cdot & \cdot & \cdot \\ \eta_2 w_{n1} & \eta_2 w_{n2} & \eta_2 w_{n3} & \cdots & \eta_2 w_{nn} \end{pmatrix} \quad (7.3)$$

The  $m^{\text{th}}$ -row of  $W$  corresponds to the channel that contained the selected BS\_ICA component and  $n$  is the number of input waveforms to BS\_ICA. For the selected BS\_ICA component, the learning rate ( $\eta$ ) was set to  $\eta_1$  and for the remaining components, it was set to  $\eta_2$ . The value of  $\eta_1$  was determined by,

$$\eta_1 = C_1 \eta_2 \left[ 1 + \frac{\phi_s}{C_2 \phi_{si}} \right] \quad (7.4)$$

where  $C_1$  and  $C_2$  are constants and  $\phi_{si}$  is the value of  $\phi_s$  after the first BS\_ICA iteration.

The justification for the approach and equation (7.4) is provided next.

BS\_ICA is an unsupervised learning algorithm. The model-based BS\_ICA however provides a form of feedback to the BS\_ICA learning rule. This is achieved by using the cost function information to provide a higher learning rate for the selected BS\_ICA component. This makes the model-based BS\_ICA a partially supervised learning algorithm where the lambda wave has become the main target for the algorithm. The aim of this operation was to emphasise the extraction of the desired component over the other components.

The expression for  $\eta_1$  has two terms. The first term, (i.e.  $C_1 \eta_2$ ) is a bias to ensure  $\eta_1$  remains always larger than  $\eta_2$ . This provides a faster convergence rate for the desired component thus emphasising its extraction over the other components. The second term (i.e.  $C_1 \eta_2 \frac{\phi_s}{C_2 \phi_{si}}$ ) is a smoothing factor for  $\eta_1$ . The term provides a dynamic adjustment of  $\eta_1$  proportional to the value of the calculated error ( $\phi_s$ ). The term  $\phi_{si}$  is a normalising factor for  $\phi_s$  to ensure that the value of the smoothing factor (second term of the expression of  $\eta_1$ ) was not out of range when compared to the first term  $C_1 \eta_2$ .  $\phi_{si}$  corresponded to the initial error, i.e. the value of

$\phi_s$  after the first BS\_ICA iteration.. The values of the constants  $C_1$  and  $C_2$  control the contribution of each term to  $\eta_1$ . Their values were determined experimentally.

Fig.7.2 shows the overall structure of the model-based BS\_ICA approach for a 2-input case.

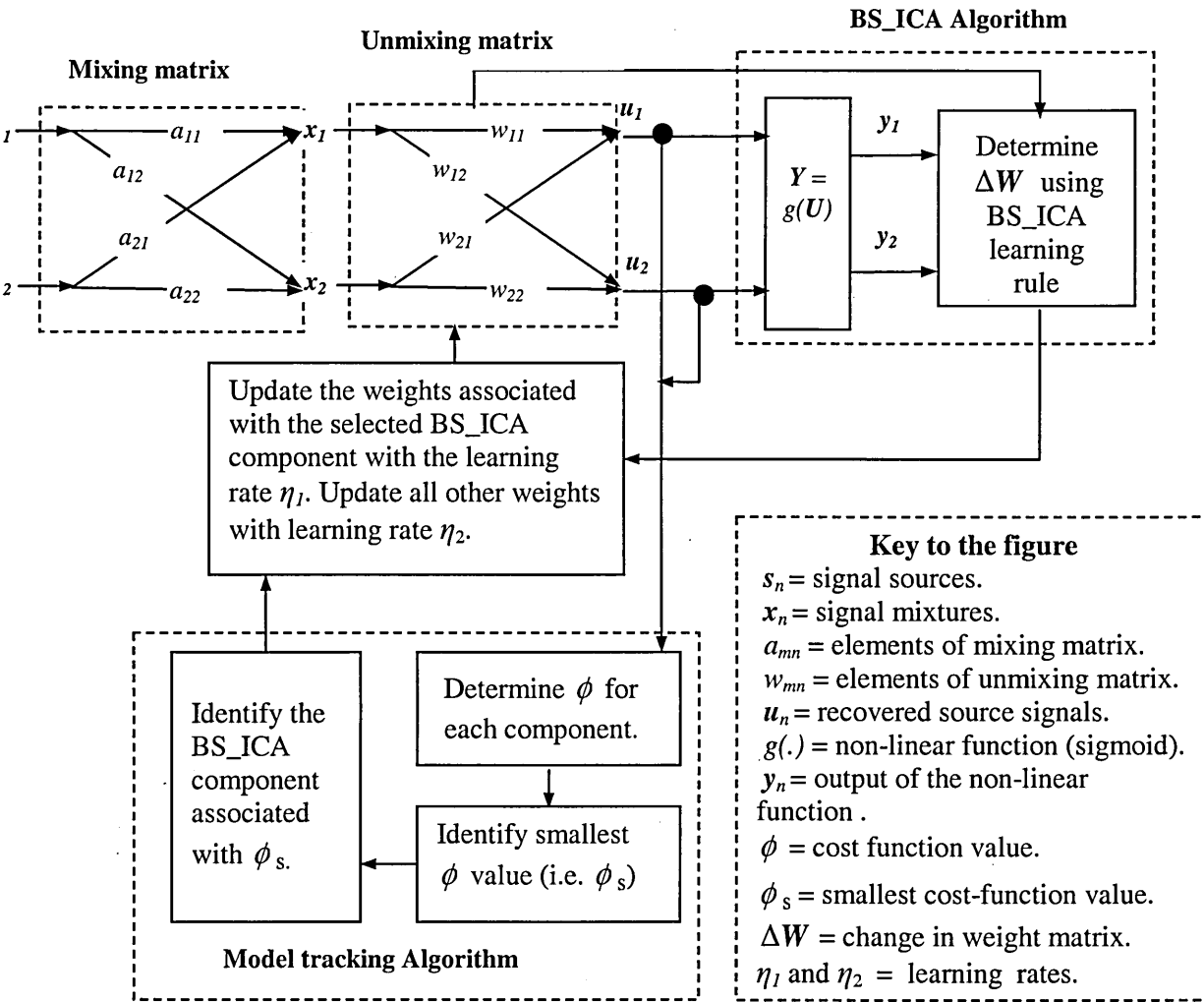


Fig.7.2 The model-based BS\_ICA operation.

## 7.4 Analysis Procedure

The performance evaluation of the two BS\_ICA approaches (i.e. with and without model) was carried out in two stages. Initially a quantitative evaluation was carried out by using artificially mixed waveforms. Then an evaluation of the approaches was carried out when applying the methods to the 22-averaged EEG waveforms (described in chapter 6, section 6.3.3).

The artificially mixed waveforms were generated by using the procedure described in chapter 6, section 6.3.6.

The two BS\_ICA approaches were applied to unmix the waveforms. The EEG mixing coefficients are shown in Table 7.1. The EOG mixing coefficients were  $a_{21} = 1 - a_{11}$  and  $a_{22} = 1 - a_{12}$ .

**Table 7.1** The mixing ratios.

$a_{11}$	0.55	0.60	0.65	0.70	0.75	0.80	0.85	0.90
$a_{12}$	0.45	0.40	0.35	0.30	0.25	0.20	0.15	0.10

The sum of  $a_{11}$  with  $a_{12}$  (similarly for  $a_{21}$  with  $a_{22}$ ) was equal to 1. Therefore, the total signals powers before and after the mixing operation remained constant. An investigation was also carried out using mixing coefficients where this condition did not apply.

The similarity between the original and recovered waveforms was assessed by calculating both the Correlation coefficient ( $\rho$ ) and the Euclidean distance ( $\varepsilon$ ) as described in chapter 6, section 6.3.6.

## 7.5 Results and Discussion

### 7.5.1 Simulated Signal Mixtures

Table 7.2a shows the values obtained for  $\rho$  and  $\varepsilon$  when extracting the EEG signal from the two simulated mixtures using BS\_ICA with and without model. The same information is shown in Table 7.2b when extracting the EOG signal.

**Table 7.2** Correlation coefficient ( $\rho$ ) and Euclidean distance ( $\varepsilon$ ) values for the two BS\_ICA approaches for (a) the EEG waveform and (b) the EOG waveform.

(a)

BS_ICA	$a_{11}$	→0.55	0.60	0.65	0.70	0.75	0.80	0.85	0.90
	$a_{12}$	→0.45	0.40	0.35	0.30	0.25	0.20	0.15	0.10
without model	$\rho$	0.116	0.451	0.641	0.789	0.890	0.957	0.992	1.000
with model	$\rho$	1.000	1.000	1.000	1.000	1.000	1.000	1.000	1.000
without model	$\varepsilon$	2.045	1.446	1.347	0.528	0.384	0.283	0.222	0.206
with model	$\varepsilon$	0.104	0.060	0.200	0.031	0.154	0.249	0.147	0.205

(b)

BS_ICA	$a_{11}$	→0.55	0.60	0.65	0.70	0.75	0.80	0.85	0.90
	$a_{12}$	→0.45	0.40	0.35	0.30	0.25	0.20	0.15	0.10
without model	$\rho$	0.985	0.997	0.997	0.999	0.992	0.998	0.996	0.995
with model	$\rho$	0.985	0.993	0.983	0.999	0.999	0.999	0.995	0.994
without model	$\varepsilon$	2.310	1.345	1.071	0.971	0.940	0.944	0.967	1.006
with model	$\varepsilon$	0.538	0.692	0.944	0.968	1.023	1.088	0.560	0.826

For values of  $a_{12}$  less than or equal to 0.2 (i.e. mild contamination of the EEG by EOG), the performance of the two approaches in recovering the EEG waveform was not significantly different. However, for larger values of  $a_{12}$  (i.e. more severe contamination of the lambda wave by the EOG), the model-based BS\_ICA performed significantly more effectively in extracting the EEG waveform with the lambda wave features (i.e. larger values of  $\rho$  and smaller values for  $\varepsilon$ ). No significant difference was observed between the 2 methods regarding the extraction of the EOG.

The mean and standard deviation (std) values of  $\rho$  and  $\varepsilon$  for the data shown in Table 7.2 are summarised in Table 7.3a. The incorporation of the model into the BS\_ICA did not deteriorate the recovery of the EOG component from the mixtures. This is demonstrated by the results in Table 7.3b.

**Table 7.3** Mean and standard deviation (Std) values of  $\rho$  and  $\varepsilon$  (in  $\mu\text{V}$ ) for the data shown in Table 2, for (a) EEG and (b) the EOG waveforms.

(a)

BS_ICA	EEG Waveform			
	$\rho$		$\varepsilon$	
	Mean	Std	Mean	Std
Without Model	0.518	0.401	1.081	0.695
With Model	1.000	0.000	0.144	0.075

(b)

BS_ICA	EOG Waveform			
	$\rho$		$\varepsilon$	
	Mean	Std	Mean	Std
Without Model	0.963	0.030	1.358	0.464
With Model	0.993	0.006	0.830	0.212

Table 7.4 shows typical results obtained for cases where the sum of  $a_{11}$  with  $a_{12}$  (similarly for  $a_{21}$  with  $a_{22}$ ) was not equal to 1. As before the model-based BS\_ICA was the more effective approach.

**Table 7.4** Correlation coefficients ( $\rho$ ) and Euclidean distance ( $\varepsilon$  in  $\mu\text{V}$ ) for the approaches. The total power of each signal within the mixtures were less than its power before mixing.

Mixing matrix	Waveform	BS_ICA Approach			
		Without model		With model	
		$\rho$	$\varepsilon$	$\rho$	$\varepsilon$
$\begin{pmatrix} 0.6 & 0.3 \\ 0.3 & 0.6 \end{pmatrix}$	EEG	0.605	1.334	1.000	0.333
	EOG	0.999	1.026	0.934	1.030
$\begin{pmatrix} 0.6 & 0.5 \\ 0.5 & 0.6 \end{pmatrix}$	EEG	0.906	0.325	1.000	0.103
	EOG	0.999	0.941	0.985	0.520

### 7.5.2 BS\_ICA Applied to the 22-Averaged Waveforms

The results obtained when the two BS\_ICA approaches were applied to the 22 spatially and temporally time-synchronised averaged waveforms for the centre-to-left saccade event are described in this section. The results for a typical subject are provided. However consistent results were observed in the other subjects and they are summarised later in this section.

The visual inspection of the 22 components extracted by each BS\_ICA approach showed two waveforms with the characteristic features of the lambda wave. These are shown in the top and middle rows of Fig.7.3. The bottom row shows the corresponding extracted EOG waveforms.

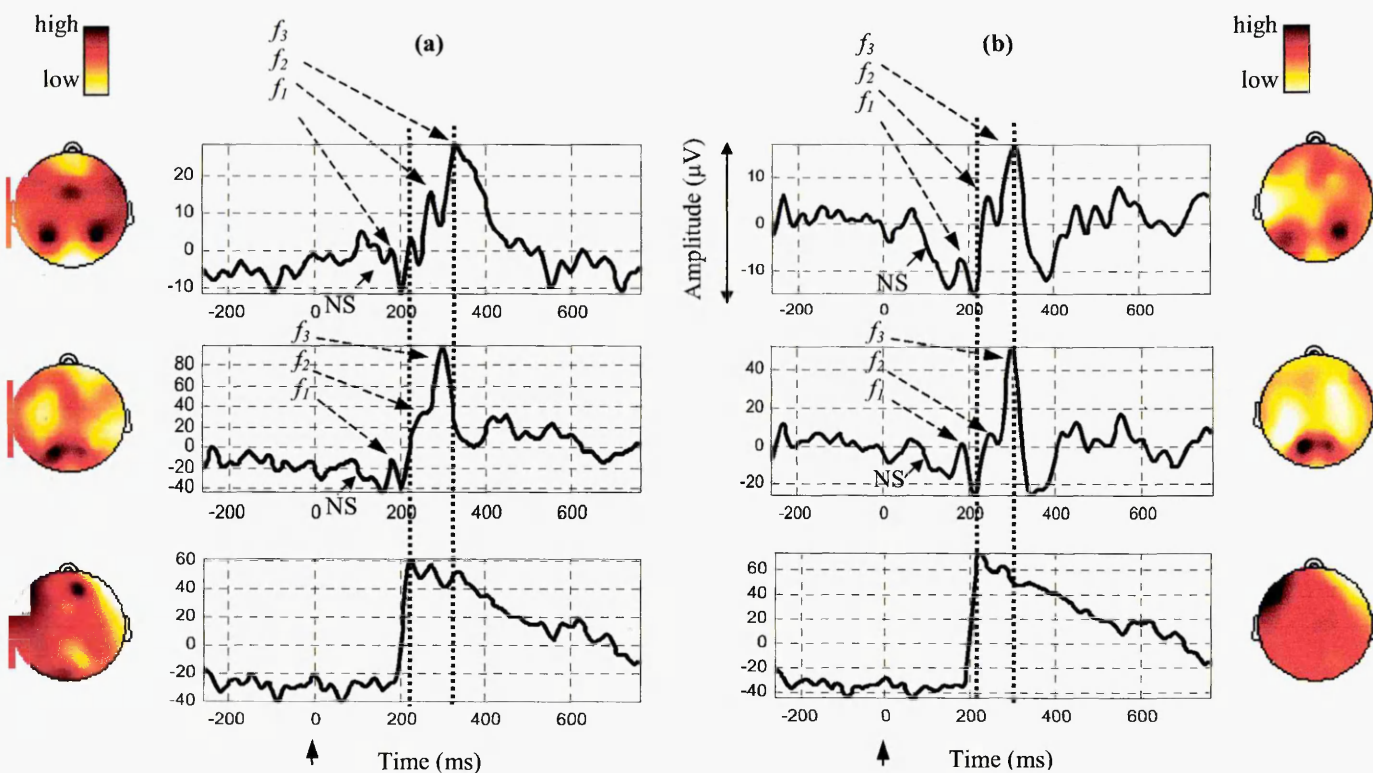


**Fig.7.3** Two Lambda wave components extracted by BS\_ICA (top and middle) with their respective scalp distributions (side) and the corresponding extracted EOG component (bottom) for (a) BS\_ICA without model, (b) model-based BS\_ICA. The vertical arrow indicates the average stimulus onset.

The following observations were made when comparing the results.

- Both BS\_ICA approaches managed to extract the lambda wave and their corresponding EOG waveforms. The features monitored were  $f_1$ ,  $f_2$ ,  $f_3$  (see Fig.7.3) and pre-saccadic negative shift (NS, a negative shift in the EEG baseline following the onset of the stimulus). The features  $f_1$ ,  $f_2$  and  $f_3$  are believed to be related to the movement of the visual field across the retina [1.5]. All these 4 features were visible in the extracted lambda wave components when both BS\_ICA approaches were applied. However, when using the model-based BS\_ICA, the features were preserved more accurately. This indicated that the model-based BS\_ICA provided a further improvement in extracting the features of the lambda wave as compared with the BS\_ICA without model.
- The peak activity of the lambda wave (observed from its scalp distribution) for both BS\_ICA approaches was dominant in the left and right sides of the parietal area (see top row in Fig.7.3) as well as in the centre of the parietal area of the cerebral cortex (see middle row in Fig.7.3). The spatial resolution of the lambda wave components however, was more concentrated in the aforementioned regions for the model-based BS\_ICA. The scalp distribution of the lambda wave obtained using the BS\_ICA approaches was in accordance with the region (parieto-occipital area of the cerebral cortex) from which the lambda wave signal was reported to have been recorded (in [1.5]).
- Table 7.5 contains a summary of the analysis results across the 7 subjects for the temporal features NS,  $f_1$ ,  $f_2$  and  $f_3$  when assessing the two BS\_ICA-based approaches to recover the lambda wave component.

**Table 7.5** Summary of the analysis results for the temporal features of the lambda wave when assessing the two BS\_ICA-based approaches to recover the lambda wave component.

Methods	Lambda wave temporal feature			
	NS	$f_1$	$f_2$	$f_3$
BS_ICA applied to averaged waveforms with time-synchronisation	7	4	6	6
Model-BS_ICA applied to averaged waveforms with time-synchronisation	7	7	7	7

The methods were:

- BS\_ICA applied to averaged waveforms with time-synchronisation.
- Model-BS\_ICA applied to averaged waveforms with time-synchronisation.

Table 7.5 contains the number of subjects in which each feature was observed for each method. The NS feature was observed in all 7 subjects for both BS\_ICA-based approaches. When BS\_ICA was applied to the averaged waveforms, the method successfully extracted features  $f_1$ ,  $f_2$  and  $f_3$  in 4, 6 and 6 subjects respectively. The best performance was achieved when the developed model-BS\_ICA algorithm was applied to the averaged waveforms as the features  $f_1$ ,  $f_2$  and  $f_3$  were visible in all 7 subjects.

- Table 7.6 contains a summary of the analysis results across the 7 subjects for the scalp distribution (spatial feature) and the amplitude range when assessing the two BS\_ICA-based methods to recover the lambda wave.

**Table 7.6** Summary of the analysis results for the scalp distribution and amplitude range features when assessing the two BS\_ICA-based approaches to recover the lambda wave component (std = standard deviation).

Methods	Percentage Scalp distribution (%)		Amplitude Range ( $\mu\text{V}$ )	
	mean	std	mean	std
BS_ICA applied to the averaged waveforms with time-synchronisation	55	9	97	25
Model-BS_ICA applied to the averaged waveforms with time-synchronisation	73	9	21	3.4

The table provides both the mean and standard deviation values for each of the two parameters across the 7 subjects. The amplitude range represents the peak-to-peak magnitude of the lambda wave as indicated in Fig.7.3. The backprojection method described in chapter 6, section 6.3.5, was applied as part of the signal separation process in order to obtain an estimate of the amplitude ranges of the extracted components. In the same section, the procedure used to estimate the percentage contribution of the BS\_ICA-extracted components to the parieto-occipital region of the cerebral cortex is provided.

When BS\_ICA was applied to the averaged waveforms the contribution of the extracted lambda wave component to the parieto-occipital region of the cerebral cortex (back of the head) was estimated to be 73% with a standard deviation of 9. When the developed model-BS\_ICA approach was applied to the averaged waveforms, the contribution was 55% with a standard deviation of 9. Therefore, the incorporation of a lambda wave temporal model into the signal separation operation of the BS\_ICA algorithm improved the spatial resolution for the extracted lambda wave.

When considering the amplitude range feature, the developed model-BS\_ICA applied to the averaged waveforms provided a mean value of 29  $\mu\text{V}$  with a standard deviation of 3.4  $\mu\text{V}$  for the amplitude range while that for BS\_ICA was 97  $\mu\text{V}$  with a standard deviation of 25  $\mu\text{V}$ . The former range is closer to the previously reported lambda wave amplitude range of about 30  $\mu\text{V}$  [1.5]. A smaller standard deviation value across subjects indicated that the developed model-BS\_ICA approach resulted in more consistent results than that obtained when normal (without model) BS\_ICA was used.

## 7.6 Discussion on the effects of the error feedback

In this section, the results obtained when experimenting with different values of the contribution of the smoothing factor (SF) to the learning rate  $\eta_1$  (of the model) are described. In Figs.7.4 to 7.6, the vertical axis represents the correlation between the BS\_ICA-extracted lambda wave and the original lambda wave, and the horizontal axis represents the number of iterations for the training process of the model-based BS\_ICA algorithm.

- Fig.7.4 shows the effect of gradually increasing the constant  $C_1/C_2$  that controls the contribution of the error-feedback (SF) to the overall model cost-function. The constant  $C_1$  that controls the contribution of the model to the overall BS\_ICA learning rule is set to a value of 45 for a the mixing ratio of ( $a_{11}=0.75$ ,  $a_{12}=0.25$ ). The value of the ratio  $C_1/C_2$  is then gradually increased from less than 0.33 to 10. This case (i.e.  $C_1 = 45$ ) was shown as a representative one, but similar results were observed for other values of  $C_1$ .

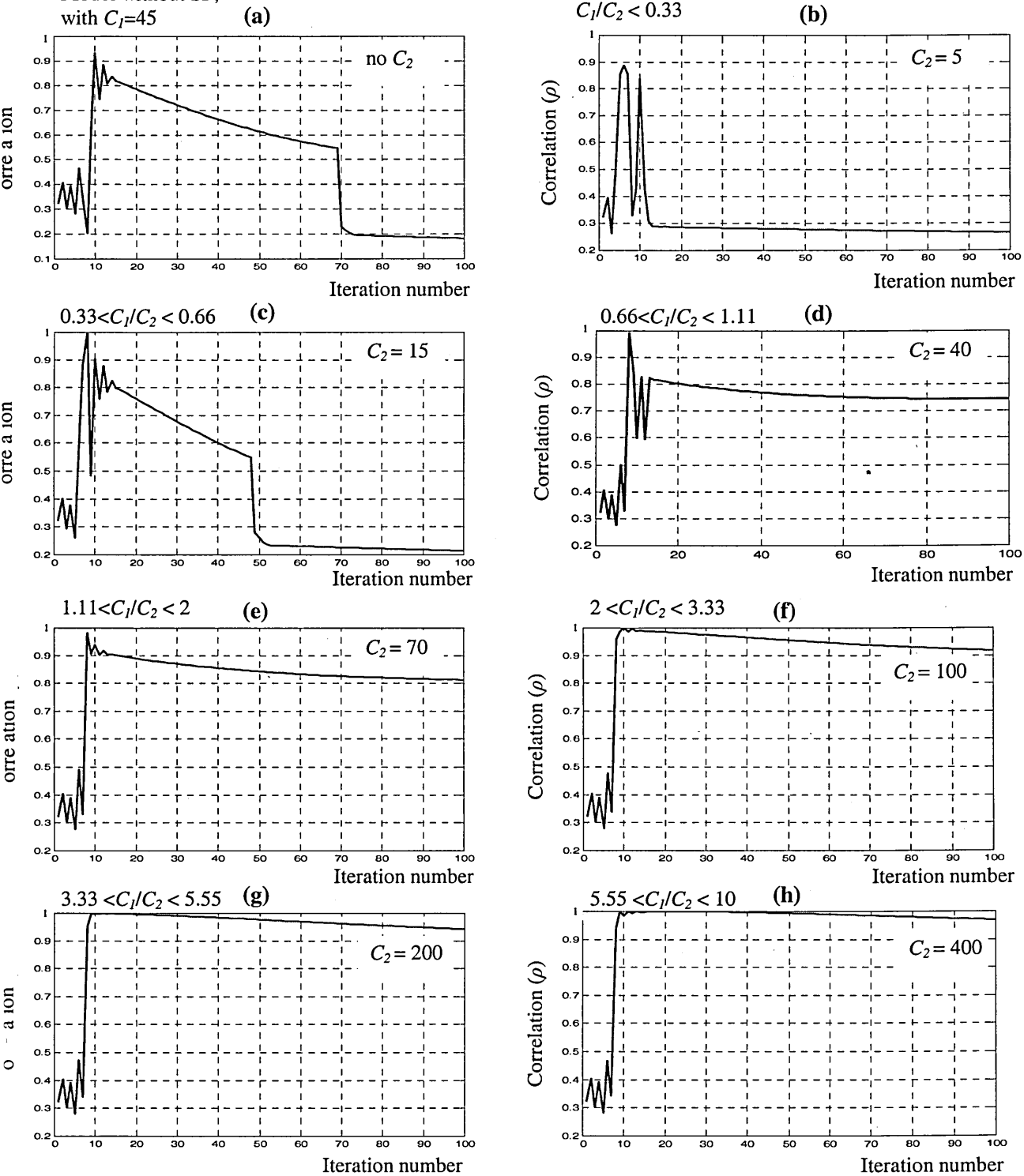


**Fig.7.4** (a) The training results when no SF was incorporated into the model cost function. (b)-(h) The effect of gradually increasing the contribution of the SF to the model cost function by increasing the value of constant ratio  $C_1/C_2$ .  $C_1$  was set to 45 for all cases.

As shown in Fig.7.4, the introduction of an error-feedback loop (or smoothing factor) into the model cost-function improved the smoothness of the learning. The learning became more gradual. Therefore the error-feedback loop provided a better stability of the adaptive training process. These results were obtained for mixing ratio ( $a_{11}=0.75$ ,  $a_{12}=0.25$ ). However, similar results were observed for other mixing ratios. The optimum value for the

ratio  $C_1/C_2$  that controls the contribution of the error-feedback cost-function to the overall model cost-function was determined experimentally. Although it was observed that the introduction of the smoothing factor improved the performance of the model cost-function, at this stage, no in-depth understanding of the reasons behind this observation was provided. However, it could be observed that within a defined range of values for  $C_2$ , the smoothing factor was effective and that very large values of  $C_2$  (i.e.  $C_2 \approx \infty$ ) will cause the smoothing factor to stop performing efficiently as shown in Fig.7.4a (cf. equation 7.4).

- A dropping effect is caused by overtraining as shown in Fig.7.5a and c, for two different values of the  $C_1$  respectively. Fig.7.5b and d show the same information when the smoothing factor was incorporated into the model cost function. In Fig.7.5a and c,  $C_1$  is set to 49 which was found to be the optimum value for the model at mixing ratio ( $a_{11}=0.75, a_{12}=0.25$ ). In Fig.7.5b and d,  $C_1$  is set to the value when the model did not perform well ( $C_1=45$ ) at the same mixing ratio. Fig.7.5a and c indicated that, in both cases, a faster drop in performances was observed when the smoothing factor was not incorporated into the model cost function. However, when the smoothing factor was incorporated into the model, this dropping effect associated with overtraining was reduced as shown in Fig.7.5b and d. These results were obtained for a mixing ratio of ( $a_{11}=0.75, a_{12}=0.25$ ). However, similar observations were made for other mixing ratios.

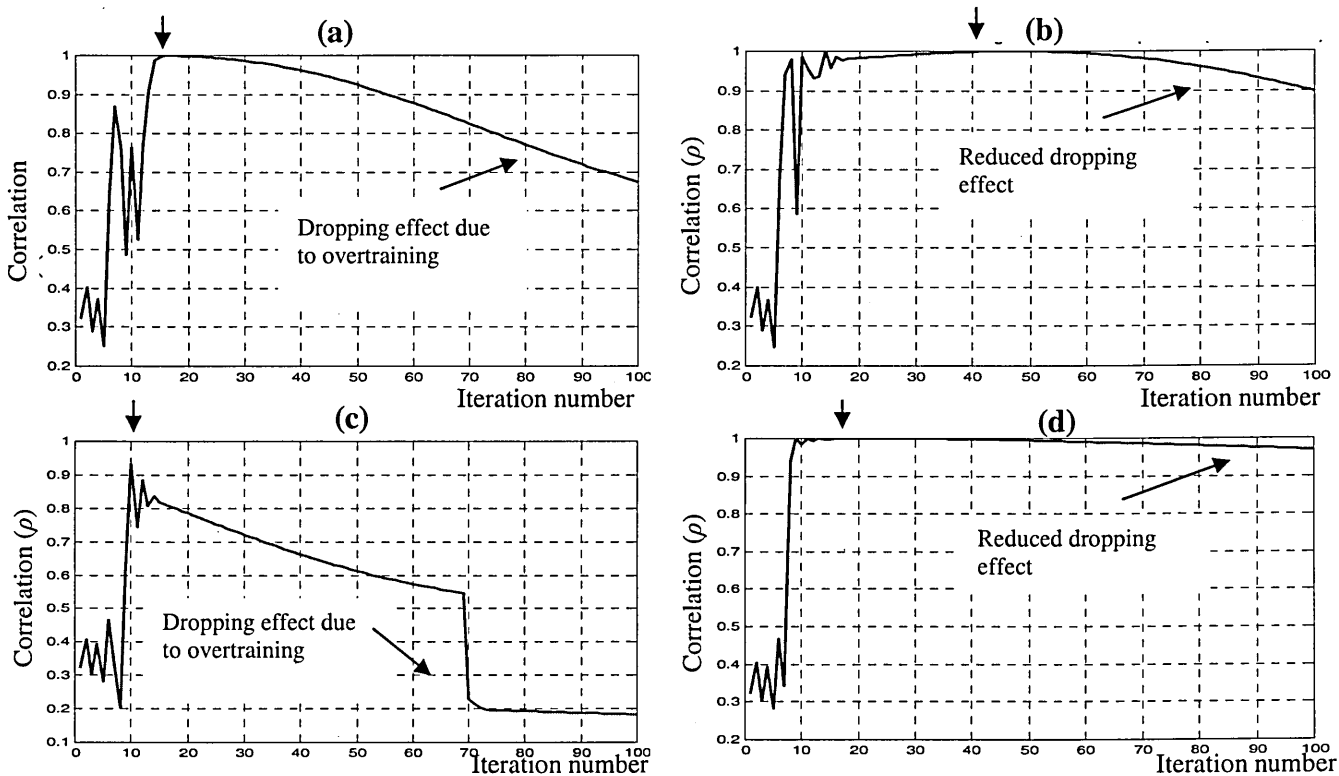


**Fig.7.5** Effect of the feedback-error on the dropping effect caused by overtraining. (a) and (c) Training results for model without smoothing factor. (b) and (d) Same information when the smoothing factor is incorporated into the model.

- Fig.7.6a shows a case when the model does not work for a given value of  $C_I$  (i.e.  $C_I=54$ ). Fig.7.6b shows the same case (i.e. with  $C_I=54$ ) when the smoothing factor was incorporated into the model. The cases where the model did not work usually involved the situations where the bias constant  $C_I$  had a very small span of possible values for the model to work. It was observed that the incorporation of the smoothing factor into the model cost-function increased the span of values which the constant  $C_I$  could take.

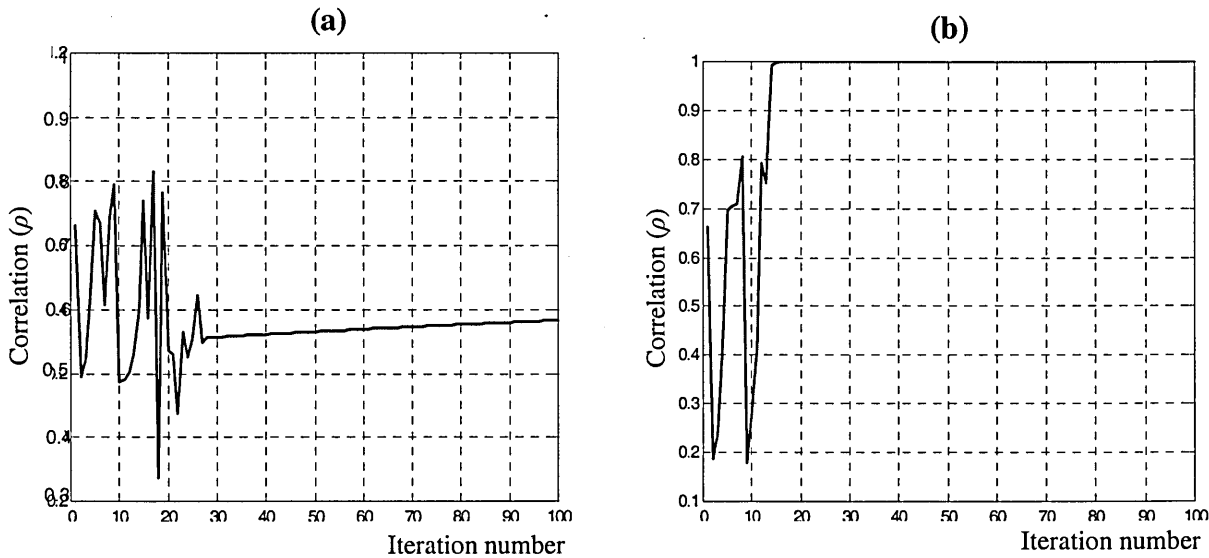


**Fig.7.6 (a)** The training results for a value of  $C_I$  ( $C_I=54$ ) when the model does not work. **(b)** The same training results for the same value of  $C_I$  ( $C_I=54$ ) when the error-feedback was incorporated into the model cost function.

- It was observed that the use of a bias constant  $C_I$  was necessary for the model to operate satisfactorily. This enabled the learning rate associated with the component of interest to always be larger than that of the other components, thus guiding the BS\_ICA algorithm in extracting the component of interest.
- It was observed that the amount of the smoothing factor (determined by the ratio  $C_I/C_2$ ) which needed to be incorporated into the model cost function, varied with respect to the mixing ratio (i.e. the level of contamination of the lambda wave by the EOG) used to generate the mixtures. This  $C_I/C_2$  parameter has to be experimentally adjusted and fine-tuned in order to find the optimum value for a given mixing ratio.

## 7.7 Conclusion

An approach for incorporating the EP signal temporal model into independent component analysis (BS\_ICA) was developed. The resulting model-based BS\_ICA was then used to perform the signal source separation of saccade-related electroencephalogram (EEG) waveforms and to extract a visual evoked potential called the lambda wave. Prior information about the time characteristic features of the lambda wave was utilised to develop the model. The model provided a means of providing extra guidance for BS\_ICA to extract the lambda wave. The effectiveness of the model-based BS\_ICA was both quantitatively and visually assessed and compared with the that of the BS\_ICA algorithm without the model. The study indicated that the model-based BS\_ICA was significantly more effective than BS\_ICA without the model, in preserving the characteristic features (both temporal and spatial) of the extracted lambda wave.

The procedure followed to incorporate the signal model into the BS\_ICA algorithm is general purpose and thus it is applicable to a number of other signal source separation applications where some prior knowledge of the time characteristics of the desired signal component is available.

# Chapter 8. An Analysis of Adaptive Non-linear PCA for EEG Signal Source Separation and the Extraction of the Lambda Wave

## 8.1 Chapter Summary

A signal source separation method called non-linear principal component analysis (NLPCA) was used to analyse saccade related EEG waveforms recorded from 7 normal subjects. The methodology and results are discussed in this chapter. The findings of this investigation using NLPCA are compared with the results obtained when BS\_ICA were used. Plots of the waveforms produced by the two approaches are provided and the results are compared.

## 8.2 Introduction

In Chapters 6 and 7, a number of signal source separation methodologies were devised and were used to extract saccade related EP components from the EEG mixtures. The methods were based on the independent component analysis algorithm of Bell and Sejnowski (BS\_ICA) [1.9]. A typical lambda wave extracted using the BS\_ICA algorithm, together with the corresponding eye-velocity EOG waveform, are shown in Fig.8.1 a and b respectively.

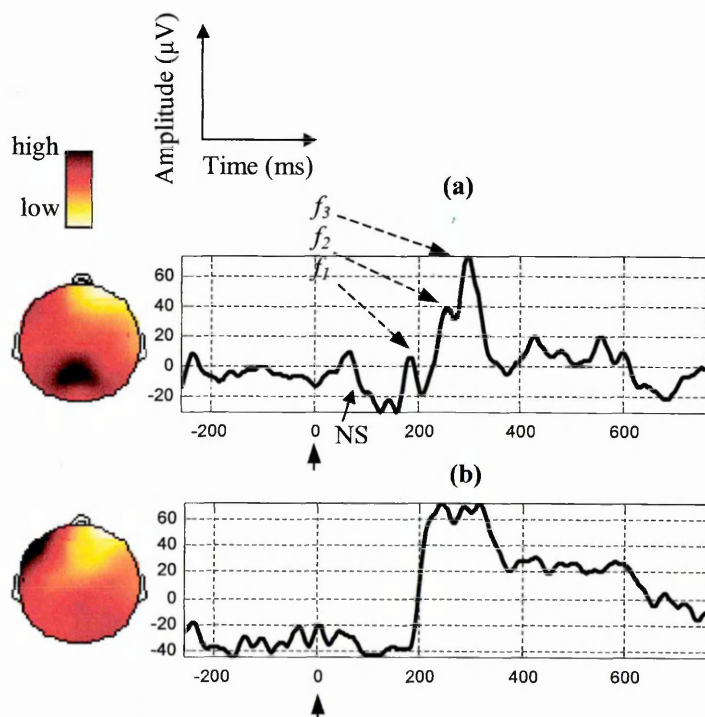


**Fig.8.1 (a)** The BS\_ICA-extracted lambda wave. **(b)** The corresponding EOG component. The vertical arrow indicates the averaged stimulus.

Three sub-components ( $f_1$ ,  $f_2$  and  $f_3$ ) related to the movement of the visual field across the retina were visible in the extracted lambda wave. The sub-components  $f_1$  and  $f_2$  are time locked to the onset of the saccade and were also observed in another study [1.5]. The sub-component  $f_3$  is time-locked to the offset of saccade and has been reported to occur at about 100 ms after the saccade offset [1.5].

The ICA algorithm of Bell and Sejnowski is a stochastic gradient algorithm. Such adaptive neural algorithms apply a coarse instantaneous estimate of the gradient and often require careful choice of the learning parameters for obtaining acceptable performance. For example, if the learning rate is too small, it could lead to a slow convergence speed but on the other hand if this parameter is too large, the learning process may become unstable. A review of different neural approaches to signal source separation is provided in [1.8]. The final accuracy of these algorithms partly depends on the chosen initial values of the learning parameters.

In this chapter, the results of applying the recursive least-squares based non-linear PCA (NLPCA) algorithm reported in [1.11] to the saccade-related EEG waveforms, are provided.

The ICA algorithm of Bell and Sejnowski uses entropy as a measure of signal independence while the NLPCA algorithm reported in [1.11] uses an adaptive signal subspaces tracking method derived using a recursive least square approach, as described in chapter 2, section 2.5. Both algorithms attempt to extract the unknown source signals from their instantaneous linear mixtures.

A review of both the NLPCA algorithm and the ICA algorithm of Bell and Sejnowski are provided in chapter 2, sections 2.5 and 2.6 respectively.

### 8.3 Experimental Procedure

Details of the data recording procedure are provided in chapter 4, section 4.4.2.

#### 8.3.1 Data Analysis

The operations to analyse the lambda wave were:

- i Signal pre-processing
- ii Iterative synchronisation
- iii Temporal and spatial averaging

Operations (i) to (iii) are described in more details in chapter 6, sections 6.3.1. to 6.3.3. respectively.

Details of operation iv) are provided in the following sections.

### 8.3.2 Signal Source Separation using NLPCA

The spatially averaged saccade-related EEG waveforms were processed by the NLPCA algorithm showed by equation (2.7) in chapter 2. Experiments were carried out to determine a suitable non-linear transfer function ( $g(\cdot)$ ), a suitable value for the forgetting factor ( $\beta$ ) and the number of iterations. The selected parameters were:  $\beta=0.9$  and  $g=\tanh(\cdot)$ . The NLPCA learning process stopped when the amount of change in the weight matrix  $W$  became less than a predefined small value (e.g.  $1E-6$ ). The number of iterations was approximately 300 for the data used in this study.

## 8.4 Results and Discussion

Typical results obtained when the NLPCA was applied to the 22 spatially-averaged saccade related EEG waveforms for the centre-to-left saccade event are described in this section. The top row of Fig.8.2 shows two extracted lambda waves from the occipital region and their respective scalp distributions. The corresponding time-locked EOG waveforms are shown in the bottom row of Fig.8.2. A number of other similar lambda waves were extracted from parietal region of the visual cortex. These are shown in the two middles rows of Fig.8.2.

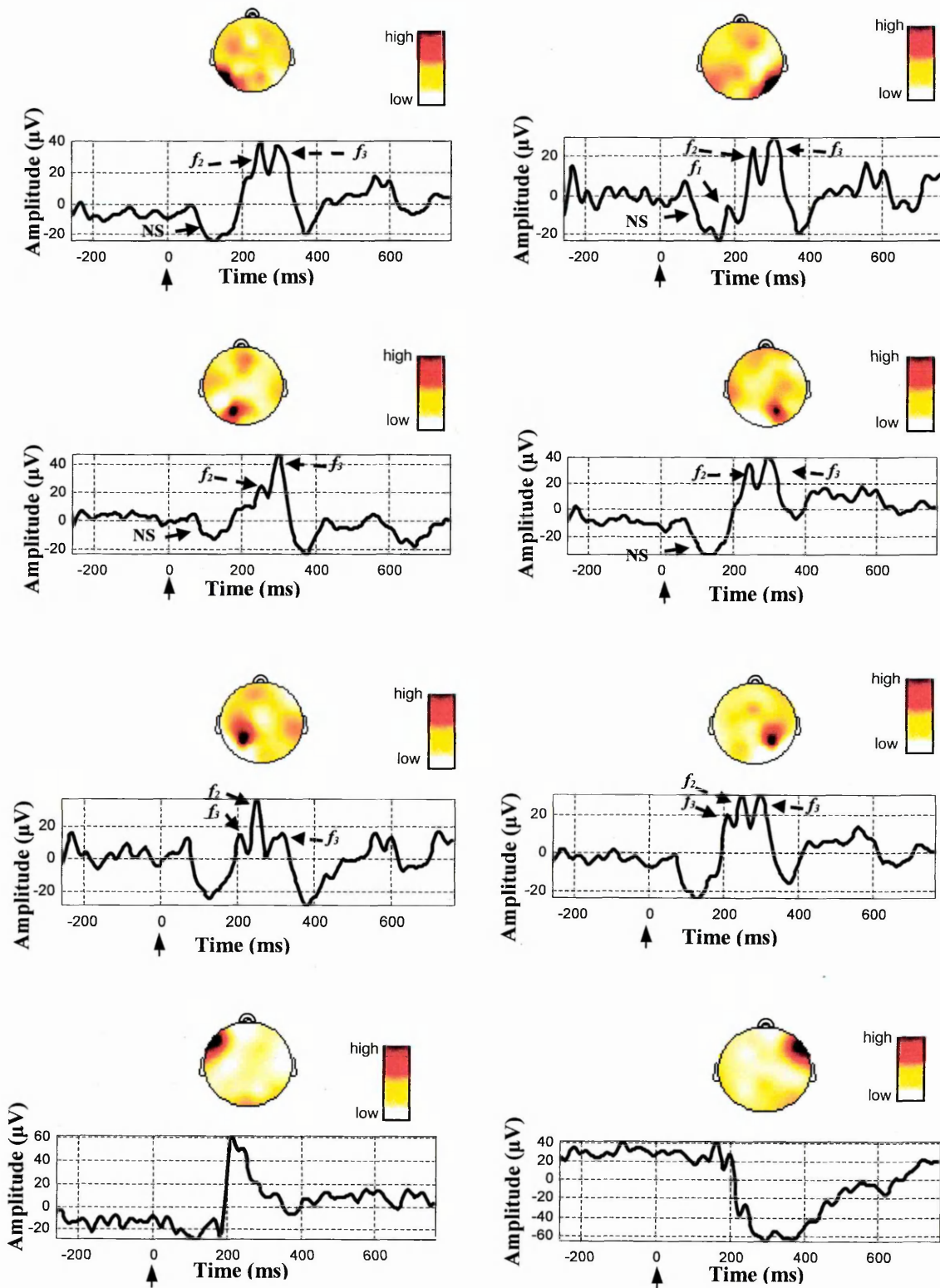


**Fig.8.2** Subject 1: Typical NLPCA extracted lambda waves with their scalp distributions (top three rows) and the corresponding extracted EOG waveforms with their scalp distributions (bottom row).

The following were observed in the study:

- The main features of the lambda wave (labelled  $f_1$ ,  $f_2$ ,  $f_3$  and negative shift, NS) were visible in the extracted waveforms. This indicated that the NLPCA algorithm extracted lambda wave like components. The shape of the extracted components was similar to the lambda wave extracted by using the ICA algorithm of Bell and Sejnowski (see Fig.8.1). Similar lambda wave like waveforms were extracted by NLPCA from the other subjects. A summary of the analysis results for the four temporal features of the lambda wave, obtained across the 7 subjects is provided in Table 8.1.

**Table 8.1** Summary of the analysis results for four temporal features of the lambda wave across the 7 subjects, when assessing the NLPCA approach to recover the lambda wave component.

	NS	$f_1$	$f_2$	$f_3$
Subject 1	✓	✓	✓	✓
Subject 2	✓	✓	✘	✓
Subject 3	✘	✘	✓	✓
Subject 4	✓	✓	✓	✓
Subject 5	✘	✘	✘	✓
Subject 6	✘	✓	✓	✘
Subject 7	✓	✘	✘	✘
<b>Total of subjects</b>	4	4	4	5

Key: ✓ = the feature was visible, ✘ = the feature was not visible

Table 8.1 indicated that not all the lambda wave features appeared in the components extracted by NLPCA. It was also observed that the four lambda wave temporal features were not all extracted for the 7 subjects. The features NS,  $f_1$ ,  $f_2$  and  $f_3$  were extracted in 4, 4, 4 and 5 subjects respectively, as indicated in Table 8.1.

- Fig 8.2 indicated that NLPCA extracted a number of components from the parieto-occipital area of the cerebral cortex. Some of these had the main characteristics of the lambda wave but showed some variations in their time courses. The peak activities of the components were

localised in distinct regions of parieto-occipital area. For each lambda wave peak activity identified over the left hemisphere a symmetrical peak of activity was observed over the right hemisphere. A typical set of lambda wave components with symmetrical peaks of activity are shown in Fig.8.2. This symmetry may be because both eyes follow the same target stimulus (red square on checkerboard).

- BS\_ICA extracted a lambda wave component with peak of activity which spread across the parieto-occipital area (see Fig.8.1). A comparison of the lambda wave peak activities obtained using the two methods indicated that NLPCA identified a number of distinct lambda wave sources within the parieto-occipital area while BS\_ICA treated the whole region as a single source. This may be due to non-linear PCA being more sensitive to the time course variations of the extracted lambda waves.
- The EOG components from both the left and the right eyes were also extracted (see bottom row of Fig.8.2). The polarity change for the left and right EOG waveforms is due to the reference electrode location ( $C_z$ ).

The above observations were consistent across the subjects included in the study. The results for three other subjects are shown in Fig.8.3, Fig.8.4 and Fig.8.5 for comparison purposes. A summary of the analysis results for the four temporal features of the lambda wave, obtained across the 7 subjects was provided in Table 8.1.

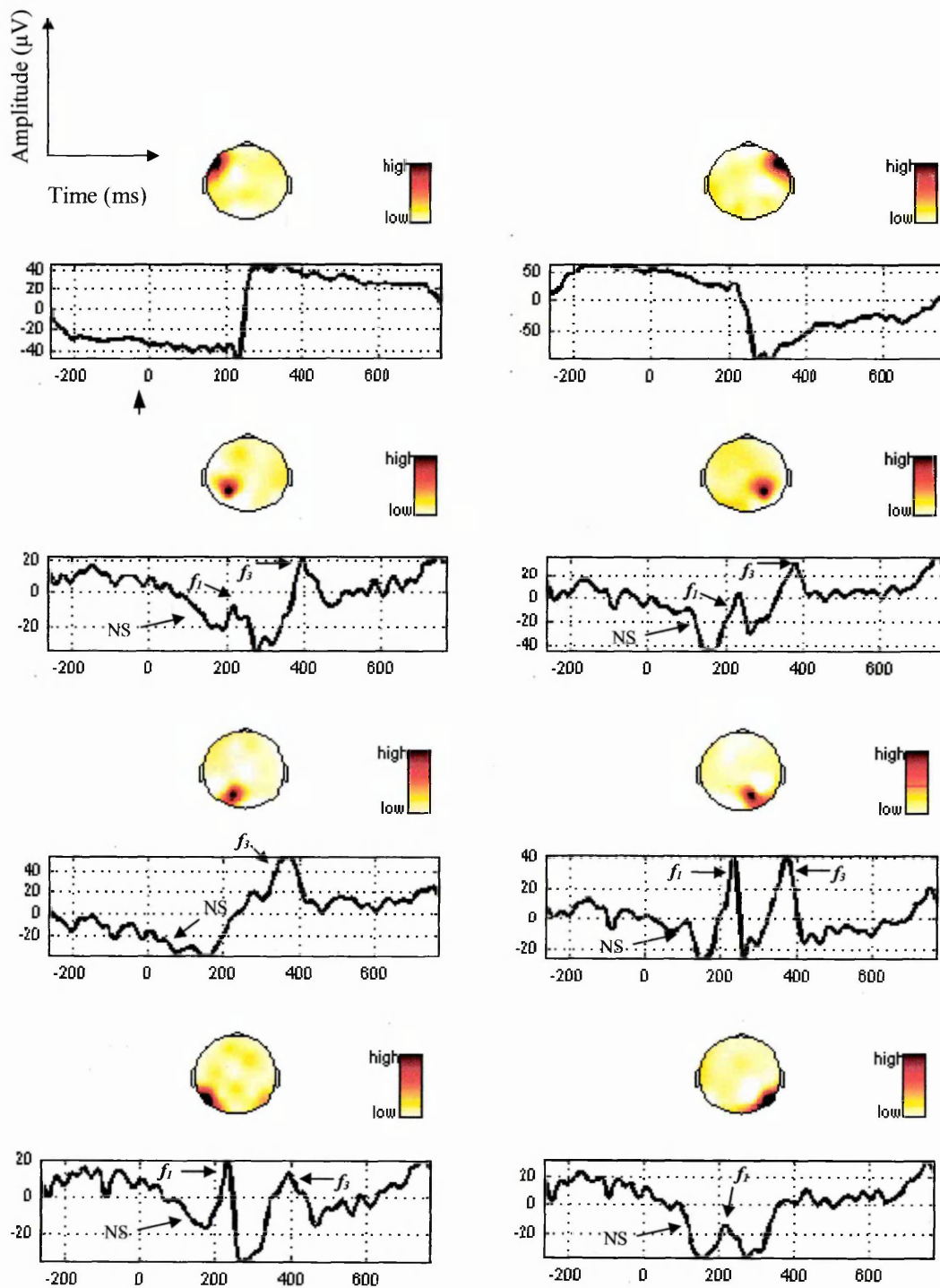


**Fig.8.3** Subject 2: The NLPCA extracted lambda waves with their scalp distributions (top three rows) and the corresponding extracted EOG waveforms with their scalp distributions (bottom row).

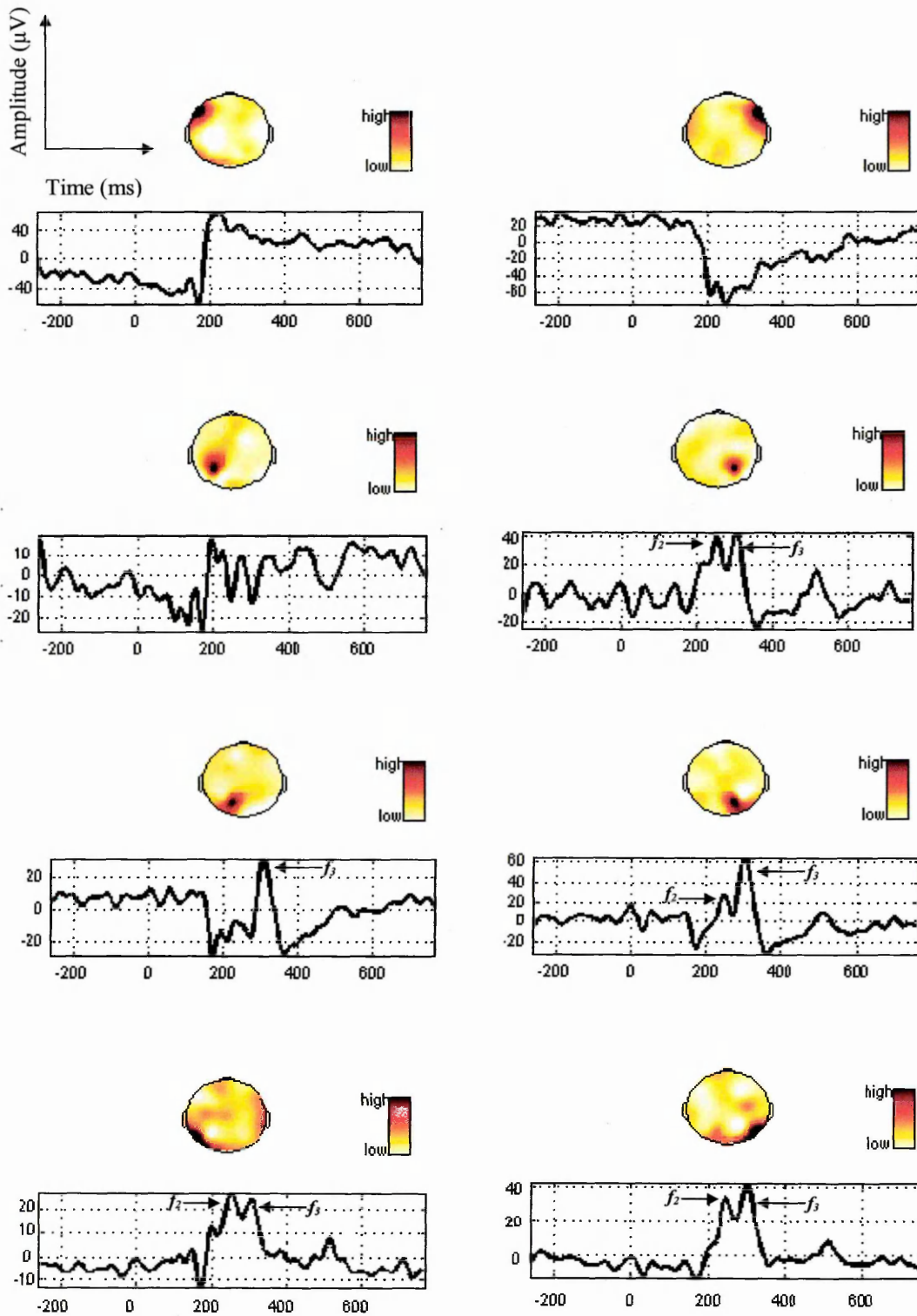


**Fig.8.4** Subject 3: The NLPCA extracted lambda waves with their scalp distributions (top three rows) and the corresponding extracted EOG waveforms with their scalp distributions (bottom row).

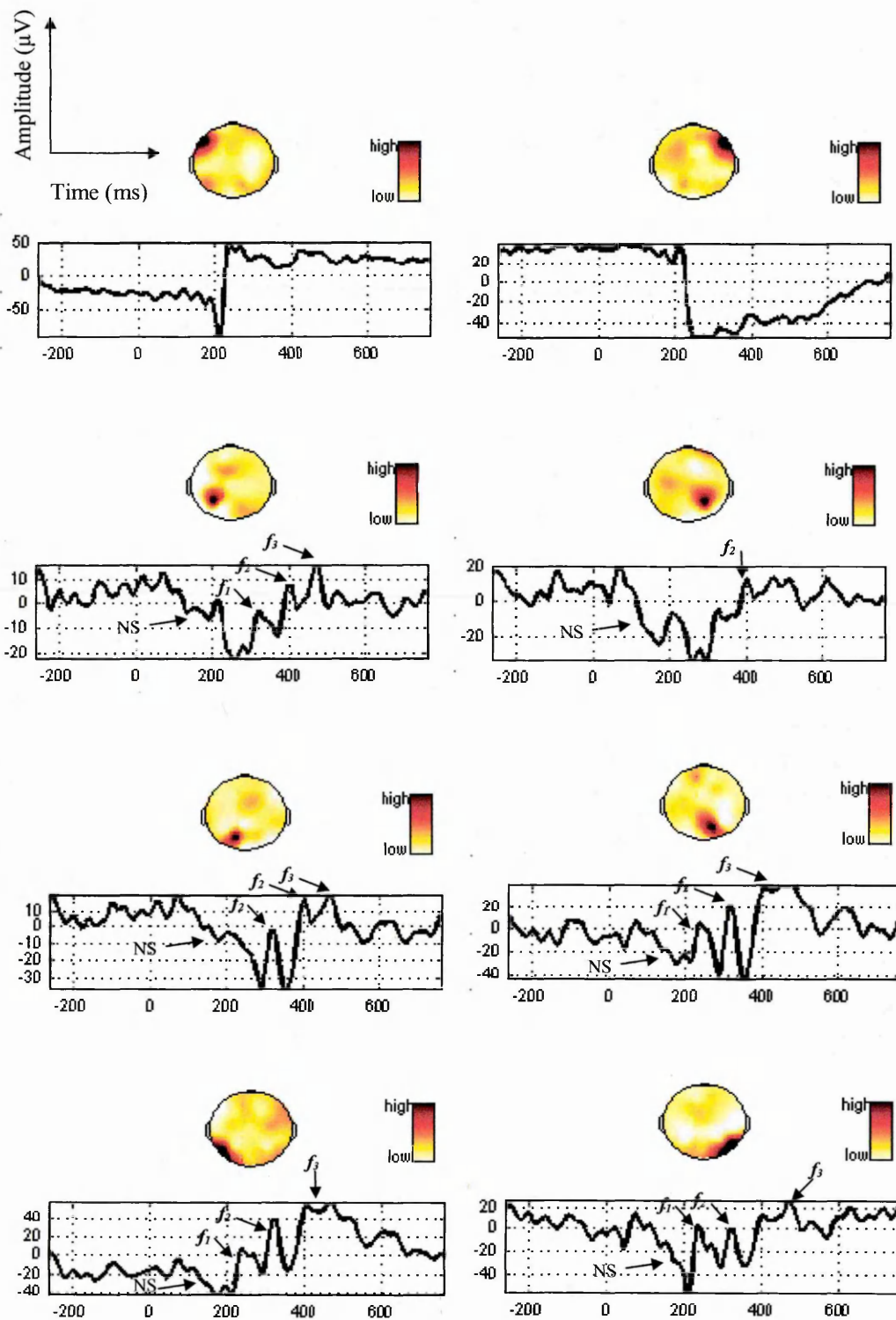


**Fig.8.5** Subject 4: The NLPCA extracted lambda waves with their scalp distributions (top three rows) and the corresponding extracted EOG waveforms with their scalp distributions (bottom row).

## 8.5 Conclusion

In this study an analysis of a signal source separation method called non-linear PCA (NLPCA) for extracting a saccade-related EEG component called the lambda wave, was carried out. A number of components with the main features of the lambda wave were extracted from the parieto-occipital area of the cerebral cortex. The peak of activities of these components corresponded to discrete locations and showed a symmetry over the left and right hemisphere. When comparing the performance of NLPCA to that of independent component analysis of Bell and Sejnowski (BS\_ICA), the study showed that NLPCA extracted the lambda wave from discrete regions of parietal-occipital area of the visual cortex while BS\_ICA treated the whole region as one source. These findings indicate that BS\_ICA considered the whole parieto-occipital area to be a single source for the lambda wave whereas NLPCA identified a number of symmetrical independent sources for the lambda wave in that region. From a clinical point of view, the brain is made of two symmetrical hemispheres. Clinicians believe that, although the two hemispheres of the brain are to some extent inter-connected, they do tend to operate independently from one another but in a symmetrical way. This viewpoint therefore seems to support the symmetrical solution of NLPCA.

The difference between the answers that NLPCA and BS\_ICA give when applied to the same data set, may be due to the difference in the assumptions made the two algorithms. NLPCA looks for subspaces in the data set whereas BS\_ICA looks for statistically independent components in the data set. As the two signal separation approaches look for different things in the data, they will probably converge to different solutions.

# **Chapter 9. Fuzzy Clustering Identification of BS\_ICA-Extracted Single-Trial Lambda Waves**

## **9.1 Chapter Summary**

The aim of the work described in this chapter was to automate the identification of the single-trial lambda waves components extracted by independent component analysis from the saccade-related background electroencephalogram (EEG) waveforms. The results obtained when a fuzzy clustering approach was used to achieve this aim are reported in this chapter.

## **9.2 Introduction**

As described in previous chapters, the analysis of lambda wave requires it to be separated from the various interfering signal components which are also picked up from the electrodes on the scalp. The application of BS\_ICA to  $n$  recorded electroencephalogram (EEG) waveforms resulted in  $n$  independent signal components. These components were visually inspected to identify specific EP components. The task of visual identification of specific EPs (specially when dealing with single-trials) was time consuming and required familiarity with the characteristic features of the components.

The aim of this study was to extract single-trial lambda waves from the background EEG and to automate their identification posterior to BS\_ICA application. The method was based on a fuzzy c-means clustering algorithm. Fuzzy logic clustering is an unsupervised pattern recognition algorithm which partitiones the data into required number of waveform categories [9.1] [9.2]. It provides the degree that an extracted BS\_ICA component belongs to a certain group.

### 9.3 Fuzzy C-Means (FCM) Clustering Pattern Recognition

The object of cluster analysis is to classify waveforms according to their similarities. Clustering is a form of unsupervised learning pattern recognition as it does not require prior information on the waveforms of known types. In a 'binary clustering' a waveform can only be allocated to a single class as shown in Fig.9.1a. However, in fuzzy clustering a waveform can belong to a number of classes with different degrees of membership as shown in Fig.9.1b. This is achieved by providing a membership value ( $\mu_{ik}$ ) which indicates the degree a waveform  $k$  belongs to the class (cluster)  $i$ .

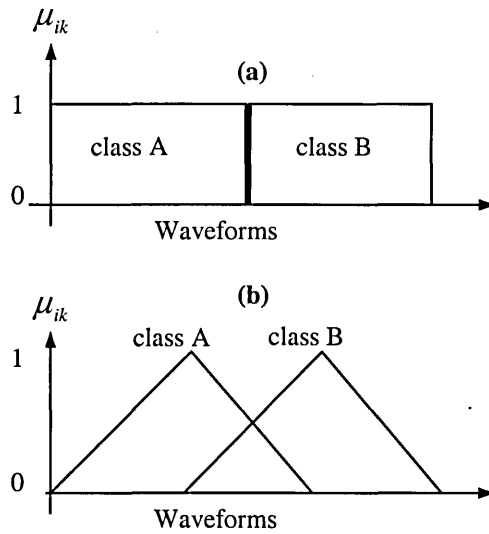


**Fig.9.1 (a)** Binary clustering membership functions and **(b)** Fuzzy logic clustering membership functions.

For a waveform  $k$  and  $c$  clusters,  $\mu_{ik}$  is normally constrained to  $0 \leq \mu_{ik} \leq 1$  and

$$\sum_{i=1}^c \mu_{ik} = 1.$$

The main advantage of fuzzy clustering over binary clustering is that a waveform is not forced to belong to one class. Therefore, an extracted single-trial component which partly resembles the lambda wave can still belong to the lambda wave category but with a degree of membership less than 1.

There are several fuzzy cluster analysis approaches. Höppner *et al.* [9.1] and Bezdek *et al.* [9.2] provided a review of fuzzy clustering algorithms. In this study the fuzzy c-means clustering algorithms [9.2] was used.

Given a set of  $N$  waveforms, each represented with  $n$  features as,

$$F = \begin{bmatrix} F_{11} & F_{12} & \dots & F_{1N} \\ F_{21} & F_{22} & \dots & F_{2N} \\ \cdot & \cdot & \cdot & \cdot \\ \cdot & \cdot & \cdot & \cdot \\ F_{n1} & F_{n2} & \cdot & F_{nN} \end{bmatrix}, \text{ the fuzzy c-means clustering partitions } F \text{ into}$$

predefined number of classes ( $c$ ) by using the algorithm described below.

**Repeat for  $\xi=1,2, \dots$**

**step 1: compute the cluster prototypes (means):**

$$v_i^{(\xi)} = \frac{\sum_{k=1}^N (\mu_{ik}^{(\xi-1)})^\delta F_k}{\sum_{k=1}^N (\mu_{ik}^{(\xi-1)})^\delta}, \quad 1 \leq i \leq c \quad (9.1)$$

where  $F_k = [F_{1k}, \dots, F_{nk}]^T$  is the  $k^{\text{th}}$  pattern and  $\delta > 1$  influences the cluster partitioning by controlling the degree of fuzziness for the membership of the waveforms to the clusters. As the value of  $\delta$  approaches 1, the membership of the clusters becomes closer to binary values (i.e. 0 for not a member and 1 for a full member). As its value becomes larger than 1, the membership of the waveforms to the clusters becomes more fuzzy, i.e. a waveform becomes more associated with a larger number of clusters.

**step 2: compute the Euclidean distances between each pattern  $k$  to the  $i^{\text{th}}$  cluster center:**

$$d_{ik}^2 = (F_k - v_i^{(\xi)})^T (F_k - v_i^{(\xi)}) \quad 1 \leq i \leq c, 1 \leq k \leq N. \quad (9.2)$$

**step 3:** update the degree of membership values:

if  $d_{ik} > 0$  for  $1 \leq i \leq c$ ,  $1 \leq k \leq N$ ,

$$\mu_{ik}^{(\xi)} = \frac{1}{\sum_{j=1}^c \left( \frac{d_{ik}}{d_{jk}} \right)^{\left( \frac{2}{\delta-1} \right)}} \quad (9.3)$$

otherwise  $\mu_{ik}^{(\xi)} = 1$

**until**  $\left\| \Psi^{(\xi)} - \Psi^{(\xi-1)} \right\| < \tau$  (9.4)

where  $\Psi$  is the matrix of degree of membership values represented by,

$$\Psi_{(N,c)} = \begin{bmatrix} \mu_{11} & \mu_{21} & \cdots & \mu_{c1} \\ \cdot & \cdot & \cdot & \cdot \\ \cdot & \cdot & \cdot & \cdot \\ \mu_{1N} & \mu_{2N} & \cdots & \mu_{cN} \end{bmatrix} \quad (9.5)$$

The parameter  $\tau > 0$  is the iteration termination tolerance.

## 9.4 Experimental method

Details of the data recording procedures are provided in chapter 4, section 4.4.2.

### 9.4.1 Operations for Extracting the Single-Trial-Components from EEG

#### Mixtures

The operations to extract the lambda wave were:

- i) Pre-processing
- ii) Spatial averaging
- iii) Abutting successive trials.
- iv) Signal source separation (i.e. whitening and application of BS\_ICA)
- v) Back-projection of the separated components to the electrode sites on the scalp.

These operations are described in the following sections.

Operations i), ii) and iii) are described in chapter 6, sections 6.3.1, 6.3.3.1 and 6.3.3.2 respectively. Section iv) and v) are described in chapter 6, sections 6.3.4 to 6.3.5 respectively.

#### **9.4.2 Inspection of BS\_ICA-Extracted Components**

990 BS\_ICA component waveforms were extracted from the spatially averaged single-trial waveforms recorded from a subject. The BS\_ICA components were divided by an expert familiar with the features of the lambda wave into 390 lambda waves and 600 non-lambda waves. This manual classification of the components was necessary in order to be able to assess the performance of the fuzzy clustering method against the decisions of the expert.

#### **9.4.3 Lambda Wave Representation by Feature Set**

The lambda wave was characterised by a spatial and three temporal features. The spatial feature represented the scalp topography of the BS\_ICA-extracted components. The spatial feature estimated the percentage contribution of each BS\_ICA-extracted component to the expected region of the scalp associated with the lambda wave (i.e. parieto-occipital). Details of its calculation are provided in chapter 6, section 6.3.5.

The three temporal features represented the gradients  $m_1$ ,  $m_2$  and  $m_3$  of the trend of the lambda wave as described in chapter 7, section 7.3.2.1. The three temporal features broadly characterised the three main sections of the lambda wave. A procedure was developed to identify the starting and end points of each section. This procedure is described in chapter 7, section 7.3.2.1. A first order polynomial was fitted into the points within each of the three sections and then the corresponding gradients were obtained.

#### 9.4.4 Classification of the BS\_ICA-Extracted Components

The operations involved in classifying the BS\_ICA-extracted components using the fuzzy c-means algorithm are shown in Fig.9.2.

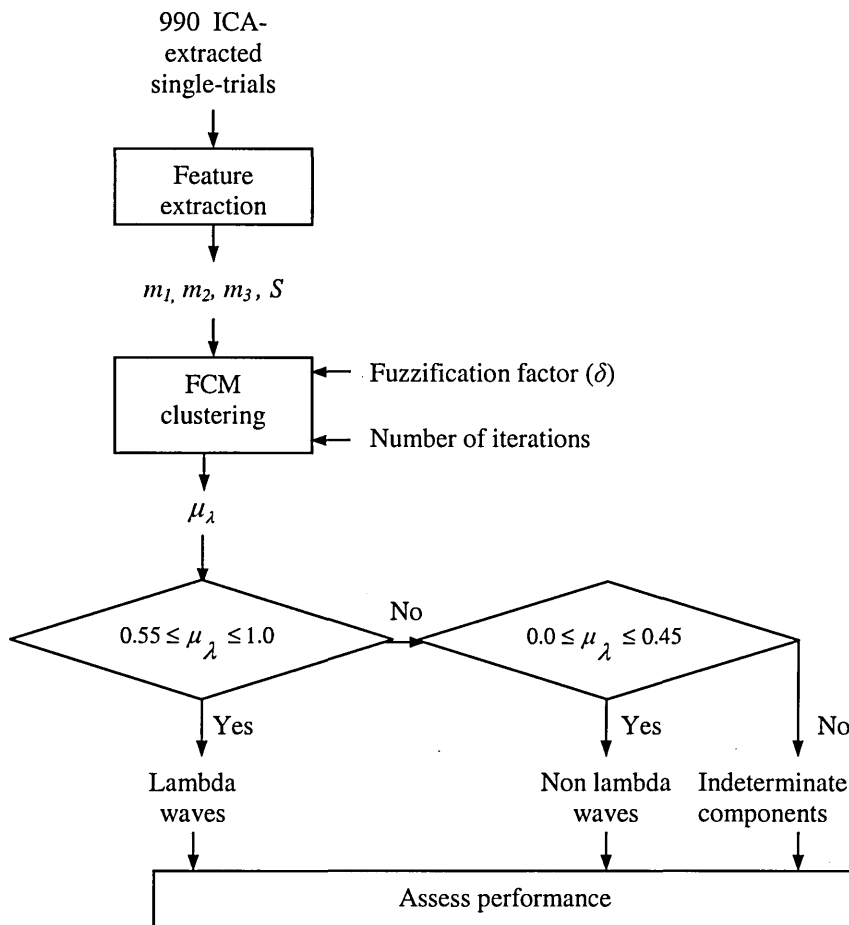


Fig.9.2 Operations involved for fuzzy c-means clustering.

The three gradient features ( $m_1, m_2$  and  $m_3$ ) together with the scalp topography feature ( $S$ ) obtained from each BS\_ICA-extracted component were processed by the fuzzy c-means clustering algorithm. Suitable values for the fuzzification factor ( $\delta$ ) and the number of iteration were determined by experimenting with a range of values as described in the result section. The algorithm provided the degree of membership ( $\mu_\lambda$ ) that an BS\_ICA-extracted component belonged to the lambda wave category (the degree that an BS\_ICA-extracted component belonged to the non-lambda wave

category was  $1-\mu_\lambda$ ). Based on the values of  $\mu_\lambda$  the components were classified as lambda waves (for  $0.55 \leq \mu_\lambda \leq 1.0$ ), non-lambda waves (for  $0.0 \leq \mu_\lambda \leq 0.45$ ) and indeterminate (for  $0.45 < \mu_\lambda < 0.55$ ). The indeterminate components could not be confidently classified as belonging to either the lambda waves or non-lambda waves categories. The results were then compared to those obtained when the BS\_ICA-extracted components were visually classified.

## 9.5 Results and Discussion

The plots of the features of the BS\_ICA-extracted single-trial components (classified visually as lambda or non-lambda waves) are shown in Figs.9.3a-d. Each feature set has been normalised between -1 and 1 across trials. The features for the lambda waveforms are represented by circles and non-lambda waveforms by crosses.

Figs.9.3a and b show 3-dimensional plots of the gradients ( $m_1$ ,  $m_2$  and  $m_3$ ). The features formed two main clusters which partially overlapped. The plots of the scalp topography feature are shown in Fig.9.3c and d. This feature tended to be mainly positive for the lambda waves and mostly negative for the non-lambda waves.

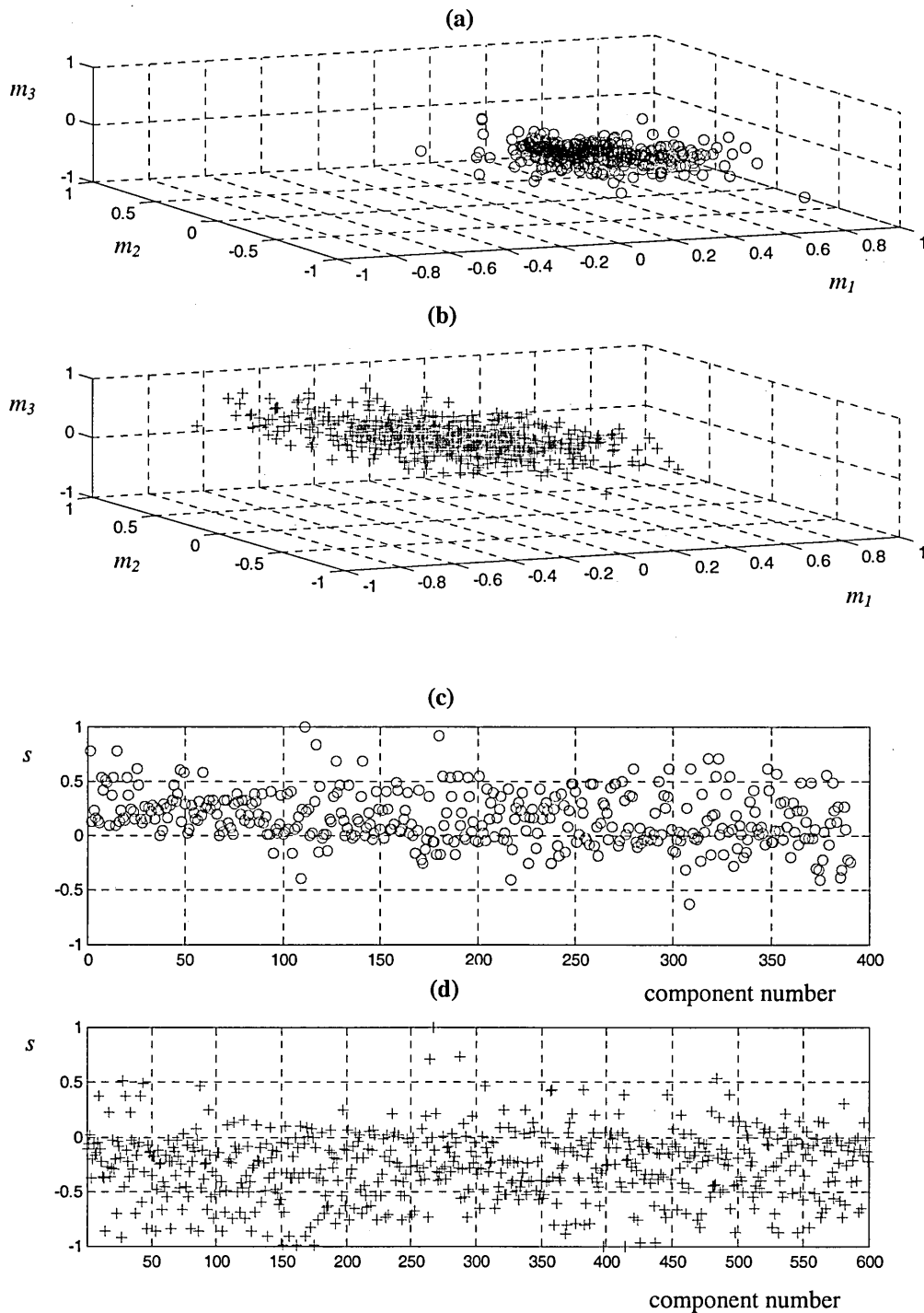


**Fig.9.3** Plot of the features of BS\_ICA-extracted single-trial components identified as either the lambda waves (o) or non-lambda waves (+). (a) and (b) represent the gradients ( $m_1$ ,  $m_2$  and  $m_3$ ) features, (c) and (d) the scalp topography feature ( $S$ ).

The results obtained when analysing the performance of the fuzzy c-means algorithm are provided in Tables 9.1. After 10 iterations, 97.4% of the lambda waves (i.e. 380 out of the 390) and 78.5% of the non-lambda waves (i.e. 471 out of 600) were classified in accordance with visual classification. The results shown are for fuzzification factor ( $\delta$ ) equal to 2 which provided the most accurate results.

**Table 9.1** Performance results of the fuzzy c-means clustering algorithm, with fuzzification factor ( $\delta$ ) = 2 and number of iteration ( $\xi$ ) =10.

**(a) the lambda waves**

$\delta$	Lambda Waves				Non-lambda Waves				Indeterminate			
	n	%C	$\mu_\lambda$ mean	$\mu_\lambda$ std	n	%C	$\mu_\lambda$ mean	$\mu_\lambda$ std	n	%C	$\mu_\lambda$ mean	$\mu_\lambda$ std
2	380	97.44	0.72	0.07	4	1.02	0.42	0.01	6	1.54	0.45	0.04

**(b) nonlambda waves**

$\delta$	Lambda Waves				Non-lambda Waves				Indeterminate			
	n	%C	$\mu_\lambda$ mean	$\mu_\lambda$ std	n	%C	$\mu_\lambda$ mean	$\mu_\lambda$ std	n	%C	$\mu_\lambda$ mean	$\mu_\lambda$ std
2	75	12.5	0.32	0.10	471	78.5	0.78	0.11	54	9	0.51	0.03

where n is the number of trial waveforms and %C =  $n/T \times 100$  where T is the total number of trial waveforms.

The main points of this study were summarised below.

- As fuzzy c-means clustering algorithm is an unsupervised learning algorithm, it did not require training on the waveforms from known types. The method provided the degree of membership for each waveform which is a measure of to what extent an BS\_ICA-extracted component belonged to the lambda wave category. Table 9.2a indicated that 97.4% of the BS\_ICA-extracted components which were identified visually as lambda wave were also classified as lambda wave by the method.

- The discrepancies between the results obtained using the fuzzy c-means clustering approach and those obtained by visual inspection may be due to a number of factors: (i) The visual inspection process may have resulted in the erroneous categorising of some of the BS\_ICA-extracted components. (ii) The feature sets used may have not been sufficiently sensitive for characterising the waveforms.

## 9.6 Conclusion

The effectiveness of a fuzzy c-means clustering approach for identifying lambda waves components extracted by BS\_ICA from single traces (or trials) of saccade-related electroencephalogram (EEG) waveforms was investigated. The BS\_ICA-extracted single-trial components for 50 trials were visually inspected and were separated into 390 lambda waves and 600 non-lambda waveforms. Each waveform was represented by one spatial and three temporal features. These features were then processed by a fuzzy c-means algorithm. Using this algorithm, 97.4% of the lambda waves and 78.5% of the non-lambda waves were identified in accordance with visual classification of the components.

The study demonstrated that it was possible to automate the identification of single-trial lambda wave using the fuzzy c-means algorithm.

# **Chapter 10. Summary of overall results, Conclusions and Future Works**

## **10.1 Chapter Summary**

This chapter provides a summary of the overall results, a conclusion to the study and future works.

## **10.2 Summary of the overall results**

The ongoing electrical activity of the brain is known as the electroencephalogram (EEG). Evoked potentials (EPs) are voltage deviations in the EEG elicited in association with stimuli. EPs therefore provide clinical information by allowing an insight into neurological processes. The amplitude of an EP potential is typically several times less than the background EEG. The background EEG has the effect of obscuring the EPs and therefore appropriate signal processing is required for their recovery.

Saccade-related EEG waveforms were recorded from 7 subjects. The saccade-related EEG waveforms recorded from electrodes placed on the scalp contain a mixture of signals. These are:

- i) Saccade-related EP components (for example the lambda wave).
- ii) Non-saccade-related EEG components, i.e. the background EEG and stimulus time-locked EP components that are not related to the saccade.
- iii) The contaminating electrophysiological signals such as the electrooculogram (EOG). EOG is generated by the eyes when eye-movements or blinks are performed.
- iv) Non-electrophysiological (external) contaminating signals, for example the noise generated by the recording system.

The conventional methods of recovering EPs from the background EEG are based on averaging. Using these methods a large number (typically about 50) of EPs are recorded and then averaged with respect to the onset of stimulus. Averaging is a valuable pre-processing tool prior to signal source separation as it can improve the 'signal-to-noise'

ratio. However, the EP recovered using averaging remains a mixture of signal components from a number of sources. A signal source separation methodology based on a technique called the independent component analysis of Bell and Sejnowski (BS\_ICA) was used to analyse the recorded waveforms.

In chapter 5, a procedure for quantifying the effectiveness of algorithms for removing EOG contamination from the EEG was developed. Four methods for OA removal were included in the study. These were the two BS\_ICA-based algorithms of extended independent component analysis (extended-ICA) and joint approximation diagonalisation of eigenmatrices (JADE), the principal component analysis (PCA) technique and the EOG subtraction method. The devised procedures made it possible for the performances of the four algorithms for OA removal to be quantified and compared.

The operation of JADE and extended-ICA is subject to amplitude scaling and channel permutation. Procedures were incorporated to estimate the amplitude of the recovered EEG waveforms and to allocate them to the correct channels. Cardoso's amplitude recovery method enabled the amplitude of the recovered EEG to be estimated for both JADE and extended-ICA. However, the results showed that the performances of Cardoso's amplitude recovery method were affected when changing the values of the mixing matrix. The proposed correlation based method provided a means for dealing with the problems of channel permutation and sign changes associated with JADE and extended-ICA algorithms.

It was demonstrated that the signal separation techniques of JADE and extended-ICA were more effective than the correlation-based techniques of EOG subtraction and PCA, for removing OA from the EEG. Statistical tests indicated that on average the performances of JADE and extended-ICA for OA removal were not significantly different. Extended-ICA method required a significantly longer time to carry out the OA removal operation as compared with JADE. This is because extended-ICA is an iterative algorithm which requires many passes through its learning algorithm to converge while JADE only requires one pass through its algorithm. However JADE provided a more consistent set of results and both JADE and extended-ICA performed significantly better than PCA and EOG subtraction. This could be because PCA only decorrelates signals while JADE and extended-ICA attempt to make the recovered signal components as independent as

possible. The EOG subtraction method was shown to cause attenuation of the recovered EEG waveforms. This is because a fraction of the EEG that contaminates the EOG signal is also subtracted from the recovered EEG component. The effect of additive Gaussian noise on the performance of the four OA removal methods was also investigated. This indicated that the performance of the methods was unaffected by an additive Gaussian noise source as long as the signal-to-noise ratio remained above 50. These investigations demonstrated the suitability of ICA-based signal source separation techniques of JADE and extended-ICA for OA removal of the EEG.

In chapter 6, an iterative time-synchronisation procedure was devised to time-synchronise the recorded waveforms across trials. The method provided the ability to optimally synchronise the trials with respect to the eye movement interest prior to averaging. This ensured that the time features of the signals components that are time-locked to the eye movement such as the lambda wave were preserved during the subsequent averaging operation for reducing the effect of background EEG. The time-synchronisation procedure was evaluated. This involved plotting the histogram of the saccade offset across the 50 trials for a given subject and experimental event. It was observed that the process has reduced the deviation of the saccade offset distribution and thus provided a less distorted averaged EOG waveform. It was observed that the process of iterative synchronisation resulted in the extraction of the lambda wave feature  $f_2$  which was not visible in the averaged lambda waves without time-synchronisation. These results showed that the devised iterative synchronise averaging method was an effective preprocessing operation prior to the application of BS\_ICA for extracting the lambda wave.

The recorded EEG waveforms were analysed using the Bell and Sejnowski ICA algorithm (BS\_ICA). The method successfully isolated the EOG waveforms caused by eye movements in both the right and left eyes, together with their scalp distribution in the region close to the right and left eye respectively. The method also enabled the extraction of a number of EPs components related to the performance and generation of saccadic eye movements, and their scalp distribution to be obtained. These were: the frontal and occipital pre-saccadic potentials, and the lambda wave. These potentials had their peak of activity in the frontal and occipital region of the cerebral cortex. The occipital pre-saccadic potential was found to occur about 30 ms after the frontal one. This finding suggested that the occipital pre-saccadic potential is an efferent feedback or copy from the frontal areas

for saccade generation. Three sub-components were extracted from the occipital area of the cerebral cortex. These appeared immediately after the saccade onset and ended shortly after the saccade offset (about 300 ms after stimulus). The fact that the occipital pre-saccadic potential and the following three sub-components were extracted separately suggested that they were generated by independent neural processes. This could not have been detected without the application of a signal source separation technique.

The characteristics of the lambda wave features depend on factors such as the saccade duration or the viewing angle ( $\alpha$ , shown in Fig.4.4 in chapter 4). In our study, where a short duration of saccade (about 20 ms) was used, we did not observe the feature  $f_I$  in either time-synchronised or not time-synchronised averaged lambda waves. This was in accordance with the observations made in [1.5] where the feature  $f_I$  was observed only in the averaged EEG waveforms of a subject for a longer duration of saccade (75 ms to 100 ms). However, in our study this feature became visible for the short duration of saccade (about 20 ms) when BS\_ICA was applied to the time-synchronised averaged waveforms. In the study reported in [1.5] they did not observe the feature  $f_I$  for such small duration of saccade. This could not have been observed without the application of a signal source separation technique such as BS\_ICA. The results revealed valuable information about the brain mechanisms involved in performing saccades.

Novel techniques were devised in order to improve the performance of BS\_ICA for extracting the lambda wave EP component.

In chapter 6, a method was devised to increase the effective length of the EEG waveforms processed by BS\_ICA, in order to enhance their stationarity property and thus to make them more suitable for BS\_ICA signal separation. This involved abutting EEG traces from an appropriate number of successive trials (a trial was a set of waveforms recorded from 64 electrode locations in an experiment involving a saccade performance). The analysis was initially carried out on artificially mixed waveforms. This allowed the approaches to be quantitatively assessed by comparing the extracted BS\_ICA components waveforms to the original signal waveforms. The correlation coefficient ( $\rho$ ) and euclidean distance ( $\varepsilon$ ) parameters were used to quantitatively assess the similarity between the original and recovered waveforms. This demonstrated that the effectiveness of BS\_ICA for extracting

the EEG waveform from the mixtures gradually improved (i.e.  $\rho$  closer to 1,  $\varepsilon$  closer to 0) when the signal length was increased (by abutting process) from 256 data points (i.e. 1 trial) to 1024 data points (i.e. 4 trials). This may be because the components of the artificially generated signal mixtures (i.e. the EOG waveform and the EEG waveform with main lambda wave characteristics) are short-duration transient signals and the abutting of the waveforms to increase their lengths improved their stationarity. As BS\_ICA relies on the stationarity of the signals, the abutting process therefore provided a means to make the waveforms more suitable for processing by BS\_ICA.

The analysis was then extended to the not-abutted and abutted 22 time-synchronised averaged waveforms and the performance of the two approaches (not-abutted and abutted) was evaluated and compared for extracting the lambda wave across the 7 subjects. One spatial and 5 temporal features of the lambda wave were monitored to assess the performance of BS\_ICA applied to both abutted and not-abutted waveforms. BS\_ICA applied to abutted trials managed to extract all 6 features across all the 7 subjects included in the study. This was not the case when BS\_ICA was applied to the not-abutted trials, where it managed to extract some of the features in only some of the subjects. Moreover, the both temporal and spatial features of the lambda wave extracted were preserved more accurately when BS\_ICA was applied to the abutted waveforms. These results demonstrated that the abutting of the trials is an effective mechanism for improving the performance of BS\_ICA in extracting evoked potentials from the recorded EEG waveforms.

In summary, the four approaches investigated were ranked in the following order of decreasing effectiveness for extracting the lambda wave.

- i) BS\_ICA applied to abutted, averaged waveforms with time-synchronisation.
- ii) BS\_ICA applied to not-abutted, averaged waveforms with time-synchronisation .
- iii) Not-abutted, averaged waveforms with time-synchronisation.
- iv) Not-abutted, averaged waveforms without time-synchronisation.

In chapter 7, a model that represented the temporal characteristics of a saccade-related EP called the lambda wave was developed and was incorporated into the BS\_ICA algorithm. The developed method consisted of utilising prior information about the time characteristic features of the lambda wave, and the use of this information in order to guide the algorithm

to extract the EP component of interest (the lambda wave). The performance of this model-based BS\_ICA approach was quantitatively assessed, and its effectiveness was compared to that of the conventional (without prior information, i.e. model-less) BS\_ICA algorithm. The performance evaluation of the two BS\_ICA approaches (i.e. with and without model) was carried out by using artificially mixed waveforms and the 22-averaged EEG waveforms. In the case of artificially generated mixtures, it was shown that the model-based BS\_ICA approach performed significantly more effectively than conventional (without model) BS\_ICA approach for extracting the lambda wave component, specially in the case of severe contamination of the lambda wave by the EOG. It was also observed that the incorporation of the model into the BS\_ICA did not deteriorate the recovery of the EOG component from the mixtures.

For the case when the BS\_ICA approaches were applied to the 22-averaged EEG waveforms, the model-based BS\_ICA managed to extract successfully the five monitored lambda wave features in all 7 subjects. This was not the case when the conventional (without model) BS\_ICA approach was used, where the five monitored features of the lambda wave were visible only in some of the subjects and were more distorted than when model-based BS\_ICA was used. The results indicated that the incorporation into the BS\_ICA algorithm of a temporal model of the lambda wave improved its signal source separation ability for extracting the lambda wave.

The characteristics of the developed model-cost function were also investigated. The results showed that the introduction of a smoothing factor into the model cost-function improved the stability of the BS\_ICA-model based algorithm.

In chapter 8, a recursive least-squares based non-linear PCA (NLPCA) algorithm was used to carry out the analysis of the 22 spatially-averaged saccade-related waveforms so as to extract the lambda wave. The results were compared with those obtained using the methodology based on the ICA algorithm of Bell and Sejnowski. The results showed that the NLPCA algorithm was effective in extracting components with the main lambda wave features. A number of components were extracted from the parieto-occipital area of the cerebral cortex. Some of these had the main characteristics of the lambda wave but showed some variations in their time courses. The peak activities of the components were localised in distinct regions of parieto-occipital area. For each lambda wave peak activity identified

over the left hemisphere a symmetrical peak of activity was observed over the right hemisphere. This symmetry may be because both eyes followed the same target stimulus (red square on checkerboard). A comparison of the lambda wave peak activities obtained using the two methods indicated that NLPCA identified a number of distinct lambda wave sources within the parieto-occipital area while BS\_ICA treated the whole region as one source. The application of NLPCA to the recorded averaged waveforms provided further insight into the saccade-related data and assisted in understanding the possible brain mechanisms involved during the generation and performance of saccadic eye movements.

In chapter 9, a procedure was implemented to automate the identification of single-trial saccade-related lambda waves. The effectiveness of a fuzzy c-means clustering method was investigated for identifying lambda waves extracted by BS\_ICA. The BS\_ICA-extracted single-trial waveforms for the 50 trials were visually inspected and were separated into 390 lambda waves and 600 non-lambda waveforms. Each waveforms was represented by one spatial and three temporal features. These features were then processed independently by the implemented fuzzy c-means pattern recognition algorithm in order to identify the single-trial lambda waves. It was shown that this method correctly identified the lambda waves with an accuracy of 97.4% in accordance with visual inspection results, as shown in Fig.10.1.

Pattern Recognition Method	Lambda waves			Non- lambda waves		
	Correctly classified (%)	Mis-classified (%)	Un-Classified (%)	Correctly classified (%)	Mis-classified (%)	Un-Classified (%)
Fuzzy c-mean clustering algorithm	97.4	1.02	1.54	78.5	12.5	9

**Fig.10.1** Results of the single-trial BS\_ICA-extracted lambda waves classification for the fuzzy c-means clustering approach.

The results demonstrated that the fuzzy c-means clustering method provided a effective means to automate the identification of the single-trial lambda wave components extracted by BS\_ICA.

### 10.3 Thesis conclusion

The study led to the development of procedures based on signal source separation techniques that facilitated the extraction of saccade-related evoked potentials (EPs) from recorded mixtures and thereby contributed towards improving the clinical understanding of vision when moving the eyes. Saccade-related evoked potential (EP) signals contained within the recorded electrical activity of the brain (EEG mixtures) have amplitudes that are typically several times less than the obscuring background electroencephalogram (EEG). Moreover, the saccade-related EP signals are susceptible to contaminations from various electrophysiological signals.

When dealing with saccade-related EEG waveforms, the ability to filter the contaminating electrooculogram (EOG) signal from the recorded EEG is essential for an accurate EPs estimation and clinical interpretation to be carried out. The ability to quantitatively assess and compare the performances of four ocular artefact (OA) removal algorithms from the EEG was demonstrated by devising a procedure that enabled the similarity between the EEG waveforms before contamination by OA and the contaminated EEG waveforms following their processing by an OA removal method to be measured. The devised procedures made it possible for the performances of the four algorithms for OA removal to be quantified and compared. They also enabled the significance of the difference between their performances to be assessed and compared.

For saccade-related EPs estimation and analysis, the ability to preserve the time features of the recorded EEG waveforms prior to averaging is essential. An iterative time-synchronisation procedure that time-synchronised the recorded waveforms across trials with respect to the eye movement was devised. The iterative time-synchronisation procedure preserved more effectively the features of the eye movement and of the signals components that were time-locked to it (e.g. lambda wave). The results indicated that the devised iterative time-synchronise averaging method was a valuable operation to be performed on the recorded waveforms prior to averaging.

The ability to separate components from the EEG mixtures recorded from electrodes placed on the scalp is essential for clinical neurophysiology. The effectiveness of a signal

source separation technique called independent component analysis (BS\_ICA) was demonstrated by extracting a number of EP components related to the performance and generation of saccadic eye movements from the recorded mixtures.

The conformation of the recorded waveforms to the BS\_ICA algorithm assumptions is essential if these waveforms are to be analysed using an BS\_ICA algorithm. The ability of a novel method of averaging devised to enhance the stationarity property of the recorded waveforms and thus to make them more suitable for BS\_ICA signal source separation, was demonstrated. This method involved abutting a number of successive EEG recording (trials) and then performing the averaging process on the abutted trials. It was quantitatively demonstrated that BS\_ICA performance for extracting the lambda wave was significantly improved when it was applied to the abutted trials.

A template-model that represented the temporal characteristics of the lambda wave was developed and its incorporation into the BS\_ICA signal separation operation was investigated. The effectiveness of the developed model-based BS\_ICA method was demonstrated by quantitatively assessing its performance in extracting the lambda wave. It was demonstrated that the incorporation into the BS\_ICA algorithm of a temporal model of the lambda wave improved its ability to extract the lambda wave from the EEG waveforms.

It can be a very time-consuming and tedious task to visually inspect the BS\_ICA-extracted components one by one, in order to identify the EP components. The ability to quickly and accurately identify the lambda waves amongst the BS\_ICA-extracted components is therefore valuable. The effectiveness of a fuzzy c-means clustering method for this task was investigated. The results showed that the method identified the single-trial lambda waves with an accuracy of 97.4%.

A recursive least-squares based non-linear PCA (NLPCA) algorithm was used to carry out further analysis of the 22 spatially-averaged saccade-related EEG waveforms. The NLPCA-extracted components were compared with those obtained using the methodology based on the ICA algorithm of Bell and Sejnowski. The results showed that the NLPCA algorithm extracted a number of EP components with the main features of the lambda wave from the parieto-occipital area of the cerebral cortex with peak activities localised in

distinct and symmetrical regions on both hemisphere of the parieto-occipital area. Comparing these results to that of BS\_ICA lead to the conclusion that NLPCA considered distinct regions of the parieto-occipital area of the cerebral cortex as being separate sources of the lambda wave where as BS\_ICA treated the whole region as one source.

The progress made so far in applying signal source separation based techniques to the recorded saccade-related EEG waveforms provided an excellent foundation for further investigations. The following sections will suggest ways to continue this work.

## **10.4 Suggestions for future work**

The effectiveness of the BS\_ICA-based algorithm could be improved in two main areas. These are (i) investigating the ability of non-linear BS\_ICA to unmix EEG waveforms as EEG signal can contain linear as well as nonlinear mixtures and (ii) devising techniques (mainly based on Bayesian mathematical approach) which will enable prior information about both the temporal and spatial characteristics features of the signal components of interest to be incorporated as part of the BS\_ICA operation.

### **10.4.1 Non-linear ICA**

In applying ICA, it is generally assumed that the mixing process is linear. However, the signal components making up the EEG waveforms propagate through complex media.

There is evidence that these components can interact producing both linear as well as nonlinear mixtures. For example, in a study the presence of quadratic phase coupling (i.e. quadratic nonlinearities) has been observed in EEG during various vigilance states [10.1].

The use of linear ICA in situations where nonlinear mixing processes are involved can result in distortion of the extracted components.

A number of nonlinear algorithms have been reported. A brief review of these algorithm is provided in Table 2.1c in chapter 2. For example [2.66] described an algorithm which

deals with nonlinear mixtures in two stages. The first stage deals with the effect of nonlinearity. This then followed by linear signal source separation.

#### **10.4.2 A Bayesian-based model approach to ICA**

In EEG signal processing, there usually exists prior information about some characteristics features of the components of interest. For example their approximate scalp distributions and temporal features may be known. Inclusion of this prior information as part of the unmixing algorithm may significantly improve the accuracy of the signal source separation.

In order to be able to use the prior information as part of the ICA algorithm, it needs to be formulated in a suitable mathematical form. Bayesian approaches are suitable for this task as the theory behind them is well developed and they have successfully been applied to numerous scientific problems (for example, differentiation of schizophrenic subjects from normal controls, [3.5]).

The use of Bayesian approaches as part of the ICA algorithm provides a number of distinct advantages which include: (i) the assumptions that go into finding a solution are made explicit. (ii) the prior knowledge about a specific problem is expressed in terms of probabilities that must be evaluated. In [10.2] for example, the technique of signal source separation was reformulated within the Bayesian framework for the application to the acoustic domain in order to solve the inverse problem by simultaneously performing source separation and localisation. An algorithm was developed that utilises information regarding both the statistics of the amplitudes of the signals emitted by the sources and the relative locations of the detectors. The Bayesian approach provided a means for incorporating prior information into a source model.

This work will result in techniques which will make the EEG a more effective tool in clinical neurophysiology. Furthermore, the processing of saccade-related EEG waveforms using ICA will result in improvements in the understanding of the signal components and mechanisms involved when saccades are performed.

### 10.4.3 Final remarks

The application of the technique of ICA to the EEG is a relatively new area in biomedical signal processing. The suggested future work will utilise nonlinear ICA and Bayesian approaches to improve the accuracy of ICA applied to EEG. Although the Bayesian theory is well developed, the process of formulating the features of the EEG signal components of interest and incorporating the resulting data as part of ICA requires further development.

The use of nonlinear ICA can reveal information about the properties of the mixing processes involved in saccade-related EEG waveforms. As the investigation is based on saccade-related EEG waveforms, the approaches devised in this study will also provide further insight into the human vision mechanisms involved in the performance of saccadic eye movements.

There are a number of other issues that could be subject to further investigations. As pointed out in chapter 2, ICA methods rely on several model assumptions that may not always be satisfied or may be inaccurate when dealing with real world data such as EEG/ERP/EP signals.

For example, EPs and ERPs are short transient signals that may not be stationary, i.e. they may appear, disappear in which case their statistical properties may vary with respect to time. In these cases, the weight matrix  $W$  may change completely from one time point to the next. Although researchers have started to work in this area of research (see Table 2.1 Part D), further investigations are still required to develop methods that can help the ICA algorithms to efficiently adjust to their changing environment.

Another example is the case where propagation delays may be introduced during the mixing process, thus resulting in the mixing transformation  $W$  not being instantaneous. Researchers have started to work in this area of research (for a sample of work reported in this area, see Table 2.1 Part B). From literature, it emerges that for applications where the propagation delays are negligible such as in the case of EEG/ERP/EP signals, the instantaneous mixing model may be appropriate. However, it may still be worth investigating whether delays may be of significant impact when dealing with the analysis and estimation of saccade-related brain signals.

ICA is a relatively new area of digital signal processing which can be of great benefit to biomedical engineering. The proposed future work provides a timely opportunity to make this technique improve the usefulness of EEG in clinical neurophysiology.

# References

- 1.1. McKinnell, I.W., Talcott, J.B., Hansen, P.C., Winter, J.L., Bacon, S.J. and Stein, J.F.: 'Visual evoked potential evidence for deficient motion processing in developmental dyslexia', *Soc. Neurosci. (SFN), 27th Annual Meeting*, New Orleans, 1997, **23**, pp.921.
- 1.2. Kubova, Z., Kuba, M., Peregrin, J. and Novakova, V.: 'Visual evoked potential evidence for magnocellular system deficit in dyslexia', *Physiological Res.*, 1996, **45**, pp.87-89.
- 1.3. Schall, J.D.: 'Neuronal basis of saccadic eye movements', *Vision and Visual Dysfunction. Volume 4: The Neural Basis of Visual Function*, Leventhal, A.G. (ed), Macmillan Press, London, 1991, pp.388-442.
- 1.4. Barlow, J.S. and Ciganek, L.: 'Lambda responses in relation to visual evoked responses in man', *Electroenceph. Clin. Neurophysiol.*, 1969, **26**, pp.183-192.
- 1.5. Thickbroom, G.W., Knezevic, W., Carroll, W.M. and Mastaglia, F.L.: 'Saccade onset and offset lambda waves – relation to pattern movement visually evoked potentials', *Brain Res.*, 1991, **551**, pp.150-156.
- 1.6. Green, J.: 'Some observations on lambda waves and peripheral stimulation', *Electroenceph. Clin. Neurophysiol.*, 1957, **22**, pp.204-209.
- 1.7. Skrandies, W. and Laschke, K.: 'Topography of visual brain activity during eye movements: lambda waves, saccadic suppression, and discrimination performance', *Int. J. Psychophysiol.*, 1997, **27**, pp.15-27
- 1.8. Hyvärinen, A.: 'Survey on independent component analysis', *Neural Computing Surveys*, 1999, **2**, pp.94-128.
- 1.9. Bell, A.J. and Sejnowski, T.J.: 'An information-maximization approach to blind separation and blind deconvolution', *Neural Computation*, 1995, **7**, pp.1129-1159.

- 1.10. Cardoso, J.-F.: 'High-order contrasts for independent component analysis', *Neural Computation*, 1999, **11** (1), pp.157-192. (A Matlab implementation of JADE is also available from the WEB site <http://sig.enst.fr/~cardoso/stuff.html>)
- 1.11. Karhunen, J. and Pajunen, P.: 'Blind source separation and tracking using nonlinear PCA criterion: a least-squares approach', *Proc. IEEE Int. Conf. Neural Networks (ICNN'97)*, Houston, Texas, 1997, pp.2147-2152.
- 1.12. Jolliffe, I.T.: 'Principal component analysis', New York: Springer-Verlag, 1986.
- 1.13. Quilter, P.M., MacGillivray, B.B. and Wadbrook, D.G.: 'The removal of eye movement artefact from the EEG signals using correlation techniques', *IEE Conf. Publication*, 1977, **159**, pp.93-100.
- 2.1. Héroult, J. and Jutten, C.: 'Space or time adaptive signal processing by neural networks models', *Int. Conf. Neural Networks for Computing*, Snowbird Utah, USA, 1986, pp.206-211.
- 2.2. Jutten, C., Héroult, J. and Guérin, A.: 'IN.C.A.: An independent component analyser based on an adaptive neuromimetic network', in Demongeot, J., Hervé, T., Rialle, V. and Roche, C. (eds), *Artificial Intelligence and Cognitive Sciences*, Manchester Univ. Press, Manchester, 1988, pp.201-219.
- 2.3. Jutten, C. and Héroult, J.: 'Blind separation of sources, part I: adaptive algorithm based on neuromimetic architecture', *Signal Processing*, 1991, **24** (1), pp.1-10.
- 2.4. Comon, P., Jutten, C. and Héroult, J.: 'Blind separation of sources, part II: Statement problem', *Signal Processing*, 1991, **24** (1), pp.11-20.
- 2.5. Cichocki, A., Unbehauen, R. and Rummert, E.: 'Robust learning algorithm for blind separation of signals', *Electronics Letters*, 1994, **30** (17), pp.1386-1387.

- 2.6. Comon, P.: 'Independent component analysis, A new concept ?', *Signal Processing* (Special issue on Higher-Order Statistics), Elsevier, 1994, **36** (3), pp.287-314.
- 2.7. Atick, J.: 'Could information theory provide an ecological theory for sensory receptive field development?', *Networks*, 1992, **3**, pp.213-251.
- 2.8. Karhunen, J. and Joutsensalo, J.: 'Learning of robust principal component subspace', *Proc. IEEE Int. Joint Conf. Neural Networks (IJCNN'93)*, Nagoya, Japan, 1993, **3**, pp.2409-2412.
- 2.9. Cichocki, A. and Unbehauen, R.: 'Robust estimation of principal components in real time', *Electronic Letters*, 1993, **29** (21), pp.1869-1870.
- 2.10. Lagerlund, T.D. , Sharbrough, F.W. and Busacker, N.E.: 'Spatial filtering of multichannel electroencephalographic recordings through principal component analysis by singular value decomposition', *J. Clin. Neurophysiol.*, 1997, **14** (1), pp.73-82.
- 2.11. Linsker, R.: 'Local synaptic learning rules suffice to maximise mutual information in a linear network', *Neural Computation*, 1992, **4**, pp.691-702.
- 2.12. Barlow, H.: 'Sensory Communication', volume Rosenblith, W.A. (ed), chapter in *Possible principles underlying the transformation of sensory messages*, MIT press, 1961, pp.217-234.
- 2.13. Nardal, J.P. and Parga, N.: 'Non linear neurons in the low noise limit: a factorial code maximises information transfer', *Network*, 1994, **5**, pp.565-581.
- 2.14. Roth, Z. and Baram, Y.: 'Multidimensional density shaping by sigmoids', *IEEE Trans. Neural Networks*, 1996, **7** (5), pp.1291-1298.
- 2.15. Cardoso, J.-F. and Laheld, B.: 'Equivariant adaptive source separation', *IEEE Trans. Signal Processing* , 1996, **45** (2), pp.434-444.

- 2.16. Cardoso J.-F. and Soudoumiac A.: 'Blind beamforming for non Gaussian signals', *IEE Proc.-F*, 1993, **140** (6), pp.362-370.
- 2.17. Gaeta, M. and Lacoume, J.-L.: 'Source separation without prior knowledge: the maximum likelihood solution', *Proc. Euro. Signal Processing Conf. (EUSIPO)*, 1990, pp.621-624.
- 2.18. Pham, D.-T., Garrat, P. and Jutten, C.: 'Separation of a mixture of independent sources through a maximum likelihood approach', *Proc. Euro. Signal Processing Conf. (EUSIPO)*, 1992, pp.771-774.
- 2.19. Pearlmutter, B. and Parra, L.: 'A context-sensitive generalisation of ICA', *Int. Conf. Neural Information Processing*, 1996, pp.151-157.
- 2.20. MacKay, D.: 'Maximum likelihood and covariant algorithm for independent component analysis', Technical Report, University of Cambridge, Cavendish Lab, 1996.
- 2.21. Cardoso, J.-F.: 'Infomax and maximum likelihood for blind source separation', *IEEE Signal Processing Letters*, 1997, **4** (4), pp.112-114.
- 2.22. Girolami, M. and Fyfe, C.: 'An extended exploratory projection pursuit network with linear and nonlinear anti-hebbian connections applied to the cocktail party problem', *Neural Networks Journal*, 1997, **10**, pp.1607-1618.
- 2.23. Girolami, M. and Fyfe, C.: 'Extraction of independent signal sources using a deflationary exploratory projection pursuit network with lateral inhibition', *IEE Proc. Vision, Image and Signal Processing*, 1997, **14** (5), pp.299-306.
- 2.24. Lee, T.-W. and Sejnowski, T.J.: 'Independent component analysis for sub-Gaussian and super-Gaussian mixtures', *Fourth Joint Symp. Neural Computation*, 1997, **7**, pp.132-139.
- 2.25. Girolami, M. and Fyfe, C.: 'Generalised independent component analysis through unsupervised learning with emergent bussgang properties', *Proc. Int. Conf. Neural Networks (ICNN'97)*, Houston, USA, 1997, pp.1788-1891.

- 2.26. Karhunen, J., and Joutsensalo, J.: 'Representation and separation of signals using non-linear PCA type learning', *Neural Networks*, 1994, **7** (1), pp.113-127.
- 2.27. Yang, B.: 'Projection approximation subspace tracking', *IEEE Trans. Signal Processing*, 1995, **43**, pp.95-107.
- 2.28. Xu, L.: 'Least mean-square error reconstruction: A principle for self-organising networks', *Neural Networks*, 1993, **6**, pp.627-648.
- 2.29. Oja, E. and Karhunen, J.: 'Signal separation by nonlinear hebbian learning', *Proc. IEEE Int. Conf. Neural Networks (ICNN'95)*, Perth, Australia, 1995, pp.83-87.
- 2.30. Oja, E.: 'The nonlinear PCA learning rule in independent component analysis', *Neurocomputing*, 1997, **17**, pp.25-45.
- 2.31. Girolami, M. and Fyfe, C.: 'Stochastic ICA contrast maximisation using Oja's nonlinear PCA algorithm', *Int. J. Neural Systems*, 1999, **8** (5-6), pp.661-678.
- 2.32. Karhunen, J., Pajunen, P. and Oja, E.: 'The nonlinear PCA criterion in blind source separation: Relations with other approaches', *Neurocomputing*, 1998, **22**, pp.5-20.
- 2.33. Hyvärinen, A. and Oja, E.: 'Simple neuron models for independent component analysis', *Int. J. Neural Systems*, 1996, **7** (6), pp.671-687.
- 2.34. Hyvärinen, A. and Oja, E.: 'A fast fixed-point algorithm for independent component analysis', *Neural Computation*, 1997, **9** (7), pp.1483-1492.
- 2.35. Hyvärinen, A.: 'A family of fixed-point algorithms for independent component analysis', *Proc. IEEE Int. Conf. Acoustics, Speech and Signal Processing (ICASSP'97)*, Munich, Germany, 1997, pp.3917-3920.
- 2.36. Hyvärinen, A.: 'Fast and Robust Fixed-Point Algorithms for Independent Component Analysis', *IEEE Trans. Neural Networks*, 1999, **10** (3), pp.626-634.

- 2.37. Karhunen, J., Hyvärinen, A., Vigario, R., Hurri, J. and Oja., E.: 'Applications of neural blind separation to signal and image processing', *Proc. IEEE Int. Conf. Acoustics, Speech and Signal Processing (ICASSP'97)*, Munich, Germany, 1997, pp.131-134.
- 2.38. Lambert., R. H.: 'Multichannel Blind Deconvolution: FIR Matrix Algebra and Separation of Multipath Mixtures', PhD thesis, Univ. of Southern California, 1996.
- 2.39. Lee, T.-W., Girolami, M. and Sejnowski., T. J.: 'Independent component analysis using an extended infomax algorithm for mixed sub-gaussian and super-gaussian sources', *Neural Computation*, 1998, pp.609-633.
- 2.40. Amari, S., Cichocki, A. and Yang, H.: 'A new learning algorithm for blind signal separation', *Advances in Neural Information Processing Systems*, 1996, **8**, pp.757-763.
- 2.41. Lee, T.-W., Girolami, M., Bell, A.J. and Sejnowski., T.J.: 'A unifying information-theoretic framework for independent component analysis', *Computers and Mathematics with Applications*, 2000, **39** (11), pp.1-21.
- 2.42. Molgedey, L. and Schuster, H. G.: 'Separation of a mixture of independent signals using time delayed correlations', *Phys. Rev. Lett.*, 1994, **72** (23), pp.3634-3636.
- 2.43. Nadal, J.-P. and Parga, N.: 'Blind source separation with time dependent mixtures', *Signal Processing*, 2000, **80** (10), pp.2187-2194.
- 2.44. Yellin, D. and Weinstein, E.: 'Criteria for multichannel signal separation', *IEEE Trans. Signal Processing*, 1994, **42**, pp.2158-2167.
- 2.45. Ngyuen-Thi, H.-L. and Jutten, C.: 'Blind Source Separation for convolutive mixtures', *Signal Processing*, 1995, **45** (2), pp.209-229.
- 2.46. Cardoso, J.-F.: 'Multidimensional independent component analysis', *Proc. IEE Int. Conf. Acoustics, Speech and Signal Processing (ICASSP'98)*, Seattle, WA, 1998, pp.1941-1944.

- 2.47. Torkkola, K.: 'Blind separation of delayed sources based on information maximization', *Proc. IEE Int. Conf. Acoustics, Speech and Signal Processing (ICASSP'96)*, Atlanta, Georgia, 1996, pp.3509-3512.
- 2.48. Lee, T.-W., Bell, A.J. and Lambert, R.: 'Blind separation of delayed and convolved sources', *Advances in Neural Information Processing Systems*, MIT Press, Cambridge MA, 1997, **9**, pp.758-764.
- 2.49. Lee, T.-W., Bell, A.J. and Orglmeister., R.: 'Blind Source Separation of Real World Signals', *Proc. IEEE Int. Conf. Neural Networks*, Houston, 1997, pp.2129-2135.
- 2.50. Amari, S., Cichocki, A. and Yang, H. H.: 'Recurrent neural networks for blind separation of sources', *Int. Symp. Nonlinear Theory and its Applications (NOLTA'95)*, Las Vegas, 1995, pp.37-42.
- 2.51. Cichocki, A. and Unbehauen., R.: 'Robust neural networks with on-line learning for blind identification and blind separation of sources', *IEEE Trans. Circuits and Systems*, 1996, **43** (11), pp.894-906.
- 2.52. Amari, S.I., Cichoki, A. and Yang, H.H.: 'Stability analysis of adaptive blind source separation', *Neural Networks*, 1997, **10** (8), pp.1345-1352.
- 2.53. Amari, S.I., Douglas, A., Cichoki, S.C. and Yang, H.H.: 'Multichannel blind deconvolution and equalization using the natural gradient', *IEEE Int. Work. Wireless Communication*, Paris, France, 1997, pp.101-104.
- 2.54. Amari, S.I.: 'Natural gradient works efficiently in learning', *Neural Computation*, 1998, **10** (4), pp.251-276.
- 2.55. Cichocki, A., Douglas, S.C. and Amari., S.-I.: 'Robust techniques for independent component analysis with noisy data', *Neurocomputing*, 1998, **22**, pp.113-129.
- 2.56. Deco, G. and Brauer, W.: 'Nonlinear higher-order statistical decorrelation by volume-conserving neural architectures', *Neural Networks*, 1995, **8** (4), pp.525-535.

- 2.57. Hermann, M. and Yang, H.H.: 'Perspectives and limitations of self-organising maps in blind separation of source signals', *Progress in Neural Information Processing, Proc. ICONIP'96*, Wan Chai, Hong Kong, Springer-Verlag, 1996, pp.1211-1216.
- 2.58. Lin, J. and Cowan, J.: 'Faithful representation of separable input distributions', *Neural Computation*, 1997, **9** (6), pp.1305-1320.
- 2.59. Pajunen, P.: 'Nonlinear Independent Component Analysis by self-organising maps', Technical report, Department of Computer Science, Helsinki University of Technology, Helsinki, 1996.
- 2.60. Burel, G.: 'Blind separation of sources: a nonlinear neural algorithm', *Neural Networks*, 1992, **5**, pp.937-947.
- 2.61. Lee, T.-W., Koehler, B.U. and Orglmeister., R.: 'Blind source separation of nonlinear mixing models', *Proc. IEEE Int. Work. Neural networks for Signal Processing (NNSP'97)*, Florida, USA, 1997, pp.406-415.
- 2.62. Taleb, A. and Jutten, C.: 'Nonlinear source separation: the post-linear mixtures', *Proc. Euro. Symp. Artificial Neural Networks (ESANN'97)*, Bruges, Belgium, 1997, pp.279-284.
- 2.63. Yang, H.H., Amari, S. and Cichocki, A.: 'Information back-propagation for blind separation of sources from non-linear mixtures', *Proc. Int. Conf. Neural Networks (ICNN'97)*, Houston, Texas, USA, 1997, pp.2141-2146.
- 2.64. Hochreiter, S. and Schmidhuber, J.: 'Lococode performs nonlinear ica without knowing the number of sources', *First Int. Work. Independent Component Analysis and Signal Separation (ICA'99)*, Aussois, France, 1999, pp.149-154.
- 2.65. Taleb, A., Jutten, C. and Olympieff, S.: 'Source separation in post nonlinear mixtures: an entropy-based algorithm', *Proc. IEE Int. Conf. Acoustics, Speech and Signal Processing (ICASSP'98)*, 1998, **4**, pp.2089-2092.

- 2.66. Taleb, A. and Jutten, C.: 'Source separation in post nonlinear mixtures', *IEEE Trans. Signal Processing*, 1999, **47** (10), pp.2807-2820.
- 2.67. Peng, H. and Chi, Z.: 'Approaching the post non-linearity of blind mixtures by hybrid neural networks', *Int. Conf. Neural Networks*, 1999, **6**, pp.4103-4106.
- 2.68. Chen, Y. and He, Z.: 'A block-adaptive blind separation algorithm for post nonlinear mixture of sub- and super- Gaussian signals', *Proc. Third Int. Conf. Information Fusion*, 2000, **2**, pp.10-17.
- 2.69. Weinstein, E., Feder, M. and Oppenheim, A.V.: 'Multi-Channel Signal Separation by Decorrelation', *IEEE Trans. Speech Audio Processing*, 1993, **1** (4), pp.405-413.
- 2.70. Matsuoka, K., Ohya, M. and Kawamoto, M.: 'A Neural Network for Blind Separation of Nonstationary Signals', *Neural Networks*, 1995, **8** (3), pp.411-419.
- 2.71. Souloumiac, A.: 'Blind source detection and separation using second order nonstationarity', *Proc. IEE Int. Conf. Acoustics, Speech and Signal Processing (ICASSP'95)*, 1995, **3**, pp.1912-1915.
- 2.72. Ehlers, F. and Schuster, H.G.: 'Blind separation of convolutive mixtures and an application in automatic speech recognition in a noisy environment', *IEEE Trans. Signal Processing*, 1997, **45** (10), pp.2608-2609.
- 2.73. Tong, L., Liu, R., Soon, V. and Huang, Y.: 'Indeterminacy and identifiability of blind identification', *IEEE Trans. Circuits and Systems*, 1991, **38** (5), pp.499-509.
- 2.74. Wee, H. and Principe, J.: 'A criterion for BSS based on simultaneous diagonalization of time correlation matrices', *Proc. IEEE Work. Neural Networks for Signal Processing (NNSP'97)*, 1997, pp.496-508.
- 2.75. Parra, L.: 'Temporal Models in Blind Source Separation', chapter in Giles, L. and Gori, M. (eds), *Adaptive Processing of Sequences and Data Structures*, Germany: Springer, 1998, pp.229-247.

- 2.76. Murata, N., Ikeda, S. and Ziehe, A.: 'An approach to blind source separation based on temporal structure of speech signals', RIKEN BSIS Technical Report No.98-2, 1998.
- 2.77. Kawamoto, M., Matsuoka, K. and Ohnishi., N.: 'A method of blind separation for convolved nonstationary signals', *Neurocomputing*, 1998, **22** (1-3), pp.157-171.
- 2.78. Parra, L. and Spence, C.: 'Convolutional blind source separation of non-stationary sources', *IEEE Trans. Speech and Audio Processing*, 2000, pp.320-327.
- 2.79. Jones, D.L.: 'A new method for blind source separation of nonstationary signals', *Proc. IEEE Int. Conf. Acoustics, Speech, and Signal Processing (ICASSP'99)*, Phoenix AZ, USA, 1999, **5**, pp.2893-2896.
- 2.80. Mansour, A.: 'The Blind separation of non-stationary signals by only using the second order statistics', *Fifth Int. Symp. Signal Processing and its Applications (ISSPA'99)*, Brisbane, Australia, 1999, pp.235-238.
- 2.81. Choi, S. and Cichocki, A.: 'Blind separation of nonstationary sources in noisy mixtures', *Electronics Letters*, 2000, **36** (9), pp.848-849.
- 2.82. Cardoso, J.-F.: 'Separation of non stationary sources: achievable performance', *Proc. IEEE Work. Statistical Signal and Array Processing (SSAP'2000)*, 2000, pp.359-363.
- 2.83. Stone, J.V. and Porrill, J.: 'Undercomplete independent component analysis for signal separation and dimension reduction', Technical report, Psychology Department, Sheffield University, England, 1997.
- 2.84. Stone, J.V. and Porrill, J.: 'Independent component analysis for step-wise separation of signals', Technical report, Psychology Department, Sheffield University, England, 1998.
- 2.85. Roberts, S.J., Rezek, I.A., Penny, W.D. and Everson, R.M.: 'The use of advanced information processing methods in EEG analysis', *Proc. IEE Colloq. Intelligent Decision*

- Support in Clinical Practice*, 1998, (the page numbers could not be found, so a webpage address is provided at this stage: URL = <http://citeseer.nj.nec.com/193842.html>).
- 2.86. Cichoki, A., Sabala, I., Choi, S., Orsier, B. and Szupiluk, R.: 'Self-adaptive independent component analysis for sub-gaussian and super-gaussian mixtures with an unknown number of sources and additive noise', *Proc. Int. Symp. Nonlinear Theory and its Applications (NOLTA'97)*, Hawaii, USA, 1997, pp.731-734.
  - 2.87. Cichoki, A., Sabala, I. and Amari, S.I.: 'Intelligent neural networks for blind signal separation with unknown number of sources', *Int. Symp. Engineering of Intelligent Systems (ESI-98)*, Tenerife, Spain, 1998, pp.148-151.
  - 2.88. Malouche, Z. and Macchi, O.: 'Adaptive separation of an unknown number of sources', *Proc. IEEE Signal Processing Work. Higher-Order Statistics (SPW-HOS'97)*, Banff, Canada, 1997, (the page numbers could not be found, so a webpage address is provided at this stage: URL = <http://dlib.computer.org/conferen/spwhos/8005/pdf/80050295.pdf>).
  - 2.89. Malouche, Z. and Machi, O.: 'Adaptive unsupervised extraction of one component of a linear mixture with a single neuron', *IEEE Trans. Neural Networks*, 1998, **9** (1), pp.123-138.
  - 2.90. Comon, P.: 'Blind channel identification and extraction of more sources than sensors', *Proc. SPIE Volume 3461: Advanced Signal Processing Algorithms, Architectures, and Implementations VIII*, San Diego, 1998, pp.2-13.
  - 2.91. Lewicki, M. and Sejnowski, T. J.: 'Learning overcomplete representations', *Advances in Neural Information Processing 10 (Proc. NIPS'97)*, MIT Press, 1998, pp.556-562.
  - 2.92. Van Hulle, M.M.: 'Clustering approach to square and non-square blind source separation', *IEEE Work. Neural Networks for Signal Processing*, Madison WI, USA, 1999, pp.315-323.

- 2.93. Lee, T.-W., Lewicki, M.S., Girolami, M. and Sejnowski, T.J.: 'Blind source separation of more sources than mixtures using overcomplete representations', *IEEE Signal Processing Letters*, 1999, **6** (4), pp.87-90.
- 2.94. Hyvärinen, A., Cristescu, R. and Oja, E.: 'A fast algorithm for estimating overcomplete ICA bases for image windows', *Proc. Int. Joint Conf. Neural Networks*, Washington D.C., USA, 1999, pp.894-899.
- 2.95. Westner, A. and Bove, V.M.: 'Blind separation of real world audio signals using overdetermined mixtures', *First Int. Work. Independent Component Analysis and Signal Separation (ICA'99)*, Aussois, France, 1999, (the page numbers could not be found, so a webpage address is provided at this stage: URL=<http://citeseer.nj.nec.com/westner99blind.html>).
- 2.96. Lee, T.-W.: 'Independent component analysis, theory and applications', Kluwer Academic Publishers, Boston, 1998.
- 2.97. Hyvärinen A., Karhunen, J. and Oja, E.: 'Independent component analysis', John Wiley and Sons, 2001.
- 2.98. Press, W.H., Teukolsky, S.A., Vetterling, W.T. and Flannery, B.P.: 'Numerical recipes in C: the art of scientific computing', 2<sup>nd</sup> ed, New-York Cambridge University Press, 1992, pp.67-70.
- 2.99. Haykin, S.: 'Adaptive filter theory', 3<sup>rd</sup> ed, Prentice Hall, 1996.
- 2.100. Cover, T.M. and Thomas, J.A.: 'Elements of Information Theory', New York: Wiley, 1991.
- 2.101. Tong, L., Liu, R., Soon, V. and Huand, Y.: 'Indeterminacy and identifiability of blind identification', *IEEE Trans. Circuits and Systems*, 1991, **38** (5), pp.499-509.
- 2.102. Golub, G.H. and Loan, C.F.V.: 'Matrix computations', The Johns Hopkins University Press, 1989.

- 3.1 Martin, J.H.: 'The collective electrical behaviour of cortical neurons: the electroencephalogram and the mechanisms of epilepsy', *Principles of Neural Sciences*, part VI, chapter 50, 3<sup>rd</sup> ed, 1995.
- 3.2 Caton, R.: 'The electric current of the brain', *British Medical Journal*, 1875, **2**, p.278.
- 3.3 Berger, H.: 'Uber des elektenkephalogram des menschen', *Arch. Psychiat.*, 1929, **87**, pp.527-570.
- 3.4 Hillyard, S.A. and Woods, D.L.: 'Electrophysiological analysis of human brain function', *Handbook of behavioural neurobiology*, 1979, **2**.
- 3.5 Saatchi, R., Oke, S., Allen, E.M., Jervis, B.W. and Hudson, N.: 'Signal processing of the contingent negative variation in schizophrenia using multilayer perceptrons and predictive statistical diagnosis', *IEE Proc. Sci. Meas. Technol.*, 1995, **142** (4), pp.269-277.
- 3.6 Pritchard, W.S.: 'Cognitive event-related potential correlates of schizophrenia', *Psychological Bulletin*, 1986, **100** (1), pp.43-66.
- 3.7 Saatchi, R.: 'Developments in signal processing for computerised diagnosis in clinical neurophysiology', PhD Thesis, Sheffield Hallam University, 1992.
- 3.8 Chaptin, J.K., Moxon, K.A., Markowitz, R.S. and Nicolelis, M.A.L.: 'Real-time control of a robot arm using simultaneously recorded neurons in the motor cortex', *Nature Neuroscience*, 1999, **2**, pp.664-670.
- 3.9 Shackell, B.: 'Eye movement recording by electrooculography', in Venables, P.H. and Martin, I. (eds), *A manual of psychological methods*, North Holland, 1967, pp.301-334.
- 3.10 Young, L.R. and Sheena, D.: 'Survey of eye movement recording methods', *Behaviour Res. Meth. Instrum.*, 1975, **7**, pp.397-429.

- 3.11 Barry, W. and Jones, G.M.: 'Influence of eyelid movement upon electro-oculographic recording of vertical eye movements', *Aerospace Med.*, 1965, **36**, pp.855-858.
- 3.12 Matsuo, F., Peters, J.F. and Reilly, E.L.: 'Electrical phenomena associated with the movements of the eyelid', *Electroenceph. Clin. Neurophysiol.*, 1975, **38**, pp.507-511.
- 3.13 Jervis, B.W., Ifeachore, E.C. and Allen, E.M.: 'The Removal of ocular artefacts from the electroencephalogram: a review', *Med. Biol. Eng. Comp.*, 1988, **26**, pp.2-12.
- 3.14 Becker, W., Hoehne, O., Iwase, K. and Kornhuber, H.H.: 'Bereitschaftspotential, prämotorische Positivierung und andere Hirnpotentiale bei sakkadischen Augenbewegungen', *Vision Res.*, 1972, **12**, pp.421-436.
- 3.15 Moster, M.L. and Goldberg, G.: 'Topography of scalp potentials preceding self-initiated saccades', *Neurology*, 1990, **40**, pp.644-648.
- 3.16 Evdokimidis, I., Mergner, T. and Lücking, C.H.: 'Dependence of presaccadic cortical potentials on the type of saccadic eye movement', *Electroenceph. Clin. Neurophysiol.*, 1992, **83**, pp.179-191.
- 3.17 Schlag, J. and Schlag-Rey, M.: 'Evidence for a supplementary eye field', *J. Neurophysiol.*, 1987, **57**, pp.179-200.
- 3.18 Goldberg, M.E. and Bruce, C.J.: 'Primate frontal eye fields. III. Maintenance of a spatially accurate saccade signal', *J. Neurophysiol.*, 1990, **64**, pp.489-508.
- 3.19 Brook-Seidelberg, B.A. and Adler, G.: 'A frontal cortical potential associated with saccades in humans', *Exp. Brain Res.*, 1992, **89**, pp.441-446.
- 3.20 Riemslog, F.C.C., van der Heide, G.L., van Dongen, M.M. and Ottenhoff, F.: 'On the origin of the pressaccadic spike potential', *Electroenceph. Clin. Neurophysiol.*, 1988, **70**, pp.281-287.

- 3.21 Scott, D.F., Groethuysen, U.C. and Bickford, R.G.: 'Lambda responses in the human electroencephalogram', *Neurology*, 1967, **17**, pp.770-778.
- 3.22 Gastaut, Y.: 'Un signe électroencéphalographique peu connu: les pointes occipitales survenant pendant l'ouverture des yeux', *Rev. Neurol.*, 1951, **84**, pp.640-643.
- 3.23 Evans, C.C.: 'Comments on Occipital sharp waves responsive to visual stimuli', *Electroenceph. Clin. Neurophysiol.*, 1952, **4**, p.111.
- 3.24 Friston, K.J.: 'Imaging neuroscience: Principle or maps?', *Proc. The National Academy of Science*, USA, 1998, **95**, pp.796-802.
- 3.25 Basar, E.: 'Brain function and oscillations', *Volume 1: Brains oscillations, Principles and Approaches*, Springer Verlag, 1998.
- 3.26 Nunez, P.L.: 'The electrical fields of the brain', Oxford University Press, 1981.
- 3.27 Frequently Asked Questions about ICA applied to EEG and MEG Data, at website:  
<http://www.cnl.salk.edu/~scott/icafaq.html>
- 3.28 Klostermann, W., Kömpf, D., Heide, W., Verleger, R., Wauschkuhn, B. and Seyfert, T.: 'The presaccadic cortical negativity prior to self-paced saccades with and without visual guidance', *Electroenceph. Clin. Neurophysiol.*, 1994, **91**, pp.219-228.
- 4.1 Halliday, A.M.: 'Evoked potentials in clinical testing', chapter in *Clinical Neurology and Neurosurgery Monographs*, **3**, Churchill Livingstone, 1982.
- 4.2 Electrical Geodesics, Inc. Internet site address: <http://www.egi.com/>.
- 5.1 Matsuo, F., Peters, J.F. and Reilly, E.L.: 'Electrical phenomena associated with eye movements of the eyelid', *Electroenceph. Clin. Neurophysiol.*, 1975, **38**, pp.507-511.
- 5.2 Girton, D.G. and Kamiya, J.: 'A simple on-line technique for removing eye movement artefacts from the EEG', *Electroenceph. Clin. Neurophysiol.*, 1973, **34**, pp.212-216.

- 5.3 Berg, P. and Scherg, M.: 'A multiple source approach to the correction of eye artifacts', *Electroenceph. Clin. Neurophysiol.*, 1994, **90**, pp.229-241.
- 5.4 Rao, K.D. and Reddy, D.C.: 'On-line method for enhancement of electroencephalogram signals in presence of electro-oculogram artefacts using non-linear recursive least squares technique', *Med. Biol. Eng. Comp.*, 1995, **33**, pp.488-491.
- 5.5 Makeig, S., Bell, A.J., Jung, T.-P. and Sejnowski, T.J.: 'Independent component analysis of electroencephalographic data', *Advances in Neural Information Processing Systems*, 1996, **8**, pp.145-151.
- 5.6 Jung, T.-P., Humphries, C., Lee, T.-W., Makeig, S., McKeown, M., Iragui, V. and Sejnowski, T.J.: 'Extended ICA removes artifacts from electroencephalographic recordings', *Advances in Neural Information Processing Systems*, 1998, **10**, pp.894-900.
- 5.7 Cardoso, J.-F.: 'Blind signal separation: statistical principles', in Liu, R.-W. and Tong, L. (eds), *Proc. IEEE Special issue on blind identification and estimation*, 1998, **90** (8), pp.2009-2026.
- 5.8 Jervis, B.W., Thomlinson, M., Mair, C., Lopez, J.M.L. and Garcia, M.I.B.: 'Residual ocular artefact subsequent to ocular artefact removal from the electroencephalogram', *IEE Proc. Sci. Meas. Technol.*, 1999, **146** (6), pp.293-298.
- 5.9 Hillyard, S.A. and Galambos, R.: 'Eye-movement artifact in the CNV', *Electroenceph. Clin. Neurophysiol.*, 1970, **28**, pp.173-182.
- 5.10 Verleger, R., Gasser, T. and Mocks, J.: 'Correction of EOG artifacts in event-related potentials of EEG: Aspects of reliability and validity', *Psychoph.*, 1982, **19**, pp.472-480.
- 5.11 Whitton, J.L., Lue, F. and Moldofsky, H.A.: 'Spectral method for removing eye-movement artifacts from the EEG', *Electroenceph. Clin. Neurophysiol.*, 1978, **44**, pp.735-741.

- 5.12 Woestenburg, J.C., Verbaten, M.N. and Slangen, J.L.: 'The removal of the eye-movement artifact from the EEG by regression analysis in the frequency domain', *Biological Psychology*, 1983, **16**, pp.127-147.
- 5.13 Barlow, J.S.: 'Computerized clinical electroencephalography in perspective', *IEEE Trans. Biomed. Eng.*, 1979, **26**, pp.377-391.
- 5.14 Verleger, R.: 'Valid identification of blinks artifacts: are they larger than 50  $\mu$ V in EEG records?', *Electroenceph. Clin. Neurophysiol.*, 1993, **87**, pp.354-363.
- 5.15 Berg, P. and Scherg, M.: 'Dipole models of eye activity and its application to the removal of eye artifacts from the EEG and MEG', *Clin. Physiol. Meas.*, 1991, **12** (supplement A), pp.49-54.
- 5.16 Weerts, T.C. and Lang, P.J.: 'The effect of eye fixation and stimulus and response location on the contingent negative variation (CNV)', *Biol. Psychol.*, 1973, **1**, pp.1-19.
- 5.17 Verleger, R.: 'The instruction from refrain from blinking affects auditory P3 and N1 amplitudes', *Electroenceph. Clin. Neurophysiol.*, 1991, **78**, pp.240-251.
- 5.18 Gratton, G., Coles, M. and Donchin, E.: 'A new method for off-line removal of ocular artefacts', *Electroenceph. Clin. Neurophysiol.*, 1983, **55**, pp.468-484.
- 5.19 Jervis, B.W., Coelbo, M. and Morgan, G.: 'Effects on EEG responses of removing ocular artifacts by proportional EOG subtraction', *Med. Biol. Eng. Comput.*, 1989, **27**, pp.484-490.
- 5.20 Huotilainen, M., Hmoniemi, R.J., Tiitinen, H., Lavaikainen, J., Albo, K., Kajola, M. and Naatanen, R.: 'The projection method in removing eye-blink artefacts from multichannel MEG measurements', *Fundamental Research and Clinical Applications (Proc. 9th Int. Conf. Biomag.)*, Elsevier, Amsterdam, 1995, pp.363-367.
- 5.21 Vigário, R.: 'Extraction of ocular artefacts from EEG using independent component analysis', *Electroenceph. Clin. Neurophysiol.*, Elsevier, 1997, **103**, pp.395-404.

- 5.22 Vigário, R., Jousmäki, V., Hämäläinen, M., Hari, R. and Oja, E.: 'Independent component analysis for identification of artifacts in magnetoencephalographic recordings', in Jordan, M.I., Kearns, M.J. and Solla, S.A. (eds), *Advances in Neural Information Processing Systems*, The MIT Press, 1998, **10**.
- 5.23 Jung, T.-P., Humphries, C., Lee, T.-W., McKeown, M., Iragui, V., Makeig, S. and Sejnowski, T.J.: 'Removing Electroencephalographic Artifacts: Comparison between ICA and PCA', *IEEE Int. Work. Neural Networks for Signal Processing*, 1998, pp.63-72.
- 5.24 Statistical Analysis System (SAS): 'SAS user's guide: statistics', SAS Institute INC, Box 8000, Cary, North Carolina 27511, 1982.
- 5.25 Cardoso, J.-F.: 'Personal communication', 1998, (address: Ecole Nationale Supérieure des Telecommunications, Telecom Paris, Department Signal, 46 rue Barrault, 75634 Paris Cedex 13, France).
- 5.26 Mardia, K.V., Kent, J.T. and Bibby, J.M.: 'Multivariate Analysis', London, Academic Press, 1979.
- 5.27 Steel, R.G.D. and Torrie, J.H.: 'Principles and procedures of statistics', 2<sup>nd</sup> ed, New York: McGraw-Hill Book Company, 1980.
- 6.1 Ditchburn, R. W.: 'Eye-movements and visual perception', Oxford: Clarendon Press, 1973.
- 6.2 Cichocki, A., Karhunen, J., Kasprzak, W. and Vigário, R.: 'Neural networks for blind separation with unknown number of sources', *Neurocomputing*, 1999, **24**, (1-3), pp.55-94.
- 6.3 'MATLAB - The language of technical computing', version 5.3.0.10183 (R11), The MathWorks Inc., (January 21) 1999.

- 7.1 Haykin, S.: 'Adaptive Filter Theory', Chap. 9., 3rd ed, Englewood Cliffs, NJ: Prentice Hall, 1996.
- 9.1 Höppner, F., Klawonn, F., Kruse, R. and Runkler, T.: 'Fuzzy cluster analysis: methods for classification, data analysis and image processing', 1999, Wiley.
- 9.2 Bezdek, J.C., Keller, J., Krisnapuram, R. and Pal, N.R.: 'Fuzzy models and algorithms for pattern recognition and image processing', Kluwer Academic Publishers, 1999.
- 9.3 Aitchison, J., Habbema, J.D.F. and Kay, J.W.: 'A critical comparison of two methods of statistical discrimination', *Applied Statistics*, 1977, **26**, pp.15-25.
- 10.1 Ning, T. and Bronzino, J.: 'Bispectral analysis of the rat EEG during various vigilance states', *IEEE Trans. Biomedical Engineering*, 1989, **36** (4), pp.497-499.
- 10.2 Knuth, K.H.: 'Bayesian Inference for Inverse Problems', *SPIE'98 Proceedings*, **3459**, Mohammad-Djafari, A. (ed), Bellingham, 1998, pp.147-158.

# Appendix A

## **Refereed Journal Publications**

put impedance condition. The two sets of solutions for the optimised feed network are shown in Table 1.

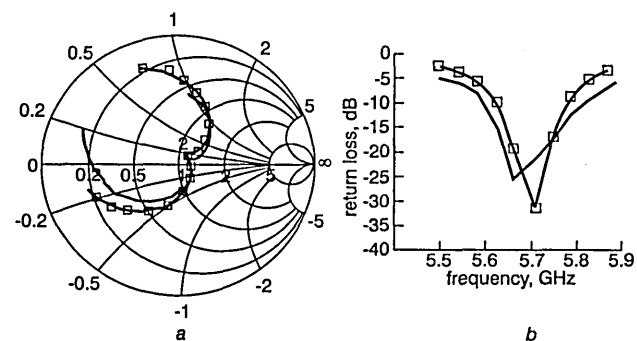


Fig. 2 Simulated and practical results of dual-feed square microstrip patch antenna

— practical  
□— simulated  
 $r = 0.79$ ,  $\epsilon_r = 2.33$

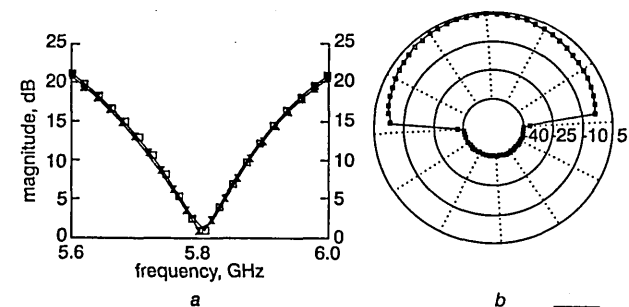


Fig. 3 Simulated results for LHCP and RHCP designs

Axial ratio  
Radiation pattern  
□— LHCP  
×— RHCP

Table 1: Two sets of solutions for optimised feed network

	$Z_1$	$\theta_2$	$Z_2$	$\theta_3$	$Z_3$	$\theta_4$	$Z_4$	$Z_{in}$	$ V_2/V_4 $	$\arg(V_2/V_4)$	CP
1	135.0	1.96	132.4	0.8	135.2	1.16	134.3	$50-0.5i$	0.97	86	RH
2	137.4	0.74	137.1	2.3	135.7	1.97	138.6	$49.5+0.5i$	1.08	89.7	LH

As can be seen in Table 1, it is possible to use an average value impedance for all four feed lines as this value is within the sign and typical manufacturing tolerances. This makes the design particularly attractive as the effect of the step discontinuity is eliminated and also spurious radiation is reduced.

Practical and simulated (full-wave analysis software) results for the reflection coefficient of the LHCP solution using  $137.2\Omega$  are shown in Fig. 2 and indicate that a good matching condition at 5.7 GHz has been obtained.

The simulated results of the axial ratio and radiation pattern of the LHCP and RHCP designs are shown in Fig. 3 with a good axial ratio and the expected radiation patterns.

**Conclusion:** It has been shown that the design of a dual-feed network for a square patch antenna for circular polarisation involves a large number of variables and that a closed form solution to the problem cannot be obtained. An MGA with specified constraints has been successfully implemented to optimise the design of a dual-feed network. A feed network with single feed impedance has been realised. The practical and simulated results for the return loss, axial ratio and radiation pattern show good agreement and confirm the validity of the approach.

© IET 2000  
Electronics Letters Online No: 20000766  
DOI: 10.1049/el:20000766

Aljibouri, E.G. Lim, H. Evans and A. Sambell (Communication Systems Research Group, University of Northumbria, United Kingdom)

- 1 LIM, B., KOROLKIEWICZ, E., and SCOTT, S.: 'Optimised design of corner microstrip fed nearly square patch antenna for circular polarisation', *Electron. Lett.*, 1996, **32**, pp. 610-612
- 2 HOWELL, J.Q.: 'Microstrip antennas', *IEEE Trans.*, 1975, **AP-23**, pp. 90-93
- 3 SOLIMAN, E.A., BREBELS, S., BEYNE, E., and VANDENBOSCH, G.: 'Circularly polarised aperture antenna fed by CPW and built in MCM-D technology', *Electron. Lett.*, 1999, **35**, pp. 250-251
- 4 DAY, P.I.: 'Transmission line transformation between arbitrary impedances using the smith chart', *IEEE Trans. Microw. Theory Techn.*, 1975, pp. 772-773
- 5 SRINIVAS, N., and KALYANMOY, D.: 'Multiobjective optimization using nondominating sorting in genetic algorithms', *Evol. Comput.*, 1995, **2**, (3), pp. 221-248

## Independent component analysis of saccade-related electroencephalogram waveforms

L. Vigon, R. Saatchi, J. Mayhew, N. Taroyan, J. Frisby, D. Johnston and O. Pascalis

A methodology based on the signal separation technique of extended independent component analysis (ICA) is devised to analyse saccade-related electroencephalogram (EEG) waveforms. The methodology enables saccade-related components to be successfully extracted from the EEG mixtures and the brain regions responsible for their generation to be identified.

**Introduction:** Saccades are rapid changes in the orientation of the eyes that are used to realign the visual axes on objects of interest. Dysfunction in this system may lead to difficulties in various visual functions such as depth perception and reading. Different neural signal components are involved in preparation and execution of saccadic eye movements. One of these is described as a pre-saccadic potential related to motor commands for saccade generation. Others, such as efferent feedback from saccade generating centres to visual cortex, are believed to provide visual stability of the surrounding world across the eye movements. The saccadic movement is accompanied by an EEG signal associated with visual information processing called the lambda-wave [1].

The investigation described in this Letter required the obscuring ongoing background EEG as well as the electrooculogram (EOG) signal caused by eye movements to be separated from the saccade components of interest. A popular signal separation technique is independent component analysis (ICA) [2]. ICA is an extension of principal component analysis (PCA) that deals with higher-order statistical dependencies. It is based on the assumption that the signal sources are statistically independent. The extended version of ICA (hereafter referred to as ICA) can handle both super- and sub-Gaussian signals [2]. In this Letter, an analysis of the saccade-related EEG waveforms is carried out by applying an ICA-based procedure. The study provides information about how the brain deals with the problem of vision with moving eyes.

**Experimental procedure:** EEG and EOG data were recorded for six healthy human adults using a network of 64 silver-silver chloride electrodes. All electrodes were referred to the vertex. The data were filtered (bandpass frequency range from 0.1 to 100 Hz) and digitised with a sampling rate of 250. The subjects were instructed to fixate a red square that appeared randomly on the screen of a computer at one of five predefined checkerboard locations: centre, left, right, up and down. For each location 50 trials were recorded. The duration of each trial was 2s.

**Analysis procedure:** The recorded signals were digitally lowpass filtered at 45 Hz and their baselines were adjusted to zero. To preserve the saccade-related EEG components, the waveforms in each trial were time synchronised with reference to the EOG signal in that trial. The synchronised averaged waveforms were decorrelated using PCA and sphered [2]. The EEG waveforms recorded from the locations close to the international 10-20 system of electrode

waveforms and enabled the ICA algorithm to operate more effectively. The back-projection technique described in [2] was used to obtain the scalp distribution of the extracted ICA components. As ICA is subject to amplitude scaling, the magnitude range for extracted components was estimated by considering both the amplitude of the averaged waveforms and the relative magnitude of the extracted components.

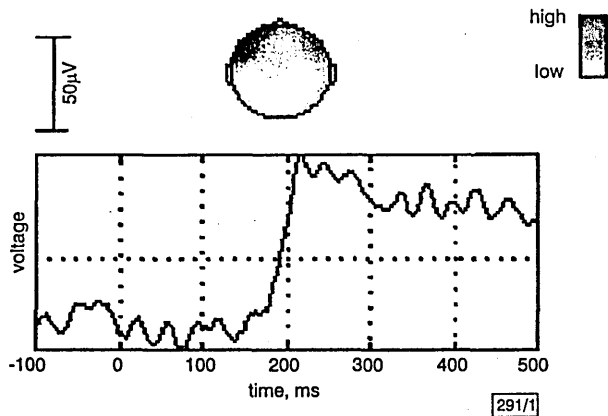


Fig. 1 Extracted EOG left waveform

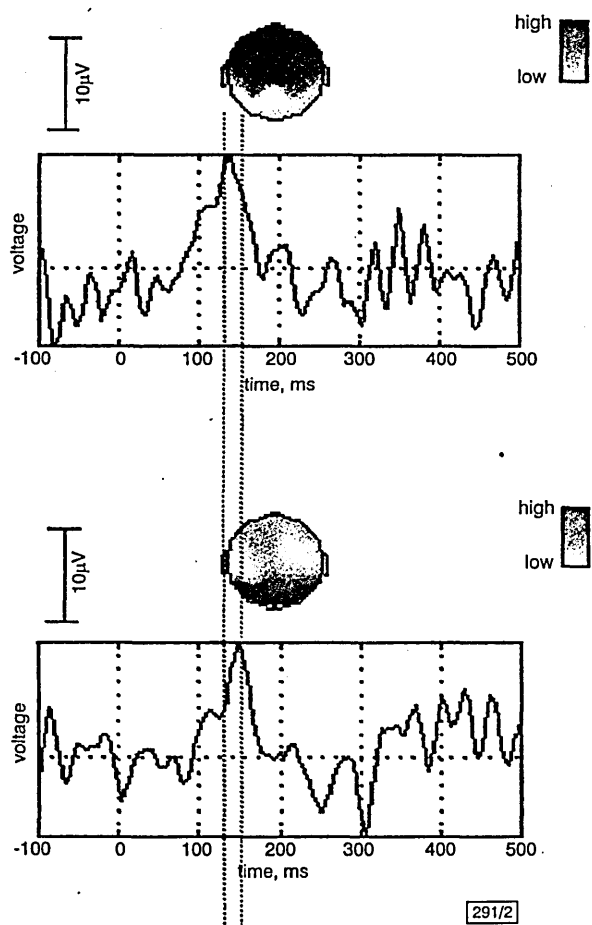


Fig. 2 Pre-saccadic potentials extracted from frontal (top) and occipital (bottom) areas

**Results and conclusion:** For this Letter, only results for the saccade to the left are reported. Figs. 1 – 3 show the waveforms for one subject, although similar waveforms were observed in the other subjects. The colour shading reflects the relative strength of an extracted component at various scalp regions. In all Figures, the onset of stimulus is shown at 0ms. Fig. 1 shows a component with peak activity close to the left eye. It had the characteristics of saccadic eye movement because of its sharp transition at ~200ms (saccade onset) after the stimulus onset. A similar component (not shown) was extracted from a region close to the right eye. The

two potentials extracted from the frontal (top picture) and occipital (bottom picture) areas. These occurred shortly prior to the saccade onset. The frontal pre-saccadic potential is believed to be related to motor commands preceding voluntary saccades [4]. The occipital pre-saccadic potential was found to occur ~30ms after the frontal one. This finding suggested that the occipital pre-saccadic potential is an efferent feedback or copy from the frontal areas for saccade generation. This is believed to be a prerequisite for visual stability during eye movements [5].

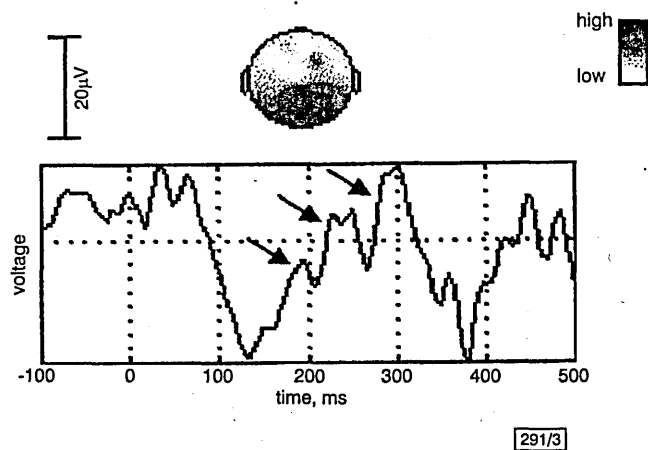


Fig. 3 Lambda wave component

Fig. 3 shows three sub-components (indicated by arrows) extracted from the occipital area. These appeared immediately after the saccade onset and ended shortly after the saccade offset (~300ms after stimulus). These are associated with visual information processing triggered by the relative movement of visual field features across the retina during a saccade [3]. The fact that the occipital pre-saccadic potential and the following three sub-components were extracted separately indicated that they were generated by independent neural processes. This could not have been detected without the application of a signal source separation technique.

An ICA-based methodology enabling saccade-related EEG waveforms to be successfully extracted has been described. Consistent results were obtained for six subjects. The study revealed valuable information about the brain mechanisms involved in performing saccades.

© IEE 2000

15 February 2000

Electronics Letters Online No: 20000732

DOI: 10.1049/el:20000732

L. Vigon and R. Saatchi, (School of Engineering, Sheffield Hallam University, Sheffield S1 1WB, United Kingdom)

J. Mayhew, N. Taroyan, J. Frisby, D. Johnston and O. Pascalis (Psychology Department, University of Sheffield S10 2TP, United Kingdom)

## References

- 1 BARLOW, J.S., and CIGANEK, L.: 'Lambda responses in relation to visual evoked responses in man', *Electroenceph. Clin. Neurophysiol.*, 1969, (26), pp. 183–192
- 2 LEE, T.-W.: 'Independent component analysis, theory and applications' (Kluwer Academic Publishers, Boston, 1998)
- 3 THICKBROOM, G.W., KNEZEVIC, W., CARROLL, W.M., and MASTAGLIA, F.L.: 'Saccade onset and offset lambda waves - relation to pattern movement visually evoked potentials', *Brain Res.*, 1991, (551), pp. 150–156
- 4 KLOSTERMANN, W., KÖMPF, D., HEIDE, W., VERLEGER, R., WAUSCHKUHN, B., and SEYFERT, T.: 'The presaccadic cortical negativity prior to self-paced saccades with and without visual guidance', *Electroenceph. Clin. Neurophysiol.*, 1994, (91), pp. 219–228
- 5 SKRANDIES, W., and LASCHKE, K.: 'Topography of visual brain activity during eye movements: lambda waves, saccadic suppression, and discrimination performance', *Int. J. Psychophysiol.*, 1997, (27), pp. 15–27

# Quantitative evaluation of techniques for ocular artefact filtering of EEG waveforms

L.Vigon, M.R.Saatchi, J.E.W.Mayhew and R.Fernandes

**Abstract:** The electrical dipoles of eyes change by eye movements and blinks, producing a signal known as an electrooculogram (EOG). A fraction of EOGs contaminate the electrical activity of the brain (electroencephalogram, EEG). Ocular artefact (OA) is a collective term used to represent EEG contaminating potentials caused by eye movements and blinks. A procedure for quantifying the effectiveness of an algorithm for removing OA from the EEG was devised. This enabled the similarity between the EEG waveforms before contamination by OA and the contaminated EEG waveforms following their processing by an OA removal method to be measured. Four methods for OA removal were included in the study: extended independent component analysis (ICA), joint approximation diagonalisation of eigenmatrices (JADE), principal component analysis (PCA) and EOG subtraction. The operation of JADE and ICA is subject to amplitude scaling and channel permutation. Procedures were incorporated to estimate the amplitude of the recovered EEG waveforms and to allocate them to the correct channels. It was demonstrated that the signal separation techniques of JADE and extended ICA were more effective than EOG subtraction and PCA for removing OA from the EEG. EOG subtraction was shown to cause attenuation of the recovered EEG waveforms. The effect of additive Gaussian noise on the performance of the four OA removal methods was also investigated. This indicated that the performance of the methods was unaffected by an additive Gaussian noise source, as long as the signal-to-noise ratio remained above 50.

## 1 Introduction

The study of electrical activity of the brain (electroencephalogram, EEG) is a tool which gives an insight into the brain and its abnormalities. The first reported observation of EEG was made by Caton [1]. Berger [2] was the first to observe EEG in human subjects by putting electrodes on the scalp. Since then there have been significant advances in both recording and interpretation of EEG waveforms. The recording of EEG is sometimes time-locked to the occurrence of discrete stimuli (events). The stimuli can be visual, auditory or cognitive processes triggered by external sources. They cause voltage fluctuations within the EEG that are known as event-related potentials (ERPs). ERPs have been extensively studied in order to improve the understanding of sensory organs and to diagnose a number of brain-related disorders including schizophrenia [3, 4].

EEG can be contaminated and thus obscured by various noise sources. The noise generated from the recording system can be significantly reduced by a careful design of the system and by following appropriate signal recording procedures. EEG can also be contaminated by a number of

electrophysiological signals, the largest of which is the electrooculogram (EOG). The human eye contains an electrical dipole caused by a positive cornea and negative retina. Eye movements and blinks change the dipole causing an electrical signal known as an EOG. The shape of the EOG waveform depends on factors such as the direction of eye movements. Vertical eye movements (eyes moving up and down) produce a square-like EOG waveform while blinks cause a spike-shaped waveform.

A fraction of the EOG spreads across the scalp and it is superimposed on the EEG. 'Ocular artefacts' (OA) is a collective term used to describe a number of EEG contaminating voltage potentials caused by eye movements and blinks [5]. In order for the EEG to be interpreted for clinical use, OAs need to be removed (filtered) from the EEG. Analogue and digital filters are not effective for this purpose, as EEG and EOG signals occupy a similar frequency band (covering a range close to DC to about 100Hz).

One of the earliest methods for OA removal was based on the use of potentiometers to balance out the effect of vertical and horizontal eye movements [6]. The required adjustments were made manually by observing the EEG and thus they were subjective. A software based OA removal method was proposed by Quilter *et al.* [7]. The method, known as EOG subtraction, involves subtracting a fraction of the EOG from the contaminated EEG. Its operation is based on the assumptions that: (i) the recorded (contaminated) EEG is a linear combination of the original (i.e. uncontaminated) EEG and OA, (ii) the contaminating OA can be estimated from the EOG, and (iii) there is no correlation between the original EEG and the EOG signals. The method can easily be implemented but it causes distortion of the recovered EEG. This is because a fraction of the

© IEE, 2000

IEE Proceedings online no. 20000475

DOI: 10.1049/ip-smt:20000475

Paper first received 14th December 1999 and in revised form 27th March 2000

L. Vigon and M.R. Saatchi are with the School of Engineering, Sheffield Hallam University, Pond Street, Sheffield S1 1WB, UK

J.E. W. Mayhew is with the Department of Psychology, Sheffield University, Northambland Road, Sheffield, UK

R. Fernandes is with the Ecole Nationale Supérieure d'Electronique et de Radi-  
oélectrique de Bordeaux, Avenue du Dr Schweitzer, BP 99 33402, Talence  
Cedex, France

process causes part of the desired EEG to be removed.

In order to improve the performance of the EOG subtraction method, a technique referred to as 'multiple source eye correction' was developed by Berg and Scherg [8]. They estimated the component of the recorded EOG that was not contaminated by the EEG. A fraction of this component was then subtracted from the recorded EEG. The method, however, required an accurate modelling of propagation paths for the signals involved.

Adaptive digital filters have also been used for OA removal. For example, Rao and Reddy [9] developed an online method of OA removal system based on this approach. They used a nonlinear recursive least-square algorithm to train an adaptive digital filter. The main limitation of the method was the need for a suitable EOG reference model for adapting (training) the filter.

Principal component analysis (PCA) [10] is a well known decorrelation technique and has provided another approach for OA removal from the EEG. PCA enables an epoch of a multichannel EEG to be decomposed into linearly uncorrelated components on the basis of their spatial distribution across channels. By omitting unwanted components (such as OA) from the linear combination, a less contaminated EEG can then be reconstructed. Lagerlund *et al.* [11] developed a variation of this technique, in which the PCA coefficients were stored in a single matrix. This allowed the matrix to be calculated on the basis of one representative epoch that contained the artefacts to be removed. The matrix was then applied to the subsequent EEG epochs, without repeating the PCA operation. The limitations of the PCA approach are that: (i) it is unable to completely separate OAs from the EEG, especially when both waveforms have similar voltage magnitudes, (ii) it requires the distribution of the signal sources to be orthogonal, (iii) its effectiveness is limited to decorrelating signals and thus it cannot deal with higher-order statistical dependencies.

In order to overcome the limitations of PCA, Makeig *et al.* [12] applied independent component analysis (ICA) for removing artefacts from the EEG. ICA is an extension of the PCA which not only decorrelates but can also deal with higher-order statistical dependencies [13]. Bell and Sejnowski [14] proposed an information-theoretic-based ICA algorithm that uses an unsupervised learning rule. It finds a linear transformation within the data to make the separated signal components as statistically 'independent' as possible. The technique does not need *a priori* knowledge of the physical location or the configuration of the sources and, unlike PCA, it does not require the distribution of the signals sources to be orthogonal. However, for it to function correctly, the signal sources must be statistically independent and the distribution of not more than one source can be Gaussian. The EEG signal sources represent the signals produced by the various signal generators of the brain and not the recorded EEG signals that represent a mixture of brain electrical activities from many sources. The ICA algorithm applied by Makeig *et al.* [12] is suitable for sources with super-Gaussian distribution (i.e. irregularly occurring signals with sharply peaked distributions and positive kurtosis). Lee and Sejnowski [15] extended the ICA algorithm to make it also suitable for signal sources with sub-Gaussian distribution (i.e. signals with negative kurtosis). Jung *et al.* [16] applied the extended ICA algorithm to isolate and remove a variety of EEG-contaminating artefacts.

An alternative approach for signal source separation was proposed by Cardoso [17]. The method is based on the

(JADE). It operates by exploiting the higher order statistical properties of the signals based on their fourth-order cumulants. Like ICA, this algorithm also requires the sources to be statistically independent and, at most, the distribution of one source can be Gaussian [18].

An investigation to analyse residual ocular artefacts subsequent to ocular artefact removal from the EEG has been carried out in another study [19]. In this study, however, a method to quantitatively evaluate the effectiveness of an algorithm for OA removal from EEG waveforms was devised. The method was used to evaluate and compare the performance of extended ICA, JADE, PCA and EOG subtraction methods for removing OAs from the EEG. EOG subtraction was included because it is a well known method. PCA was included in order to investigate the need for considering the higher statistical dependencies in OA removal process. Extended ICA and JADE were included as they are well established signal source separation techniques. Both extended ICA and JADE are based on information theoretic principles, however ICA uses entropy while JADE exploits the fourth-order cumulants [20]. EOG subtraction, PCA and ICA have all been previously applied to the problem of OA removal, however the aim of this study is to extend the information available by providing a quantitative evaluation and comparison of their (including JADE) performance based on a series of statistical tests. As the operations of JADE and extended ICA are subject to amplitude scaling and channel permutation, procedures were incorporated as part of these two methods to estimate the amplitude of the separated signals and to allocate them to the correct channels.

Initially, a brief description of the theory of the four methods is provided. Then the experimental procedures are outlined and the results obtained are discussed.

## 2 Theoretical review of the four OA removal methods

### 2.1 EOG subtraction

The operation of EOG subtraction method for removing OA from an EEG waveform consisting of  $N$  data points is outlined in this Section. The contaminated EEG waveform ( $EEG_c$ ) can be expressed as the sum of the original EEG ( $EEG_0$ ) and a fraction ( $\hat{\theta}$ ) of the EOG waveform, i.e.

$$EEG_c(i) = EEG_0(i) + \hat{\theta}EOG(i) \quad i = 1, 2, \dots, N \quad (1)$$

The correlation (at zero lag) between the EOG and contaminated EEG waveforms is given by

$$correlation = \sum_{i=1}^N EEG_c(i)EOG(i) \quad (2)$$

Substituting  $EEG_c$  from eqn. 1 into eqn. 2 results,

$$correlation = \sum_{i=1}^N EEG_0(i)EOG(i) + \hat{\theta} \sum_{i=1}^N EOG(i)^2 \quad (3)$$

Equating eqns. 2 and 3 provides

$$\sum_{i=1}^N EEG_c(i)EOG(i) = \sum_{i=1}^N EEG_0(i)EOG(i) + \hat{\theta} \sum_{i=1}^N EOG(i)^2 \quad (4)$$

correlation between the original EEG and EOG, therefore  $\sum_{i=1}^N EEG_0(i) EOG(i) = 0$ . This simplifies eqn. 4 and from it the value of  $\hat{\theta}$  can be determined by

$$\hat{\theta} = \frac{\sum_{i=1}^N EEG_c(i) EOG(i)}{\sum_{i=1}^N EOG(i)^2} \quad (5)$$

The original EEG waveform can be obtained by inserting  $\hat{\theta}$  in eqn. 1. Therefore,

$$EEG_0(i) = EEG_c(i) - \hat{\theta} EOG(i) \quad i = 1, 2, \dots, N \quad (6)$$

## 2.2 Principal component analysis

Principal component analysis (PCA) is a multivariate data analysis procedure that transforms a set of  $n$  correlated variables,  $X = (x_1, x_2, \dots, x_n)$ , into a set of uncorrelated variables called principal components ( $p_1, p_2, \dots, p_n$ ) [10]. The first principal component accounts for most of the variability in the data, while each of the succeeding components in turn account for the highest amount of the remaining variability. Each principal component is a linear combination of the variables,  $X$ . The  $i$ th principal component can thus be expressed as

$$y_i = e_i^T X \quad (7)$$

where  $e_i$  is the eigenvector of the covariance matrix ( $R$ ) of  $X$  ( $e_i^T$  is the transpose of  $e_i$ ). The variance of the  $i$ th principal component is given by

$$Var(Y_i) = e_i^T R e_i = \lambda_i \quad i = 1, 2, \dots, n \quad (8)$$

where  $\lambda_i$  is the  $i$ th eigenvalue.

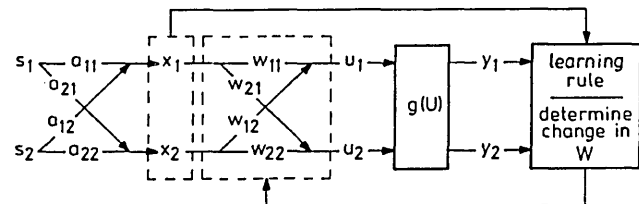


Fig. 1 Diagram to illustrate the operation of ICA

## 2.3 Independent component analysis

The concept of ICA for a situation involving two signal sources  $S$  is illustrated in Fig. 1. The mixtures  $X$  are generated by the operation

$$X = AS \quad (9)$$

where

$$S = \begin{bmatrix} s_1 \\ s_2 \end{bmatrix}, X = \begin{bmatrix} x_1 \\ x_2 \end{bmatrix}$$

and the mixing matrix  $A$  is given by

$$A = \begin{bmatrix} a_{11} & a_{12} \\ a_{21} & a_{22} \end{bmatrix}$$

The aim is to estimate an unmixing matrix  $W$  which, in turn, enables an estimate of the signal sources  $U$  to be obtained by

$$U = WX \quad (10)$$

where

$$W = \begin{bmatrix} w_{11} & w_{12} \\ w_{21} & w_{22} \end{bmatrix}, U = \begin{bmatrix} u_1 \\ u_2 \end{bmatrix}$$

described by the following steps.

(i) The unmixing matrix  $W$  is initialised to an identity matrix.

(ii) The signal sources are estimated by eqn. 10 and then they are transformed by a nonlinear transfer function. For a sigmoidal transfer function, the resulting signals ( $Y$ ) are expressed as

$$Y = g(U) = \frac{1}{1 + e^{-(U + \omega_0)}} \quad (11)$$

where  $\omega_0$  is a vector of bias weights which is initialised to a zero vector.

(iii) The nonlinearly transformed signals ( $Y$ ) are processed by a learning rule which maximises their joint entropy (i.e. minimises their mutual information). This is achieved by changing the weight matrix by the amount  $\Delta W$  [14], where

$$\Delta W = [W^T]^{-1} + (1 - 2y)x^T \quad (12)$$

and the superscripts  $T$  and  $-1$  represent matrix transpose and inversion, respectively. The change in the bias weight is expressed by [14]

$$\Delta \omega_0 = 1 - 2y \quad (13)$$

(iv) The ICA algorithm is trained by repeating steps (ii) and (iii). After each iteration the unmixing matrix  $W$  is updated by  $\Delta W$  until convergence is achieved. The algorithm stops training when the rate of change falls below a predefined small value, e.g.  $1.0 \times 10^{-6}$ . The rate of change is computed by squaring the difference between corresponding elements of the unmixing matrix before and after each iteration and then summing the values.

The ICA algorithm of Bell and Sejnowski [14] which uses a sigmoidal activation function is specifically suited to separate signals with super-Gaussian distribution (i.e. positive kurtosis). Lee and Sejnowski [15] proposed an extension of ICA that is able to separate signals with sub- as well as super-Gaussian distributions. This preserves the ICA architecture of Bell and Sejnowski [14] but it uses a learning rule derived by Girolami and Fyfe [21]. It determines the sign changes (positive to negative and vice versa) required by the algorithm to handle both sub- and super-Gaussian distributions. This is achieved by considering the normalised fourth-order kurtosis ( $k_4$ ) of the estimated signal sources. In extended ICA, the amount of change ( $\Delta W$ ) required to update the unmixing weight matrix  $W$  is given by

$$\Delta W = \frac{\partial H(Y)}{\partial W} W^T W = [I - \text{sign}(k_4)(1 - 2y)u^T - uu^T]W \quad (14)$$

where  $W^T W$  is the 'natural gradient' of Amari *et al.* [22] used as an optimiser for speeding up the convergence.

For a detailed description of ICA and its extended version, the reader may refer to the book by Lee [20].

## 2.4 Joint approximate diagonalisation of eigenmatrices (JADE)

The second signal source separation technique used in this study was the joint approximation diagonalisation of eigenmatrices (JADE). A description of this method is provided by Cardoso [17]. JADE algorithm exploits the fourth-order moments in order to separate signals in a mixture. The operation of JADE is outlined in the following:

(i) The covariance matrix ( $\hat{R}_x$ ) of the mixtures is obtained. This operation is based on the assumption that the signal

to ensure their amplitude information is contained in the mixing matrix  $A$ . This enables  $\hat{R}_x$  to be expressed as  $\hat{R}_x = AA^H$ , where  $A^H$  is the Hermitian matrix of  $A$ . The whitening matrix  $\hat{Q}_x$  is computed by considering the whitening condition  $I = \hat{Q}_x \hat{R}_x \hat{Q}_x^H$ . Replacing  $\hat{R}_x$  gives  $I = \hat{Q}_x AA^H \hat{Q}_x^H$ , where  $I$  is the identity matrix. This implies that  $\hat{Q}_x A$  is a unitary matrix ( $V$ ) and therefore  $A$  can be factorised as  $A = \hat{Q}_x^H V$ .

(ii) The mixtures are then whitened according to  $\hat{Z} = \hat{Q}_x X$ . The whitened mixtures ( $\hat{Z}$ ) obey the linear model  $\hat{Z} = \hat{Q}_x AS$ . Substituting for  $A$  gives  $\hat{Z} = \hat{Q}_x \hat{Q}_x^H VS = VS$ .

(iii) In order to determine  $V$ , the fourth-order cumulants of the whitened mixtures are computed. Their  $n$  most significant eigenvalues ( $\lambda_i$ ) and their corresponding eigenmatrices ( $M_i$ ) are determined. An estimate of the unitary matrix ( $\hat{V}$ ) is obtained by maximising the criteria  $N = \lambda_i M_i$  by means of joint diagonalisation. If  $N$  cannot be exactly jointly diagonalised, the maximisation of the criteria defines a 'joint approximate diagonalisation'.

(iv) An estimate of the unmixing matrix ( $\hat{W}$ ) is obtained by  $\hat{W} = \hat{Q}_x \hat{V}$ . This is then used to compute an estimate of the original signal sources  $U$  as shown in Fig. 2.

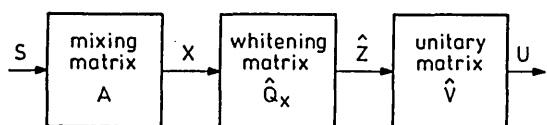


Fig. 2 Diagram to illustrate the operation of JADE

### 3 Experimental method

To quantify the effectiveness of each OA removal method, the recovered EEG waveforms were compared with the original (uncontaminated) EEG. A measure of similarity indicated how well the OA removal method had performed. The operation required the availability of the EEG waveforms before and after OA contamination. Furthermore, extended ICA and JADE required the original signal sources to be independent. The steps for satisfying these requirements are described as part of the overall experimental method. The experiments consisted of: (i) comparison of the four OA removal methods based on single EEG and EOG channels, (ii) analysis of the effect of mixing matrix values on the recovered (separated) EEG waveforms, (iii) analysis of the effect of additive Gaussian noise on the operation of the four OA removal methods, and (iv) comparison of JADE and extended ICA based on multiple EEG and EOG channels.

#### 3.1 Data recording procedure

The EEG and EOG data were recorded in an EEG data recording room with subjects relaxed and fixating at a white board. Four sets of EEG waveforms were recorded from four subjects. Each set consisted of thirty-two waveforms. By recording each EEG data set from a different subject, the condition for independence of the signal sources was satisfied. Thirty-two EOG waveforms were recorded from another subject. By recording the EOG data from a separate subject it was ensured that they had not contaminated any of the EEG data sets. The subjects were asked to avoid eye movements and blinks during each EEG recording in order to minimise OA contamination. EEG data were recorded from the scalp (location CZ in accordance with the 10–20 standard electrode positions). EOG data were recorded using a pair of electrodes placed adjacent to the right eye. The reference for both EEG and

the ear lobes. Silver-silver chloride electrodes were used for all recordings. The sampling rate was 125Hz and the signals were band limited to 30Hz. Each waveform contained 1250 data points (i.e. 10 seconds).

#### 3.2 Generation of required signal sources and mixtures

Mixing matrices used in this analysis are

$$A_1 = \begin{bmatrix} 0.8 & 0.2 \\ 0.2 & 0.8 \end{bmatrix}, A_2 = \begin{bmatrix} 0.5 & 0.2 \\ 0.3 & 0.5 \end{bmatrix}$$

In order to carry out the analysis based on single EEG and EOG channels, 32 pairs of EEG and EOG mixtures were generated using the mixing matrix  $A = A_1$ . The mixing operation was carried out by performing

$$\begin{bmatrix} EEG_c \\ EOG_c \end{bmatrix} = A \begin{bmatrix} EEG_0 \\ EOG_0 \end{bmatrix}$$

where  $EEG_0$  and  $EOG_0$  were the original EEG and EOG, respectively, and  $EEG_c$  and  $EOG_c$  were the resulting contaminated mixtures. The operation caused the original EEG waveforms to be contaminated by one fifth of the EOG (and vice versa). This mixing matrix was considered appropriate as only a fraction of the EOG and EEG can contaminate each other. The mixing operation resulted in 32 pairs of contaminated EEG and EOG mixtures.

The distribution of the EEG and EOG waveforms was tested by the UNIVARIATE procedure using the Statistical Analysis System [23]. This indicated that the EEG waveforms had a Gaussian distribution while the EOG were not Gaussian. Therefore, the requirement for JADE and ICA, where not more than one source can be Gaussian, was not breached.

The 32 pairs of EEG and EOG mixtures generated using the mixing matrix  $A = A_1$  were also used to investigate the effect of additive Gaussian noise on the operation of the four OA removal algorithms. Gaussian noise (band limited to 50Hz) was added to the 32 pair of mixtures and then the four methods for OA removal were applied to recover the EEG waveforms. Statistical parameters (described in Section 3.2) were calculated to determine the ability of each method in recovering the EEG when contaminated by additive Gaussian noise. For each test the results obtained for recovering the 32 EEG waveform were averaged. The experiment was repeated for different amounts of noise. The signal-to-noise ratio (SNR) values represented the signal power (before addition of the noise) to the noise power.

The mixing matrix  $A$  used in this analysis conformed to a unity value for the sum of elements in its columns. To investigate the effect of not conforming to this condition, the experiment for the recovery of EEG waveforms was repeated using the mixing matrix  $A = A_2$ .

The analysis based on multiple EEG and EOG channels was carried out by using the four EEG and EOG data sets. The condition for independence of sources was ensured as each of the four EEG data sets had been recorded from a different subject. The UNIVARIATE statistical procedure [23] was used to test the EEG and EOG distribution. This indicated that while the EOG data were not Gaussian, the EEG data had a Gaussian distribution, and therefore they could not be considered as valid signal sources for ICA and JADE algorithms. The required EEG signal sources were obtained by transforming the recorded EEG data. The transformation involved the following steps: (i) a DC offset was added to the EEG signals so that their minimum

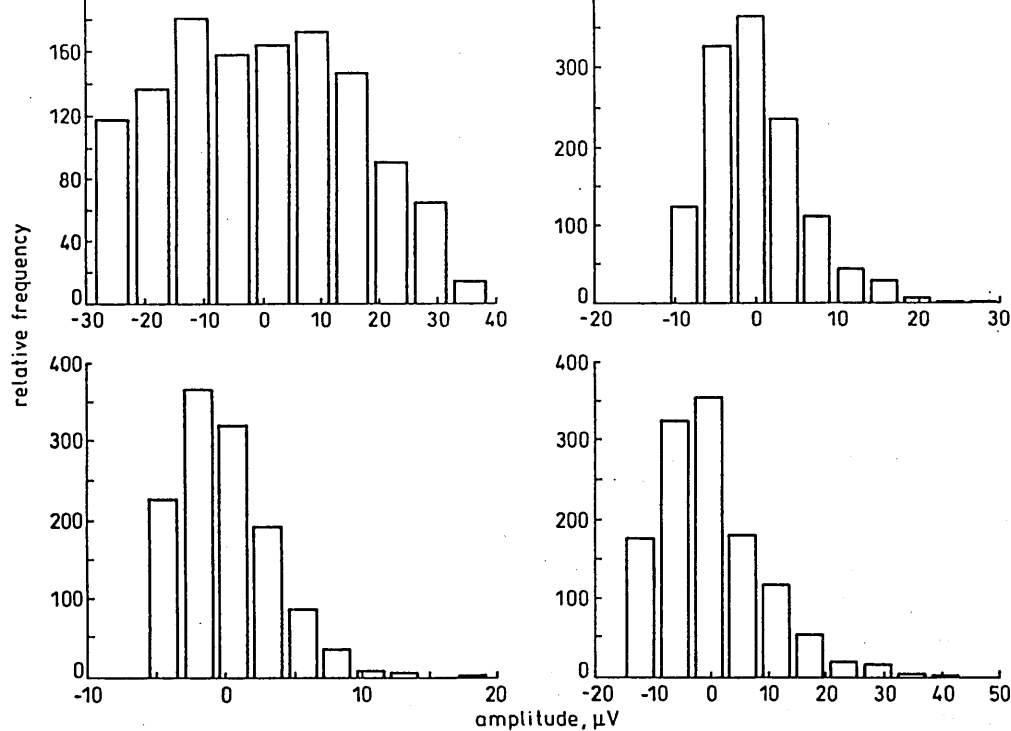


**Fig. 3** Typical distributions of transformed EEG waveforms

values became zero, (ii) they were squared and their mean values were removed, (iii) the resulting signals were rescaled to the original amplitude ranges, and (iv) the UNIVARIATE statistical procedure [23] was applied to the transformed EEG waveforms to ensure they had the required non-Gaussian distribution. Typical distributions of transformed EEG waveform are shown in Fig. 3.

Thirty-two sets, each consisting of five signal mixtures were generated by carrying out the mixing operation,

$$\begin{bmatrix} EEG_{1c} \\ EEG_{2c} \\ EEG_{3c} \\ EEG_{4c} \\ EOG_c \end{bmatrix} = A \begin{bmatrix} EEG_{1t} \\ EEG_{2t} \\ EEG_{3t} \\ EEG_{4t} \\ EOG_0 \end{bmatrix}$$

where  $EEG_{1c}$  to  $EEG_{4c}$  were the contaminated EEG signals and the  $EOG_c$  was the contaminated EOG.  $EEG_{1t}$  to  $EEG_{4t}$  were the transformed EEG signals and  $EOG_0$  was the original EOG waveform. The mixing matrix  $A$  was given by

$$A = \begin{bmatrix} 0.5 & 0.125 & 0.125 & 0.125 & 0.125 \\ 0.125 & 0.5 & 0.125 & 0.125 & 0.125 \\ 0.125 & 0.125 & 0.5 & 0.125 & 0.125 \\ 0.125 & 0.125 & 0.125 & 0.5 & 0.125 \\ 0.125 & 0.125 & 0.125 & 0.125 & 0.5 \end{bmatrix}$$

### 3.3 Procedures to enable JADE and ICA deal with the problems of amplitude scaling and channel permutation

JADE and ICA scale and may invert the recovered signals. Furthermore, the recovered signals may not appear in the correct channels (channel permutation). In order to deal with the channel permutation problem, each recovered signal was compared with each mixture and their correlation coefficient was calculated. A recovered signal was then allocated to the channel which corresponded to the highest correlation coefficient value. The operation assumed that each mixture contained a larger contribution from the original signal source than from the contaminating source. The pos-

sible sign change (i.e. signal inversion) was corrected by considering the sign of the correlation coefficient.

In order to estimate the amplitude of the recovered signals for both JADE and extended ICA, a procedure proposed by Cardoso [Note 1] was implemented. The steps are outlined in the following for a case involving two signal sources, however the method can be extended to situations involving more than two sources:

(i) The inverse of the unmixing matrix  $W^{-1}$  was obtained. This provided an estimate of the mixing matrix.  $W^{-1}$  is given by

$$W^{-1} = \begin{bmatrix} w_{11} & w_{12} \\ w_{21} & w_{22} \end{bmatrix}$$

(ii) The total contribution of each original signal source to the mixtures was estimated from  $W^{-1}$ . This required summing the squared elements in each of its columns. The resulting sums were square rooted and then multiplied by a scaling factor ( $k_j$ ). This produced a row vector,  $p = [k_1\sqrt{(w_{11}^2 + w_{21}^2)}, k_2\sqrt{(w_{12}^2 + w_{22}^2)}]$ . The squaring of the elements was necessary to ensure negative values did not cancel positive values during the summing process. The scaling factor  $k_1$  and  $k_2$  were required to deal with the mathematical inequality that, for any two values ( $x$  and  $y$ ),  $x + y \neq \sqrt{(x^2 + y^2)}$ . The expression for  $k_j$  ( $j = 1, 2$ ) is given by

$$k_j = \frac{\sum_{i=1}^2 w_{ij}}{\sqrt{\sum_{i=1}^2 (w_{ij})^2}} \quad (15)$$

where  $w_{ij}$  represents an element (in the  $i$ th row and  $j$ th column) of the matrix  $W^{-1}$ . The unmixing matrix  $W$  was rescaled by multiplying its columns by the corresponding columns of the row vector  $p$ .

Note 1: Cardoso, J.-F.: Personal communication, 1998, (address: Ecole Nationale Supérieure des Telecommunications, Telecom Paris, Department Signal, 46 rue Barrault, 75634 Paris Cedex 13, France)

### methods

In order to assess the performance of each OA removal method, the similarity between the original and recovered EEG waveforms was measured. This required quantifying any change in the amplitude and shape of the waveforms. The required measurements were carried out by using the correlation coefficient, standard deviation and Euclidean distance parameters. The justification for using these parameters is provided by the following:

(i) *Correlation coefficient*: This provided a measure of the similarity in shape for the recovered and original EEG waveforms. A value of 1 indicated that the recovered and original waveforms had exactly the same shape. However, this parameter did not provide any information about amplitude changes.

(ii) *Standard deviation ratio*: This was the ratio of the original EEG standard deviation to that of the recovered EEG. A value of 1 indicated that the original and recovered

a loss in the recovered signal power. As both ICA and JADE scale the amplitude of the recovered signals, this parameter indicated how well (for a particular mixing matrix) the Cardoso's amplitude estimation operates as part of JADE and extended ICA algorithms.

(iii) *Euclidean distance*: This provided a measure of similarity in both shape and amplitude. The Euclidean distance between two signals ( $x$  and  $y$ ) can be expressed as [24]

$$\text{Euclidean distance} = \sqrt{\sum_{i=1}^N (x_i - y_i)^2} \quad (16)$$

### 3.5 Statistical tests for determining the significance of differences

In order to determine the significance of the differences between the performance of the four OA removal methods, a number of tests were carried out using the Statistical

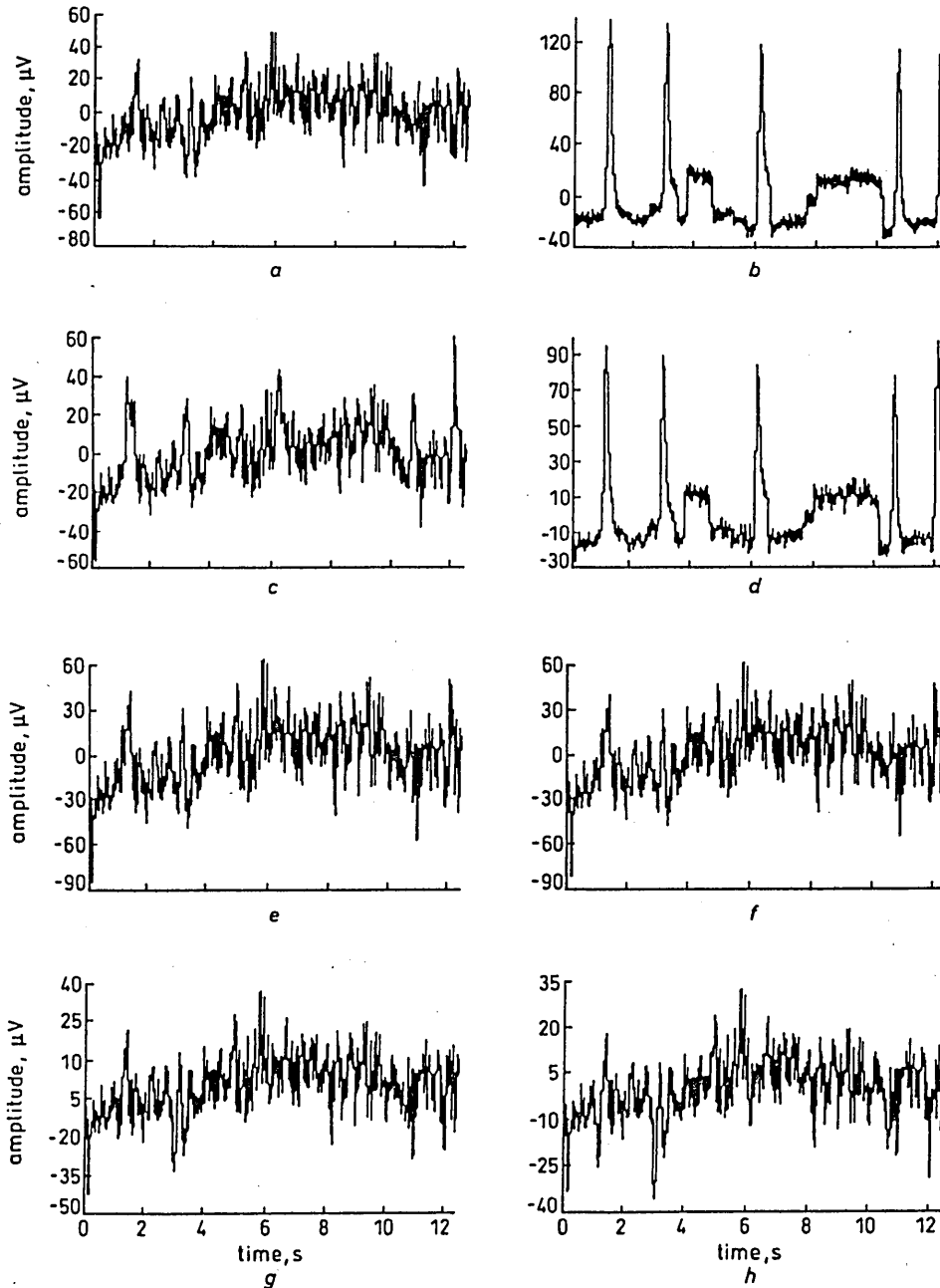


**Fig. 4** Typical plots

a Original EEG  
b Original EOG  
c Contaminated EEG

d Contaminated EOG  
e Recovered EEG waveforms using JADE  
f Extended ICA

g EOG subtraction  
h PCA

F-statistic test [25] to be carried out on the mean values (over thirty-two trials) for each of the three parameters (correlation coefficient, Euclidean distance and standard deviation ratio) across the four OA removal methods. The F-statistic was suitable because it tested the null hypothesis that a significant difference did not exist between the means for a given parameter. An F value close to 1 resulted in accepting the null hypothesis, otherwise it was rejected.

Although the F-statistic indicated whether means were significantly different across the four OA removal methods, it did not however indicate which mean differed significantly from the other means. In order for this to be determined, Tukey's studentised range test [23] was performed. This test was based on analysing the pairwise differences between the means.

The results obtained for JADE and extended ICA were computed after incorporating the amplitude estimation procedure as part of their algorithms. The mixtures were processed by the four OA removal methods in order to recover the original EEG waveforms. The results are described in the following Sections.

#### 4.1 Single EEG and EOG data set analysis

This investigation used the signals generated with the mixing matrix  $A = A_1$ .

Typical plots for one pair of original EEG and EOG waveforms, their mixtures and the recovered EEG waveforms following the application of the four OA removal algorithms are shown in Figs. 4a-l.

The standard deviation ratio, Euclidean distance and correlation coefficient values were computed for the EEG

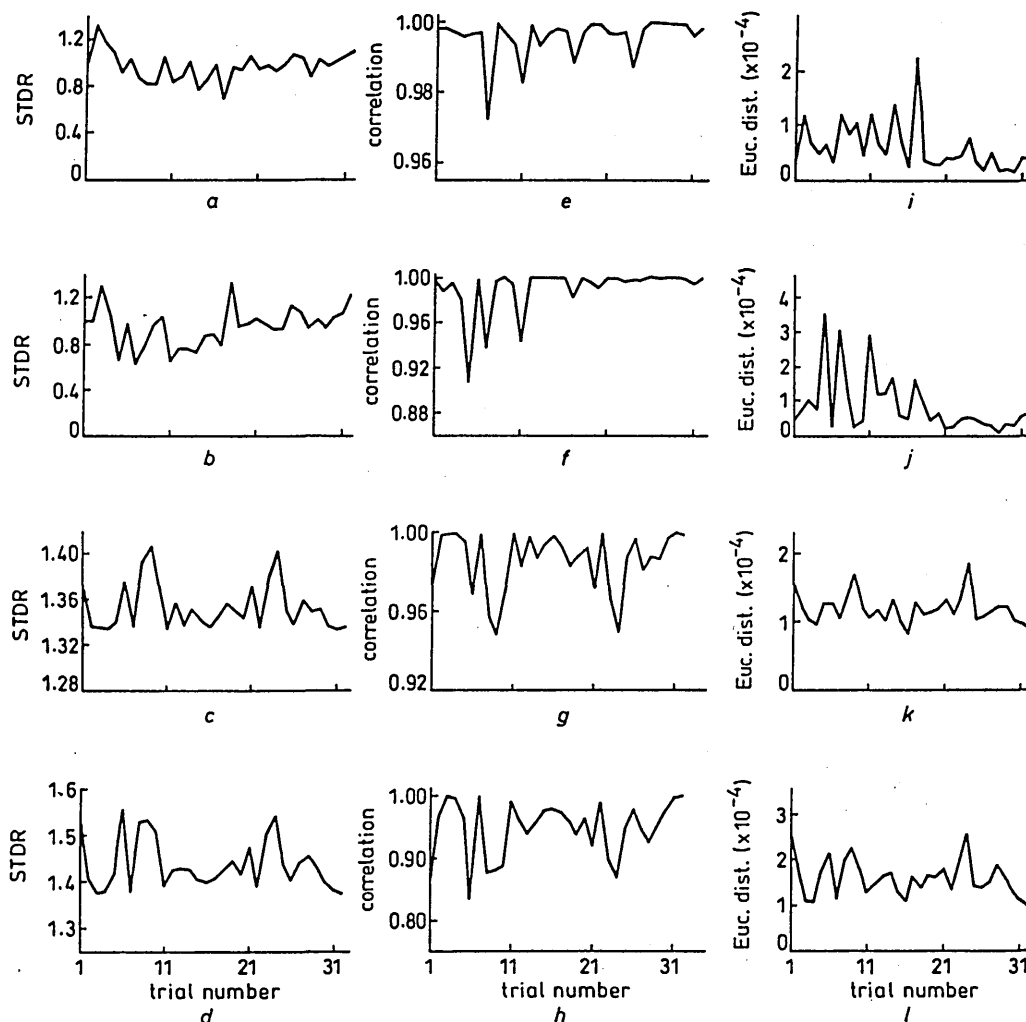


**Fig.5** Plots of standard deviation ratio (STDR), correlation coefficient and Euclidean distance for different techniques

Top to bottom: JADE, extended-ICA, EOG subtraction, PCA

a-d STDR

e-h Correlation coefficient

i-l Euclidean distance

**Table 1: Means and variances for the three parameters over 32 trials**

Methods	Standard deviation ratio		Correlation coefficient		Euclidean distance	
	Mean	Variance ( $\times 10^{-3}$ )	Mean	Variance ( $\times 10^{-3}$ )	Mean ( $\times 10^{-4}$ )	Variance ( $\times 10^{-9}$ )
PCA	1.45	3.0	0.95	2.2	1.59	1.7
Extended ICA	0.95	29.4	0.99	0.43	0.85	7.4
JADE	0.97	15.9	1.00	0.034	0.60	2.1
EOG subtraction	1.35	0.4	0.99	0.23	1.18	0.48

provided in Table 1.

The following observations were made for the standard deviation ratio parameter. The EOG subtraction method provided smallest variance and thus the highest consistency. However, it was always larger than 1 indicating a loss of amplitude in the recovered EEG. This confirmed the limitation of the EOG subtraction method, in which the part of the EEG which contaminates the EOG is also subtracted from the recovered EEG, resulting in a loss of its amplitude (this was first referred to in the Introduction, Section 1). The PCA technique also reduced the amplitude of the recovered EEG. This indicated that PCA could not completely separate the mixtures. This may be because PCA is unable to deal with higher-order statistical dependencies. For extended ICA and JADE, the standard deviation ratio parameter assessed, not only their ability to separate the signal components in the mixtures, but also the ability of the Cardoso's amplitude estimation in rescaling the separated signals. The results show that JADE and extended ICA, together with the Cardoso's amplitude estimation procedure, have provided an accurate recovery of the original EEG waveforms.

JADE provided a correlation coefficient closest to 1 and a Euclidean distance value closest to 0. It was also the most consistent (i.e. smallest variance) for these two parameters.

To determine the significance of the difference between the observed means, two statistical tests were carried out by using the analysis of variance (ANOVA) technique [23]. These were F-statistics and Tukey's studentised range test.

The F-statistic test was performed for each measured parameter (standard deviation ratio, correlation coefficient and Euclidean distance) across the four OA removal methods. This indicated that significant differences ( $p < 0.0001$ ) existed between the means for each of the three parameters across the four methods.

The Tukey's studentised range test was then performed to determine the sign (positive or negative) of the pair-wise differences between the means. This indicated whether a mean was significantly smaller or larger than another mean. The results are shown in Table 2.

Regarding the standard deviation ratio parameter, the performance of PCA and EOG subtraction was significantly different from JADE and extended ICA. The per-

formance of PCA was significantly different (smaller mean) from the other three algorithms. The latter did not show significant differences between their performances. This parameter indicated that PCA was the least effective in preserving the shape of the recovered EEG waveforms.

Considering the results for Euclidean distance parameter, JADE and extended ICA differed significantly from PCA and EOG subtraction, however they did not differ significantly from each other.

#### 4.2 Analysis to determine the effect of mixing matrix

The results shown in Table 1 were obtained using a mixing matrix that conformed to unity for the sum of elements in its columns. To investigate the effect of not conforming to this condition, the experiment was repeated using the mixing matrix  $A = A_2$ . The results are shown in Table 3.

**Table 3: Performance evaluation results when the mixing matrix  $A = A_2$**

Methods	Standard deviation ratio	Correlation coefficient	Euclidean distance ( $\times 10^{-4}$ )
PCA	3.15	0.89	2.93
Extended ICA	1.23	0.98	1.06
JADE	1.27	0.99	0.87
EOG subtraction	2.77	0.95	2.68

The results for standard deviation ratio (from Table 3) indicated that JADE and extended ICA performed better than PCA and EOG subtraction. Both PCA and EOG subtraction methods resulted in a significant loss in the recovered EEG amplitude. The results also showed that the performance of the amplitude estimation procedure was affected by the mixing matrix values. The results for correlation coefficients were all still close to 1 indicating that the values associated with the mixing matrix do not affect the recovered signals' shape. The experiment was repeated with several other mixing matrices. The results were consistent with these observations.

**Table 2: Tukey's test (at level of significance 0.05) for pair-wise differences between algorithms**

Pair-wise differences between the algorithms		Standard deviation ratio	Correlation coefficient	Euclidean distance
PCA-	EOG subtraction	s(+)	s(-)	s(+)
	JADE	s(+)	s(-)	s(+)
	Extended ICA	s(+)	s(-)	s(+)
EOG subtraction	PCA	s(-)	s(+)	s(-)
	JADE	s(+)	ns(-)	s(+)
	Extended ICA	s(+)	ns(-)	s(+)
JADE	PCA	s(-)	s(+)	s(-)
	EOG subtraction	s(-)	ns(+)	s(-)
	Extended ICA	ns(+)	ns(+)	ns(+)
Extended ICA	PCA	s(-)	s(+)	s(-)
	EOG subtraction	s(-)	ns(+)	s(-)
	JADE	ns(-)	ns(-)	ns(-)

s = significant, ns = not significant

of the four OA removal methods was also investigated. The plots for the observations are shown in Figs. 6a–c. The results indicated that the performances of all four algorithms for OA removal degrade rapidly for signal-to-noise ratios below 50.

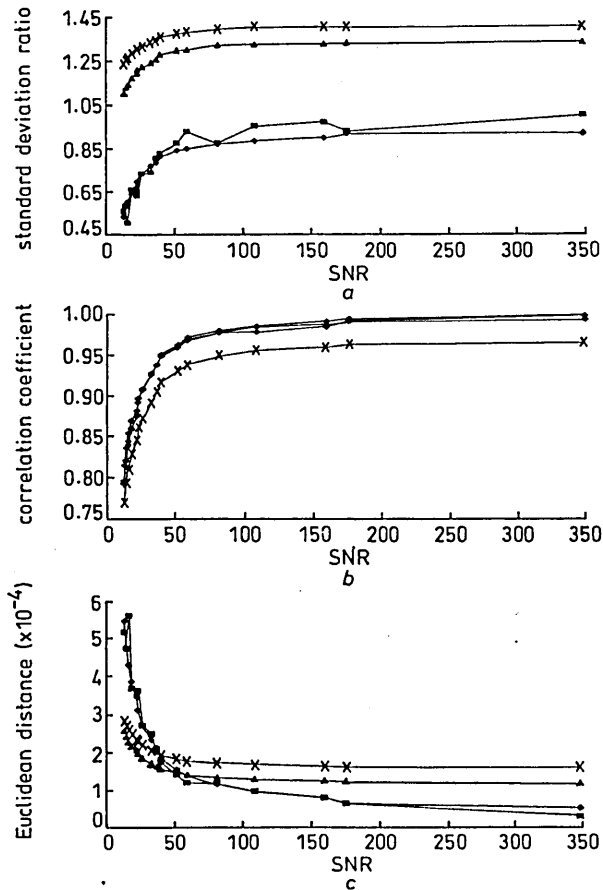


**Fig. 6** Plots to demonstrate the effect of noise on the performances of different methods  
 —■— extended-ICA  
 —◆— JADE  
 —×— PCA  
 —▲— EOG subtraction

#### 4.4 Multiple EEG channels analysis

The results obtained for the data consisting of four sets of thirty-two transformed EEG waveforms ( $EEG_{1t}$  to  $EEG_{4t}$ ) are presented in Table 4. The mean value for each parameter was obtained by averaging the results over thirty-two waveforms. The results obtained were consistent with those obtained involving one set of EEG waveforms. Only JADE and extended ICA were included in this analysis because they had performed significantly better than PCA and EOG subtraction methods, when analysing one set of EEG and EOG data.

**Table 4: Results obtained when the algorithms were applied to four transformed EEG sources**

Transformed EEG data	Standard deviation ratio		Correlation coefficient means		Euclidean distance means ( $\times 10^{-5}$ )	
	JADE	Ext. ICA	JADE	Ext. ICA	JADE	Ext. ICA
$EEG_{1t}$	1.04	1.08	0.95	0.95	11.75	11.48
$EEG_{2t}$	1.15	1.10	0.95	0.96	8.00	7.80
$EEG_{3t}$	1.00	0.97	0.96	0.96	6.28	7.62
$EEG_{4t}$	1.05	1.02	0.98	0.97	7.87	9.31

- The devised procedures made it possible for the performances of the four algorithms for OA removal to be quantified and compared.
- Cardoso's amplitude recovery method enabled the amplitude of the recovered EEG to be estimated for both JADE and extended ICA. However, the results were affected by changing the values of the mixing matrix.
- The proposed correlation-based method provided a means for dealing with the problems of channel permutation and sign changes problems associated with JADE and extended ICA algorithms.
- JADE and extended ICA performed significantly better than PCA. This could be because PCA only decorrelates signals while JADE and extended ICA attempt to make the recovered signal components as independent as possible.
- The EOG subtraction attenuated the recovered EEG signals. This is because a fraction of the EEG that contaminates the EOG signal is also subtracted from the recovered EEG component.
- Extended ICA method required a significantly longer time to carry out the OA removal operation when compared with JADE. This is because extended ICA is an iterative algorithm, which requires many passes through its learning algorithm in order to converge, while JADE only requires one pass through its algorithm.
- Statistical tests showed that, on average, the performances of JADE and extended ICA, for OA removal, were not significantly different. However, JADE provided a more consistent set of results and both JADE and extended ICA performed significantly better than PCA and EOG subtraction.
- The performances of the four OA removal methods were not significantly affected by an additive Gaussian noise source for a signal-to-noise ratio above 50.

## 5 Conclusion

The performances of four methods for removing ocular artefacts from the EEG were quantified and compared. The methods were extended independent component analysis (ICA), joint approximation diagonalisation of eigenmatrices (JADE), principal component analysis and electrooculogram (EOG) subtraction. The study indicated that JADE and extended ICA performed significantly better than the other two methods. The performances of JADE and extended ICA were not, on average, significantly different, however JADE provided a more consistent set of results. All four algorithms could tolerate additive Gaussian noise, provided the signal-to-noise ratio remained above 50.

ICA are various methods for the removal of the EEG. However, their main weaknesses are amplitude scaling and channel permutation. Further work will be carried out to improve the accuracy of the recovered signal amplitudes. Other approaches to deal with the problem of channel permutation will also be investigated.

## 6 Acknowledgments

The authors are grateful to Professor J.-F. Cardoso for being able to use the JADE algorithm and his kindness in providing his amplitude recovery procedure. They are grateful to Dr S. Makeig for being able to access and use his extended ICA algorithm. The helpful comments of Dr David K. Johnston and of the IEE Honorary Editor on the contents of this paper are also greatly appreciated.

## 7 References

- 1 CATON, R.: 'The electric current of the brain', *Br. Med. J.*, 1875, 2, pp. 278
- 2 BERGER, H.: 'Über des elektenkephalogram des menschen', *Arch. Psychiat.*, 1929, 87, pp. 527-570
- 3 SAATCHI, M.R., OKE, S., ALLEN, E.M., JERVIS, B.W., and HUDSON, N.: 'Signal processing of the contingent negative variation in schizophrenia using multilayer perceptrons and predictive statistical diagnosis', *IEE Proc., Sci. Meas. Technol.*, 1995, 142, (4), pp. 269-277
- 4 PRITCHARD, W.S.: 'Cognitive event-related potential correlates of schizophrenia', *Psycholog. Bull.*, 1986, 100, (1), pp. 43-66
- 5 JERVIS, B.W., IFEACHOR, E.C., and ALLEN, E.M.: 'The removal of ocular artefacts from the electroencephalogram: a review', *Med. Biol. Eng. Comput.*, 1988, 26, pp. 2-12
- 6 GIRTON, D.G., and KAMIYA, J.: 'A simple on-line technique for removing eye movement artefacts from the EEG', *Electroencephalogr. Clin. Neurophysiol.*, 1973, 34, pp. 212-216
- 7 QUILTER, P.M., MacGILLIVRAY, B.B., and WADBROOK, D.G.: 'The removal of eye movement artefact from the EEG signals using correlation techniques'. IEE Conf. Publ., 1977, Vol. 159, pp. 93-100
- 8 BERG, P., and SCHERG, M.: 'A multiple source approach to the correction of eye artifacts', *Electroencephalogr. Clin. Neurophysiol.*, 1994, 90, pp. 229-241
- 9 facts using non-linear recursive least squares technique', *Neural. Com. Eng. Comput.*, 1995, 33, pp. 488-491
- 10 JOLLIFFE, I.T.: 'Principal component analysis' (Springer-Verlag, New York, 1986)
- 11 LAGERLUND, T.D., SHARBROUGH, F.W., and BUSACKER, N.E.: 'Spatial filtering of multichannel electroencephalographic recordings through principal component analysis by singular value decomposition', *J. Clin. Neurophysiol.*, 1997, 14, (1), pp. 73-82
- 12 MAKEIG, S., BELL, A.J., JUNG, T., and SEJNOWSKI, T.J.: 'Independent component analysis of electroencephalographic data', *Adv. Neural Inf. Process. Syst.*, 1996, 8, pp. 145-151
- 13 COMON, P.: 'Independent component analysis, A new concept?', *Signal Process.*, 1994, 36, (3), pp. 287-314
- 14 BELL, A.J., and SEJNOWSKI, T.J.: 'An information-maximization approach to blind separation and blind deconvolution', *Neural Comput.*, 1995, 7, pp. 1129-1159
- 15 LEE, T.-W., and SEJNOWSKI, T.J.: 'Independent component analysis for sub-Gaussian and super-Gaussian mixtures'. Proceedings of 4th joint symposium on *Neural computation*, 1997, Vol. 7, pp. 132-139
- 16 JUNG, T.-P., HUMPHRIES, C., LEE, T.-W., MAKEIG, S., McKEOWN, M., IRAGUI, V., and SEJNOWSKI, T.J.: 'Extended ICA removes artifacts from electroencephalographic recordings', *Adv. Neural Inf. Process. Syst.*, 1998, 10, pp. 894-900
- 17 CARDOSO, J.-F.: 'High-order contrasts for independent component analysis', *Neural Comput.*, 1999, 11, (1), pp. 157-192 (A Matlab implementation of JADE is also available from the WEB site <http://sig.enst.fr/~cardoso/stuff.html>)
- 18 CARDOSO, J.-F.: 'Blind signal separation: statistical principles', *Proc. IEEE*, 1998, 90, (8), pp. 2009-2026 (Special issue on blind identification and estimation)
- 19 JERVIS, B.W.: 'Residual ocular artefact subsequent to ocular artefact removal from the electroencephalogram', *IEE Proc., Sci. Meas. Technol.*, 1999, 146, (6), pp. 293-298
- 20 LEE, T.-W.: 'Independent component analysis, theory and applications' (Kluwer Academic Publishers, Boston, 1998)
- 21 GIROLAMI, M., and FYFE, C.: 'Extraction of independent signal sources using a deflationary exploratory projection pursuit network with lateral inhibition', *IEE Proc., Vis. Image Signal Process.*, 1997, 144, (5), pp. 299-306
- 22 AMARI, S., CICHOCKI, A., and YANG, H.: 'A new learning algorithm for blind signal separation', *Adv. Neural Inf. Process. Syst.*, 1996, 8, pp. 757-763
- 23 'SAS user's guide: statistics'. Statistical Analysis System (SAS), SAS Institute INC, Box 8000, Cary, North Carolina 27511, 1982
- 24 MARDIA, K.V., KENT, J.T., and BIBBY, J.M.: 'Multivariate analysis' (Academic Press, London, 1979)
- 25 STEEL, R.G.D., and TORRIE, J.H.: 'Principles and procedures of statistics' (Mcgraw-Hill Book Company, New York, 1980, 2nd edn.)

Society Proceedings

The British Society for Clinical Neurophysiology,  
London, 20 October 2000

*Hon. Meetings Secretary: Dr L.M. Henderson\**

*University Hospital, Queen's Medical Centre NHS Trust, Nottingham, NG7 2UH, UK*

**1 Peripheral neuropathy in HIV infection – G. Kanabar, S. Gunasekera, H. Longhurst, A.T. Pinching and K. Nagendran (Barts and The London NHS Trust)**

We studied 147 consecutive HIV +ve patients referred to our department with possible diagnosis of peripheral neuropathy for assessment. All had sural SAP, common peroneal motor conduction, and F and H wave studies. Ninety-two in addition had quantitative thermal thresholds.

The summary of findings in the 92 patients who had large and small fibre studies include 21 normal, 25 small fibre neuropathy (SFN) only, 6 large fibre neuropathy alone, 10 radiculopathy with small fibre dysfunction and 30 small and large fibre neuropathy. Six patients fulfilled the criteria for demyelinating neuropathy but none had significant conduction block, temporal dispersion to proximal stimulation or significant F wave prolongation except in one case. Ankle jerks were frequently absent, and nearly all had retained or brisk knee jerks despite the presence of well-established neuropathy, suggestive of co-existing UMN dysfunction. A small group of patients had significantly reduced MCV (without fulfilling the criteria for demyelinating neuropathy) but preserved sural SAP and EDB CMAP.

We conclude that small fibre studies are more frequently abnormal (70.6%) in HIV neuropathy. Demyelinating neuropathy affects predominantly distal segments without conduction block or temporal dispersion.

**2 Initial clinical experience with vibration threshold testing in repetitive strain injury – D.S. Holder, V. Morris and M. Boland (University College, London)**

Greening and Lynn (1998) recently measured hand vibration thresholds in subjects with repetitive strain injury (RSI) and found that they were elevated ( $>0.6 \mu\text{m}$ ) and increased by more than 50% after use of a keyboard for 5 min. We report initial clinical experience in patients with presumed RSI, using these criteria.

Vibration thresholds were recorded from median, ulnar and radial territories in each hand in 20 patients with RSI on clinical grounds, mainly referred in the hope of providing support in a medicolegal claim.

Twelve subjects had a raised vibration threshold in median territory in either hand, but only two of these met the above criteria.

This method could be of considerable value if it is able to provide objective evidence of RSI, but this initial clinical experience in this patient group suggests a low sensitivity with the proposed conservative criteria. It may be possible to increase sensitivity by adjusting criteria in the light of larger clinical studies. The median abnormalities support the hypothesis that there is median nerve dysfunction in this condition.

Greening J, Lynn B. Vibration sense in the upper limb in patients with repetitive strain injury and a group of at-risk office workers. *Int Arch Occup Environ Health* 1998;71:29–34.

**3 The clinical utility of visual evoked responses in the assessment of pituitary structural lesions – B. Anand, R.C. Pottinger and D.A. Ingram (Barts and The London NHS Trust)**

The advent of high-resolution neuroimaging has prompted re-evaluation of the role of visual evoked responses (VERs) in the management of pituitary structural lesions. We have therefore retrospectively examined the results of VERs in 29 patients (mean age  $46.8 \pm 16.0$  (SD) years; 18 females) with various pituitary lesions and compared these with clinical and radiological evidence of impingement on suprasellar visual pathways. Whole-field and hemi-field pattern-evoked responses, obtained using standardized techniques, were evaluated blind for latency and amplitude measurements by one author (B.A.). These findings were then compared with the results of computed tomography and magnetic resonance imaging findings and carefully mapped visual fields to 5 mm red stimuli.

Fourteen (48%) patients had radiological evidence of suprasellar involvement of visual pathways and all demonstrated various VER abnormalities. Of the remaining 15 (52%) patients without radiological evidence of visual pathway involvement, 5 (17%) had normal VERs and 10 (34%) had a VER abnormality. Of those with a VER abnormality 5 (17%) (two macroadenomas, one microadenoma, one TSHoma and one resected supraclinoid tumour) had a visual field defect. The remaining 5 (17%), including 3 who had undergone previous transphenoidal surgery, had no associated visual field defect. This suggests that in almost one-fifth of cases, evidence of subclinical involvement of chiasmal visual pathways may be detected using VERs.

**4 Signal source separation of saccade-related evoked potentials – L. Vigon<sup>a</sup>, M.R. Saatchi<sup>a</sup>, J.E.H. Mayhew<sup>b</sup>, N. Taroyan<sup>b</sup> and J.P. Frisby<sup>b</sup> (<sup>a</sup>Sheffield Hallam University and <sup>b</sup>Sheffield University)**

The independent component analysis (ICA) signal source separation algorithm was extended by incorporating the template model of a visual evoked potential (EP) called the lambda-wave (Thickbroom et al., 1991) into the algorithm's cost function. The template-model ICA algorithm was evaluated in this study by analyzing saccade-related EEG data.

Saccade related EEG waveforms were recorded from 64 locations on the scalp. Seven subjects participated in the experiments. Each subject sat 0.5 m from a computer screen which displayed a checkerboard pattern. They were asked to visually follow a red square which appeared randomly at one of 5 pre-defined locations (up, down, left, right and centre) on the checkerboard. The peripheral-to-centre viewing angle was 12 degrees. Up to 50 trials were recorded per event (i.e. a direction of saccade). Each trial lasted about 2 s.

The template-model ICA algorithm was applied to the averaged saccade-related EEG waveforms to extract the lambda wave and identify its saccade time-locked subcomponents. Its corresponding scalp distribution obtained using the developed method showed peak activity in the parieto-occipital area of the cerebral cortex.

The results of the study demonstrated that the incorporation of a

\* Tel.: +44-115-970-9146; fax: +44-115-849-3225.

template-model into ICA significantly improved the extraction of the lambda wave from the EEG data. The technique is applicable for the extraction and analysis of other EPs and event-related potentials for which models can be developed.

Thickbroom et al., *Brain Res* 1991;551:150–156.

**5 Motor abnormalities in patients with chronic pain? – A.M. Purves and M.S. Chong (Medway Maritime Hospital, Orpington Hospital and Kings College Hospital, London)**

Patients who present with chronic pain syndromes may have abnormalities of function which are quite separate from the pain. They often also complain of more subtle difficulties using the hand or arm, with loss of power or dexterity, and the neurological basis for this is not well understood.

We have used a recently described motor reflex (the group III reflex) (Priori et al., 1998; Burne and Lippold, 1996) as a probe for changes in motor unit excitability in patients with pain in one limb of unknown cause, and have found 3 patterns of abnormality. In some patients ( $n = 19$ ) there is greater inhibition of the rectified averaged EMG signal in the forearm muscles on the affected side after stimulation ( $P < 0.01$ , Mann–Whitney  $U$  test), in others ( $n = 5$ ) a more tonic inhibition and in a few ( $n = 3$ ) a failure of recruitment of motor units with or without stimulation. The possible significance of these findings for our understanding of pain syndromes in the clinic will be discussed.

Priori et al. *Brain* 1998;121:373–380.

Burne JA, Lippold OC. Loss of tendon organ inhibition in Parkinson's disease. *Brain* 1996;119:1115–1121.

**6 Electrocorticographic findings in cortical dysplasia and dysembryoplastic neuroepithelial tumour – C.D. Binnie, G. Alarcon, A. Dean, R.D.C. Elwes, C. Ferrier and C.E. Polkey (Guys, Kings and St. Thomas' School of Medicine, London)**

Of all patients treated surgically for epilepsy over a 20 year period and whose medical records were available, 17 underwent frontal resection for cortical dysplasia (CD), 18 underwent frontal resection for other pathology, 12 underwent temporal resection for CD as the only pathology, 22 DNET, and 17 other, non-atrophic lesions. The intraoperative electrocorticograms (EcoGs) were related blind to the pathology before and after resection, with reference to ictal or continuous epileptiform discharges (ICEDs) and discontinuous sporadic spike or spike-and-wave discharges.

In the frontal group, pre-resection ICEDs were strongly associated with CD (16/17 versus 4/18 in non-CD subjects,  $P < 0.001$ ). Sporadic spikes did not discriminate between CD and non-CD subjects (11/17 and 14/18). The presence of ICEDs was associated with favourable surgical outcome (type I or II) ( $P < 0.05$ ) but neither sporadic spikes nor the topography of discharges was predictive of outcome. Post-resection, only 3 CD subjects continued to exhibit ICEDs – all with unfavourable outcome, whereas overall 9/17 patients had good outcome. ICEDs were abolished in all non-CD patients but appeared de novo in one – with good outcome.

In the temporal group, pre-resection ICEDs were associated with CD (9/12) and also occurred with DNET (6/22), but never with other pathology. Sporadic spikes did not discriminate between pathologies. Neither the presence nor post-resective persistence of ICEDs was predictive of surgical outcome.

**7 Bizarre prolongation of distal motor latency is a robust sign of active motor axonal regeneration – K. Nagendran (Barts and The London NHS Trust)**

Sixteen patients showed a markedly delayed distal motor latency to target muscles (values ranging from 10.5 to 71 ms) during recovery following severe or total axonopathic lesions such as severe traumatic nerve injuries and severe compressive nerve lesions. Recordings were made using concentric needle electrodes. The presence of 'nascent units' and the appropriate time of occurrence confirmed that the recorded potentials were re-innervating motor units. The phenomenon is probably due to a relatively rapid advancement of axonal growth combined with a delayed myelination process.

These findings provide (1) a useful electrodiagnostic test for motor axonal regeneration and (2) a human model to study motor axonal regeneration.

**8 Monitoring intercostal nerve function during thoracotomy – L.M. Henderson<sup>a</sup>, M.I. Rogers<sup>b</sup> and J.P. Duffy<sup>b</sup> (<sup>a</sup>University Hospital, Queen's Medical Centre, Nottingham and <sup>b</sup>City Hospital, Nottingham)**

Chronic postoperative pain persisting beyond 3 months is a distressing and common complication of thoracotomy. Pain may result from intercostal nerve injury by retraction or dissection, but the mechanism of injury intraoperatively has not been demonstrated.

We used intraoperative motor conduction studies of intercostal nerves above and below the level of original incision to identify nerve injury.

Thirteen patients undergoing first thoracotomy were recruited. Bipolar recording needle electrodes were placed anteriorly in the muscles of the two intercostal spaces either side of the planned incision and additionally one space above or below. A monopolar probe stimulated each intercostal nerve in turn with a 3.5 mA current giving a visible twitch. Motor responses produced were recorded before (1) and after (2) the intercostal space was entered and ribs retracted. After intrathoracic surgery was completed, the rib retractor was removed and motor responses were again recorded (3) with a fourth recording after closing intercostal spaces.

The mean velocity (1,2) was 35.3 m/s and recording (3) in 12 cases showed conduction block. In the nerve above the incision, the block was total in 3 cases and at the level of the retractor in 9. In the nerve below, the block was total in 3 cases, at retractor level in 8 and partial in one. One patient without rib spreading showed no conduction change in (3).

We conclude that multiple nerves are routinely injured during thoracotomy due to rib spreading. The relation to post-thoracotomy pain has still to be demonstrated.

# Adaptive Non-linear Principal Component Analysis of a Saccade Related EEG Component

L. Vigon and R. Saatchi

School of Engineering - Sheffield Hallam University  
Pond Street, Sheffield S1 1WB  
Email: r.saatchi@shu.ac.uk

## 1. Summary

Saccades are rapid changes in the orientation of the eyes for realigning the visual axes on objects of interest. Dysfunction in this system may affect various visual functions such as depth perception and reading. A signal source separation method called non-linear principal component analysis (NLPCA) was used to analyse saccade related EEG waveforms recorded from 7 normal subjects. A number of components with the main features of the lambda wave were extracted from the parieto-occipital area of the visual cortex. The peak of activities of these components corresponded to discrete locations and showed a symmetry over the left and right hemisphere. In a previous study the application of another signal source separation method called independent component analysis (ICA) to the same data had indicated that the peak of activity of the lambda wave spread across the whole parieto-occipital area. The findings of this study indicated that ICA considered the whole parieto-occipital area to be a single source for the lambda-wave whereas NLPCA identified a number of symmetrical independent sources for the lambda wave in that region.

## 2. Introduction

The study of electrical activity of the brain (electroencephalogram, EEG) is a tool for studying the neuronal mechanisms associated with the brain functions and its abnormalities. Evoked potentials (EPs) are voltage deviations in the EEG which are time-locked to the onset of stimuli. Saccades are rapid changes in the orientation of the eyes for realigning the visual axes on objects of interest. Saccade mechanisms are associated with vision when moving the eyes. Therefore their study provides valuable information about various visual functions such as depth perception and reading. A saccade performance generates a number of EPs which are time locked to the onset of the stimulus and the eye movement waveform (known as electrooculogram, EOG). The lambda wave is a saccade-related EP which has been reported to originate in the parieto-occipital area (back of the head) of the cerebral cortex [1]. It is believed to be related to visual information processing triggered by the relative movement of features of the visual field

across the retina. The occurrence of the lambda wave is time-locked to the saccade onset (i.e. initiation of the eye-movement) and to the saccade offset (i.e. termination of the eye-movement). It has a pronounced positive peak which appears within a 200 ms period after the saccade offset.

The EEG waveforms recorded from the scalp during a saccade-related performance are signal mixtures consisting of: (i) Saccade-related EP components (such as the lambda wave). These components overlap in time and may also have overlapping spatial topographies. (ii) The obscuring background EEG and EPs that are not associated with the saccade performance and generation. (iii) The contaminating electrophysiological signal artefacts such as the EOG generated by the eyes and the electromyogram (EMG) caused by muscle activity. (iv) Non-electrophysiological (external) sources of contamination, for example the mains interference.

The conventional method for extracting saccade-related EPs from the EEG waveforms involves averaging a large number of recorded trials. The process of averaging reduces the obscuring effect of the background EEG. This is because the background EEG components vary from one trial to the next while the EPs have a more consistent pattern. A typical lambda wave (obtained by the averaging method) together with the corresponding time-locked EOG waveform are shown in Fig.1.

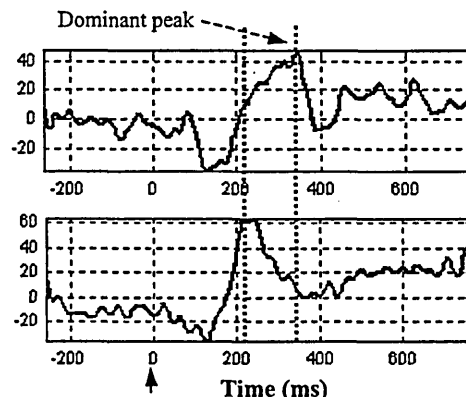


Fig.1 The lambda wave extracted using conventional averaging method and the corresponding EOG component. The vertical arrow indicates the onset of stimulus.

Averaging on its own is not sufficient when accurate interpretation of the saccade-related components such as the lambda wave is required. For example, the operation cannot separate the individual components of the saccade-related EPs within the recorded EEG mixtures. It also does not provide the scalp distribution of the individual saccade-related EP components. As a result, the brain regions responsible for their generation cannot be accurately identified. Procedures that can separate the independent components in the mixtures are therefore valuable.

In a previous study, a signal source separation methodology was devised and was successfully used to extract saccade related EP components from the EEG mixtures [2]. The method was based on a signal source separation (blind deconvolution) called independent component analysis (ICA) [6]. A typical extracted lambda wave, its scalp distribution, together with the corresponding time-locked EOG waveform are shown in Fig.2.

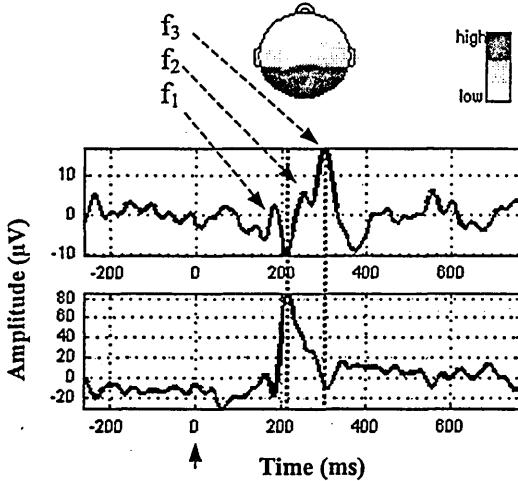


Fig.2 The lambda wave extracted using ICA and the corresponding EOG component.

Three sub-components ( $f_1$ ,  $f_2$  and  $f_3$ ) related to the movement of the visual field across the retina were visible in the extracted lambda wave. Sub-components  $f_1$  and  $f_2$  are time locked to the onset of the saccade and have also been observed in another study [1]. The sub-component  $f_3$  is time-locked to the offset of saccade and has been reported to occur at about 100 ms after the saccade offset [1].

The aim of this study was to carry out an analysis of the lambda wave using non-linear PCA (NLPCA) and to compare the results with those obtained in our previous study using ICA [2]. The ICA algorithm uses entropy as a measure of signal independence

while NLPCA uses a recursive least square algorithm. Both algorithms attempt to extract the unknown source signals from their instantaneous linear mixtures.

### 3. Brief Review of Non-Linear PCA and ICA

A recursive least square algorithm for adaptive tracking of signal subspaces was reported by Yang [3]. The algorithm is derived from the cost function,

$$J_2(W) = E\{\|x - WW^T x\|^2\} \quad (1)$$

where,  $x = [x_1, x_2, \dots, x_n]^T$  is the matrix of signal mixtures,  $n$  is the number of mixtures,  $W$  is an  $m \times m$  weight matrix ( $m$  is the number of sources,  $m$  is assumed to be equal to  $n$  in this study),  $^T$  represents a matrix transpose, and  $E$  is the expectation operation. The minimum of this cost function is provided by any orthogonal matrix  $W$  whose columns span the PCA subspace defined by the principal eigen-vectors of the covariance matrix of  $x$ . Karhunen and Pajunen [4] have extended Yang's recursive least square algorithm so that it can be used for minimising the NLPCA cost function reported in [5] given as,

$$J_2(W) = E\{\|x - Wg(W^T x)\|^2\} \quad (2)$$

where  $g(\cdot)$  is a non-linear transfer function. This transfer function enables the method to deal with the higher-order statistics of the data.

This resulted in an adaptive learning algorithm described by the following steps.

$$\begin{aligned} z(t) &= g(W^T(t-1) v(t)) = g(y(t)), \\ h(t) &= P(t-1)z(t), \\ m(t) &= h(t) / (\beta + z^T(t)h(t)), \\ P(t) &= \frac{1}{\beta} \text{Tri}[P(t-1) - m(t)h^T(t)], \\ e(t) &= v(t) - W(t-1)z(t), \\ W(t) &= W(t-1) + e(t)m^T(t). \end{aligned} \quad (3)$$

The matrix  $v(t)$  is the input to the algorithm and is produced by whitening  $x(t)$ . The covariance of  $v(t)$  is expressed as  $E\{v(t)v(t)^T\}$  and is equal to the identity matrix,  $I$ . The constant  $0 < \beta \leq 1$  is a forgetting term which is normally set close to 1.  $P$  is a symmetrical matrix where its upper triangular part is computed by operation  $\text{Tri}$  and its transpose is copied to the lower triangular part.

The block diagram of NLPCA operation when applied to 2 sources is shown in Fig.3.

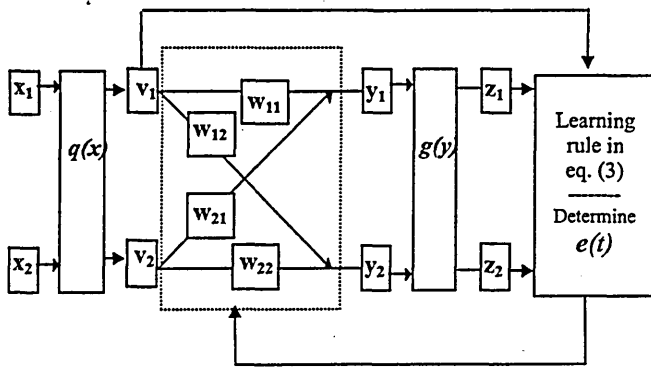


Fig.3 Block diagram of the operation of NLPCA when applied to 2 sources;  $q(\cdot)$  is the whitening process.

Another signal source separation algorithm, called independent component analysis (ICA), was proposed by Bell and Sejnowski [6]. It uses an unsupervised learning rule that maximises the joint entropy (i.e. minimises the mutual information) of the separated components with respect to the weight matrix (i.e.  $\frac{\partial H(\mathbf{y})}{\partial \mathbf{W}}$ ). The change in the weight matrix ( $\Delta \mathbf{W}$ ) at each iteration is given as,

$$\Delta \mathbf{W} = \frac{\partial H(\mathbf{y})}{\partial \mathbf{W}} = \left[ \mathbf{W}^T \right]^{-1} + (1 - 2\mathbf{y})\mathbf{x}^T \quad (4)$$

$$\text{where } \mathbf{y} = g(\mathbf{u}) = \frac{1}{1 + e^{-(\mathbf{u} + \boldsymbol{\omega}_o)}} \quad (5)$$

$\boldsymbol{\omega}_o$  is a vector of bias weight, the symbol  $^{-1}$  represent matrix inversion,  $g(\cdot)$  is a non-linear transfer function such as sigmoid and the estimate of the signal sources is given by  $\mathbf{u} = \mathbf{x}\mathbf{W}$ . The change in the bias weight at each iteration is given by,

$$\Delta \boldsymbol{\omega}_o = 1 - 2\mathbf{y} \quad (6)$$

Amari *et al.* [7] modified the ICA algorithm of Bell and Sejnowski in order to avoid matrix inversion and thus speed up the convergence of the learning rule. The modification involved the incorporation of  $\mathbf{W}^T \mathbf{W}$  into (4) as,

$$\begin{aligned} \Delta \mathbf{W} &= \frac{\partial H(\mathbf{Y})}{\partial \mathbf{W}} \mathbf{W}^T \mathbf{W} \\ &= \left[ \mathbf{I} + (\mathbf{I} - 2\mathbf{Y})\mathbf{U}^T \right] \mathbf{W} \end{aligned} \quad (7)$$

## 4. Experimental Procedures

### 4.1 Data Recording

Seven healthy adults (3 males, 4 females) mean age 27 years (standard deviation 6) with normal or corrected-to-normal vision participated in the study. The subjects had no history of a neurological or ophthalmologic disease and were all right-handed. They were seated in an EEG recording laboratory at about 60 cm from a computer that displayed a black and white checkerboard pattern background.

A red square visual target stimulus (hereafter referred to as the stimulus) appeared on a computer screen at one of five predefined checkerboard locations: centre, left, right, up and down as shown in Fig.4. The sequence of the stimulus appearance on the checkerboard was random to reduce the effect of expectancy.

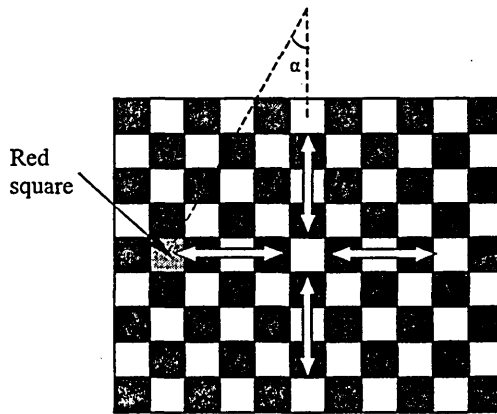


Fig.4 The checkerboard showing the directions of saccade and the viewing angle.

The subjects were instructed to visually follow the stimulus as fast as possible. They were also asked to avoid head movements and blinks. The viewing angle ( $\alpha$ , shown in Fig.4) of the peripheral positions from the centre was about 10 degrees. There were 8 directions of saccade and a steady fixation. These were: 4 centre-to-peripherals, 4 peripherals-to-centre and a centre-to-centre (i.e. no eye-movement) as indicated in Fig.4. In order to avoid the effect of anticipating the onset of the stimulus, the 'pre-stimulus period' was varied randomly.

The EEG and EOG data were recorded using a network of 64 silver-silver chloride electrodes. The EOG data were recorded to monitor the eye-movements. All channels (EEG and EOG) were referred to the vertex ( $C_z$ ) electrode. The recording system bandpass filter had a frequency range of 0.01 to 100 Hz. The digitisation sampling rate was

250 Hz. Up to fifty trials (a trial being a set of 64 recorded waveforms) were recorded per saccade direction. Each trial lasted about 2 seconds. A group of 50 trials is called an event. The total number of recorded trials per subject was up to 450 (i.e. 50 trials  $\times$  (8 directions of saccade + 1 steady fixation)).

## 4.2 Data Analysis

The operations to analyse the lambda wave were:

- i Signal pre-processing
- ii Iterative synchronisation
- iii Temporal and spatial averaging
- iv Signal source separation using NLPCA.

These operations are described in the following sections.

### 4.2.1 Signal Pre-Processing

The recorded data were digitally lowpass filtered at 45 Hz in order to remove any 50 Hz mains interference and unwanted high frequency signal components. The baseline for each waveform was adjusted by calculating the mean of the pre-stimulus section and subtracting it from the waveform. This operation ensured that the waveforms started at a zero reference level. The trials with magnitudes larger than 200  $\mu$ V were rejected offline in order to remove severely contaminated waveforms (typically 3-4 trials per event). The 200  $\mu$ V threshold ensured that the eye-movement waveforms (which were needed for the analysis) were retained. The trials were sorted into their respective directions of saccade and synchronised-averaged using the procedure described in the next section.

### 4.2.2 Iterative Synchronisation

The lambda wave is time-locked to the eye movement waveform (EOG). The initiation of the eye movement (saccade onset time) and its termination (saccade offset time) vary from one trial to the next. This means that the lambda waves from different recorded trials are not synchronised in time. Therefore the averaging of the trials causes their features to be distorted. An algorithm which time synchronised the trials was devised. This algorithm ensured that the features of the lambda wave were preserved during the signal averaging operation. The EOG waveform was chosen as the reference signal for performing the synchronisation because the lambda wave is time-locked to it. The operation of the algorithm is outlined in [8].

### 4.2.3 Averaging Process

Both temporal and spatial averaging of the waveforms were carried out. The reasons and procedures for these operations are provided in the next two sections.

#### 4.2.3.1 Temporal Averaging

Temporal averaging was necessary to reduce the obscuring effect of the background EEG on the features of the signal of interest (i.e. the lambda wave). The synchronised trials obtained in section 4.2.2 were time averaged producing a mean waveform for each channel.

#### 4.2.3.2 Spatial Averaging

In our previous study [2], it was found that the effectiveness of ICA in extracting saccade-related EEG components was improved when the saccade related EEG waveforms recorded from the 64 channels were spatially averaged. The operation consisted of averaging together the waveforms from channels close to the international 10-20 system of electrode site placement. This resulted in 20 EEG and 2 EOG waveforms which were input to ICA. In this study, this form of averaging was used when applying NLPCA.

### 4.2.4 Signal Source Separation using NLPCA

This spatially averaged saccade related EEG waveforms were processed by the NLPCA algorithm outlined in eq.(3). Experiments were carried out to investigate the effect of using different types of non-linear transfer functions ( $g(\cdot)$ ), different values of forgetting factor ( $\beta$ ) and the number of iterations in order to determine the optimum NLPCA parameters for processing the data. The selected parameters were:  $\beta=0.9$  and  $g=\tanh(\cdot)$ . The NLPCA learning process stopped when the amount of change in the weight matrix  $W$  became less than a predefined small value. The number of iterations was approximately 300 for the data used in this study.

## 5. Results and Discussion

Typical results obtained when the NLPCA was applied to the 22 spatially-averaged saccade related EEG waveforms for the centre-to-left saccade event are described in this section. Fig.5 a and b show two extracted lambda waves from the occipital region, their respective scalp distributions and the time locked EOG waveforms. A number of other similar lambda waves were extracted from parietal region of the visual cortex.

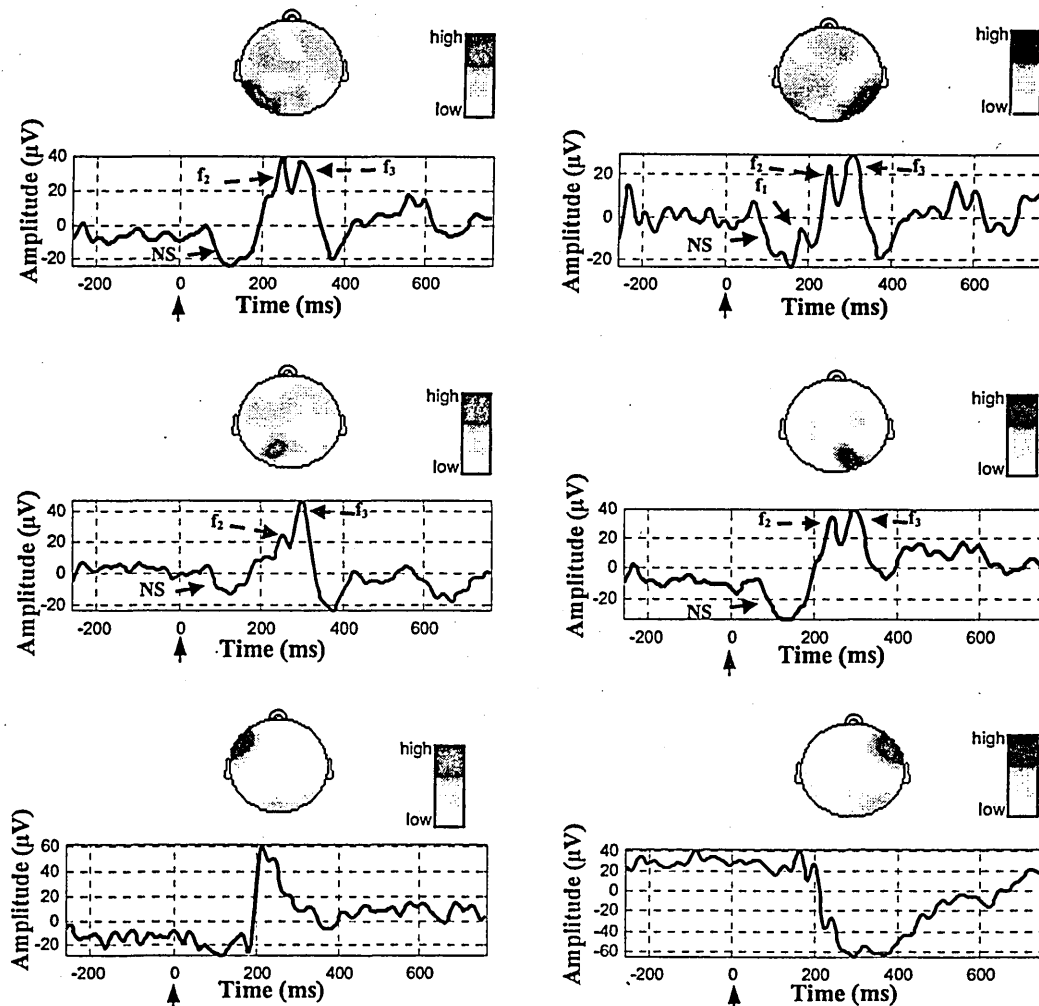


Fig. 5 The NLPCA extracted lambda waves with their scalp distributions (top two rows) and the corresponding extracted EOG waveforms with their scalp distributions (bottom row).

The following were observed in the study:

- The main features of the lambda wave (labelled  $f_1$ ,  $f_2$ ,  $f_3$  and negative shift, NS) were clearly visible. This indicated the effectiveness of NLPCA in extracting the lambda wave. The shape of the extracted lambda waves was similar to that extracted by using ICA (see Figs 2 and 5).
- NLPCA extracted a number of components from the parieto-occipital area of the cerebral cortex. Some of these had the main characteristics of the lambda wave but showed some variations in their time courses. The peak activities of the components were localised in distinct regions of parieto-occipital area. For each lambda wave peak activity identified over the left hemisphere a symmetrical peak of activity was observed over the right hemisphere. A typical set of lambda wave components with symmetrical peaks of activity are shown in Fig.5. This symmetry may be

because both eyes follow the same target stimulus (red square on checkerboard).

- ICA extracted a lambda wave component with peak of activity which spread across the whole parieto-occipital area (see Fig.2). A comparison of the lambda wave peak activities obtained using the two methods indicated that NLPCA identified a number of distinct lambda wave sources within the parieto-occipital area while ICA treated the whole region as one source. This may be due to non-linear PCA being more sensitive to the time course variations of the extracted lambda waves.
- The EOG components from both the left and the right eyes were also extracted (see Fig. 5). The polarity change for the left and right EOG waveforms is due to the reference electrode location ( $C_z$ ).

The above observations were consistent across the subjects included in the study.

## 6. Conclusion and Further Work

In this study an analysis of a signal source separation method called non-linear PCA (NLPCA) was carried out for extracting a saccade related EEG component called the lambda wave. Its performance was compared with that of independent component analysis (ICA). The study showed that NLPCA extracted the lambda wave from discrete regions of parietal-occipital area of the visual cortex while ICA treated the whole region as one source. These findings indicate that ICA considered the whole parieto-occipital area to be a single source for the lambda-wave whereas NLPCA identified a number of symmetrical independent sources for the lambda wave in that region.

Further work will be carried out to determine the significance of the findings reported in this study and will include the use of non-linear ICA for analysing the saccade related EEG waveforms.

## 7. Acknowledgements

This study is supported by a joint Sheffield Hallam University - Sheffield University research grant. The authors are grateful to Prof. J.E.W. Mayhew, Prof. J.P. Frisby and Dr N.A. Taroyan for their valuable discussions and support, Dr P. Furness and Dr D. Buckley for helping with the data recording procedures. This study would not have been possible without the kind co-operation of the subjects who took part in the experiments.

## 8. References

1. Thickbroom, G.W., Knezevic, W., Carroll, W.M. and Mastaglia, F.L.: 'Saccade onset and offset lambda waves - relation to pattern movement visually evoked potentials', *Brain Res.*, 1991, vol.551, pp.150-156.

2. Vigon, L., Saatchi, R., Mayhew, J., Taroyan, N.A., Frisby, J.P.: 'Independent component analysis of saccade-related electroencephalogram waveforms', *IEE Electronics Letters*, 2000, vol.36, no.12, pp.1006-1007.
3. Yang, B.: 'Projection approximation subspace tracking', *IEEE Transaction on Signal Processing*, 1995, vol.43, pp.95-107.
4. Karhunen, J. and Pajunen, P.: 'Blind source separation and tracking using nonlinear PCA criterion: a least-squares approach'. *Proc. of IEEE 1997 International Conference on Neural Networks (ICNN97)*, Houston, Texas, June 9-12, 1997, pp.2147-2152.
5. Karhunen, J., and Joutsensalo, J.: 'Representation and separation of signals using non-linear PCA type learning', *Neural Networks*, 1994, vol.7, no.1, pp.113-127.
6. Bell, A.J. and Sejnowski, T.J.: 'An information-maximization approach to blind separation and blind deconvolution', *Neural Computation*, 1995, vol.7, pp.1129-1159.
7. Amari, S., Cichocki, A. and Yang, H.: 'A new learning algorithm for blind signal separation', *Advances in Neural Information Processing Systems*, 1996, vol.8, pp.757-763.
8. Vigon, L., Saatchi, R., Mayhew, J.E.W., Taroyan, N.A., Frisby, J.P. and Buckley, D.: 'Optimising independent component analysis performance for extracting the lambda wave', submitted to *IEE Proc. Image, Vision and Signal Processing*, 2001.

# Effect of signal length on the performance of independent component analysis when extracting the lambda wave

L. Vigon<sup>1</sup> R. Saatchi<sup>1</sup> J. E. W. Mayhew<sup>2</sup> N. A. Taroyan<sup>2</sup> J. P. Frisby<sup>2</sup>

<sup>1</sup>School of Engineering, Sheffield Hallam University, Sheffield, UK

<sup>2</sup>Department of Psychology, Sheffield University, Sheffield, UK

**Abstract**—The aim of the study was to investigate the effect of signal length on the performance of a signal source separation method, independent component analysis (ICA), when extracting the visual evoked potential (EP) lambda wave from saccade-related electro-encephalogram (EEG) waveforms. A method was devised that enabled the effective length of the recorded EEG traces to be increased prior to processing by ICA. This involved abutting EEG traces from an appropriate number of successive trials (a trial was a set of waveforms recorded from 64 electrode locations in a study investigating saccade performance). ICA was applied to the saccade-related EEG and electro-oculogram (EOG) waveforms recorded from the electrode locations. One spatial and five temporal features of the lambda wave were monitored to assess the performance of ICA applied to both abutted and non-abutted waveforms. ICA applied to abutted trials managed to extract all six features across all seven subjects included in the study. This was not the case when ICA was applied to the non-abutted trials. It was quantitatively demonstrated that the process of abutting EEG waveforms was useful for ICA preprocessing when extracting lambda waves.

**Keywords**—Independent component analysis, Evoked potentials, Saccade analysis, Lambda wave, Electro-encephalogram

Med. Biol. Eng. Comput., 2002, 40, 260–268

## 1 Introduction

AN ELECTRO-ENCEPHALOGRAM (EEG) is a record of the electrical activity of the brain. It contains valuable information about the brain functions and its abnormalities. Evoked potentials (EPs) are voltage deviations in the EEG that are time-locked to the onset of stimuli. They contain information about the neuronal mechanisms involved in sensory functions.

This study was based on a saccade-related visual EP called the lambda wave. Saccades are rapid changes in the orientation of the eyes for realigning the visual axes on objects of interest. Dysfunction in this system can affect various visual functions, such as depth perception and reading (LEVENTHAL, 1991). The lambda wave is believed to be related to visual information processing triggered by the relative movement of features of the visual field across the retina (BARLOW and CIGANEK, 1969). The lambda wave has a number of sub-components. These are generated by the brain when a subject visually follows a target stimulus (such as a red square) appearing at different locations

on a black and white checker-board background. These sub-components are time-locked to the saccade onset (i.e. initiation of the eye movement) and its offset (i.e. termination of the eye movement) (THICKBROOM *et al.*, 1991). One of these sub-components has a pronounced positive peak that appears within a 200 ms time window after the saccade offset (THICKBROOM *et al.*, 1991). A typical lambda wave, together with its saccadic eye-movement electro-oculogram (EOG) waveform, is shown in Fig. 1.

It is reported that the lambda wave originates in the parieto-occipital area (back of the head) of the cerebral cortex (GREEN, 1957). The study of saccade-related EPs provides valuable information about how the brain deals with vision when eye movements are performed (SKRANDIES and LASCHKE, 1997).

Saccade-related EEG waveforms recorded from electrodes placed on the scalp contain a mixture of signals. These are

- (i) saccade-related EP components (for example, the lambda wave)
- (ii) non-saccade-related EEG components, i.e. the background EEG and stimulus time-locked EP components that are not related to the saccade
- (iii) contaminating electrophysiological signals, such as the EOG; EOG is generated by the eyes when eye movements or blinks are performed

Correspondence should be addressed to Dr R. Saatchi;  
e-mail: r.saatchi@shu.ac.uk

Paper received 26 September 2001 and in final form 4 February 2002

MBEC online number: 20023661

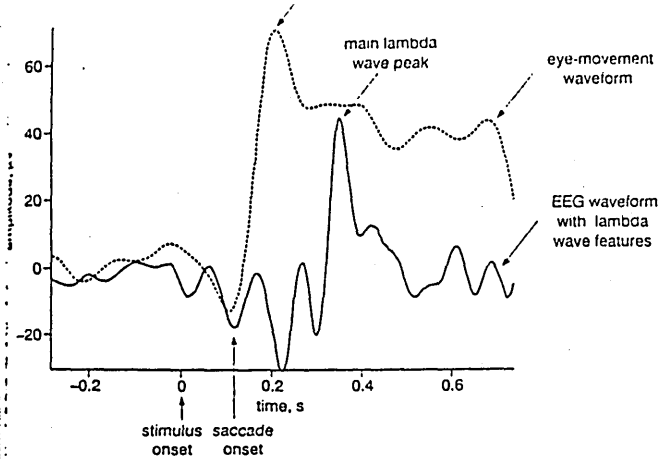


Fig. 1 Typical lambda wave together with its saccadic EOG waveform

iv) non-electrophysiological (external) contaminating signals, for example the noise generated by the recording system.

Therefore signal source separation techniques that allow the recorded EEG waveforms to be unmixed are valuable for extracting and studying specific EP components, such as the lambda wave. A technique that can be used for this purpose is independent component analysis (ICA). The goal of ICA is to recover the independent source signals given only the recorded mixtures. Its operation is based on a number of assumptions. These are

- a) the mixing process is linear
- b) not more than one source signal has a Gaussian distribution
- c) the source signals are stationary and statistically independent.

When ICA is applied to the EEG waveforms, the source signals are considered to be concurrent electromagnetic activities that are temporally independent of each other and that are generated by spatially fixed sources. These signals are mixed as they propagate from their sources to the electrode locations on the scalp.

The ICA technique is reviewed by HYVÄRINEN (1999). BELL and SEJNOWSKI (1995) proposed a method for implementing ICA that extracts independent components by maximising the joint entropy (i.e. minimising the mutual information) of the separated components. CARDOSO (1999) proposed an approach for implementing ICA that exploits the fourth-order cumulant. A study showed that both of these approaches provided a more accurate means for removing EOG-based contamination from the EEG than a number of correlation-based methods (VIGON *et al.*, 2000a).

For the EEG to conform to the stationarity requirement of ICA, the statistical properties of its signal components should be time-invariant. However, EEG signal components (such as EPs) are short-duration transient signals and may not fully conform to the stationarity assumption of ICA. In this study, a method was devised to increase the effective length of the EEG waveforms processed by ICA so as to increase their stationarity pre-requisite. The performance of ICA for extracting the lambda wave was assessed for different length EEG waveforms. Initially, a brief description of the ICA algorithm of BELL and SEJNOWSKI (1995) is provided (this algorithm was used in our study). The experimental methodologies are outlined, and the results obtained are presented.

AND SEJNOWSKI

The ICA algorithm of BELL and SEJNOWSKI (1995) receives  $n$  signal mixtures

$$X = \begin{bmatrix} x_1 \\ x_2 \\ \vdots \\ x_n \end{bmatrix}$$

and determines an unmixing matrix

$$W = \begin{bmatrix} w_{11} & w_{12} & \cdots & w_{1n} \\ w_{21} & w_{22} & \cdots & w_{2n} \\ \vdots & \vdots & \ddots & \vdots \\ w_{n1} & w_{n2} & \cdots & w_{nn} \end{bmatrix}$$

that enables the original source signals

$$U = \begin{bmatrix} u_1 \\ u_2 \\ \vdots \\ u_n \end{bmatrix}$$

to be estimated using the matrix operation

$$U = WX \tag{1}$$

It is assumed that the number of original signals and the recorded mixtures are equal. The unmixing matrix  $W$  is initially set to the identity matrix, and then its elements are updated iteratively by an amount  $\Delta W$ , in such a way as to minimise the mutual information between the extracted signal components. The ICA algorithm of BELL and SEJNOWSKI achieves this by maximising the rate of change of entropy of  $Y$  with respect to  $W$ . Therefore, to derive the ICA learning rule,  $\Delta W$  is first expressed as

$$\Delta W = \frac{\partial H(Y)}{\partial W} \tag{2}$$

where

$$Y = \begin{bmatrix} y_1 \\ y_2 \\ \vdots \\ y_n \end{bmatrix}$$

is obtained by a non-linear transformation of the signal components  $U$  using a function such as sigmoid. (2) can be expanded as (BELL and SEJNOWSKI, 1995)

$$\Delta W = \frac{\partial}{\partial W} \left( \ln \left| \frac{\partial Y}{\partial X} \right| \right) = \left( \frac{\partial Y}{\partial X} \right)^{-1} \frac{\partial}{\partial W} \left( \frac{\partial Y}{\partial X} \right) \tag{3}$$

where  $\ln|\cdot|$  is the natural logarithm of the magnitude of a variable, and the symbol  $^{-1}$  represents matrix inversion. For a sigmoid transfer function,  $Y$  is determined by

$$Y = \frac{1}{1 + e^{-(U+w_o)}} \tag{4}$$

where  $w_o$  is a bias term (initially set to zero vector). It can be shown that (BELL and SEJNOWSKI, 1995)

$$\frac{\partial Y}{\partial X} = WY(1 - Y) \tag{5}$$

$$\frac{\partial}{\partial W} \left( \frac{\partial Y}{\partial X} \right) = Y(1 - Y)(1 + WX(1 - 2Y)) \tag{6}$$

and bias term ( $\Delta W_0$ ) are expressed as

$$\Delta W = [W^T]^{-1} + (1 - 2Y)X^T \quad (7)$$

$$\Delta W_0 = 1 - 2Y \quad (8)$$

where  $T$  represents the matrix transpose operation. The matrix inversion is avoided by incorporating  $W^T W$  into (7) (AMARI *et al.*, 1996). This provides

$$\Delta W = \eta [I + (1 - 2Y)U^T] W \quad (9)$$

where  $\eta$  is the learning rate for controlling the speed of convergence.

### 3 Experimental method

#### 3.1 Data recording

Seven healthy adults (three males and four females), mean age 27 years (standard deviation 6), with normal or corrected-to-normal vision, participated in the study. The subjects had no history of neurological or ophthalmological disease and were all right-handed. They were seated in an EEG recording laboratory at about 60 cm from a computer that displayed a black and white checker-board pattern background.

A red square visual target stimulus (hereafter referred to as the stimulus) appeared on a computer screen at one of five pre-defined checker-board locations: centre, left, right, up and down, as shown in Fig. 2. The sequence of the stimulus appearance on the checker-board was random to reduce the effect of expectancy.

The subjects were instructed to follow visually the red square as fast as possible, without head movements, and to minimise blinks. The viewing angle ( $\alpha$ , shown in Fig. 2) of the peripheral positions from the centre was about 10 degrees. This value was also used in one of the saccade experiments reported in THICKBROOM *et al.* (1991). This made it possible to compare the lambda waves observed in both studies. To avoid the effect of anticipating the onset of the stimulus, the pre-stimulus period was varied randomly (between 850 ms and 1500 ms).

The EEG and EOG waveforms were recorded using a network of 64 silver-silver chloride electrodes. The type of EEG recording machine, its features and the details of the electrode locations can be found at reference (Electrical Geodesics Inc.). The EOG waveforms were recorded to monitor eye movements. All channels were referenced to the vertex  $C_z$  electrode. The recording system bandpass filter had a frequency range of

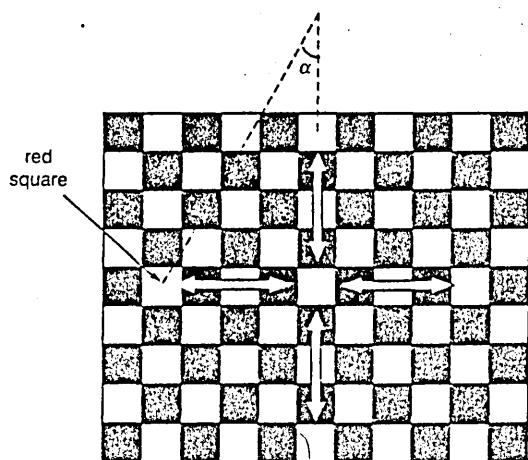


Fig. 2 Representation of checker-board showing directions of saccade and viewing angle

collection of the waveforms recorded from the 64 electrodes when a saccade was performed was referred to as a trial. Up to 50 trials were recorded per saccade direction. A collection of 50 trials is referred to as an event. Each trial lasted about 2 s. However only a 1 s window of each trial contained the lambda wave. This was selected and processed for this study.

#### 3.2 Preprocessing procedures

The recorded data were digitally lowpass filtered at 45 Hz to remove any 50 Hz mains interference and the unwanted high-frequency signal components. The baseline for each waveform was adjusted by calculating the mean of the pre-stimulus section and subtracting it from the whole waveform. The trials were sorted into their respective directions of saccade and time-synchronised using a procedure described in the following Section.

**3.2.1 Iterative time-synchronisation operation and its evaluation:** Temporal averaging of the waveforms across trials was carried out to reduce the effect of background EEG before processing by ICA (this is described in Section 3.2.2). The lambda wave is time-locked to the eye-movement EOG waveforms. The initiation of the eye movement (i.e. the saccade onset time) and its termination (saccade offset time) vary between trials. This means that the lambda waves from different trials are not time-synchronised. Therefore the averaging process would produce a distorted waveform. To overcome this, an algorithm that time-synchronised the trials was devised. The algorithm ensured that the temporal features of the lambda wave from different trials were aligned to a single reference signal prior to averaging. The EOG waveform was chosen as the reference signal for the synchronisation process because the lambda wave was time-locked to it. The operations involved when performing the time synchronisation are as follows:

- (i) The EOG waveforms across all trials for the desired event were averaged with respect to the stimulus onset. The resulting EOG waveform provided the averaged stimulus onset information.
- (ii) A section of the averaged EOG waveform that contained both the onset and the offset of the saccade was selected by the software as the reference signal.
- (iii) The reference signal and the EOG waveform from the trial being synchronised were correlated at each time point (sample value). The maximum correlation coefficient value between the two waveforms indicated the amount of shift required to synchronise the EOG waveform in that trial. This synchronisation was repeated for the EOG waveforms in the remaining trials.
- (iv) The newly synchronised EOG waveforms from all trials were then averaged. The resulting waveform retained the averaged stimulus onset information. Steps (ii)–(iv) (i.e. one iteration) were repeated until the reference signal did not change significantly from one iteration to the next. The changes in the reference signal from one iteration to the next were measured by computation of the Euclidean distance between the corresponding waveforms. The synchronisation improved the alignment of EOG waveforms across all trials after each iteration.
- (v) The last iteration in the above process produced the required reference EOG signal. This signal was then correlated with the original (not synchronised) EOG waveform for each trial, and the amount of shift required for their alignment was determined. All 64 waveforms in the corresponding trial were then time-shifted by the

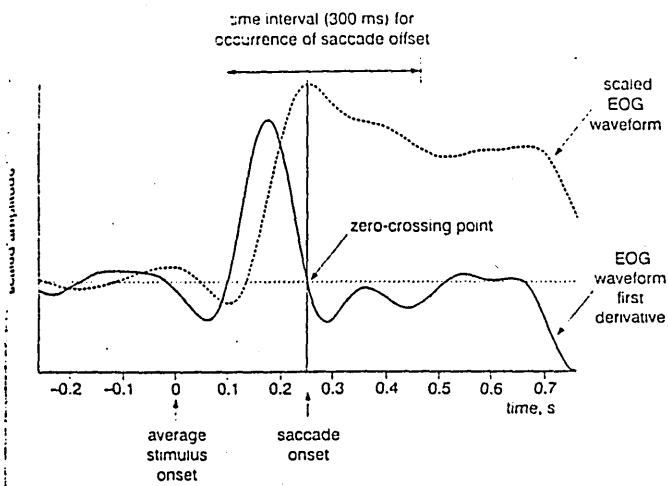


Fig. 3 Scaled eye-movement EOG waveform and its first derivative

calculated amount. The algorithm therefore synchronised all waveforms in all trials to the reference EOG signal.

The performance of the time-synchronisation procedure was evaluated. This involved plotting the histogram of the saccade offset across the 50 trials for a given subject and experimental event. To determine the saccade offset of the EOG waveforms, the following procedure was followed.

It takes about 160–200 ms for a subject to start moving his/her eyes in response to the appearance of the stimulus at a new location on the checker-board (VIGON *et al.*, 2000b). Furthermore, it can be assumed that the saccade is complete within the following 300 ms (DITCHBURN, 1973). The saccade offset corresponded to the largest peak in the eye-movement EOG waveform within this 300 ms time interval. To locate this peak, the first derivative of the eye-movement EOG waveform was computed, as shown in Fig. 3.

The maximum value of the derivative within the 300 ms time window was identified by a computer program. This

corresponded to the highest peak in the waveform within this time interval. The first zero-crossing after this peak represented the saccade offset for an EOG waveform of a given trial. The statistical distribution (histogram) of the saccade offsets across the 50 trials could then be obtained by repeating the procedure for each trial.

**3.2.2. Averaging process:** Both spatial and temporal averaging of the waveforms were carried out. A description of each follows.

**Spatial averaging:** In a previous study (VIGON *et al.*, 2000b), it was found that ICA was more effective in extracting the lambda wave when the saccade-related EEG waveforms recorded from the 64 channels were spatially averaged. The operation involved averaging together the waveforms from channels close to the International 10-20 system of electrode site placement, as denoted by the regions circled with broken lines in Fig. 4a. This resulted in 20 EEG waveforms obtained from the 20 locations highlighted by the alpha-numeric designation of electrodes placement in Fig. 4b and two EOG waveforms ( $EOG_L$  and  $EOG_R$  for the left and right sides, respectively), which were then used as input to ICA.

**Temporal averaging:** This was performed to reduce the obscuring effect of the background EEG on the EP component of interest (i.e. the lambda wave). For evaluation purposes, temporal averaging was carried out in three forms

- (a) non-abutted, averaged waveforms without time synchronisation; this involved obtaining the mean of the waveforms for each channel across the 50 trials
- (b) non-abutted, averaged waveforms with time synchronisation; this was similar to the first form, except that the waveforms were time-synchronised prior to averaging
- (c) abutted, averaged waveforms with time synchronisation; this involved abutting time-synchronised waveforms from a suitable number of successive trials and then obtaining the mean; the number of trials abutted was determined experimentally, as described in Section 3.2.5.

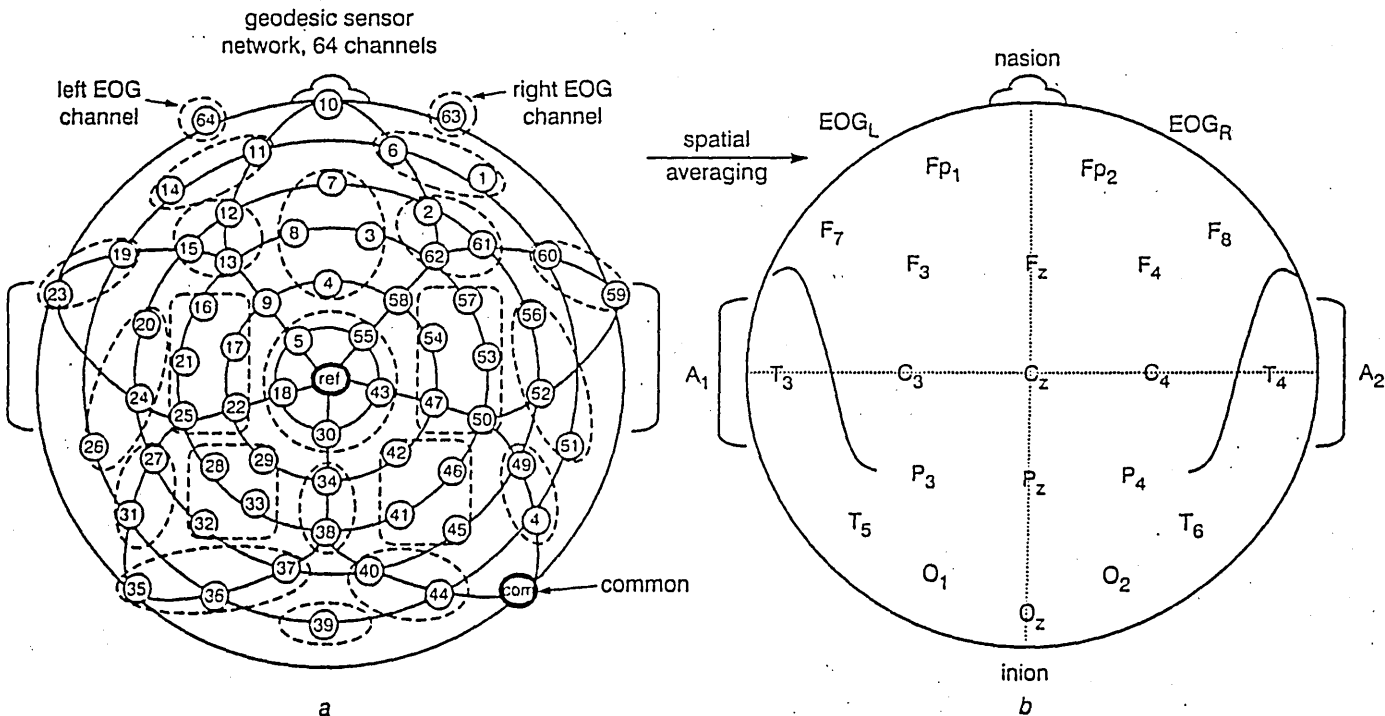


Fig. 4 Spatial averaging operation: (a) Electrical Geodesics sensor network of 64 electrodes and (b) International 10-20 system of electrode placement with alpha-numeric designation of electrodes placement on scalp for EEG recordings

3.2.3 *Whitening process and application of ICA:* The averaged waveforms were whitened. Whitening is a process that makes the mixtures mutually uncorrelated, as well as ensuring that they have unity variance (CICHOCKI *et al.*, 1999). By decorrelating the data beforehand, ICA can concentrate on the higher-order statistical dependencies of the waveforms.

ICA has a number of parameters that need to be initialised. One of these is the learning rate  $\eta$ , described in Section 2. It was heuristically found that a value of  $5 \times 10^{-4}$  was an appropriate initial value for this parameter. The value of  $\eta$  gradually decreased during the learning process until the rate of change was less than  $1 \times 10^{-6}$ . The weight matrix  $W$  was initialised to the identity matrix and then updated during the learning process by the amounts  $\Delta W_0$  and  $\Delta W$ , using (8) and (9), respectively. The training of ICA stopped when the value of  $\Delta W$  became less than a predefined small value ( $1 \times 10^{-9}$ ).

3.2.4 *Backprojection of the separated components:* The whitened waveforms were then input into ICA. The resulting ICA time series were backprojected to the 22 scalp locations (i.e. the 10-20 International EEG and EOG electrode placement locations) to obtain their scalp distributions. This involved multiplying the inverse of the unmixing matrix  $W$  by the ICA time series to obtain an estimate of the contributions of the separated components at each of the 22 scalp locations.

A procedure was devised to assess the effectiveness of ICA for determining the scalp distribution of the lambda wave. This estimated the percentage contribution of each ICA-extracted component to the expected region of the scalp associated with the lambda wave (i.e. parieto-occipital). The procedure used was as follows:

- (i) The estimated contributions of each extracted component to all electrode sites were normalised between 0 and 1.
- (ii) The sum  $S_1$  of the resulting contributions was obtained.
- (iii) The sum  $S_2$  of the contributions for the parieto-occipital area of the cerebral cortex (i.e. the region defined by the eight electrodes  $P_3, P_4, P_z, O_1, O_2, O_z, T_5$  and  $T_6$ , as shown in Fig. 4b) was calculated.
- (iv) The required percentage contribution was then determined as  $(S_2/S_1) \times 100$ .

3.2.5 *Analysis procedure:* The analysis was initially carried out on artificially mixed waveforms. This allowed the approaches to be quantitatively assessed. The analysis was then extended to the 22 spatially and temporally averaged waveforms (described in Section 3.2.2). The details of the investigations follow.

For the artificially mixed signals, the 22 averaged waveforms were visually inspected, and two waveforms were selected. These two waveforms were selected from different subjects to ensure their independence. One waveform was an EEG waveform with the temporal features of the lambda wave (as described in the literature, such as THICKBROOM *et al.* (1991)). The other was an eye-movement EOG waveform (recorded from EOG<sub>L</sub> site in Fig. 4b). Different lengths of averaged waveforms were produced by the abutting of successive trials (described in Section 3.2.2). The abutted EEG and EOG waveforms for waveform length corresponding to three trials are shown in Figs 5 and 6, respectively. EOG can be hundreds of microvolts in magnitude and contain the signal components caused by blinks and eye movements. The EOG waveforms shown in Fig. 6 are caused by eye movements. The magnitude of this type of EOG is affected by the amount that the eyes are moved when performing

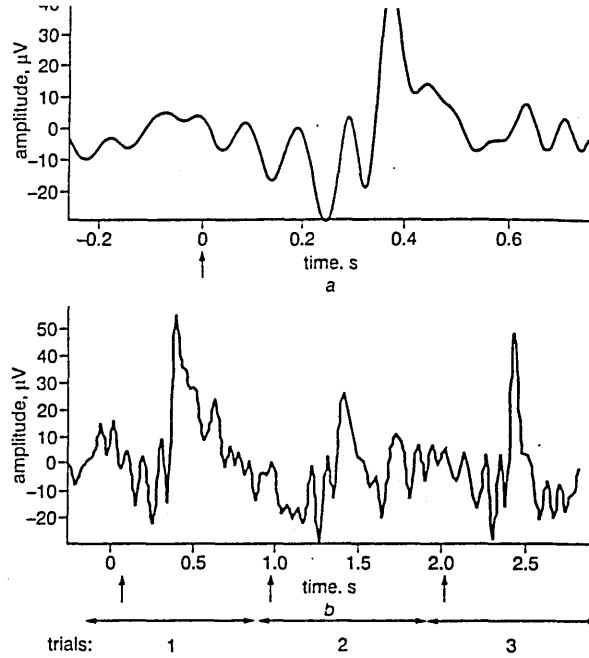


Fig. 5 Averaged EEG waveform with lambda wave features: (a) non-abutted, (b) abutted for three trials. Vertical arrow indicates average stimulus onset

saccade (i.e. the viewing angle defined in Section 3.1). The viewing angle of 10 degrees used in this study causes a small deviation of the eyes, thus generating eye-movement waveforms of the range shown in Fig. 6.

The univariate statistical procedure (SAS, 1982) was used to test the degree to which the selected EEG and EOG signals were Gaussian. The univariate procedure tested the null hypothesis that the input data values were a random sample from a normal distribution. To decide whether to reject the null hypothesis of the test for normality, it was necessary to examine the probability associated with the test statistic (i.e. the probability value for the Shapiro-Wilk statistic). The value obtained was less than 0.05

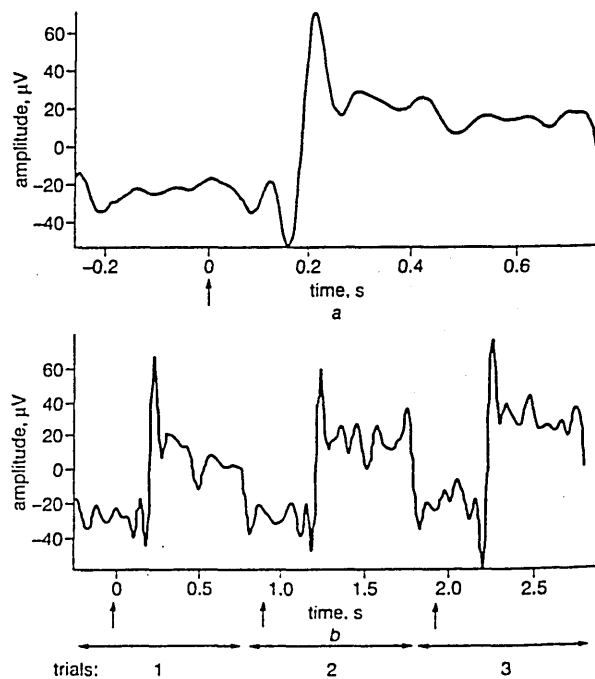


Fig. 6 Averaged eye-movement EOG waveform: (a) non-abutted, (b) abutted for three trials. Vertical arrow indicates average stimulus onset

$a_{11}$	0.55	0.65	0.75	0.85
$a_{12}$	0.45	0.35	0.25	0.15

e. 95% confidence level) for all four waveforms (the non-abutted and abutted time-synchronised averaged EEG and EOG waveforms). Therefore the null hypothesis was rejected, and it was concluded that the four waveforms were not significantly Gaussian.

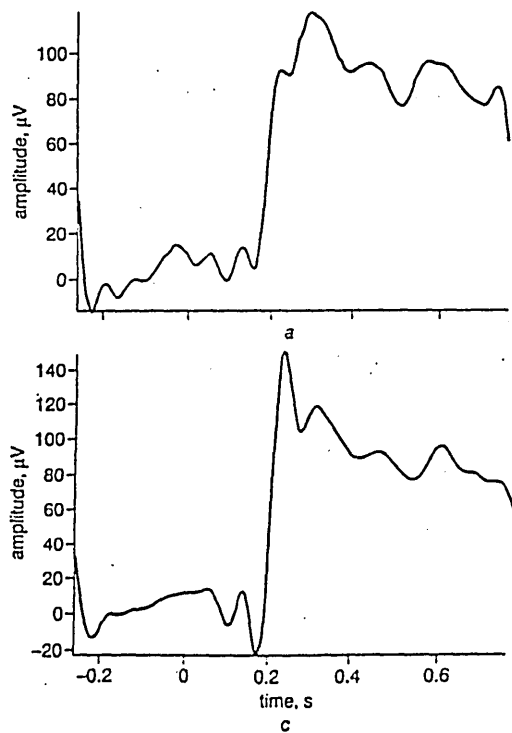
Artificial mixtures were generated by carrying out the matrix operation

$$\begin{pmatrix} EEG_m \\ EOG_m \end{pmatrix} = \begin{pmatrix} a_{11} & a_{12} \\ a_{21} & a_{22} \end{pmatrix} \begin{pmatrix} EEG \\ EOG \end{pmatrix} \quad (10)$$

where  $EEG$  and  $EOG$  were the original signal sources,  $EEG_m$  and  $EOG_m$  were the resulting mixtures,  $a_{11}$  and  $a_{12}$  were the mixing coefficients for the EEG signal, and  $a_{21}$  and  $a_{22}$  were the mixing coefficients for the EOG signal. The ICA algorithm of BELL and SEJNOWSKI (1995) was applied to unmix the mixtures. The effect of signal length on the performance of ICA was investigated by gradually increasing the length of the averaged waveforms from 256 data points (corresponding to one trial) to 536 data points (corresponding to six abutted trials). This was carried out for the mixing coefficients shown in Table 1.

The EOG mixing coefficients were  $a_{21} = 1 - a_{11}$  and  $a_{22} = 1 - a_{12}$ . The gradual increase in the waveforms' length was carried out in such a way that each waveform always contained an integer number of lambda wave sections. Indeed, as the lambda wave occurred within the 500 ms time interval following the onset of the stimulus, the abutting process ensured that the end point of the resulting abutted trials did not lie within this 500 ms window.

The similarity between the original and recovered waveforms was quantified by calculating the following parameters:



- (a) correlation  $c$ : zero indicated no similarity, and  $-1$  and  $1$  indicated 100% similarity in shape ( $-1$  meant an inversion in polarity of the extracted component)
- (b) euclidean distance  $\epsilon$ : this provided a measure of similarity in both magnitude and shape of the waveforms and was calculated by

$$\epsilon = \sqrt{\sum_{i=1}^k (o(i) - r(i))^2} \quad (11)$$

where  $o$  and  $r$  were the original and recovered signals, respectively, and  $k$  was their length.

## 4 Results and discussion

### 4.1 Evaluation of iterative synchronised averaging

Fig. 7a shows a typical average of 50 eye-movement EOG waveforms prior to iterative synchronisation. Fig. 7b shows the histogram (distribution) of the saccade offsets of the EOG waveforms. The saccade offset of each trial was determined using the procedure described in Section 3.2.1. Figs 7c and d show the same information once the iterative synchronisation has been performed. It can be observed that the process has reduced the deviation of the saccade offset distribution and thus provided a less distorted, averaged EOG waveform.

Fig. 8a shows the averaged lambda wave (over 50 trials) without time synchronisation, together with its eye-movement EOG waveform. The waveforms following iterative synchronisation are shown in Fig. 8b. The process of iterative synchronisation resulted in the extraction of the lambda wave feature  $f_2$ , which was not visible in the averaged lambda wave without time synchronisation. The significance of the features  $f_2$ ,  $f_3$  and negative shift  $NS$ , which are shown in Fig. 8, are outlined in Section 4.3.

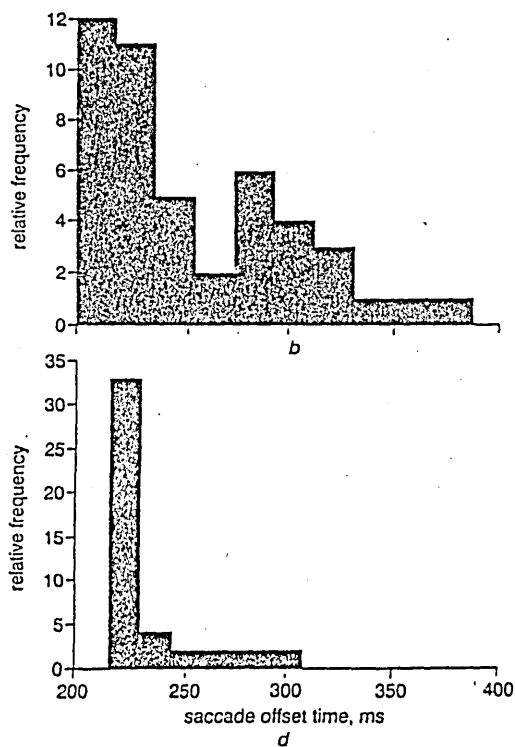


Fig. 7 (a) Averaged eye movement EOG waveform before synchronisation; (b) saccade offset distribution; (c) averaged eye-movement EOG waveform after synchronisation; (d) saccade offset distribution

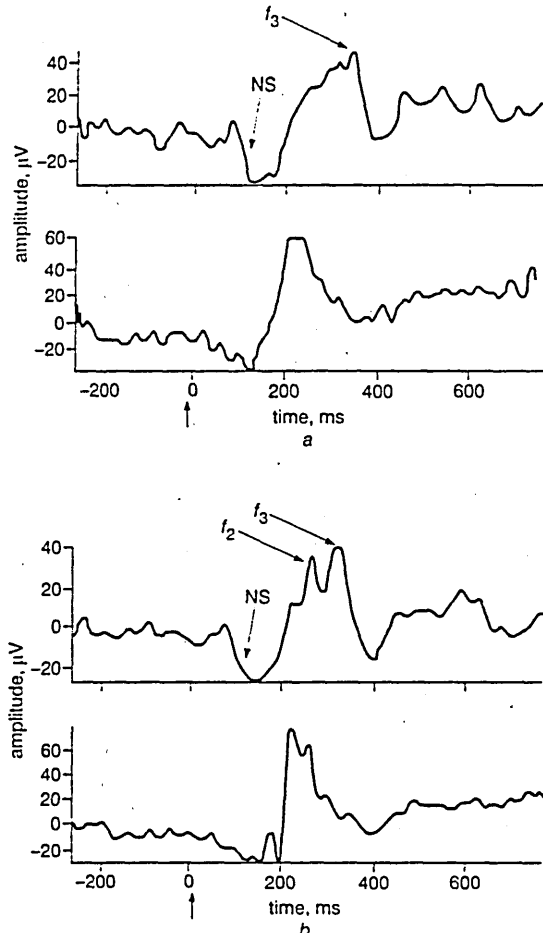


Fig. 8 Lambda wave (top) and eye movement EOG waveform (bottom) obtained by (a) averaging without time synchronisation, (b) averaging with time synchronisation. Vertical arrow indicates average stimulus onset

#### 4.2 ICA applied to artificial mixtures

Figs 9a and b show the effect of signal length on ICA performance when the artificially mixed waveforms were processed. The points on the graphs correspond to the mixing ratios indicated in Table 1. The effectiveness of ICA for extracting the EEG waveform from the mixtures gradually improved (i.e.  $\rho$  closer to 1,  $\epsilon$  closer to 0) when the signal length was increased (by the abutting process) from 256 data points (i.e. one trial) to 1024 data points (i.e. four trials).

The components of the artificially generated signal mixtures (i.e. the EOG waveform and the EEG waveform with main lambda wave characteristics) are short-duration transient signals. The abutting of the waveforms to increase their lengths improved their stationarity. As ICA relies on the stationarity of the signals, the abutting process therefore provided a means to make the waveforms more suitable for processing by ICA. For waveforms greater than 1024 data points, no further improvement was observed.

#### 4.3 ICA applied to 22 spatially and temporally averaged waveforms

The results for the centre-to-left saccade event are presented in this Section. As a finite number of trials had been recorded (i.e. 50 trials per subject), increasing the number of trials for the abutting process would have resulted in the averaging being carried out over a smaller number of trials, thus reducing the ability to attenuate the background EEG prior to ICA operation. It was decided to set the length of the abutted waveforms to three trials. This was considered to be a reasonable compromise for

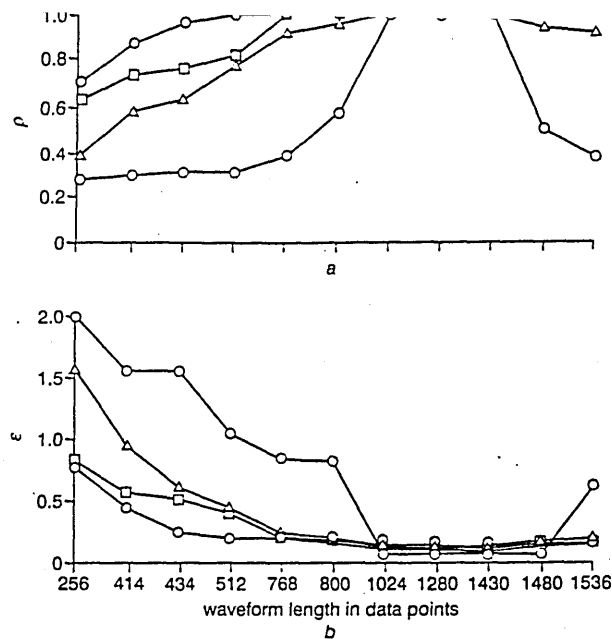


Fig. 9 (a) Correlation coefficient values and (b) Euclidean distance values, between original and recovered EEG waveforms. EEG mixing ratios  $a_{11}$ ,  $a_{12}$ : (—○—) 0.85, 0.15; (—□—) 0.75, 0.25; (—△—) 0.65, 0.35; (—○—) 0.55, 0.45

satisfying these two criteria. Once the components were extracted by ICA, a further averaging across the trials was carried to produce a single lambda wave.

Fig. 10 shows typical ICA-extracted lambda waves (top row) and eye movement (bottom row) together with their corresponding scalp distributions, for the non-abutted (Figs 10a and b) and abutted (Figs 10c and d) time-synchronised, averaged approaches. Similar results were obtained for the other subjects, and the results when the methods for all subjects were assessed are summarised later in this Section.

The following are the main observations of this part of the study:

First, ICA managed to extract the lambda wave and the eye-movement waveform when it was applied to both abutted and non-abutted averaged time-synchronised waveforms. However, the features of the lambda wave extracted when ICA was applied to the abutted waveforms were preserved more accurately. The features considered for this evaluation were  $f_1$ ,  $f_2$  and  $f_3$  and the pre-saccadic negative shift NS (negative shift in the EEG that appears from the onset of the stimulus and ends once the saccade is performed). The features  $f_1$ ,  $f_2$  and  $f_3$  are believed to be related to the movement of the visual field across the retina (THICKBROOM *et al.*, 1991). The features  $f_1$  and  $f_2$  were reported to be time-locked to the onset of the saccade, and the feature  $f_3$  was reported to be time-locked to the offset of the saccade (THICKBROOM *et al.*, 1991). The characteristics of these features depend on factors such as the saccade duration or the viewing angle ( $\alpha$ , shown in Fig. 2).

In our study, where a short duration of saccade (about 20 ms) was used, we did not observe the feature  $f_1$  in either time-synchronised or not time-synchronised, averaged lambda waves (see Fig. 8b). This was in accordance with the observations made in THICKBROOM *et al.* (1991). However, in our study, this feature became visible when ICA was applied to either non-abutted or abutted time-synchronised, averaged waveforms. The feature  $f_1$  was observed by THICKBROOM *et al.* (1991) only in the averaged EEG waveform of a subject for a longer duration of saccade (75–100 ms).

Secondly, Table 2 contains a summary of the analysis results across the seven subjects for the temporal features NS,  $f_1$ ,  $f_2$  and

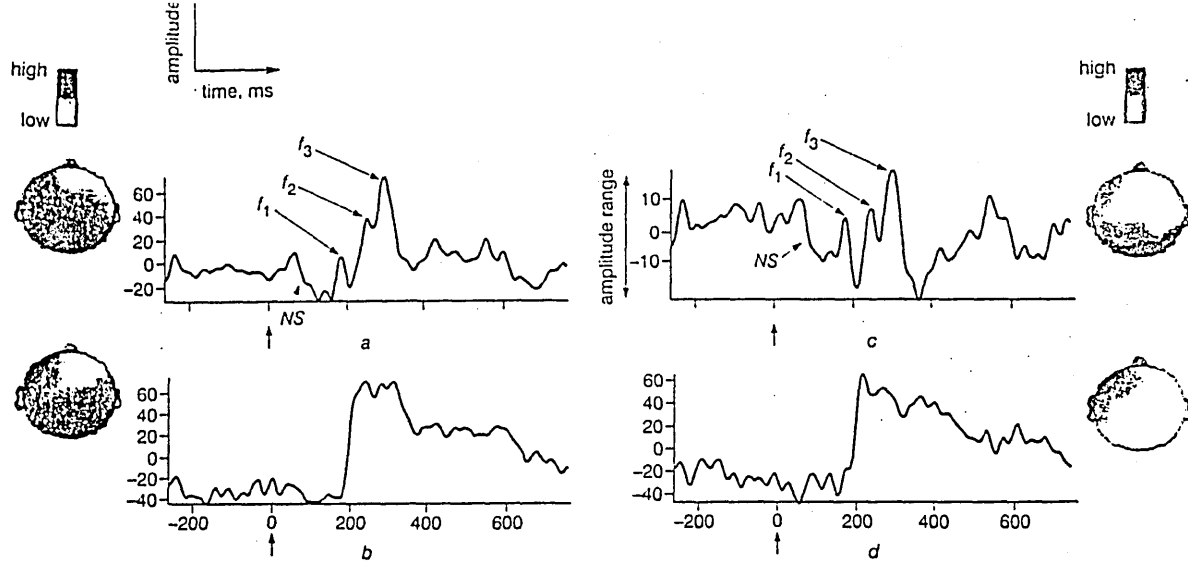


Fig. 10 ICA-extracted lambda waves (top row) and eye movements (bottom row), together with respective scalp distributions for (a), (b) non-abutted and (c), (d) abutted approaches. Vertical arrow indicates average stimulus onset

$f_3$  when the methods to recover the lambda wave component were assessed.

The methods were

- (i) non-abutted, averaged waveforms without time synchronisation
- (ii) non-abutted, averaged waveforms with time synchronisation
- (iii) ICA applied to non-abutted, averaged waveforms with time synchronisation
- (iv) ICA applied to abutted, averaged waveforms with time synchronisation.

An expert familiar with the features of the lambda wave inspected the recovered lambda waves for each method. Four features of the recovered lambda waves ( $NS$ ,  $f_1$ ,  $f_2$  and  $f_3$ ) were monitored for their visibility. Table 2 contains the number of subjects in which each feature was observed for each method. The  $NS$  feature was observed in all seven subjects for all four methods. The averaging method without time synchronisation was least effective, as, with this method, each one of the features  $f_1$ ,  $f_2$  and  $f_3$  were observed only once across the seven subjects. Averaging with time synchronisation was more effective than averaging

Table 2 Summary of analysis results for temporal features of lambda wave when four methods to recover lambda wave component were assessed

Methods	Lambda wave temporal feature			
	$NS$	$f_1$	$f_2$	$f_3$
non-abutted, averaged waveforms without time synchronisation	7	1	1	1
non-abutted, averaged waveforms with time synchronisation	7	2	5	4
ICA applied to non-abutted, averaged waveforms with time synchronisation	7	4	6	6
ICA applied to abutted, averaged waveforms with time synchronisation	7	7	7	7

without synchronisation, as the method managed to preserve features  $f_1$ ,  $f_2$  and  $f_3$  in two, five and four subjects, respectively. The results were further improved when ICA was applied to non-abutted, time-synchronised averaged waveforms. The method successfully extracted features  $f_1$ ,  $f_2$  and  $f_3$  in four, six and six subjects, respectively. The best performance was achieved when ICA was applied to the abutted, time-synchronised averaged waveforms, as the features  $f_1$ ,  $f_2$  and  $f_3$  were visible in all seven subjects.

Thirdly, Table 3 contains a summary of the analysis results across the seven subjects for the scalp distribution (spatial feature) and the amplitude range, when the four methods to recover the lambda wave were assessed.

The amplitude range represents the peak-to-peak magnitude of the lambda wave, as indicated in Fig. 10. The Table provides both the mean and standard deviation values for each of the two parameters across the seven subjects. Neither averaging method (i.e. with or without time synchronisation) provided the scalp distribution of the recovered lambda wave. When using ICA, the backprojection method described in Section 3 was applied to obtain an estimate of the amplitude ranges. In the same Section, the procedure used to estimate the percentage contribution of the ICA-extracted components to the parieto-occipital region of the cerebral cortex is provided.

When ICA was applied to the abutted, averaged, time-synchronised waveforms the contribution of the extracted lambda wave component to the parieto-occipital region of the cerebral cortex (back of the head) was estimated to be 73%. When ICA was applied to non-abutted, averaged, time-synchronised waveforms, the contribution was 55%. Therefore the abutting process improved the spatial resolution for the extracted lambda wave. When we consider the amplitude range feature, the averaging methods, with or without time synchronisation, provided mean values of  $48 \mu\text{V}$ . ICA applied to the abutted, averaged, time-synchronised waveforms provided a mean value of  $29 \mu\text{V}$  for the amplitude range, whereas that for ICA applied to the non-abutted, averaged, time-synchronised waveforms was  $97 \mu\text{V}$ . The former range is closer to the previously reported lambda wave amplitude range of about  $30 \mu\text{V}$  (THICKBROOM *et al.*, 1991).

In summary, the four approaches reported in this study were ranked in the following order of decreasing effectiveness for extracting the lambda wave:

Methods	Percentage scalp distribution, %		Amplitude range, $\mu\text{V}$	
	mean	SD	mean	SD
non-abutted, averaged waveforms without time synchronisation	–	–	48	13
non-abutted, averaged waveforms with time synchronisation	–	–	48	18
ICA applied to non-abutted, averaged waveforms with time synchronisation	55	9	97	25
ICA applied to abutted, averaged waveforms with time synchronisation	73	11	29	7

- (a) ICA applied to abutted, averaged waveforms with time synchronisation
- (b) ICA applied to non-abutted, averaged waveforms with time synchronisation
- (c) non-abutted, averaged waveforms with time synchronisation
- (d) non-abutted, averaged waveforms without time synchronisation.

## 5 Conclusion

The effect of waveform length on the performance of independent component analysis for extracting a visual evoked potential called the lambda wave from saccade-related EEG waveforms was investigated. Experiments were carried out using both artificially generated mixtures and the recorded EEG and EOG waveforms. The length of the waveforms was increased by a process that involved abutting successive trials. The study demonstrated that increasing the length of the EEG waveforms by the abutting process increased the accuracy of ICA for extracting the lambda wave.

*Acknowledgments*—This study was supported by a joint Sheffield Hallam University – Sheffield University research grant. The authors are grateful to Dr Peter Furness, for helping with the data recording procedures, and Dr David Buckley, for his help in designing the experiment. This study would not have been possible without the kind co-operation of the subjects who took part in the data recordings.

## References

- AMARI, S., CICHOCKI, A., and YANG, H. (1996): 'A new learning algorithm for blind signal separation', *Adv. Neural Inf. Process. Syst.*, **8**, pp. 757–763
- BARLOW, J. S., and CIGANEK, L. (1969): 'Lambda responses in relation to visual evoked responses in man', *Electroenceph. Clin. Neurophysiol.*, **26**, pp. 183–192
- BELL, A. J., and SEJNOWSKI, T. J. (1995): 'An information-maximization approach to blind separation and blind deconvolution', *Neural Comput.*, **7**, pp. 1129–1159
- CARDOSO, J.-F. (1999): 'High-order contrasts for independent component analysis', *Neural Comput.*, **11**, pp. 157–192
- CICHOCKI, A., KARHUNEN, J., KASPRZAK, W., and VIGÁRIO, R. (1999): 'Neural networks for blind separation with unknown number of sources', *Neurocomputing*, **24**, pp. 55–94
- DITCHBURN, R. W. (1973): 'Eye-movements and visual perception' (Clarendon Press, Oxford, 1973)
- Electrical Geodesics, Inc. Internet site address: <http://www.egi.com/>

- GREEN, J. (1957): 'Some observations on lambda waves and peripheral stimulation', *Electroenceph. Clin. Neurophysiol.*, **22**, pp. 204–209
- HYVÄRINEN, A. (1999): 'Survey on independent component analysis', *Neural Comput. Surv.*, **2**, pp. 94–128
- LEVENTHAL, A. G. (Ed.) (1991): 'The neural basis of visual function. Vol. 4' (Macmillan, Vision and Visual Dysfunction Series, Basingstoke, 1991)
- SKRANDIES, W., and LASCHKE, K. (1997): 'Topography of visual brain activity during eye movements: lambda waves, saccadic suppression, and discrimination performance', *Int. J. Psychophysiol.*, **27**, pp. 15–27
- STATISTICAL ANALYSIS SYSTEM (SAS) (1982): 'SAS user's guide: statistics' (SAS Institute Inc., Box 8000, Cary, North Carolina 27511)
- THICKBROOM, G. W., KNEZEVIC, W., CARROLL, W. M., and MASTAGLIA, F. L. (1991): 'Saccade onset and offset lambda waves – relation to pattern movement visually evoked potentials', *Brain Res.*, **551**, pp. 150–156
- VIGON, L., SAATCHI, M. R., MAYHEW, J. E. W., and FERNANDES, R. (2000a): 'A quantitative evaluation of techniques for ocular artefact filtering of EEG waveforms', *IEE Proc. Sci. Meas. Technol.*, **147**, pp. 219–228
- VIGON, L., SAATCHI, R., MAYHEW, J., TAROYAN, N., and FRISBY, J. (2000b): 'Independent component analysis of saccade-related electroencephalogram waveforms', *Electron. Lett.*, **36**, pp. 1006–1007

## Authors' biographies

L. VIGON obtained her MSc in Electronics and Communication Engineering in 1997. She is currently a research student at Sheffield Hallam University investigating independent component analysis for the interpretation of the electroencephalogram.

R. SAATCHI is a Reader in Computer Engineering and Digital Signal Processing at Sheffield Hallam University. His research interests include signal source separation and artificial intelligence methods for analysing the electroencephalogram.

J. E. W. MAYHEW is a full-time research professor and holds a Personal Chair in the University of Sheffield. His research activities involve electrophysiology, optical imaging spectroscopy, laser Doppler flowmetry and magnetic resonance imaging.

N. A. TAROYAN is currently working as a postdoctoral researcher in the Psychology Department of Sheffield University. Her research interests include psychophysical and electrophysiological aspects of stereopsis and eye movements.

J. P. FRISBY was appointed Professor of Psychology at the University of Sheffield in 1976. His research interests lie mainly in psychophysical studies of human stereopsis, guided by computational models, and in clinical tests of stereopsis.